Complex sine-Gordon theory: solitons, defects and boundaries

Umpleby, James

Complex sine-Gordon theory: Solitons, defects and boundaries

James Umpleby

A Thesis presented for the degree of
Doctor of Philosophy

Centre of Particle Theory
Department of Mathematical Sciences
Durham University
UK

September 2008

This thesis is dedicated to the memory of my grandma,

Eileen Umpleby

1922 - 2008

Complex sine-Gordon theory: Solitons, defects and boundaries

James Umpleby

Submitted for the degree of Doctor of Philosophy
September 2008

Abstract

This thesis presents research into the properties and features of the complex sine-Gordon theory. The CSG theory is a 1+1 dimensional integrable field theory that admits soliton solutions which carry a Noether charge due to the $U(1)$ invariance of the theory. Integrable CSG defects and boundaries are constructed and interactions between solitons, defects and boundaries are analysed at the classical and quantum level.

The introduction of defects into the theory is facilitated by a new Bäcklund transformation involving two parameters. Defect conditions, constructed so they maintain the integrability of the theory and found to be exactly the BT, are used to sew two CSG theories together. How solitons interact with the defect is investigated, in particular whether as in the SG theory solitons can be absorbed and emitted by the defect. The classical time-delay and phase-shift are calculated for soliton-defect and particle-defect scattering.

Using the CSG defect to dress the Dirichlet boundary a new CSG boundary theory is produced. Its integrability is checked by the explicit construction of conserved charges. The various interactions between solitons and the boundary are analysed, compared and contrasted with the defect theory. Finally aspects of the quantum CSG boundary theory are examined, culminating in a conjecture for the quantum reflection matrix for a $Q = +1$ soliton reflecting from an unexcited boundary. Reflection and boundary bootstrap procedures are used to generate the general reflection matrix for any charged soliton reflecting from any excited boundary.

Declaration

The work in this thesis is based on research carried out at the Centre for Particle Theory, Department of Mathematical Sciences, Durham University, UK. No part of this thesis has been submitted elsewhere for any other degree or qualification and it is all my own work unless referenced to the contrary in the text.

Chapters 2 and 3 form a review, apart from the work on classical bound states in ShG defect theory, section 3.4. Chapters 4 and 7 include a review into classical and quantum CSG theory respectively. The content in chapters 4, 5, 6 and 7 is work in collaboration with Dr. Peter Bowcock, the classical aspects appear in *"Defects and Dressed Boundaries in Complex Sine-Gordon Theory"* [1] and the quantum aspects in *"Quantum complex sine-Gordon dressed boundaries"* [2].

Acknowledgements

First a big thank you to my supervisor Peter Bowcock; for introducing me to the world of solitons; the guidance offered and the endless hours of interesting debate and discussion during my studies. To Ed Corrigan and Patrick Dorey for allowing me to tap into their expertise and EPSRC for funding my PhD.

To all the fantastic people I have met during my PhD, especially my housemates John, Kemal, Martyn, Simon and Liz. To meet one such friend, one would count yourself very lucky, so I am not sure what that makes me. Thank you for all the good times that we have shared and putting up with my Boro obsession.

Thank you to the groups of people who have made my time in Durham such an enjoyable one; my office mates Bina, James, Jackie and especially Derek and Andy for many discussions on all things solitonic!; the members of Ustinov Darts and Hockey teams; fellow salsa dancers and Stokesley 2nd XI cricketers. Thank you to the whole of the Maths department; the "Sharry v Patrick" Friday footballers; to Pamela, Mike and the secretary girls for making it so welcoming.

Thank you to my Mum, Dad and sister Helen for all your continual support and encouragement, without which I don't think it would have been possible.

Finally to the City of Durham, the place I have called home for the best part of a decade! The memories of my time here will stay with me forever. Where ever the rest of my life takes me, I will be sure to return frequently. I'll leave the last words to the University of Durham Chancellor Bill Bryson, with whom I fully concur [3]

"I got off at Durham... and fell in love with it instantly in a serious way. Why, it's wonderful - a perfect little city.... If you have never been to Durham, go there at once. Take my car. It's wonderful."

Contents

List of Figures

List of Tables

Chapter 1

Introduction

This thesis continues the research into integrable field theories on restricted domains [4–8]. Specifically we investigate whether defects and dressed boundaries can be introduced into the complex sine-Gordon theory while preserving the classical integrability of the original theory. The complex sine-Gordon theory is a quantum field theory of a complex field in 1+1 dimensions which like many other integrable models exhibits soliton solutions. Solitons in the CSG theory carry a Noether charge due to the $U(1)$ invariance of the theory, this leads to additional interesting phenomena in the interactions between solitons, defects and boundaries, beyond those found in the well studied sine-Gordon theory.

Solitons or solitary waves were first observed by John Scott Russell on the Edinburgh-Glasgow canal in 1834 and reported on in his *"Report on waves"* [9] in 1844, including the passage

"I was observing the motion of a boat which was rapidly drawn along a narrow channel by a pair of horses, when the boat suddenly stopped - not so the mass of water in the channel which it had put in motion; it accumulated round the prow of the vessel in a state of violent agitation, then suddenly leaving it behind, rolled forward with great velocity, assuming the form of a large solitary elevation, a rounded, smooth and well-defined heap of water, which continued its course along the channel apparently without change of form or diminution of speed. I followed it on horseback, and overtook it still rolling on at a rate of some eight or nine miles an hour, preserving its original figure some thirty feet long and a foot to a foot and a half in height. Its

height gradually diminished, and after a chase of one or two miles I lost it in the windings of the channel. Such, in the month of August 1834, was my first chance interview with that singular and beautiful phenomenon which I have called the Wave of Translation".

Russell's "wave of translation" became known as the soliton which plays an important part in the study of non-linear systems. They are dispersionless localised solutions which retain their form when they scatter with other solitons. Solitons were first studied in the KdV equation and then found to be present in many non-linear theories, including the sine-Gordon theory and complex sine-Gordon theory.

The integrability of the complex sine-Gordon theory adds further interest to the theory. Quantum field theories that are integrable have been an extensive area of study over the past 25 years since Zamolodchikov and Zamolodchikov [10] showed in the case of the sine-Gordon model that the S-matrices can be found exactly. The S-matrix of a theory governs the particle scattering in the theory. It was realised that the integrability, which we define as the existence of an infinite number of conserved charges, simplifies the S-matrix in 1+1 dimensions. The S-matrix in 1+1 dimensions has the following properties:

- no particle production
- the sets of incoming and outgoing momenta are equal
- $n \to n$ S-matrix can be factorised into $2 \to 2$ S-matrices.

These properties mean that the scattering in the theory is totally determined once the S-matrix governing $2 \to 2$ scattering is known. The factorisability and integrability of the $n \to n$ S-matrix also gives added constraints on the $2 \to 2$ S-matrices through the Yang-Baxter equation. We illustrate the factorisability of the $3 \to 3$ S-matrix in figure 1.1 where the integrability allows the world lines of the particles to be shifted, so the $3 \to 3$ scattering can be factorised into three $2 \to 2$ scatterings. The Yang-Baxter equation is the equality of figures 1.1(b) and 1.1(c), which gives the constraint

$$S_{ab}^{\alpha\beta}(\theta_a-\theta_b)\, S_{ac}^{n\gamma}(\theta_a-\theta_c)\, S_{\beta\gamma}^{ml}(\theta_b-\theta_c) = S_{bc}^{\beta\gamma}(\theta_b-\theta_c)\, S_{a\gamma}^{al}(\theta_a-\theta_c)\, S_{\alpha\beta}^{nm}(\theta_a-\theta_b)\,, \quad (1.0.1)$$

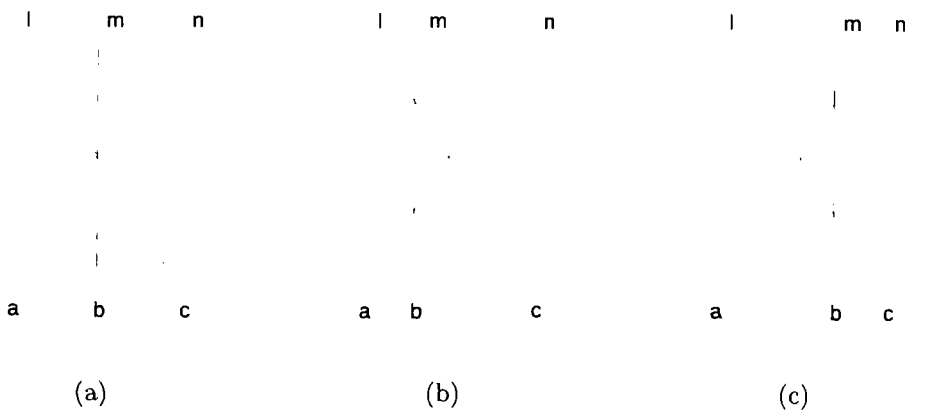

Fig. 1.1: Factorisability of S-matrix and Yang-Baxter equation, with time flowing up the diagrams.

if the S-matrix is non-diagonal. If the S-matrix is diagonal then the Yang-Baxter equation is trivially satisfied. The Yang-Baxter equation along with unitarity, analyticity and crossing constraints mean that the S-matrix is exactly solvable (see [11] for a review).

In 1993 Ghoshal and Zamolodchikov [4] initiated the study into integrable field theories on restricted domains when they considered the sine-Gordon theory on the halfline. They found that the integrability of the theory could be preserved in the boundary theory if the boundary conditions at $x = 0$ were carefully chosen. The study of boundaries is relevant in condensed matter physics and also in string theory. A generalisation of the Yang-Baxter equation exists describing the scattering from a boundary and the reflection matrices K can be solved for. In theories with solitons, asking how they interact with the boundary is an interesting question.

Progressing on from the study of boundary theories Bowcock, Corrigan and Zambon [8] first considered the possibility of studying an internal boundary or defect between two integrable field theories from a Lagrangian point of view. Again it was found that if the defect conditions used to sew the two theories together are carefully chosen, the defect theories are able to maintain the classical integrability of the original theory. Defects allow impurities to be studied, but in the context of integrable models the conditions on the defect are chosen specifically to maintain the mathematical properties of the model.

The complex sine-Gordon theory exhibits many of the same interesting properties of the sine-Gordon theory, integrability and the existence of soliton solutions, while adding more complexity. It is a theory of complex fields and exhibits a $U(1)$ symmetry which generates a Noether charge. The solitons carry this extra internal degree of freedom. The study of the complex sine-Gordon theory with boundary and defect provides a testing ground to see whether properties found in the sine-Gordon and other theories are general to all integrable boundary and defect theories, and whether the richness of the complex sine-Gordon theory adds to the previously witnessed phenomena. The examination of the interactions between the charged complex sine-Gordon solitons and the boundary and defect is of particular interest.

This thesis will be structured as follows, in the next chapter we use the sine-Gordon and sinh-Gordon theories to introduce common properties and techniques prevalent in the study of all 1+1 dimensional field theories in preparation for the study into the more complicated complex sine-Gordon theory. Chapter 3 will continue the introduction by describing the sine-Gordon boundary and defect theories, including a brief overview of the soliton interactions with defect and boundary. The sinh-Gordon defect theory is introduced and we present new analysis on classical solutions to the field equations.

Chapter 4 starts the main body of research with an introduction into the bulk complex sine-Gordon theory. A new description of the theory is presented allowing new Bäcklund transformation and two-soliton solution to be formulated. In chapter 5 we construct the complex sine-Gordon defect theory, generate defect conditions so the lower spin Lorentz charges are conserved. We thoroughly analyse the defect theory in the original 'two field' description and the new description introduced in the chapter 4. Soliton and particle interactions with the defect are studied.

In chapter 6 a new complex sine-Gordon boundary theory is constructed by using the defect to dress the Dirichlet boundary. We formulate boundary conditions and lower spin conserved charges. Similarly to the defect theory, soliton and particle interactions with the boundary are analysed.

Chapter 7 covers the study of quantum aspects of the dressed boundary theory after properties of the quantum complex sine-Gordon theory are introduced. We

use semi-classical methods to approximate the quantum boundary spectrum, before providing a conjecture for the fully quantum reflection matrices. We check our conjecture with classical results and give a preliminary analysis of the pole structure present in the reflection matrices.

The final chapter summarises the findings of this thesis and comments on possible avenues of research leading on from the work presented.

Chapter 2

Sine and sinh-Gordon theories

Two examples of 1+1 dimensional integrable quantum field theories are the sine-Gordon theory (SG) and its sister theory the sinh-Gordon theory (ShG), recovered by analytically continuing the coupling constant in the SG theory. In this chapter we use both theories to introduce features displayed by the complex sine-Gordon theory and techniques which we use in later chapters. The two theories, despite being described by virtually the same Lagrangian, have very different properties and features.

2.1 Sine-Gordon theory

The SG theory exhibits the more interesting properties due to the topological nature of the vacuum. These include the existence of soliton solutions that carry topological charge. The starting point in the overview for the SG theory is the Lagrangian density

$$\mathcal{L}_{SG} = \frac{1}{2}\left(\frac{\partial\phi}{\partial t}\right)^2 - \frac{1}{2}\left(\frac{\partial\phi}{\partial x}\right)^2 - \frac{2m^2}{\beta^2}(1-\cos(\sqrt{2}\beta\phi))\,, \qquad (2.1.1)$$

where ϕ is a real scalar field, m the mass parameter and β the coupling constant. The presence of the $\cos(\sqrt{2}\beta\phi)$ term introduces the interactions into the theory. Expanding the cosine as a sum shows that as well as the standard mass term $\sim \phi^2$, there are an infinite number of interaction terms ϕ^4, $\phi^6, \ldots$. Varying the action

$S = \int \mathrm{dt} \int \mathrm{dx}\ \mathcal{L}$ with respect to the field gives the equation of motion

$$0 = \frac{\partial^2\phi}{\partial t^2} - \frac{\partial^2\phi}{\partial x^2} + \frac{2\sqrt{2}m^2}{\beta}\sin(\sqrt{2}\beta\phi)\,. \tag{2.1.2}$$

From the Lagrangian, formulae for the energy and momentum can be constructed

$$\begin{aligned} E &= \int_{-\infty}^{\infty} \mathrm{dx}\ \frac{1}{2}\left(\frac{\partial\phi}{\partial t}\right)^2 + \frac{1}{2}\left(\frac{\partial\phi}{\partial x}\right)^2 + \frac{2m^2}{\beta^2}(1-\cos(\sqrt{2}\beta\phi))\,, \\ P &= \int_{-\infty}^{\infty} \mathrm{dx}\ \frac{\partial\phi}{\partial t}\frac{\partial\phi}{\partial x}\,. \end{aligned} \tag{2.1.3}$$

The oscillating nature of the cosine function present in the energy leads to multiple vacuum solutions, namely $\phi = \frac{\sqrt{2}\pi n}{\beta}$, $n \in \mathbb{Z}$, with energy $E = 0$.

2.1.1 Classical integrability

The SG theory is classically integrable. That means that as well as having conserved energy and momentum, there are infinitely many related higher spin charges that are also conserved. The energy and momentum satisfy the condition

$$\frac{\partial\mathcal{E}}{\partial t} - \frac{\partial\mathcal{P}}{\partial x} = 0\,, \tag{2.1.4}$$

where $E = \int dx\ \mathcal{E}$, $P = \int dx\ \mathcal{P}$. Using this condition we show that the energy is conserved

$$\begin{aligned} \frac{\partial E}{\partial t} &= \int_{-\infty}^{\infty} dx\ \frac{\partial\mathcal{E}}{\partial t} = \int_{-\infty}^{\infty} dx\ \frac{\partial\mathcal{P}}{\partial x} \\ &= \Big[\mathcal{P}\Big]_{-\infty}^{\infty} = 0\,. \end{aligned} \tag{2.1.5}$$

Similarly the condition

$$\frac{\partial\mathcal{P}}{\partial t} - \frac{\partial\mathcal{E}^*}{\partial x} = 0\,, \tag{2.1.6}$$

where

$$\mathcal{E}^* = \frac{1}{2}\left(\frac{\partial\phi}{\partial t}\right)^2 + \frac{1}{2}\left(\frac{\partial\phi}{\partial x}\right)^2 - \frac{2m^2}{\beta^2}(1-\cos(\sqrt{2}\beta\phi))\,, \tag{2.1.7}$$

can be used to show that the momentum is conserved. As well as the energy and momentum there are higher spin versions, so called due to the how their light-cone co-ordinate versions transform under a Lorentz boost, which are also conserved.

Scalar field theories, the class of field theories SG and ShG belong to, are described by the Lagrangian

$$\mathcal{L} = \frac{1}{2}\left(\frac{\partial\phi}{\partial t}\right)^2 - \frac{1}{2}\left(\frac{\partial\phi}{\partial x}\right)^2 - V(\phi)\,. \tag{2.1.8}$$

We show that for the next higher spin versions to be conserved there is a restriction on the potential term in the scalar field theory and that the SG theory is one of the allowed theories. For any scalar field theory the next charge related to the energy has the form

$$\begin{aligned}\mathcal{E}_2 &= \frac{\lambda^2}{4}\left((\partial_t\phi)^4 + 6(\partial_t\phi)^2(\partial_x\phi)^2 + (\partial_x\phi)^4\right) + \frac{1}{4}\frac{\partial^2 V}{\partial\phi^2}\left((\partial_t\phi)^2 + (\partial_x\phi)^2\right)\\ &\quad + \frac{1}{4}\left((\partial_{tt}\phi)^2 + 2\,\partial_{tt}\phi\;\partial_{xx}\phi + 4(\partial_{tx}\phi)^2 + (\partial_{xx}\phi)^2\right)\,.\end{aligned} \tag{2.1.9}$$

Similarly the next momentum-like charge is

$$\mathcal{P}_2 = \lambda^2\left(\partial_t\phi\,(\partial_x\phi)^3 + \partial_x\phi\,(\partial_t\phi)^3\right) + \partial_{tx}\phi\,(\partial_{tt}\phi + \partial_{xx}\phi) + \frac{1}{2}\frac{\partial^2 V}{\partial\phi^2}\partial_x\phi\;\partial_t\phi\,. \tag{2.1.10}$$

Using the scalar field theory equation of motion

$$\phi_{tt} - \phi_{xx} + \frac{\partial V}{\partial\phi} = 0\,, \tag{2.1.11}$$

they can be shown to satisfy the conditions

$$\frac{\partial\mathcal{E}_2}{\partial t} - \frac{\partial\mathcal{P}_2^*}{\partial x} = 0\,, \qquad \frac{\partial\mathcal{P}_2}{\partial t} - \frac{\partial\mathcal{E}_2^*}{\partial x} = 0\,, \tag{2.1.12}$$

where

$$\begin{aligned}\mathcal{E}_2^* &= \frac{\lambda^2}{4}\left((\partial_t\phi)^4 + 6(\partial_t\phi)^2(\partial_x\phi)^2 + (\partial_x\phi)^4\right) - \frac{1}{4}\frac{\partial^2 V}{\partial\phi^2}\left((\partial_t\phi)^2 + (\partial_x\phi)^2\right)\\ &\quad + \frac{1}{4}\left((\partial_{tt}\phi)^2 + 2\,\partial_{tt}\phi\;\partial_{xx}\phi + 4(\partial_{tx}\phi)^2 + (\partial_{xx}\phi)^2\right)\,,\\ \mathcal{P}_2^* &= \lambda^2\left(\partial_t\phi\,(\partial_x\phi)^3 + \partial_x\phi\,(\partial_t\phi)^3\right) + \partial_{tx}\phi\,(\partial_{tt}\phi + \partial_{xx}\phi) - \frac{1}{2}\frac{\partial^2 V}{\partial\phi^2}\partial_x\phi\;\partial_t\phi\,,\end{aligned} \tag{2.1.13}$$

if the potential is such that

$$\frac{\partial^3 V}{\partial\phi^3} = 4\lambda^2\frac{\partial V}{\partial\phi}\,. \tag{2.1.14}$$

As before for the energy the conditions (2.1.12) are used to show that $E_2 = \int dx\;\mathcal{E}_2$ and $P_2 = \int dx\;\mathcal{P}_2$ are conserved. We note that the starred quantities are not

conserved. The condition (2.1.14) shows that there are only certain scalar field theories for which the higher spin energy and momentum are conserved. SG is one of the few theories with [4]

$$\lambda^2 = -\frac{\beta^2}{2}, \quad V(\phi) = \frac{2m^2}{\beta^2}\left(1 - \cos(\sqrt{2}\beta\phi)\right). \tag{2.1.15}$$

There are infinite more quantities like the ones displayed above involving higher derivative terms, it is the conservation of all these charges that make the SG theory integrable and give it many of its remarkable properties.

2.1.2 SG soliton solutions

Rewriting the energy formula (2.1.3) as a sum of squares we generate a Bogomolny bound on the energy of the field configurations

$$\begin{aligned} E &= \int_{-\infty}^{\infty} \mathrm{dx}\, \frac{1}{2}\left(\frac{\partial\phi}{\partial t}\right)^2 + \frac{1}{2}\left(\frac{\partial\phi}{\partial x} - \frac{2\sqrt{2}m}{\beta}\sin\left(\frac{\beta\phi}{\sqrt{2}}\right)\right)^2 - \frac{\partial}{\partial x}\left(\frac{4m}{\beta^2}\cos\left(\frac{\beta\phi}{\sqrt{2}}\right)\right) \\ &\geq -\left[\frac{4m}{\beta^2}\cos\left(\frac{\beta\phi}{\sqrt{2}}\right)\right]_{-\infty}^{\infty}. \end{aligned} \tag{2.1.16}$$

The bound is satisfied when the squares are identically zero, explicitly when

$$\phi_t = 0, \quad \phi_x = \frac{2\sqrt{2}m}{\beta}\sin\left(\frac{\beta\phi}{\sqrt{2}}\right), \tag{2.1.17}$$

which are solved by the stationary solution

$$\phi_{kink} = \frac{2\sqrt{2}}{\beta}\arctan(e^{2m(x-c)}), \tag{2.1.18}$$

with energy $E = \frac{8m}{\beta^2}$ and momentum $P = 0$. This solution is the famous sine-Gordon kink solution connecting two of the vacua with $\phi \to \frac{\sqrt{2}\pi}{\beta}$ as $x \to \infty$ and $\phi \to 0$ at $x \to -\infty$. This kink solution has topological charge $+1$ which is defined by $Q_{top} = \frac{\beta}{\sqrt{2}\pi}[\phi]_{x=-\infty}^{\infty}$. There is another solution

$$\phi_{anti-kink} = \frac{2\sqrt{2}}{\beta}\arctan(e^{-2m(x-c)}), \tag{2.1.19}$$

the anti-kink solution with the same energy and topological charge -1. In figure 2.1 we illustrate both the kink and anti-kink solutions. These soliton solutions can be Lorentz boosted so that they are moving with rapidity θ. The kink solution becomes

$$\phi = \frac{2\sqrt{2}}{\beta}\arctan(e^{2m(\cosh(\theta)(x-c)-\sinh(\theta)t)}), \tag{2.1.20}$$

with the increased energy $E = \frac{8m}{\beta^2}\cosh(\theta)$ and momentum $P = -\frac{8m}{\beta^2}\sinh(\theta)$.

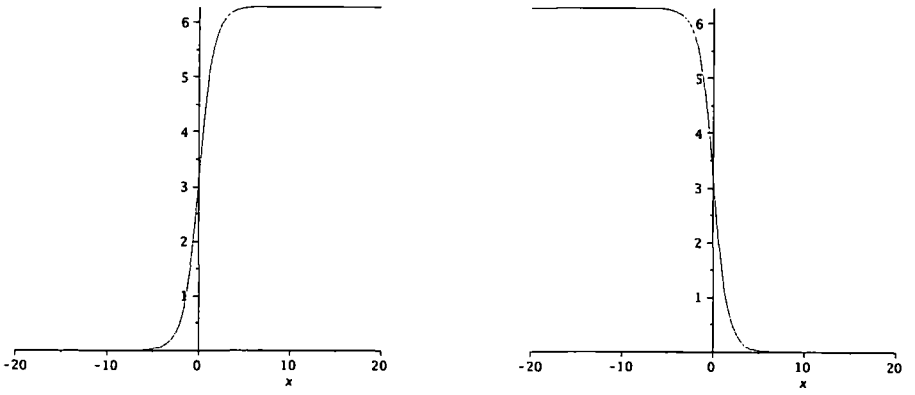

(a) (b)

Fig. 2.1: Sine-Gordon (a) kink and (b) anti-kink solution.

2.1.3 Bäcklund transformation

In SG theory there exists Bäcklund transformation (BT)

$$\begin{aligned} \partial_+(\phi+\psi) &= \frac{2m}{\beta}e^{-x}\sin\left(\frac{\beta(\phi-\psi)}{\sqrt{2}}\right), \\ \partial_-(\phi-\psi) &= -\frac{2m}{\beta}e^{x}\sin\left(\frac{\beta(\phi+\psi)}{\sqrt{2}}\right), \end{aligned} \tag{2.1.21}$$

a pair of coupled first order differential equations in the fields ϕ and ψ. Written here in light-cone co-ordinates where $\partial_+ = \frac{1}{\sqrt{2}}(\partial_t + \partial_x)$, $\partial_- = \frac{1}{\sqrt{2}}(\partial_t - \partial_x)$. In these co-ordinates the SG equation becomes

$$\partial_+\partial_-\phi + \frac{\sqrt{2}m^2}{\beta}\sin(\sqrt{2}\beta\phi) = 0\,. \tag{2.1.22}$$

These BT (2.1.21) imply that both the fields satisfy the SG equation, this can be explicitly seen, first we cross-differentiate the BT

$$\begin{aligned} \partial_-\partial_+(\phi+\psi) &= \sqrt{2}me^{-x}\,\partial_-(\phi-\psi)\cos\left(\frac{\beta(\phi-\psi)}{\sqrt{2}}\right), \\ \partial_+\partial_-(\phi-\psi) &= -\sqrt{2}me^{x}\,\partial_+(\phi+\psi)\cos\left(\frac{\beta(\phi+\psi)}{\sqrt{2}}\right). \end{aligned} \tag{2.1.23}$$

We remove the first order derivative terms in these resultant equations by again using the BT

$$\begin{aligned} \partial_-\partial_+(\phi+\psi) &= -\frac{2\sqrt{2}m^2}{\beta}\cos\left(\frac{\beta(\phi-\psi)}{\sqrt{2}}\right)\sin\left(\frac{\beta(\phi+\psi)}{\sqrt{2}}\right), \\ \partial_+\partial_-(\phi-\psi) &= -\frac{2\sqrt{2}m^2}{\beta}\cos\left(\frac{\beta(\phi+\psi)}{\sqrt{2}}\right)\sin\left(\frac{\beta(\phi-\psi)}{\sqrt{2}}\right). \end{aligned} \tag{2.1.24}$$

Adding these equations together and expanding the cosine and sine functions and using the double angle formula for sine gives the familiar SG equation in ϕ, while subtracting one equation from the other and performing similar manipulation gives the SG equation in ψ. This property that there exists coupled first order equations that imply the equation of motions makes these BT a remarkable pair of equations and very useful for finding solitonic solutions to the SG equation. In fact starting with the vacuum solution $\phi = 0$ means that ψ satisfies the simplified BT

$$\begin{aligned} \partial_t \psi &= \frac{\sqrt{2}m}{\beta}\left(e^{-\chi} - e^{\chi}\right) \sin\left(\frac{\psi\beta}{\sqrt{2}}\right), \\ \partial_x \psi &= \frac{\sqrt{2}m}{\beta}\left(e^{-\chi} + e^{\chi}\right) \sin\left(\frac{\psi\beta}{\sqrt{2}}\right). \end{aligned} \tag{2.1.25}$$

It can be checked that these equations are satisfied by the kink solution (2.1.20) with $\theta = \chi$. The BT have therefore allowed a one-soliton solution to be produced from the vacuum with the rapidity of the soliton governed by the parameter that appears in the BT. This is a general property of BT and as we shall now show provides a way to generate multi-soliton solutions algebraically via Bianchi's Theorem of Permutability [12].

2.1.4 Theorem of Permutability

The Theorem of Permutability (ToP) [13] states that the process using BT to generate higher soliton solutions is commutative. With the original theory proved for the SG theory, where the proof involves computing the two-soliton solution and then shows that it is indeed a solution to the equation of motion. This allows a two-soliton solution to be formulated by solving no further differential equations and only algebraic ones. The diagram in figure 2.2 shows schematically the process used to generate a two-soliton solution ϕ_{12}. The two-soliton solution generated by the two routes can be made identical by the free choices on the constants of integration which are generated when solving the first order BT.

The result of the ToP is that the same two-soliton solution is generated if either route on the diagram is used. Explicitly, if first a one-soliton is made from the vacuum using the BT with parameter e^{θ_1} and then this soliton is used as the input to the BT with parameter e^{θ_2} or if the BTs are used with their parameters reversed,

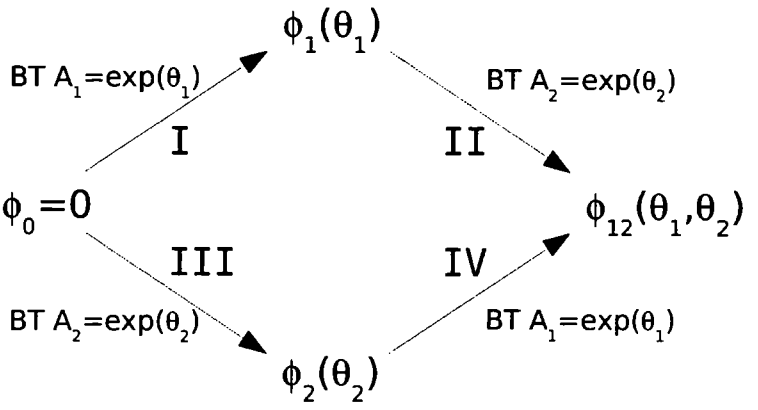

Fig. 2.2: Theorem of Permutability used to generate a two-soliton solution. The theorem states that the order in which BT are applied to generate multi-soliton solutions is commutative. So either route on the diagram (from left to right) results in the same two-soliton solution.

i.e. a one-soliton is generated with parameter e^{θ_2} and then e^{θ_1} is used, then the same two-soliton solution is produced. In practice that gives eight equations, two for each BT on all four legs of the ToP diamond, but in fact only four of these equations are needed, one from each leg of the diamond. These four equations link the vacuum solution $\phi_0 = 0$, the two one-soliton solutions $\phi_i = \phi_i(\theta_i)$ and the two-soliton solution ϕ_{12}

$$\begin{aligned}
\partial_+(\phi_0+\phi_1) &= \frac{2m}{\beta}e^{-\theta_1}\sin\left(\frac{\beta(\phi_0-\phi_1)}{\sqrt{2}}\right), \\
\partial_+(\phi_0+\phi_2) &= \frac{2m}{\beta}e^{-\theta_2}\sin\left(\frac{\beta(\phi_0-\phi_2)}{\sqrt{2}}\right), \\
\partial_+(\phi_1+\phi_{12}) &= \frac{2m}{\beta}e^{-\theta_2}\sin\left(\frac{\beta(\phi_1-\phi_{12})}{\sqrt{2}}\right), \\
\partial_+(\phi_2+\phi_{12}) &= \frac{2m}{\beta}e^{-\theta_1}\sin\left(\frac{\beta(\phi_2-\phi_{12})}{\sqrt{2}}\right). \qquad (2.1.26)
\end{aligned}$$

The idea is to combine these four equations to produce the form of the two-soliton solution. We simplify by eliminating the derivatives of the one-solitons by subtract-

ing the first equation from the third and the second from the fourth

$$\begin{aligned}\partial_+(\phi_{12}+\phi_0) &= \frac{2m}{\beta}\left(e^{-\theta_2}\sin\left(\frac{\beta(\phi_1-\phi_{12})}{\sqrt{2}}\right)-e^{-\theta_1}\sin\left(\frac{\beta(\phi_0-\phi_1)}{\sqrt{2}}\right)\right),\\ \partial_+(\phi_{12}+\phi_0) &= \frac{2m}{\beta}\left(e^{-\theta_1}\sin\left(\frac{\beta(\phi_2-\phi_{12})}{\sqrt{2}}\right)-e^{-\theta_2}\sin\left(\frac{\beta(\phi_0-\phi_2)}{\sqrt{2}}\right)\right).\end{aligned} \tag{2.1.27}$$

As the left hand sides of both equations are the same derivative term, we are able to eliminate all the derivatives to give a sole algebraic equation. After simplifying the trigonometric functions this becomes

$$\tan\left(\frac{\beta}{2\sqrt{2}}\phi_{12}-\phi_0\right)=\left(\frac{e^{\theta_1}+e^{\theta_2}}{e^{\theta_1}-e^{\theta_2}}\right)\tan\left(\frac{\beta}{2\sqrt{2}}\left(\phi_1-\phi_2\right)\right). \tag{2.1.28}$$

We rearrange this to give a formula for the two-soliton solution in terms of the two BT parameters and the constituent one-soliton solutions

$$\phi_{12}=\frac{2\sqrt{2}}{\beta}\arctan\left(\frac{1}{\mu}\tan\left(\frac{\beta}{2\sqrt{2}}\left(\phi_1-\phi_2\right)\right)\right), \tag{2.1.29}$$

where $\mu=\tanh(\frac{\theta_1-\theta_2}{2})$. In a similar way to this construction of the two-soliton solution another BT can be added to the ToP to construct a three-soliton solution and similarly for higher soliton solutions.

2.1.5 Soliton-soliton scattering

The two-soliton solution models the elastic scattering of two SG soliton solutions, one moving with rapidity θ_1 and the other with θ_2. We can re-express the one and two soliton solutions, the one-soliton as

$$e^{\frac{i\beta}{\sqrt{2}}\phi_1}=\frac{1+ie^{\xi}}{1-ie^{\xi}}, \tag{2.1.30}$$

where $\xi=2m(\cosh(\theta)x-\sinh(\theta)t)$ and the two-soliton solution in the form

$$e^{\frac{i\beta}{\sqrt{2}}\phi_{12}}=\frac{1+\frac{i}{\mu}(e^{\xi_1}-e^{\xi_2})+e^{\xi_1+\xi_2}}{1-\frac{i}{\mu}(e^{\xi_1}-e^{\xi_2})+e^{\xi_1+\xi_2}}. \tag{2.1.31}$$

The scattering process of two SG solitons described by the two-soliton solution is shown in figure 2.3. It shows the world lines of two solitons with positive rapidity coming together, experience a non-zero time interaction before continuing through

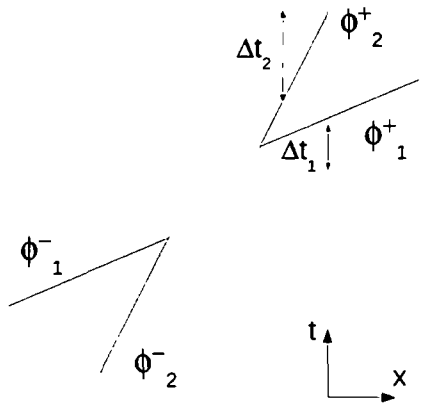

Fig. 2.3: World lines of solitons involved in soliton-soliton scattering illustrating the time-delay Δt_1 and time-advance Δt_2 experienced by the solitons.

each other at the same rapidities as before the scattering. To analyse the properties of the scattering we need to examine the solution around the constituent one-solitons at the temporal infinities. For example to examine the solution around the faster soliton ϕ_1 (setting $\theta_1 > \theta_2$ without loss of generality) as $t \to -\infty$, we constrain x and t by setting

$$x = \tanh(\theta_1)\, t + x' , \tag{2.1.32}$$

which sends

$$\xi_1 = 2m\, \cosh(\theta_1) x' \tag{2.1.33}$$

and

$$\xi_2 = 2m \left(\frac{\sinh(\theta_1 - \theta_2)}{\cosh(\theta_1)}\, t - \cosh(\theta_2)\, (x' - d) \right) \quad \to \quad -\infty , \tag{2.1.34}$$

collapsing the two-soliton solution to

$$e^{\frac{i\beta}{\sqrt{2}}\phi_1^-} = e^{\frac{i\beta}{\sqrt{2}}\phi_{12}} \to \frac{1 + \frac{i}{\mu} e^{\xi_1}}{1 - \frac{i}{\mu} e^{\xi_1}} . \tag{2.1.35}$$

In ϕ_1^-, the subscript and superscript denotes that we are examining soliton ϕ_1 in the far past. Similarly in the other temporal limits the two-soliton solution reduces to

$$e^{\frac{i\beta}{\sqrt{2}}\phi_1^+} = -\frac{1 + i\mu e^{\xi_1}}{1 - i\mu e^{\xi_1}} , \qquad e^{\frac{i\beta}{\sqrt{2}}\phi_2^-} = -\frac{1 - i\mu e^{\xi_2}}{1 + i\mu e^{\xi_2}} , \qquad e^{\frac{i\beta}{\sqrt{2}}\phi_2^+} = \frac{1 - \frac{i}{\mu} e^{\xi_2}}{1 + \frac{i}{\mu} e^{\xi_2}} . \tag{2.1.36}$$

As expected in these limits the two-soliton solution reduces to the form of a one-soliton solution, with additional multiplicative factors. We note that by choosing the constituent solitons to have the form of a kink solution, the scattering process described is actually kink-anti-kink scattering. When we examine around solution ϕ_1 the two-soliton solution results in a kink solution, while when we examine around ϕ_2 it reduces to an anti-kink solution. We re-express these factors as time-delays and phase shifts

$$\Delta t_1 = \frac{\ln(\mu)}{m\,\sinh(\theta_1)}\,, \qquad \Delta t_2 = -\frac{\ln(\mu)}{m\,\sinh(\theta_2)}\,, \qquad e^{i\psi_1} = e^{i\psi_2} = -1\,, \tag{2.1.37}$$

experienced by the two solitons during the scattering process. An example of this kink-anti-kink scattering is illustrated in figure 2.4, the time-delays experienced are not easy to gather from the figures but it does show the elastic nature of soliton-soliton scattering.

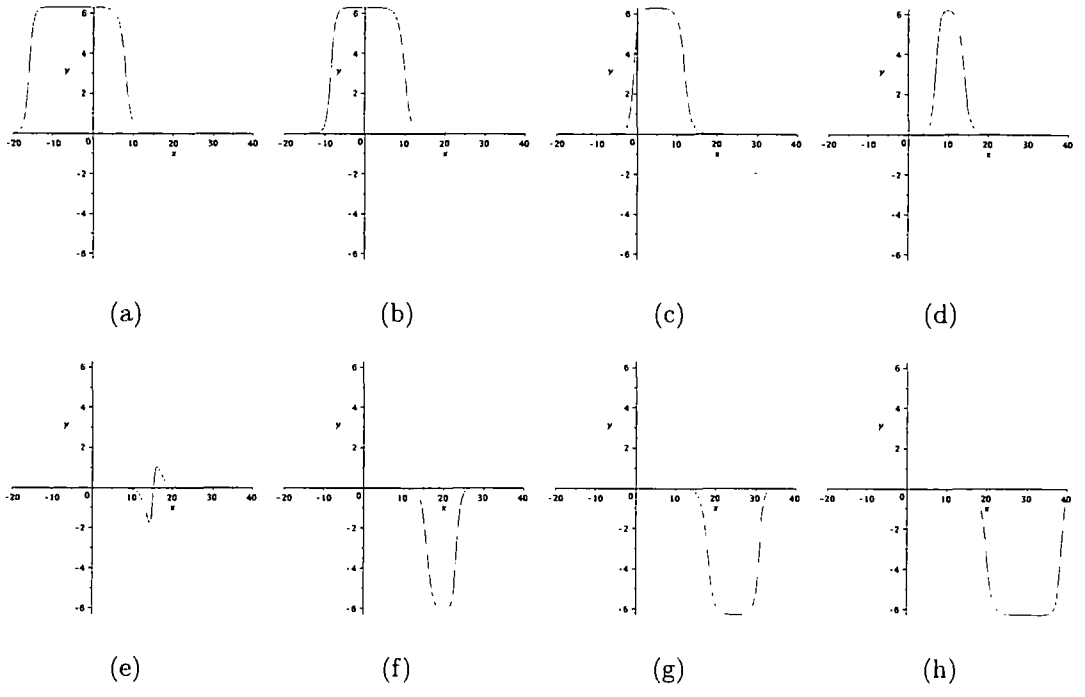

Fig. 2.4: SG kink and anti-kink scattering, with parameters set $m = \frac{1}{2}$, $\beta = \frac{1}{\sqrt{2}}$, $\theta_1 = 1$, $\theta_2 = 0.2$, $c = -4$, $d = 10$ with the time evolving from t= (a) -15, (b)-5, (c)5, (d)15, (e)25, (f)35, (g)45, (h)55.

The two-soliton solution describes kink-kink scattering if we make the constituent ϕ_2 soliton an anti-kink, by the transformation $\xi_2 \longrightarrow -\xi_2$. In this case the temporal

limits of the solution become

$$e^{\frac{i\beta}{\sqrt{2}}\phi_1^-} = -\frac{1+i\mu e^{\xi_1}}{1-i\mu e^{\xi_1}}, \qquad e^{\frac{i\beta}{\sqrt{2}}\phi_1^+} = \frac{1+\frac{i}{\mu}e^{\xi_1}}{1-\frac{i}{\mu}e^{\xi_1}},$$

$$e^{\frac{i\beta}{\sqrt{2}}\phi_2^-} = \frac{1+\frac{i}{\mu}e^{\xi_2}}{1-\frac{i}{\mu}e^{\xi_2}}, \qquad e^{\frac{i\beta}{\sqrt{2}}\phi_2^+} = -\frac{1+i\mu e^{\xi_2}}{1-i\mu e^{\xi_2}}. \tag{2.1.38}$$

Figure 2.5 illustrates this kink-kink scattering process. The two solitons connect adjacent vacua, initially the faster soliton -2π to 0 and the slower soliton 0 to 2π. After the scattering the kink solutions remain unchanged but the faster soliton now connects the vacua 0 to 2π.

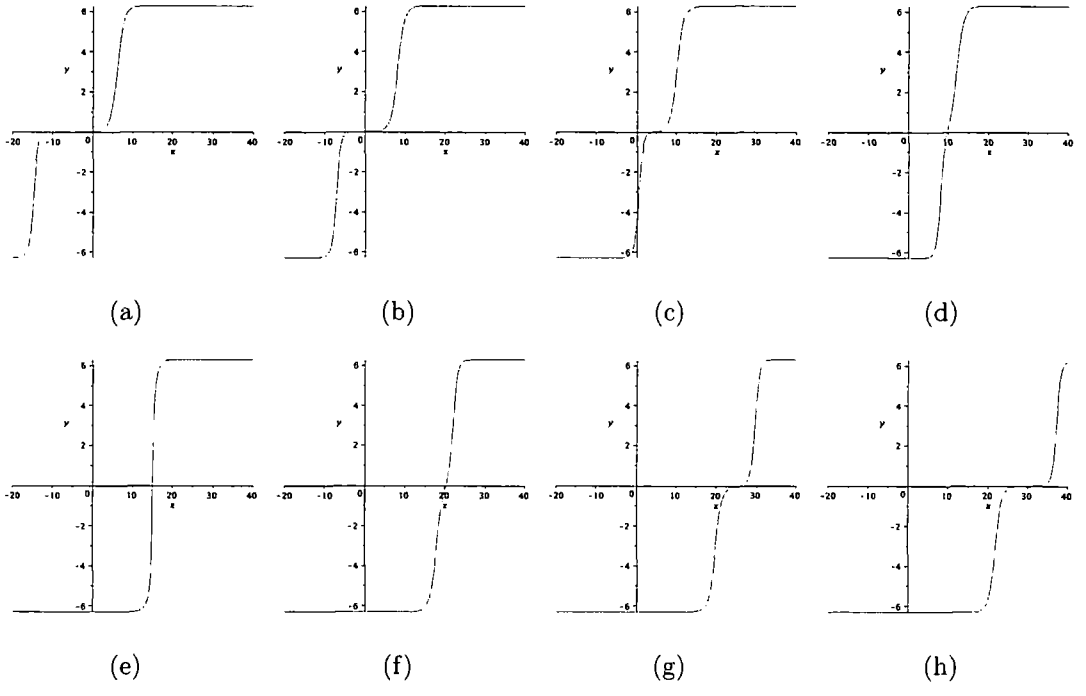

Fig. 2.5: SG kink and kink scattering, with parameters set $m = \frac{1}{2}$, $\beta = \frac{1}{\sqrt{2}}$, $\theta_1 = 1$, $\theta_2 = 0.2$, $c = -4$, $d = 10$ with the time evolving from t= (a)−15, (b)−5, (c)5, (d)15, (e)25, (f)35, (g)45, (h)55.

2.1.6 Breather solution

The two-soliton solution can demonstrate quite different behaviour to the soliton-soliton scattering described above. By setting the constituent solitons rapidities very carefully the two-soliton solution can be transformed into a breather solution.

If we set the rapidities of the two constituent solitons to be the complex conjugate of each other $\theta_1 = \psi + i\theta$, $\theta_2 = \psi - i\theta$, then the two-soliton solution becomes a solution that breathes. Unlike in the scattering processes where the constituent solitons start and finish infinitely separated, in the breather solution the solitons remain finitely separated for all time. The breather solution is a bound state of two solitons and appears as such in the quantum S-matrix.

Figure 2.6 illustrates the nature of a breather solution. It shows a stationary breather soliton ($\psi = 0$) composed of a kink and anti-kink solution. The process starts similarly to scattering with the solitons approaching each other (2.6(b) $\rightarrow$ 2.6(c)), they move through each other 2.6(d) and away from each other 2.6(e). Unlike during scattering they do not move away to infinity but slow and change direction to repeat the process in the opposite direction (2.6(f) $\rightarrow$ 2.6(h)), before returning to their starting configuration 2.6(a). This breathing process is periodic and continues forever. The breather solution can be given its own rapidity by setting ψ to be non-zero. This concludes the introduction into the SG theory.

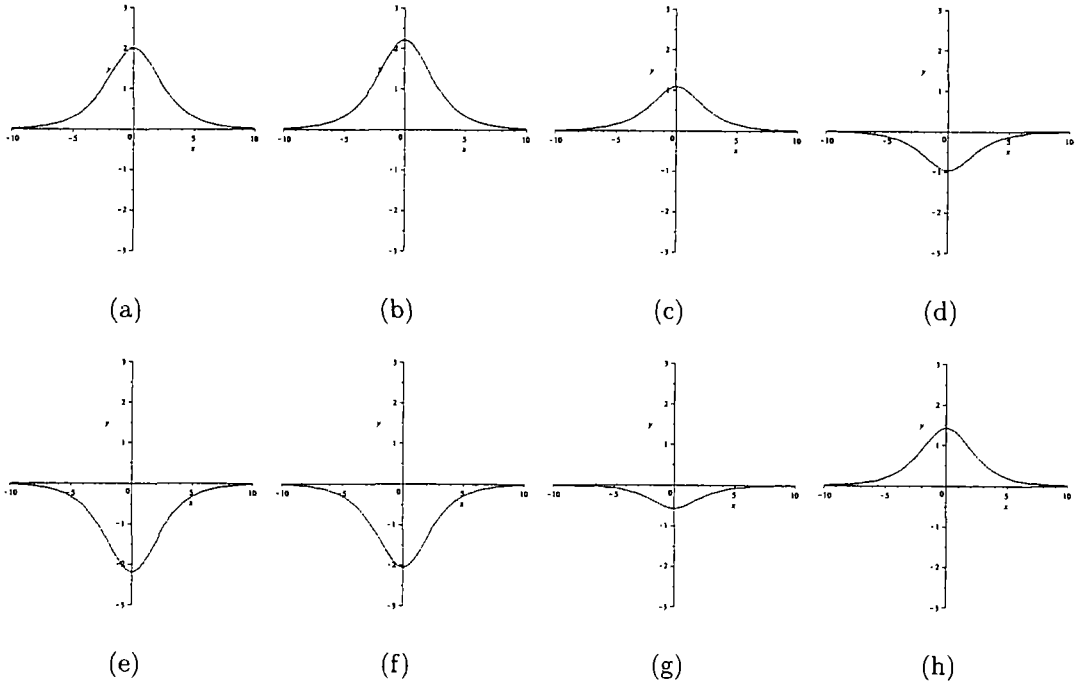

Fig. 2.6: SG two-soliton breather solution, with parameters set $m = \frac{1}{2}$, $\beta = \frac{1}{\sqrt{2}}$, $\theta_1 = i$, $\theta_2 = -i$, $c = 0$, $d = 0$ with the time evolving from t=(a) $t - 10$, (b)-9, (c)-8, (d)-7, (e)-6, (f)-5, (g)-4, (h)-3.

2.2 Sinh-Gordon theory

The sinh-Gordon (ShG) theory is recovered from the SG theory by analytically continuing the coupling constant $\beta \to i\beta$. ShG theory describes a real scalar field in 1+1 D with exponential interaction terms. It is described by the Lagrangian density

$$\mathcal{L}_{ShG} = \frac{1}{2}(\partial_t\phi)^2 - \frac{1}{2}(\partial_x\phi)^2 - \frac{2m^2}{\beta^2}(\cosh(\sqrt{2}\beta\phi) - 1)\,, \tag{2.2.1}$$

when the cosh term is expanded it produces the standard kinetic term then every even point interaction. Again we vary the action in the normal way to produce the ShG equation of motion

$$\partial_{tt}\phi - \partial_{xx}\phi + \frac{\sqrt{8}m^2}{\beta}\sinh(\sqrt{2}\beta\phi) = 0\,. \tag{2.2.2}$$

The formula for the energy

$$E = \int_{-\infty}^{\infty} \mathrm{dx}\ \frac{1}{2}(\partial_t\phi)^2 + \frac{1}{2}(\partial_x\phi)^2 + \frac{2m^2}{\beta^2}(\cosh(\sqrt{2}\beta\phi) - 1) \tag{2.2.3}$$

follows from the Lagrangian. Using the Bogomolny energy bound, as before, gives the form of the solution which in the SG theory would be the static soliton solution, however in the ShG theory this solution does not really exist since it is not a finite energy solution. We remark upon it here as it we use it when we move away from the bulk theory to the defect theory. The static ShG 'soliton' is given by

$$\phi \;=\; \frac{2\sqrt{2}}{\beta}\,\mathrm{arctanh}(e^{2m(x-c)})\,. \tag{2.2.4}$$

Figure 2.7 illustrates the form of the ShG 'soliton' solutions, explicitly showing the field going to infinite ruining the possibility of energy finiteness. Since the spectrum of the bulk theory contains no soliton solution and only the massive scalar field, it is uninteresting to study. In the next chapter we show that adding a boundary or defect to the theory does allow the existence of solitonic objects.

2.3 Summary

This concludes the brief overview of the SG and ShG theories. We have introduced the Lagrangian of both theories and generated the equations of motion. General

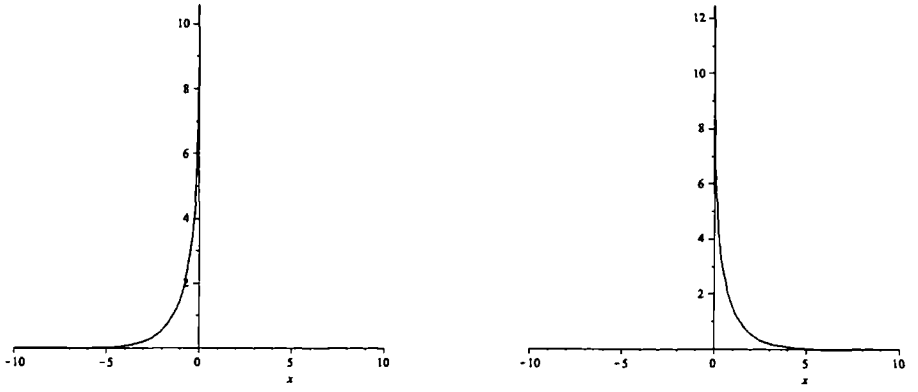

(a) (b)

Fig. 2.7: Sinh-Gordon (a) 'soliton' and (b) anti-'soliton' solution.

techniques to generate solitons solutions were covered, explicitly using the BT and the ToP in the SG theory to give the one and two-soliton solutions. The topological nature of SG solitons and the different processes that the two-soliton solution can model have been shown. In the ShG theory we have seen that no soliton solution exists in the bulk. In the next chapter we use the same two theories to introduce the ideas of adding boundaries and defects into 1+1 D integrable field theories.

Chapter 3

Introducing boundaries and defects

In this chapter we introduce the idea of boundaries and defects in integrable field theories using the sine-Gordon and sinh-Gordon theories. We show that the classical integrability of the bulk theories can be maintained with the introduction of boundaries and defects and comment on the different features and properties of the models. What we learn is used in the analysis of the complex sine-Gordon theory in chapters 5 and 6. The work presented here on the SG theory is a review but the analysis of finite energy field configurations in the ShG defect theory is new research.

The first theory we explore is the SG theory with boundary, this was historically the first 1+1 D integrable field theory to be studied. Ghoshal and Zamolodchikov conjectured [4] the form of the quantum reflection matrix and this work led to various other research into the theory [5, 14, 15]. The next section concentrates on introducing the set up of a boundary theory and shows the construction of the SG boundary theory Lagrangian.

3.1 Sine-Gordon theory with boundary

The motivation to study theories with boundaries has many guises; to help in the understanding of boundary statistical systems near criticality; to get a handle on the boundary interactions in open string theory. However the mathematical ele-

gance that integrability brings to the theories and the presence of non-perturbative effects are motivation enough to make the study into integrable field theories with boundaries both interesting and rewarding.

The general idea for a boundary theory is to restrict the theory to the halfline $x < 0$. In the case of integrable field theories the boundary conditions at $x = 0$ are constructed so that they preserve the integrability of the theory. It is of interest to investigate how solitons interact with the boundary. The set up for the SG boundary theory is illustrated in figure 3.1, with the SG field ϕ restricted to the bulk region $x < 0$ and satisfying to be determined boundary conditions at $x = 0$.

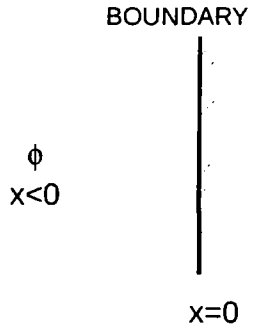

Fig. 3.1: The set up for a theory with boundary.

We show how the boundary Lagrangian is constructed for a general scalar field theory, starting by hypothesising the boundary Lagrangian to have the form

$$L = \int_{-\infty}^{0} dx \, \frac{1}{2}(\partial_t \phi)^2 - \frac{1}{2}(\partial_x \phi)^2 - V(\phi) - \Big[B(\phi)\Big]\Big|_{x=0} , \tag{3.1.1}$$

with the standard Lagrangian restricted to the halfline and a term $B(\phi)$ added at the boundary. The minimal choice for the form of the boundary potential is chosen purely for simplicity, i.e. it is assumed to be only a function of the field and no field derivatives. It is possible to add more complicated boundary terms and in this thesis we describe a way of introducing boundary theories with such terms. Varying

the action $S = \int dt\ L$

$$\begin{aligned}\delta S &= \int_{-\infty}^{\infty} dt \int_{-\infty}^{0} dx \left(\partial_t\phi\,\delta(\partial_t\phi) - \partial_x\phi\,\delta(\partial_x\phi) - \frac{\partial V}{\partial\phi}\delta\phi\right) - \left[\frac{\partial B}{\partial\phi}\delta\phi\right]\Big|_{x=0} \\ &= \int_{-\infty}^{\infty} dt \int_{-\infty}^{0} dx \left(-\partial_{tt}\phi + \partial_{xx}\phi - \frac{\partial V}{\partial\phi}\right)\delta\phi + \left[\left(-\frac{\partial B}{\partial\phi} - \partial_x\phi\right)\delta\phi\right]\Big|_{x=0},\end{aligned} \tag{3.1.2}$$

with respect to the field and field derivatives generates the Euler-Lagrange type equations that the field satisfies. This shows that the scalar field ϕ does indeed satisfy the standard equation of motion in the bulk region $x < 0$

$$\partial_{tt}\phi - \partial_{xx}\phi + \frac{\partial V}{\partial\phi} = 0 \tag{3.1.3}$$

and the boundary condition

$$\partial_x\phi = -\frac{\partial B}{\partial\phi}, \tag{3.1.4}$$

at $x = 0$. The form of the boundary energy

$$E = \int_{-\infty}^{0} dx\ \frac{1}{2}(\partial_t\phi)^2 + \frac{1}{2}(\partial_x\phi)^2 + V(\phi) + \Big[B(\phi)\Big]\Big|_{x=0} \tag{3.1.5}$$

can be read from the Lagrangian and we check that it is conserved $\frac{dE}{dt} = 0$ with no added restriction on $B(\phi)$. Explicitly

$$\begin{aligned}\frac{dE}{dt} &= \int_{-\infty}^{0} dx \left(\partial_t\phi\,\partial_{tt}\phi + \partial_x\phi\,\partial_{xx}\phi + \frac{\partial V}{\partial\phi}\,\partial_t\phi\right) + \left[\frac{\partial B}{\partial\phi}\,\partial_t\phi\right]\Big|_{x=0} \\ &= \int_{-\infty}^{0} dx\ \frac{d}{dx}\left(\partial_x\phi\,\partial_t\phi\right) + \left[\frac{\partial B}{\partial\phi}\,\partial_t\phi\right]\Big|_{x=0} \\ &= \left(\partial_x\phi + \frac{\partial B}{\partial\phi}\right)\partial_t\phi\Big|_{x=0} \\ &= 0.\end{aligned} \tag{3.1.6}$$

As the introduction of the boundary breaks the spatial translational invariance of the theory there is no conserved momentum. Therefore to derive the form of the boundary potential that maintains integrability, we have to consider a higher spin generalisation of the energy. In the bulk this has the form $\mathcal{E}_2$ (2.1.9). For classical integrability to be maintained in the boundary theory this charge with added boundary contribution should be conserved $\frac{dE_2}{dt} = 0$ where

$$E_2 = \int_{-\infty}^{0} dx\ \mathcal{E}_2 + \Big[B_2(\phi)\Big]\Big|_{x=0}. \tag{3.1.7}$$

Explicitly

$$\begin{aligned}\frac{dE_2}{dt} &= \int_{-\infty}^{0} dx\ \frac{d\mathcal{E}_2}{dt} + \left[\frac{d}{dt}B_2(\phi)\right]\Big|_{x=0} \\ &= \left[\mathcal{P}_2^* + \frac{dB_2(\phi)}{dt}\right]\Big|_{x=0},\end{aligned} \tag{3.1.8}$$

with $\mathcal{P}_2^*$ (2.1.13). Using the scalar field theory equation of motion (3.1.3) and boundary condition (3.1.4) along with the bulk constraint on the potential term (2.1.14), we find the form of B_2 to be

$$B_2 = \lambda^2 B\ (\partial_t\phi)^2 + \left(\lambda^2 B\ \left(\frac{\partial B}{\partial\phi}\right)^2 - \frac{2\lambda^4}{3}B^3\right) + \left(\frac{B}{2}\frac{\partial^2 V}{\partial\phi^2} - \frac{\partial B}{\partial\phi}\frac{\partial V}{\partial\phi}\right), \tag{3.1.9}$$

with the constraint on the boundary potential [4]

$$\lambda^2\ B = \frac{\partial^2 B}{\partial\phi^2}. \tag{3.1.10}$$

In the specific case of the SG theory

$$\lambda^2 = -\frac{\beta^2}{2}, \quad V(\phi) = \frac{2m^2}{\beta^2}\left(1 - \cos(\sqrt{2}\beta\phi)\right), \quad B(\phi) = -\frac{4m}{\beta^2}e^{\chi}\cos\left(\frac{\beta}{\sqrt{2}}(\phi - d)\right). \tag{3.1.11}$$

Similar expressions exist for the ShG theory [16, 17]. Therefore it is possible to adapt the bulk energy and next energy-like conserved charge so that they are also conserved in the boundary theory. All the infinitely many higher spin energy-like charges present in the bulk can similarly be adapted and so the boundary theories for both the SG and ShG constructed in this way are classically integrable. Both boundary theories have subsequently been thoroughly analysed. Without presenting any detail, their interesting characteristics include SG solitons being reflected from the boundary and the existence of boundary ShG breather states. The above derivation of the boundary theories provides a sufficient introduction into integrable boundary theories for the work on complex sine-Gordon boundary theory in chapter 6.

3.2 Scalar field theory with defect

The idea of studying an internal boundary or defect in 1+1 D integrable field theories was reintroduced in [8] following an earlier exploration by Delfino et al. [7].

Other early work on the study of impurities and defects include [18,19]. Similar techniques have been used in spin chains [20] and conformal field theories [21], while the connection between defects and boundaries has previously been commented on [22]. We reproduce the method used by Bowcock et al. [8] to derive the defect conditions required to maintain the classical integrability for a scalar field theory.

The defect is introduced as an internal boundary between two separate field theories with defect conditions at $x = 0$ governing any interaction between the fields of the left and right theories. Figure 3.2 shows the defect set up. As in the

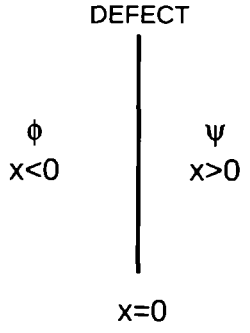

Fig. 3.2: The set up for a theory with defect.

boundary case, the starting point for the construction of an integrable defect theory is to conjecture the form of the Lagrangian

$$\begin{aligned} L &= \int_{-\infty}^{0} dx \ \frac{1}{2}(\partial_t\phi)^2 - \frac{1}{2}(\partial_x\phi)^2 - V_\phi(\phi) + \int_{0}^{\infty} dx \ \frac{1}{2}(\partial_t\psi)^2 - \frac{1}{2}(\partial_x\psi)^2 - V_\psi(\psi) \\ &\quad + \left[\frac{1}{2}(\phi\,\partial_t\psi - \psi\,\partial_t\phi) - D(\phi,\psi)\right]\Big|_{x=0} . \end{aligned} \tag{3.2.1}$$

In this case we have two bulk Lagrangians restricted to their respective bulk regions ($x < 0$ and $x > 0$) where two different fields ϕ, ψ reside and two types of defect term at $x = 0$, a defect potential term which depends on the left and right fields and a term anti-symmetric in the first order time derivatives of the fields. Varying

the action with respect to the field and field derivatives gives

$$\begin{aligned}\delta S &= \int_{-\infty}^{\infty} dt \int_{-\infty}^{0} dx \left(\partial_t\phi\,\delta(\partial_t\phi) - \partial_x\phi\,\delta(\partial_x\phi) - \frac{\partial V_\phi}{\partial\phi}\right) \\ &\quad + \int_{0}^{\infty} dx \left(\partial_t\psi\,\delta(\partial_t\psi) - \partial_x\psi\,\delta(\partial_x\psi) - \frac{\partial V_\psi}{\partial\psi}\right) \\ &\quad + \left(\frac{1}{2}\partial_t\psi - \frac{\partial D}{\partial\phi}\right)\delta\phi - \left(\frac{1}{2}\partial_t\phi + \frac{\partial D}{\partial\psi}\right)\delta\psi + \frac{1}{2}\phi\,\delta(\partial_t\psi) - \frac{1}{2}\psi\,\delta(\partial_t\phi)\Big|_{x=0} .\end{aligned} \tag{3.2.2}$$

As in the boundary calculation we continue by integrating by parts to get

$$\begin{aligned}\delta S &= \int_{-\infty}^{\infty} dt \int_{-\infty}^{0} dx \left(-\partial_{tt}\phi + \partial_{xx}\phi - \frac{\partial V_\phi}{\partial\phi}\right) \\ &\quad + \int_{0}^{\infty} dx \left(-\partial_{tt}\psi + \partial_{xx}\psi - \frac{\partial V_\psi}{\partial\psi}\right) \\ &\quad + \left(\partial_t\psi - \partial_x\phi - \frac{\partial D}{\partial\phi}\right)\delta\phi - \left(\partial_t\phi - \partial_x\psi + \frac{\partial D}{\partial\psi}\right)\delta\psi\Big|_{x=0} ,\end{aligned} \tag{3.2.3}$$

which implies the standard scalar field theory equation of motion (3.1.3) in the bulk regions and the defect conditions

$$\partial_t\psi - \partial_x\phi = \frac{\partial D}{\partial\phi} , \qquad \partial_t\phi - \partial_x\psi = -\frac{\partial D}{\partial\psi} , \tag{3.2.4}$$

which hold on the defect. We notice that the defect conditions are not symmetric in ϕ and ψ and therefore the defect theory is not invariant under a parity transformation. We read the energy straight from the Lagrangian to be

$$\begin{aligned}E &= \int_{-\infty}^{0} dx\ \frac{1}{2}(\partial_t\phi)^2 + \frac{1}{2}(\partial_x\phi)^2 + V_\phi(\phi) \\ &\quad + \int_{0}^{\infty} dx\ \frac{1}{2}(\partial_t\psi)^2 + \frac{1}{2}(\partial_x\psi)^2 + V_\psi(\psi) + \big[D(\phi,\psi)\big]\big|_{x=0} .\end{aligned} \tag{3.2.5}$$

Using the equations of motion and defect conditions we see that it is conserved

$$\begin{aligned}\frac{dE}{dt} &= \int_{-\infty}^{0} dx\ \frac{d}{dx}(\partial_x\phi\,\partial_t\phi) + \int_{0}^{\infty} dx\ \frac{d}{dx}(\partial_x\psi\,\partial_t\psi) + \left(\frac{\partial D}{\partial\phi}\phi_t + \frac{\partial D}{\partial\psi}\psi_t\right)\Big|_{x=0} \\ &= \left[\left(\partial_x\phi + \frac{\partial D}{\partial\phi}\right)\partial_t\phi + \left(-\partial_x\psi + \frac{\partial D}{\partial\psi}\right)\partial_t\psi\right]\Big|_{x=0} \\ &= \partial_t\psi\,\partial_t\phi - \partial_t\phi\,\partial_t\psi \\ &= 0 ,\end{aligned} \tag{3.2.6}$$

without any restriction on $D(\phi,\psi)$. Despite the fact that the defect breaks the translational invariance of the theory, it is possible to add a defect term to the bulk

momentum to make it conserved in the defect theory. The property that the defect conditions hold at all points not just $x = 0$ allows this to be possible [8, 23]. The defect momentum has the form

$$P = \int_{-\infty}^{0} dx \quad \partial_t\phi\,\partial_x\phi + \int_{0}^{\infty} dx \quad \partial_t\psi\,\partial_x\psi + \Big[\mathcal{P}_{def}(\phi,\psi)\Big]\Big|_{x=0}, \tag{3.2.7}$$

where we choose $\mathcal{P}_{def}(\phi,\psi)$ so that the defect momentum is conserved. To explicitly see this we differentiate the momentum with respect to t and use the equations of motion to simplify

$$\begin{aligned}\frac{dP}{dt} = &\int_{-\infty}^{0} dx \quad \frac{d}{dx}\left(\frac{1}{2}(\partial_t\phi)^2 + \frac{1}{2}(\partial_x\phi)^2 - V_\phi(\phi)\right)\\ &+\int_{0}^{\infty} dx \quad \frac{d}{dx}\left(\frac{1}{2}(\partial_t\psi)^2 + \frac{1}{2}(\partial_x\psi)^2 - V_\psi(\psi)\right)\\ &+\frac{\partial P}{\partial\phi}\partial_t\phi + \frac{\partial P}{\partial\psi}\partial_t\psi\Big|_{x=0},\end{aligned} \tag{3.2.8}$$

we continue by integrating the bulk expressions and use the defect conditions to give

$$\begin{aligned}\frac{dP}{dt} = &\,\partial_t\phi\left(\frac{\partial\mathcal{P}_{def}}{\partial\phi} - \frac{\partial D}{\partial\psi}\right) + \partial_t\psi\left(\frac{\partial\mathcal{P}_{def}}{\partial\psi} - \frac{\partial D}{\partial\phi}\right)\\ &+\frac{1}{2}\left(\left(\frac{\partial D}{\partial\phi}\right)^2 - \left(\frac{\partial D}{\partial\psi}\right)^2\right) + V_\psi - V_\phi\,.\end{aligned} \tag{3.2.9}$$

Demanding that the defect momentum is conserved results in the conditions

$$\frac{\partial\mathcal{P}_{def}}{\partial\phi} = \frac{\partial D}{\partial\psi}, \quad \frac{\partial\mathcal{P}_{def}}{\partial\psi} - \frac{\partial D}{\partial\phi}, \quad \frac{1}{2}\left(\left(\frac{\partial D}{\partial\phi}\right)^2 - \left(\frac{\partial D}{\partial\psi}\right)^2\right) = V_\phi - V_\psi\,. \tag{3.2.10}$$

We cross-differentiate the first two conditions to give $\partial_{\phi\phi}D - \partial_{\psi\psi}D = 0$, which is solved by the ansatz $D = f_1(\phi+\psi) + f_2(\phi-\psi)$. Substituting this ansatz into the third condition gives $2f_1'f_2' = V_\phi - V_\psi$, which further implies

$$\frac{f_1'''}{f_1'} = \frac{f_2'''}{f_2'} = \kappa^2, \tag{3.2.11}$$

where $f_1' = \partial_{\phi+\psi}f_1$ and $f_2' = \partial_{\phi-\psi}f_2$. This is solved by

$$\begin{aligned}&\kappa \neq 0 \quad f_1' = \alpha_1 e^{\kappa(\phi+\psi)} + \beta_1 e^{-\kappa(\phi+\psi)}, \quad f_2' = \alpha_2 e^{\kappa(\phi-\psi)} + \beta_2 e^{-\kappa(\phi-\psi)},\\ &\kappa = 0 \quad f_1' = \gamma_1(\phi+\psi), \quad f_2' = \gamma_2(\phi-\psi)\,.\end{aligned} \tag{3.2.12}$$

These solutions cover the whole set of defect conditions that allow the conservation of the defect momentum. We now explore the different possibilities.

3.2.1 Free massive - free massive

First we consider the case when $\kappa = 0$, this forces the bulk potentials to have the form

$$V_\phi = 2\gamma_1\gamma_2\,\phi^2\,, \qquad V_\psi = 2\gamma_1\gamma_2\,\psi^2\,, \tag{3.2.13}$$

which means both bulk theories are free and massive, with the same mass. The defect term and the momentum defect contribution are calculated to be

$$\begin{aligned} D &= (\gamma_1+\gamma_2)\frac{1}{2}\phi^2 + (\gamma_1-\gamma_2)\,\phi\,\psi + (\gamma_1+\gamma_2)\frac{1}{2}\psi^2\,, \\ \mathcal{P}_{def} &= (\gamma_1-\gamma_2)\frac{1}{2}\phi^2 + (\gamma_1+\gamma_2)\,\phi\,\psi + (\gamma_1-\gamma_2)\frac{1}{2}\psi^2\,. \end{aligned} \tag{3.2.14}$$

3.2.2 Free massless / Liouville - free massless / Liouville

The case when $\kappa \neq 0$ is slightly more complicated with the bulk potentials having the form

$$V_\phi = 2\alpha_1\alpha_2 e^{2\kappa\phi} + 2\beta_1\beta_2 e^{-2\kappa\phi}\,, \qquad V_\psi = -2\alpha_1\beta_2 e^{2\kappa\psi} - 2\beta_1\alpha_2 e^{-2\kappa\psi}\,, \tag{3.2.15}$$

which unlike the previous case still leaves a freedom over the bulk theories. Different bulk theories result from different choices of the parameters α_i, β_i. By setting $\alpha_1 = \beta_1 = 0$, both bulk theories are free and massless

$$V_\phi = V_\psi = 0\,, \tag{3.2.16}$$

while if $\alpha_1 = \beta_2 = 0$ then V_ϕ remains zero but

$$V_\phi = 0\,, \quad V_\psi = -2\beta_1\alpha_2 e^{-2\kappa\psi}\,, \tag{3.2.17}$$

which gives a massless free field theory on the left hand side of the defect and Liouville theory on the right. Similarly the reverse set up with Liouville on the left and free massless on the right can be obtained, as can Liouville theory on both sides of the defect, for example by setting $\alpha_1 = 0$.

3.2.3 Sine-Gordon - sine-Gordon

The parameter choice of

$$\alpha_1 = \frac{m}{i\sqrt{2}\beta\delta}\,, \quad \alpha_2 = \frac{m\,\delta}{i\sqrt{2}\beta}\,, \quad \beta_1 = -\frac{m}{i\sqrt{2}\beta\delta}\,, \quad \beta_2 = -\frac{m\,\delta}{i\sqrt{2}\beta}\,, \tag{3.2.18}$$

with $\kappa = \frac{i\beta}{\sqrt{2}}$, gives the sine-Gordon theory on both sides of the defect

$$V_\phi = -\frac{2m^2}{\beta^2}\cos(\sqrt{2}\beta\phi)\,, \quad V_\psi = -\frac{2m^2}{\beta^2}\cos(\sqrt{2}\beta\psi)\,, \tag{3.2.19}$$

with both theories forced to have the same mass and coupling constant. The defect term in the Lagrangian and the term in the momentum become

$$\begin{aligned} D &= -\frac{2m}{\beta^2}\left(\frac{1}{\delta}\cos\left(\frac{\beta}{\sqrt{2}}(\phi+\psi)\right) + \delta\cos\left(\frac{\beta}{\sqrt{2}}(\phi-\psi)\right)\right)\,, \\ \mathcal{P}_{def} &= -\frac{2m}{\beta^2}\left(\frac{1}{\delta}\cos\left(\frac{\beta}{\sqrt{2}}(\phi+\psi)\right) - \delta\cos\left(\frac{\beta}{\sqrt{2}}(\phi-\psi)\right)\right)\,. \end{aligned} \tag{3.2.20}$$

3.2.4 Sinh-Gordon - sinh-Gordon

Similarly the parameter choice of

$$\alpha_1 = -\frac{m}{\sqrt{2}\beta\delta}\,, \quad \alpha_2 = -\frac{m\,\delta}{\sqrt{2}\beta}\,, \quad \beta_1 = \frac{m}{\sqrt{2}\beta\delta}\,, \quad \beta_2 = \frac{m\,\delta}{\sqrt{2}\beta}\,, \tag{3.2.21}$$

with $\kappa = \frac{\beta}{\sqrt{2}}$, gives the sinh-Gordon theory on both sides of the defect

$$V_\phi = \frac{2m^2}{\beta^2}\cosh(\sqrt{2}\beta\phi)\,, \quad V_\psi = \frac{2m^2}{\beta^2}\cosh(\sqrt{2}\beta\psi)\,, \tag{3.2.22}$$

again with the same mass and coupling constant. The defect term in the Lagrangian and the term in the momentum become

$$\begin{aligned} D &= -\frac{2m}{\beta^2}\left(\frac{1}{\delta}\cosh\left(\frac{\beta}{\sqrt{2}}(\phi+\psi)\right) + \delta\cosh\left(\frac{\beta}{\sqrt{2}}(\phi-\psi)\right)\right)\,, \\ \mathcal{P}_{def} &= -\frac{2m}{\beta^2}\left(\frac{1}{\delta}\cosh\left(\frac{\beta}{\sqrt{2}}(\phi+\psi)\right) - \delta\cosh\left(\frac{\beta}{\sqrt{2}}(\phi-\psi)\right)\right)\,. \end{aligned} \tag{3.2.23}$$

This concludes all the scalar field theory choices on either side of the defect for which the defect momentum is conserved. The conservation of momentum is sufficient to fully determine the form of the defect Lagrangian, but as for the bulk and boundary theories the conservation of energy and momentum is not sufficient to claim integrability of the theory. In [8] the next energy-like charge has been shown to be conserved in these theories. In the next section we analyse the properties of the defect SG theory.

3.3 Sine-Gordon theory with defect

In the previous chapter we presented the derivation of the defect SG Lagrangian (3.2.1) where the bulk potentials are the standard (3.2.19) and defect potential (3.2.20) is chosen specifically to ensure the integrability of the theory. The conserved energy has the form (3.2.5) and the conserved momentum (3.2.7) with the momentum defect term (3.2.20) chosen to ensure the defect momentum is conserved.

This Lagrangian means the defect conditions (DC) (3.2.4) take the form

$$\begin{aligned} \partial_t\psi - \partial_x\phi &= \frac{\sqrt{2}m}{\beta\,\delta}\sin\left(\frac{(\phi+\psi)\beta}{\sqrt{2}}\right) + \frac{\sqrt{2}m}{\beta}\delta\sin\left(\frac{(\phi-\psi)\beta}{\sqrt{2}}\right), \\ \partial_t\phi - \partial_x\psi &= -\frac{\sqrt{2}m}{\beta\,\delta}\sin\left(\frac{(\phi+\psi)\beta}{\sqrt{2}}\right) + \frac{\sqrt{2}m}{\beta}\delta\sin\left(\frac{(\phi-\psi)\beta}{\sqrt{2}}\right). \end{aligned} \tag{3.3.1}$$

It is noted by Bowcock et al. [24] that these defect conditions are exactly the SG auto-Bäcklund transformation (2.1.21). As we see later in this thesis, this seems to be a general feature of integrable defect theories and it plays an important role in determining the properties of the defect theory. Using this complete description of the defect SG theory we analyse its properties. The defect SG theory has been thoroughly analysed [24–26] since the construction of the model [8].

3.3.1 Vacuum

The defect vacuum is the trivial $\phi = 0,\ \psi = 0$ when $\delta > 0$, with energy and momentum

$$E = -\frac{2m}{\beta^2}\left(\delta + \frac{1}{\delta}\right), \qquad P = \frac{2m}{\beta^2}\left(\delta - \frac{1}{\delta}\right). \tag{3.3.2}$$

There is another trivial solution $\phi = 0,\ \psi = \frac{\sqrt{2}\pi}{\beta}$ to the defect conditions which due to the half angles that appear in the defect term has different energy and momentum

$$E = \frac{2m}{\beta^2}\left(\delta + \frac{1}{\delta}\right), \qquad P = -\frac{2m}{\beta^2}\left(\delta - \frac{1}{\delta}\right). \tag{3.3.3}$$

These two field configurations are shown in figure 3.3, with figure 3.3(a) showing the zero topological vacuum and figure 3.3(b) showing the defect with topological charge $Q = +1$. The topologically charged defect has positive energy if $\delta > 0$ and is called an excited defect, while the defect vacuum has negative energy and is called

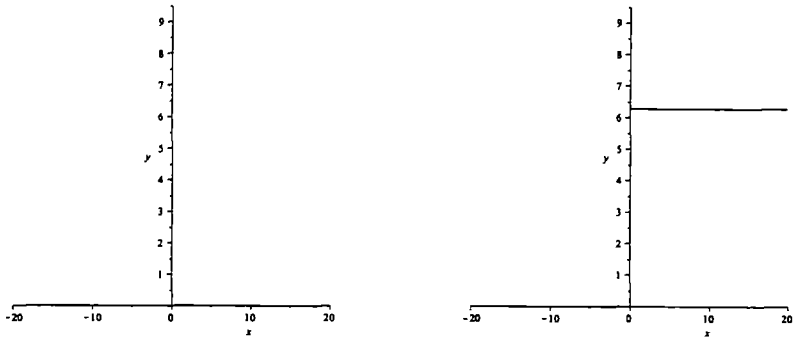

(a) (b)

Fig. 3.3: (a) Unexcited defect and (b) excited defect when $\delta > 0$.

an unexcited defect, the opposite is true for $\delta < 0$. The reason for these labels will become clear when we examine the interaction between solitons and defects and discover that the sign of the energy and the momentum determines how they interact.

3.3.2 Soliton absorption and emission

The realisation that the defect conditions and Bäcklund transformation are one and the same thing prompts the idea that solitons can be absorbed and emitted by the the defect. Since BT allow the construction of higher soliton solutions and specifically from the vacuum a one-soliton solution can be produced. This suggests that the defect conditions should be satisfied by the vacuum on one side of the defect and a one-soliton solution on the other.

First we solve the defect conditions with a one-soliton solution

$$\phi = \frac{2\sqrt{2}}{\beta}\arctan(e^{2m(\cosh(\theta)\,x-\sinh(\theta)\,t)}), \tag{3.3.4}$$

on the left hand side of the defect and the vacuum $\psi = 0$ on the right hand side. Substituting the above values for the fields into the DC, we find that the condition $\delta = -e^{\theta}$ is required for the DC to be satisfied. By assuming that the one-soliton solution describes a right-moving kink solution $\theta > 0$ then this set up describes a kink being absorbed by a defect with parameter $\delta < -1$. Figure 3.4 illustrates this scenario with time progressing from $t \to -\infty$ in figure 3.4(a) through to $t \to +\infty$ in figure 3.4(d).

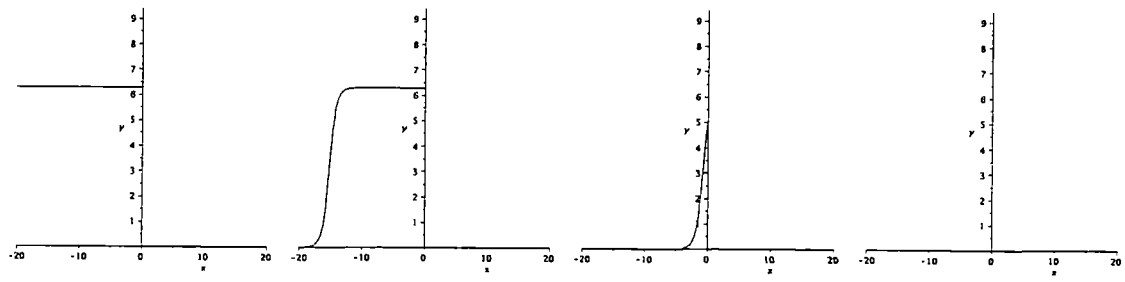

(a) (b) (c) (d)

Fig. 3.4: SG kink absorbed by a defect, with time progressing from (a) to (d).

Similarly for the set up of a right-moving anti-kink solution on the left

$$\phi = \frac{2\sqrt{2}}{\beta}\arctan(e^{-2m(\cosh(\theta)\,x-\sinh(\theta)\,t)}) \tag{3.3.5}$$

and $\psi = 0$ on the right hand side, the defect conditions are satisfied when $\delta = e^{\theta}$. This describes a defect with parameter $\delta > 1$ absorbing a right-moving anti-kink. Figure 3.5 illustrates this scenario with time progressing from $t \to -\infty$ in figure 3.5(a) through to $t \to +\infty$ in figure 3.5(d).

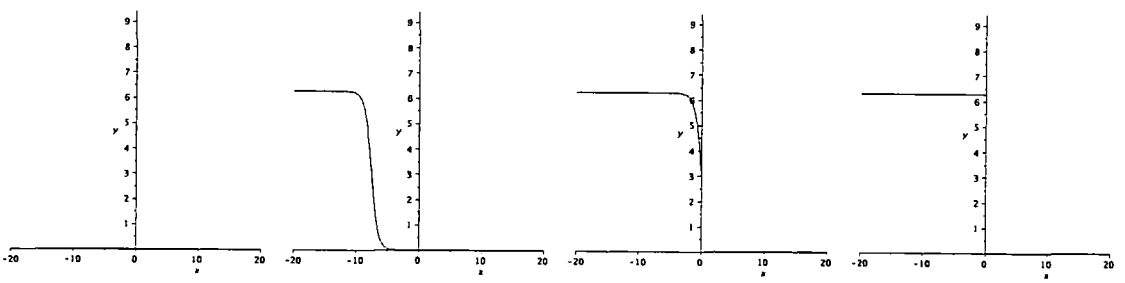

(a) (b) (c) (d)

Fig. 3.5: SG anti-kink absorbed by a defect, with time progressing from (a) to (d).

In both of these absorption processes the energy of the original defect configuration is negative and the momentum positive. This has to be the case for the defect to be able to absorb a right-moving soliton which has positive energy and negative momentum. The absorption leaves the final defect configuration with positive energy and negative momentum. In fact the energy of the soliton is twice the energy of the final defect state when the parameters are matched as to allow absorption, so the final energy is the equal and opposite of the initial energy. The conservation of

the total energy is schematically shown

$$E^{total}_{before} = E_{sol} + E^{def}_{before} = 2E - E = E = E^{def}_{after} = E^{total}_{after}. \tag{3.3.6}$$

We have described that an unexcited defect can absorb a soliton and become excited, the reverse process is also possible with an excited defect decaying to an unexcited one by emitting a soliton. The defect conditions are satisfied by a right-moving kink solution on the right hand side of the defect and $\phi = 0$ on the left with the condition $\delta = e^{\theta}$. So a defect with topological charge $+1$ described by parameter $\delta > 1$ can decay to a defect with no topological charge. Figure 3.6 illustrates this process with the initial defect shown in figure 3.6(a) and time evolving through the diagrams to the right with the figure 3.6(d) showing the final defect state.

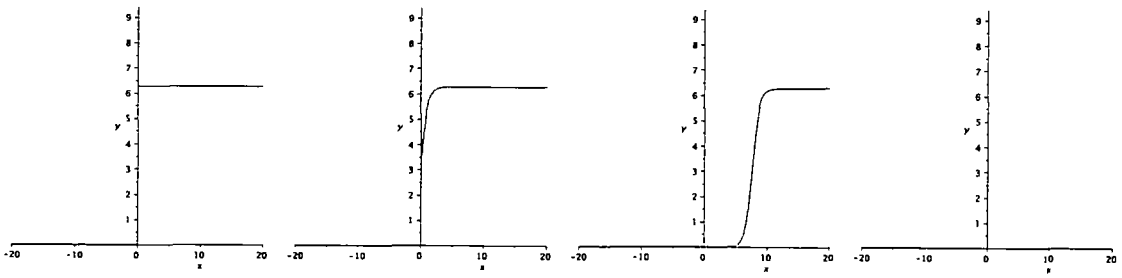

(a) (b) (c) (d)

Fig. 3.6: SG kink emitted by a defect, with time progressing from (a) to (d).

As expected a defect can also emit an anti-kink, in fact a defect with zero topological charge can decay into a defect with topological charge $+1$ by emitting an anti-kink (topological charge -1). The defect conditions are satisfied when $\delta = -e^{\theta}$ with a right moving anti-kink solution on the right of the defect and $\phi = 0$ on the left. Figure 3.7 shows this process where time flows from figure 3.7(a) to figure 3.7(d).

In all four examples illustrated the $\phi = 0$ or $\psi = 0$ solution has been taken opposite the one-soliton solution, but $\phi = \frac{\sqrt{2}\pi}{\beta}$ or $\psi = \frac{\sqrt{2}\pi}{\beta}$ also satisfies the SG equation. Therefore we can also analyse absorption and emission processes with these values. Figure 3.8 shows a SG kink being absorbed by a defect with $\delta > 1$ and zero topological charge. This scenario of ϕ being a right-moving kink solution and $\psi = \frac{\sqrt{2}\pi}{\beta}$ satisfies the defect conditions when $\delta = e^{\theta}$. Analysing the energies more

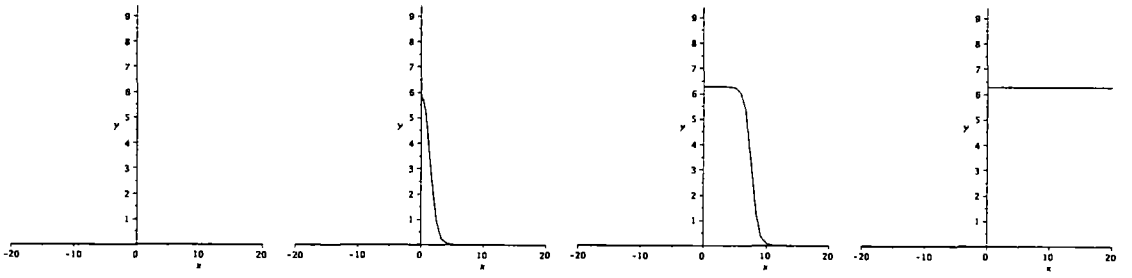

(a) (b) (c) (d)

Fig. 3.7: SG anti-kink emitted by a defect, with time progressing from (a) to (d).

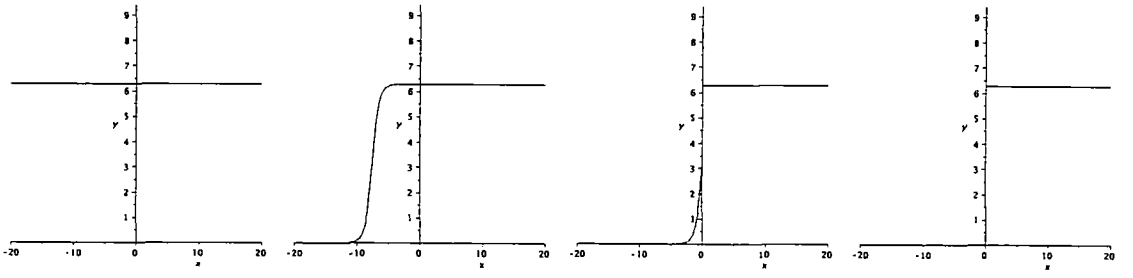

(a) (b) (c) (d)

Fig. 3.8: SG kink absorbed by a zero topological charge defect, with time progressing from (a) to (d).

explicitly, the initial defect state (figure 3.8(a)) has energy and momentum

$$E = -\frac{2m}{\beta^2}\left(\delta + \frac{1}{\delta}\right) < 0\,, \qquad P = \frac{2m}{\beta^2}\left(\delta - \frac{1}{\delta}\right) > 0 \tag{3.3.7}$$

and the final defect state (figure 3.8(d)) has energy and momentum

$$E = \frac{2m}{\beta^2}\left(\delta + \frac{1}{\delta}\right) > 0\,, \qquad P = -\frac{2m}{\beta^2}\left(\delta - \frac{1}{\delta}\right) < 0\,, \tag{3.3.8}$$

which fits consistently with energy and momentum conservation since the SG kink that is absorbed has energy and momentum

$$E_{sol} = \frac{8m}{\beta^2}\cosh(\theta)\,, \qquad P_{sol} = -\frac{8m}{\beta^2}\sinh(\theta)\,. \tag{3.3.9}$$

Topological charge is also conserved, initially the defect has charge zero and the incoming soliton has charge $Q = +1$ and the final defect state has topological charge $Q = +1$.

3.3.3 Soliton - defect scattering

In the previous section we showed that solitons with specific rapidity can be absorbed or emitted by a defect, but what happens to solitons travelling at a rapidity other than this specific rapidity? These solitons scatter through the defect and by analysing a one-soliton solution on each side of the defect we can find the relationship between the incoming and outgoing soliton.

For a right-moving kink solution on each side of the defect with the same rapidity $\theta > 0$, which is necessary for any chance of energy and momentum to be conserved, with the position of the left kink shifted by $x \to x - c$ and the right kink's position by $x \to x - d$

$$\phi = \frac{2\sqrt{2}}{\beta}\arctan(e^{2m(\cosh(\theta)(x-c)-\sinh(\theta)\,t)}), \quad \psi = \frac{2\sqrt{2}}{\beta}\arctan(e^{2m(\cosh(\theta)(x-d)-\sinh(\theta)\,t)}), \tag{3.3.10}$$

the defect conditions are satisfied when

$$e^{2m(d-c)\cosh(\theta)} = \frac{\delta - e^{\theta}}{\delta + e^{\theta}}. \tag{3.3.11}$$

We convert this condition into a time-delay

$$\Delta t = \frac{1}{2m\sinh(\theta)}\ln\left(\frac{\delta + e^{\theta}}{\delta - e^{\theta}}\right), \tag{3.3.12}$$

on the outgoing soliton where

$$\phi = \frac{2\sqrt{2}}{\beta}\arctan(e^{2m(\cosh(\theta)\,x-\sinh(\theta)\,t)}), \quad \psi = \frac{2\sqrt{2}}{\beta}\arctan(e^{2m(\cosh(\theta)\,x-\sinh(\theta)(t-\Delta t))}). \tag{3.3.13}$$

Analysing the time-delay formula, assuming $\theta > 0$ and the incoming soliton is a kink solution, shows that when $\delta > e^{\theta}$ then the outgoing solution is a kink with a positive time-delay $\Delta t > 0$. Figure 3.9 shows this process, figure 3.9(a) shows initially the left soliton far from the defect and the fields at the defect taking the values $\phi = \psi = \frac{\sqrt{2}\pi}{\beta}$. The left kink approaches and is absorbed by the defect before the right kink is emitted after a time-delay. The final state shown in figure 3.9(e) is again a zero topological charge defect but now with $\phi = \psi = 0$. The energy of the initial and final defect states are the same, as are the energy of the absorbed and emitted solitons. It is therefore trivial to see that the energy is conserved with the

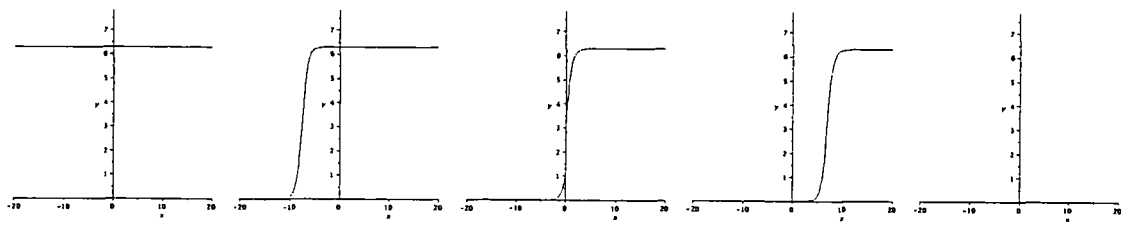

(a) (b) (c) (d) (e)

Fig. 3.9: SG kink scattering through a defect, time flowing from (a) to (e).

total energy of the system being

$$E_{tot} = E_{sol}(\theta) + E^{def}_{\phi=0,\ \psi=0}(\delta) = \frac{8m}{\beta^2}\cosh(\theta) - \frac{2m}{\beta^2}\left(\delta + \frac{1}{\delta}\right). \qquad (3.3.14)$$

Different scattering processes are possible when the δ the parameter on the defect takes different values. Figure 3.10 shows the process when $0 < \delta < e^{\theta}$ where the outgoing soliton still experiences a time-delay but also the incoming kink gets flipped to an anti-kink. Topological charge is still conserved as the initial defect state has charge -2 and the final defect state has zero topological charge.

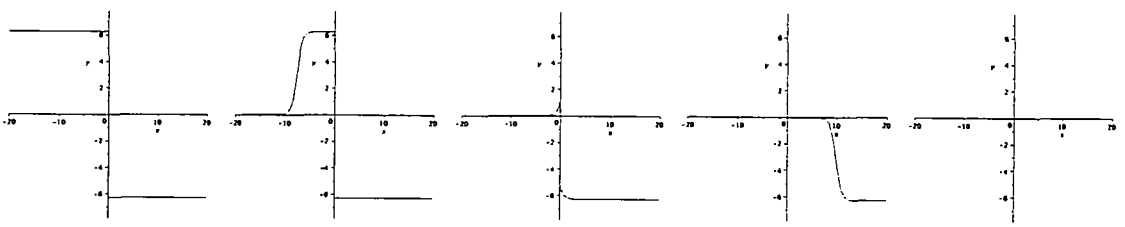

(a) (b) (c) (d) (e)

Fig. 3.10: SG kink scattering through a defect and changing into an anti-kink, time flowing (a) to (e).

As well as the right hand side soliton being time-delayed it is possible for it to be time-advanced. Figure 3.11 shows the kink-kink scattering process where $\delta < -e^{-\theta}$ and the right kink is time-advanced. This time-advancement is shown in figure 3.11(b) where the right kink is being emitted from the defect before the left kink has been absorbed. We note that in all processes where the scattering soliton is time-advanced the initial defect state has positive energy, this is necessary so that the defect can transfer energy to the right soliton before it gains energy from the

the left soliton. Likewise processes where the right soliton is time-delayed the initial defect state has negative energy.

Comparing the SG soliton-defect time-delay (3.3.12) with the SG soliton-soliton time-delay (2.1.37) shows that if we match the parameters between the defect and soliton then the time-delay experienced when scattering through the defect is exactly half of that experienced when scattering through another soliton. This might point towards defects actually being the fundamental objects of the theory and somehow two defects are equal to a soliton [24].

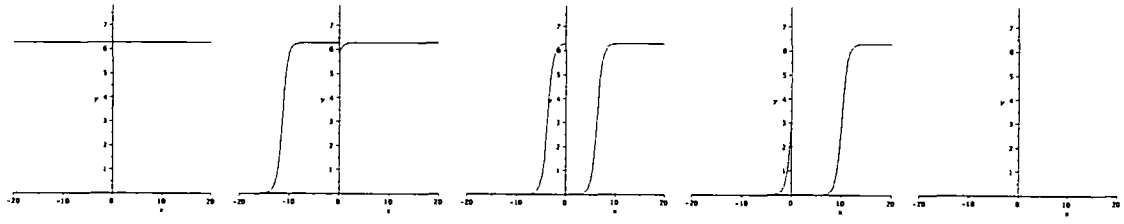

(a) (b) (c) (d) (e)

Fig. 3.11: SG kink scattering through a defect with time-advance, time flowing (a) to (e).

3.3.4 Particle - defect scattering

The particle of the theory is taken to be linearised fluctuations around the vacuum and therefore the particle-defect scattering factor is found by solving the linearised defect conditions. The linearised SG equation of motion is solved by the usual plane wave solution with mass shell condition $\omega^2 = k^2 + 4m^2$. For the zero topologically charged defect $\phi = 0,\ \psi = 0$ the linearised defect conditions are

$$\begin{aligned} \partial_t\psi_\epsilon - \partial_x\phi_\epsilon &= m\,e^{-\chi}(\phi_\epsilon + \psi_\epsilon) + m\,e^{\chi}(\phi_\epsilon - \psi_\epsilon)\,, \\ \partial_t\phi_\epsilon - \partial_x\psi_\epsilon &= -m\,e^{-\chi}(\phi_\epsilon + \psi_\epsilon) + m\,e^{\chi}(\phi_\epsilon - \psi_\epsilon)\,, \end{aligned} \tag{3.3.15}$$

which has solutions (strictly speaking the real part of these expressions)

$$\phi_\epsilon = e^{ikx}e^{-i\omega t} + R\,e^{-ikx}e^{-i\omega t}\,, \quad \psi_\epsilon = T\,e^{ikx}e^{-i\omega t}\,, \tag{3.3.16}$$

where

$$R = 0\,, \quad T = \frac{wi + m(e^{\chi} - e^{-\chi})}{-ki + m(e^{\chi} + e^{-\chi})}\,. \tag{3.3.17}$$

Similarly for the topologically charged defect $\phi = 0\,,\ \psi = \frac{\sqrt{2}\pi}{\beta}$ the linearised SG equation remains the same but the linearised defect conditions become

$$\begin{aligned} \partial_t\psi_\epsilon - \partial_x\phi_\epsilon &= -m\,e^{-x}(\phi_\epsilon + \psi_\epsilon) - m\,e^{x}(\phi_\epsilon - \psi_\epsilon)\,, \\ \partial_t\phi_\epsilon - \partial_x\psi_\epsilon &= m\,e^{-x}(\phi_\epsilon + \psi_\epsilon) - m\,e^{x}(\phi_\epsilon - \psi_\epsilon)\,, \end{aligned} \tag{3.3.18}$$

which has the same solution (3.3.16), this time with

$$R = 0\,, \quad T = \frac{-wi + m(e^x - e^{-x})}{ki + m(e^x + e^{-x})}\,. \tag{3.3.19}$$

Both of these solutions have the property that the reflection factor is zero and therefore the defect is purely transmitting.

This concludes the introduction of the defect SG theory, after the derivation of the theory we have concentrated on the classical properties of the theory. We have shown that the defect can store energy, momentum and topological charge and can have these charges transferred to and away from it during absorption, emission and scattering processes with SG solitons. Solitons with specific rapidity can be absorbed or emitted by the defect and during scattering the rapidity of the incoming soliton in reference with the defect rapidity parameter governs whether the soliton changes flavour or not. We have seen that a kink can either remain a kink or swap to an anti-kink. It has been commented that this property could allow the SG defect to be used as a logic gate [26]. The property that the particle transmission factor is purely transmitting is startling and is a result of integrability. Further analysis has been completed on aspects of the quantum theory [25] which are not mentioned here.

Other field theories with defects have since been studied including the non-linear Schrödinger model [27, 28] and some supersymmetric theories [29]. In the next section we introduce the sinh-Gordon theory with defect.

3.4 Sinh-Gordon theory with defect

In section 3.2.4 we showed that it is possible to construct a defect theory with ShG theory on both sides so that the defect conditions preserve the integrability of the ShG theory. The ShG defect Lagrangian has the form (3.2.1) with the defect term

(3.2.23) and the standard bulk Lagrangian pieces (2.2.1) restricted to $x < 0$ and $x > 0$. The conserved defect energy (3.2.5) and defect momentum (3.2.7) with defect term (3.2.23) have contributions from the bulk regions and the defect. The ShG defect conditions are

$$\begin{aligned} \partial_x\phi - \partial_t\psi &= \frac{\sqrt{2}m}{\beta}\left(\frac{1}{\delta}\sinh\left(\frac{\beta(\phi+\psi)}{\sqrt{2}}\right) + \delta\sinh\left(\frac{\beta(\phi-\psi)}{\sqrt{2}}\right)\right), \\ \partial_x\psi - \partial_t\phi &= \frac{\sqrt{2}m}{\beta}\left(-\frac{1}{\delta}\sinh\left(\frac{\beta(\phi+\psi)}{\sqrt{2}}\right) + \delta\sinh\left(\frac{\beta(\phi-\psi)}{\sqrt{2}}\right)\right). \end{aligned} \quad (3.4.1)$$

This model was derived along with the other scalar field defect theories [8] but the analysis that follows here is new work.

In the earlier introduction into the bulk sinh-Gordon theory in section 2.2, we showed that the 'soliton' solutions in the ShG theory are not finite energy configurations in the bulk theory. This makes the bulk theory uninteresting as it is a theory of just a scalar particle. This property certainly implies that 'solitons' moving with real rapidity will still have infinite energy in the defect theory. However as we show, it is possible to hide the infinities present in the 'soliton' solution behind the defect allowing a finite energy field configuration to be constructed using ShG 'soliton' solutions.

3.4.1 Defect bound states

The vacuum of the ShG defect theory is the trivial $\phi = 0$, $\psi = 0$ with energy and momentum

$$E = -\frac{2m}{\beta^2}\left(\delta + \frac{1}{\delta}\right), \quad P = \frac{2m}{\beta^2}\left(\delta - \frac{1}{\delta}\right). \quad (3.4.2)$$

We analyse the field configuration with a static one-'soliton' solution (2.2.4) on both sides of the defect

$$\phi = \frac{2\sqrt{2}}{\beta}\text{arctanh}(e^{2m(x-c)}), \quad \psi = \frac{2\sqrt{2}}{\beta}\text{arctanh}(e^{2m(-x-d)}). \quad (3.4.3)$$

Due to the asymptotic behaviour of the 'soliton' solution, the two solutions are taken to be the parity inverse of each other. This is achieved by flipping the sign of x in the ψ solution, meaning that the ϕ solution tends to zero as $x \to -\infty$ and the ψ solution tends to zero as $x \to +\infty$. This choice at least allows the possibility of

hiding the infinities from both solutions behind the defect and therefore achieving the aim of creating a finite energy field configuration.

We substitute these solutions into the ShG defect conditions (3.4.1) and simplify them to give the constraint

$$e^{2md} = \frac{1}{e^{2mc}} \left(\frac{\delta+1}{\delta-1}\right), \tag{3.4.4}$$

on the parameters c and d which govern the position of the two solutions. We calculate the energy and momentum of this configuration to be

$$E = \frac{2m}{\beta^2}\left(\delta + \frac{1}{\delta}\right) - \frac{8m}{\beta^2}, \qquad P = -\frac{2m}{\beta^2}\left(\delta - \frac{1}{\delta}\right), \tag{3.4.5}$$

although the energy is only this value if both infinities are absent from their respective bulk regions. The position of the infinities are at $x = c$ and $x = -d$ giving the range of finite energies to be

$$\begin{aligned} 1 < e^{2md} < \tfrac{\delta+1}{\delta-1}, &\qquad \text{for} \quad \delta > 1, \\ -1 < e^{2md} < \tfrac{\delta+1}{\delta-1}, &\qquad \text{for} \quad 0 < \delta < 1. \end{aligned} \tag{3.4.6}$$

In figure 3.12 we show that the ShG defect bound state does have greater energy than the vacuum for $\delta > 0$, the range where the defect bound state exists. For the particular value of $\delta = 1$, the energies of the two configurations coincide.

Figures 3.13 and 3.14 each show three examples of the static 'solitons' in positions where the energy of the configuration is finite. Figures 3.13(a), 3.14(a) are where the left 'soliton' has its infinity at $x = 0$, which coincides with $e^{2md} = \frac{\delta+1}{\delta-1}$. Figures 3.13(c), 3.14(c) show when the right 'soliton' has its infinity at $x = 0$, where $d = 0$ (actually for $\delta < 1$, $d = \frac{\pi i}{2m}$). Figures 3.13(b), 3.14(b) show the 'solitons' where e^{2md} lies in the internal region of the range (3.4.6). When $\delta > 1$ then the right 'soliton' is the same flavour as the left, illustrated in figure 3.13, while if $0 < \delta < 1$ then the 'solitons' are the opposite flavour, shown in figure 3.14.

Unlike the bulk ShG theory there are finite energy configurations involving ShG 'solitons' in the defect theory, as there are in the boundary theory [16, 17]. The straightforward extension to this result is to ask whether higher soliton solutions can form other finite energy configurations.

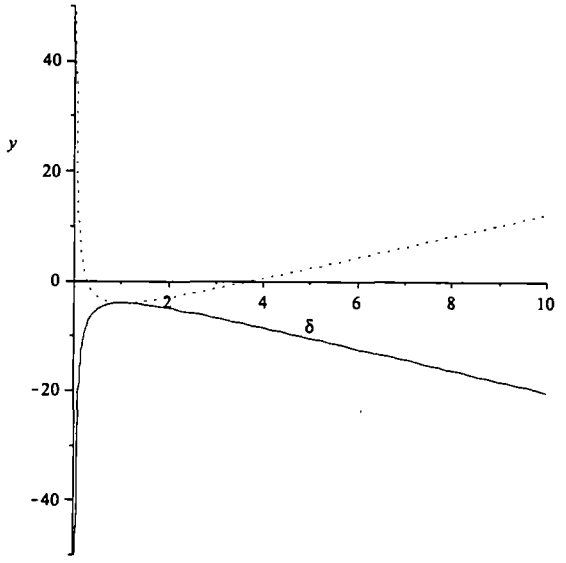

Fig. 3.12: Energy of the defect states for different values of δ ($m = \frac{1}{2}$, $\beta = \frac{1}{\sqrt{2}}$). Solid line = energy of the $\phi = \psi = 0$ state, dotted line = energy of ShG defect bound state.

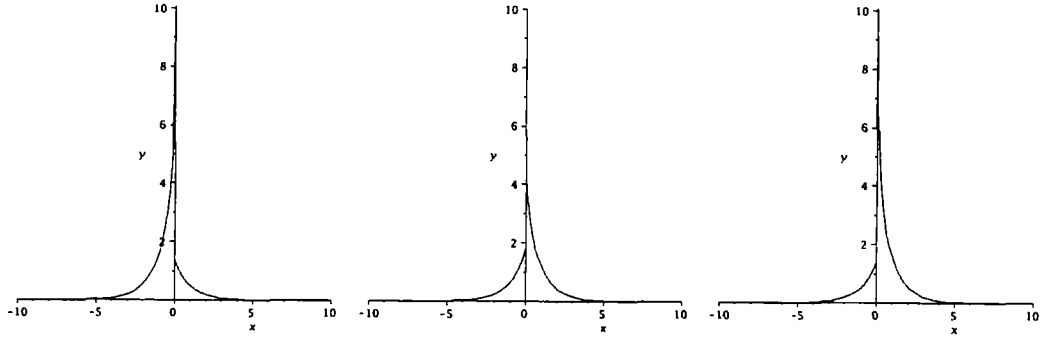

Fig. 3.13: Defect static 'soliton' solution with $\delta = 2$ with the positions of the 'solitons' at the extremal values and one in the middle of the range.

As in the SG theory (section 2.1.6) there exists a ShG breather solution, similarly constructed by giving the two constituent one-'solitons' in the two-'soliton' solution rapidities the complex conjugate of each other. As for the 'soliton' this breather solution is not a finite energy solution in the bulk theory. If the breather solution is moving, when the rapidities are not purely imaginary, then this automatically rules out the chance of the energy being finite in the defect theory. Therefore we

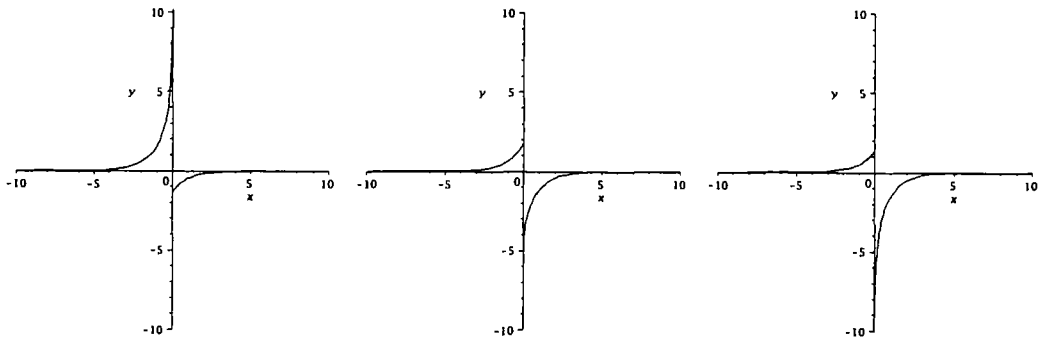

(a) (b) (c)

Fig. 3.14: Defect static 'soliton' solution with $\delta = 0.5$ with the positions of the 'solitons' at the extremal values and one in the middle of the range.

consider the stationary breather solution. We illustrate the ShG breather solution in figure 3.15, where similarly to the SG breather the constituent 'solitons' are bound to each other, moving through each other periodically and never escaping to infinite separation.

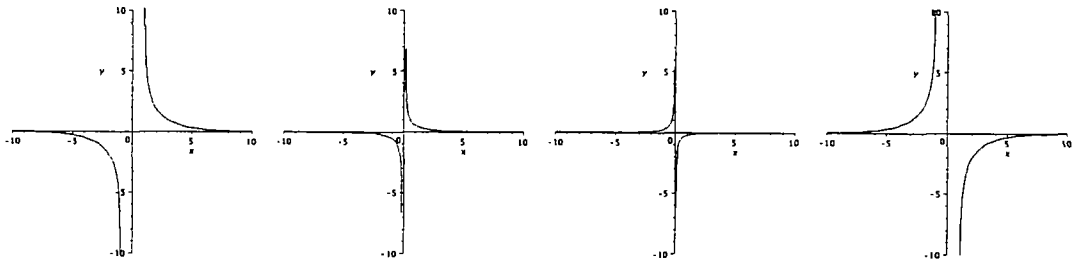

(a) (b) (c) (d)

Fig. 3.15: ShG breather solution, time flowing (a) to (d).

The most useful way to write down a ShG breather solution is

$$\phi = \frac{\sqrt{2}}{\beta} \ln\left(\frac{\tau_0}{\tau_1}\right), \tag{3.4.7}$$

where

$$\tau_0 = 1 + \frac{f}{\mu} - \frac{g}{\mu} - fg, \qquad \tau_1 = 1 - \frac{f}{\mu} + \frac{g}{\mu} - fg \tag{3.4.8}$$

and

$$f = e^{2m((x-c)\cos(\theta) - i\,t\sin(\theta))}, \quad g = e^{2m((x-c)\cos(\theta) + i\,t\sin(\theta))}, \quad \mu = \frac{e^{i\theta} - e^{-i\theta}}{e^{i\theta} + e^{-i\theta}}. \tag{3.4.9}$$

In this breather solution we have made it stationary by giving the constituent 'solitons' rapidities $\pm i\theta$. We place this solution on the left hand side of the defect and a similar one for ψ

$$\psi = \frac{\sqrt{2}}{\beta} \ln\left(\frac{\sigma_0}{\sigma_1}\right), \tag{3.4.10}$$

where

$$\sigma_0 = 1 + \frac{p}{\nu} - \frac{q}{\nu} - pq, \qquad \sigma_1 = 1 - \frac{p}{\nu} + \frac{q}{\nu} - pq \tag{3.4.11}$$

and

$$p = e^{2m((x-d)\cos(\theta) - i\,(t-t_0)\sin(\theta))}, \quad q = e^{2m((x-d)\cos(\theta) + i\,(t-t_0)\sin(\theta))}, \quad \nu = \frac{e^{i\theta} - e^{-i\theta}}{e^{i\theta} + e^{-i\theta}} \tag{3.4.12}$$

on the right hand side of the defect. We find that the defect conditions (3.4.1) are satisfied by

$$e^{4m(c-d)} = \frac{\cosh(\chi) - \cos(\theta)}{\cosh(\chi) + \cos(\theta)}, \qquad e^{4mt_0} = \frac{\sinh(\chi) - i\sin(\theta)}{\sinh(\chi) + i\sin(\theta)}, \tag{3.4.13}$$

where $\delta = e^{\chi}$. Generating these conditions is not a trivial matter due to the complexity of the breather solutions and the defect conditions themselves. However by realising that the conditions must hold for all time, a Taylor series in an exponentiated time variable can be made leaving equations proportional to each term that can be individually solved. As in the static 'soliton' configuration the important question is whether there is a range of the parameters where the energy of a breather-breather solution is finite? Once again it is necessary to "hide" the infinities behind the defect, after extensive analysis it is thought that this is impossible although we offer no formal proof.

Continuing to the next possible defect solution, we consider a three-'soliton' solution on each side of the defect. Again the three-'soliton' solutions are best written in the same form as for the breathers (3.4.7), (3.4.10) this time with

$$\begin{aligned}
\tau_0 &= 1 + \frac{f}{\nu\rho} - \frac{g}{\mu\nu} + \frac{h}{\mu\rho} - \frac{fg}{\mu\rho} + \frac{fh}{\mu\nu} - \frac{gh}{\nu\rho} - fgh, \\
\tau_1 &= 1 - \frac{f}{\nu\rho} + \frac{g}{\mu\nu} - \frac{h}{\mu\rho} - \frac{fg}{\mu\rho} + \frac{fh}{\mu\nu} - \frac{gh}{\nu\rho} + fgh, \\
\sigma_0 &= 1 + \frac{p}{\epsilon\eta} - \frac{q}{\delta\epsilon} + \frac{r}{\epsilon\eta} - \frac{pq}{\delta\eta} + \frac{pr}{\delta\epsilon} - \frac{qr}{\epsilon\eta} - pqr, \\
\sigma_1 &= 1 - \frac{p}{\epsilon\eta} + \frac{q}{\delta\epsilon} - \frac{r}{\epsilon\eta} - \frac{pq}{\delta\eta} + \frac{pr}{\delta\epsilon} - \frac{qr}{\epsilon\eta} + pqr.
\end{aligned} \tag{3.4.14}$$

We choose the constituent 'solitons' so that two of the 'solitons' form a breather and the third is a stationary 'soliton' with flavour to ensure that $\phi \to 0$ as $x \to -\infty$ and $\psi \to 0$ as $x \to +\infty$. These choices mean the solution has the form

$$\begin{aligned} f &= e^{2m(x-b)}, \quad g = e^{2m(\cos(\theta)(x-a)-i\,t\sin(\theta))}, \quad h = e^{2m(\cos(\theta)(x-a)+i\,t\sin(\theta))}, \\ p &= e^{2m(-x-c)}, \quad q = e^{2m(\cos(\theta)(-x-d)-i\,(t-e)\sin(\theta))}, \quad r = e^{2m(\cos(\theta)(-x-d)+i\,(t-e)\sin(\theta))} \end{aligned} \tag{3.4.15}$$

and

$$\mu = \delta = \frac{e^{i\theta} - e^{-i\theta}}{e^{i\theta} + e^{-i\theta}}, \qquad \nu = \epsilon = \frac{1 - e^{i\theta}}{1 + e^{i\theta}}, \qquad \rho = \eta = \frac{1 - e^{-i\theta}}{1 + e^{-i\theta}}. \tag{3.4.16}$$

We solve the defect conditions (3.4.1) for these breather plus static 'soliton' configurations and find they are satisfied when

$$e^{2m(a+d)} = \sqrt{\frac{\cosh(\chi) + \cos(\theta)}{\cosh(\chi) - \cos(\theta)}}, \qquad e^{2me} = \sqrt{\frac{\sinh(\chi) + i\sin(\theta)}{\sinh(\chi) - i\sin(\theta)}},$$

$$e^{2m(c+b)} = \coth\left(\frac{\chi}{2}\right). \tag{3.4.17}$$

After more analysis we found that for no range of the parameters is it possible to hide all the infinities of this configuration behind the defect and we conjecture that there are no non-static finite energy defect states in the defect ShG theory.

3.4.2 Particle - defect scattering

In the previous section we analysed different field configurations in the ShG defect theory, despite being able to solve the defect conditions for complicated time-dependent solutions only the trivial vacuum and static solution were found to be finite energy. In this section linearised calculations are performed on both of these configurations which models the scattering of the ShG particle through the two defect states. Strictly speaking the fields are the real parts of the plane wave type solutions which follow. The ShG equation linearises to the Klein-Gordon equation which has the standard plane wave solution

$$\phi_\epsilon = \alpha_1\, e^{ikx} e^{-i\omega t} + \alpha_2\, e^{ikx} e^{i\omega t}, \tag{3.4.18}$$

with the mass-shell condition $\omega^2 - k^2 = 4m^2$. The linearised defect conditions around the vacuum $\phi = 0, \quad \psi = 0$ are

$$\begin{aligned} \frac{\partial \psi_\epsilon}{\partial t} - \frac{\partial \phi_\epsilon}{\partial x} &= -m\, e^{-\chi}(\phi_\epsilon + \psi_\epsilon) - m\, e^{\chi}(\phi_\epsilon - \psi_\epsilon)\,, \\ \frac{\partial \phi_\epsilon}{\partial t} - \frac{\partial \psi_\epsilon}{\partial x} &= m\, e^{-\chi}(\phi_\epsilon + \psi_\epsilon) - m\, e^{\chi}(\phi_\epsilon - \psi_\epsilon)\,. \end{aligned} \tag{3.4.19}$$

We solve the defect conditions for a plane wave solution moving in from left infinity

$$\phi_\epsilon = e^{ikx} e^{-iwt} + R\, e^{ikx} e^{iwt}\,, \quad \psi_\epsilon = T\, e^{ikx} e^{-iwt}\,, \tag{3.4.20}$$

which we find are satisfied when

$$R_{vac} = 0\,, \quad T_{vac} = \frac{w + im\left(\delta - \frac{1}{\delta}\right)}{-k + im\left(\delta + \frac{1}{\delta}\right)}\,. \tag{3.4.21}$$

As in the SG defect theory, the plane wave (ShG particle) is purely transmitted through the defect.

To find the transmission factor for the particle scattering through the static 'soliton' defect state needs more work, first we need to find the linearised equation of motion around the static configuration. The solutions have the form

$$\phi = \frac{2\sqrt{2}}{\beta}\mathrm{arctanh}(e^{2m(x-c)}) + \phi_\epsilon\,, \qquad \psi = \frac{2\sqrt{2}}{\beta}\mathrm{arctanh}(e^{2m(-x-d)}) + \psi_\epsilon \tag{3.4.22}$$

and the linearised equations of motion become

$$\begin{aligned} 0 &= \ddot{\phi}_\epsilon - \phi_\epsilon'' + 4m^2\left(1 + \frac{2}{\sinh^2(2m(x-c))}\right)\phi_\epsilon\,, \\ 0 &= \ddot{\psi}_\epsilon - \psi_\epsilon'' + 4m^2\left(1 + \frac{2}{\sinh^2(2m(-x-d))}\right)\psi_\epsilon\,. \end{aligned} \tag{3.4.23}$$

To solve the ϕ equation we use the ansatz $\phi_\epsilon = e^{-iwt} f(x)$ to eliminate the time dependence, this reduces the equation to a Schrödinger type equation

$$-f'' + 4m^2\left(1 + \frac{2}{\sinh^2(2m(x-c))}\right) f = w^2 f\,. \tag{3.4.24}$$

We rewrite this in the form $A^+ A f = w^2 f$

$$\left(-\frac{d}{dx} + \frac{2m}{\tanh(2m(x-c))}\right)\left(\frac{d}{dx} + \frac{2m}{\tanh(2m(x-c))}\right) f = w^2 f\,, \tag{3.4.25}$$

where

$$A = \frac{d}{dx} + \frac{2m}{\tanh(2m(x-c))}\,. \tag{3.4.26}$$

By considering the related equation $AA^+g = w^2g$ and noticing that if $g(x)$ is a solution to this equation then $f(x) = A^+g(x)$ is a solution to the original equation. This reduces the problem to solving the related equation. Expanding out the related equation $AA^+g = w^2g$, we find that it has the simple form

$$-g'' + 4m^2g = w^2g\,, \tag{3.4.27}$$

which is solved by $g(x) = e^{\pm ikx}$ with $w^2 - k^2 = 4m^2$. Therefore $f(x) = A^+g(x)$ is a solution to the original equation (3.4.24) and has the explicit form

$$f(x) = \left(\mp ik + \frac{2m}{\tanh(2m(x-c))}\right) e^{\pm ikx}\,. \tag{3.4.28}$$

We solve the similar linearised ψ equation of motion (3.4.23) by the same method and find

$$\psi_\epsilon = \left(\mp ik - \frac{2m}{\tanh(2m(-x-b))}\right) e^{\pm ikx}e^{-iwt}\,. \tag{3.4.29}$$

We have the solutions in the bulk and to proceed we find the form of the linearised form of the defect conditions

$$\begin{aligned}
\partial_t\psi_\epsilon - \partial_x\phi_\epsilon &= \frac{2\sqrt{2}m}{\beta}\frac{1}{S(c)} \\
&\quad -\frac{\sqrt{2}m}{\beta\delta}\left\{\left(\frac{\phi_\epsilon+\psi_\epsilon}{\sqrt{2}}\beta\right)\left[\frac{C(c)C(d)+1}{S(c)S(d)}\right] + \left[\frac{C(c)+C(d)}{S(c)S(d)}\right]\right\} \\
&\quad -\frac{\sqrt{2}m\delta}{\beta}\left\{\left(\frac{\phi_\epsilon-\psi_\epsilon}{\sqrt{2}}\beta\right)\left[\frac{C(c)C(d)-1}{S(c)S(d)}\right] + \left[\frac{C(d)-C(c)}{S(c)S(d)}\right]\right\}, \\
\partial_t\phi_\epsilon - \partial_x\psi_\epsilon &= -\frac{2\sqrt{2}m}{\beta}\frac{1}{S(d)} \\
&\quad +\frac{\sqrt{2}m}{\beta\delta}\left\{\left(\frac{\phi_\epsilon+\psi_\epsilon}{\sqrt{2}}\beta\right)\left[\frac{C(c)C(d)+1}{S(c)S(d)}\right] + \left[\frac{C(c)+C(d)}{S(c)S(d)}\right]\right\} \\
&\quad -\frac{\sqrt{2}m\delta}{\beta}\left\{\left(\frac{\phi_\epsilon-\psi_\epsilon}{\sqrt{2}}\beta\right)\left[\frac{C(c)C(d)-1}{S(c)S(d)}\right] + \left[\frac{C(d)-C(c)}{S(c)S(d)}\right]\right\},
\end{aligned} \tag{3.4.30}$$

where $C(c) = \cosh(2mc)$, $S(c) = \sinh(2mc)$. This is before we have applied the constraint between the positions of the two 'solitons' (3.4.4) bound to the defect. Solving the linearised defect conditions for an incoming particle from left infinity and allowing the defect to both reflect and transmit

$$\begin{aligned}
\phi_\epsilon &= \left[\left(-ik + \frac{2m}{\tanh(2m(x-c))}\right)e^{ikx} + R\left(ik + \frac{2m}{\tanh(2m(x-c))}\right)e^{-ikx}\right]e^{-iwt}, \\
\psi_\epsilon &= T\left(-ik - \frac{2m}{\tanh(2m(-x-d))}\right)e^{ikx}e^{-iwt},
\end{aligned} \tag{3.4.31}$$

we find

$$R_{bs} = 0\,, \qquad T_{bs} = \frac{-w + im\left(\delta - \frac{1}{\delta}\right)}{k + im\left(\delta + \frac{1}{\delta}\right)}\,. \tag{3.4.32}$$

Again the scattering is reflectionless so the particle is purely transmitted through the defect bound state.

3.4.3 Transmission factor analysis

We have calculated the particle-defect transmission factor for the vacuum T_{vac} (3.4.21) and the defect bound state T_{bs} (3.4.32), finding in both cases that they have modulus one, another way of saying that the defects are reflectionless.

There exists a pole in T_{vac} at $k = i\,m(\delta + \delta^{-1})$ which corresponds to the configuration

$$\phi \sim 0\,, \qquad \psi \sim e^{\pm m(\delta - \delta^{-1})t} e^{-m(\delta + \delta^{-1})x}\,, \tag{3.4.33}$$

this is normalisable in x which suggests the existence of a defect bound state but damped in t, except when $\delta = 1$ where it is static. This corresponds to the defect bound state found in the previous section, since the bound state was static and in the limit $\delta \longrightarrow 1$ the solution is small as the left and right bound 'solitons' are positioned far behind the defect. Similar analysis of T_{bs} should help to confirm whether or not we are correct in conjecturing that there are no higher bound states. T_{bs} has a pole at $k = -i\,m(\delta + \delta^{-1})$ which corresponds to the configuration

$$\phi \sim 0\,, \qquad \psi \sim e^{-i\omega t} e^{m(\delta + \delta^{-1})x}\,, \tag{3.4.34}$$

this is non-normalisable for $\delta > 0$ suggesting that there are no higher bound states. We can rewrite the transmission factors in the form

$$T_{vac} = i\frac{\sinh\left(\frac{\theta - \chi}{2} + \frac{i\pi}{4}\right)}{\sinh\left(\frac{\theta - \chi}{2} - \frac{i\pi}{4}\right)}\,, \qquad T_{bs} = -i\frac{\sinh\left(\frac{\theta - \chi}{2} - \frac{i\pi}{4}\right)}{\sinh\left(\frac{\theta - \chi}{2} + \frac{i\pi}{4}\right)}\,. \tag{3.4.35}$$

Using the classical formula for particle-particle scattering in ShG theory [25]

$$S_{11}(\theta) = -\frac{\sinh\left(\frac{\theta}{2}\right)\sinh\left(\frac{\theta}{2} - \frac{i\pi}{2}\right)}{\sinh\left(\frac{\theta}{2}\right)\sinh\left(\frac{\theta}{2} + \frac{i\pi}{2}\right)}\,, \tag{3.4.36}$$

we check that the transmission factors satisfy the classical defect bootstrap equation, illustrated in figure 3.16.

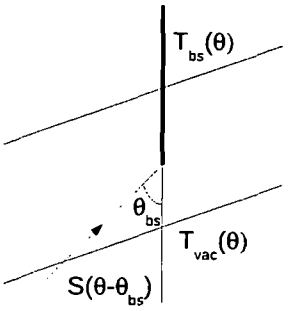

Fig. 3.16: Defect Bootstrap from vacuum to bound state.

$$T_{vac}(\theta)\, S_{11}(\theta - \theta_{bs}) = T_{bs}(\theta)\,, \tag{3.4.37}$$

where $\theta_{bs} = \chi + \frac{i\pi}{2}$ the pole that appears in T_{vac}.

3.5 Summary

This concludes the introductory part of this thesis, in the past two chapters we have introduced and analysed some aspects of 1+1 D field theories. Using SG and ShG theories to describe properties of the integrable field theories and general techniques which are common place in this area of research. We have concentrated purely on the classical aspects of the theory which dominates the analysis of the complex sine-Gordon theory to come.

We reviewed the topological solitons solutions present in the SG theory, both by using the Bogomolny energy bound and the Bäcklund transformation. Using the Theorem of Permutability we have generated a two-soliton solution and described how higher soliton solutions could in principle be generated. The two-soliton solution can describe soliton-soliton scattering, where the solitons experience a time-delay or time-advance, or a breather solution where the two constituent solitons are bound in periodic motion. Unlike the SG soliton, the ShG 'soliton' does not have finite energy, meaning the spectrum of the model is a sole scalar particle. For the SG theory the conservation of higher spin charges was shown which is the first step on the way to proving the integrability of the theory, which is responsible for many of

its interesting properties.

Moving on from the bulk theory we have introduced boundaries and defects in scalar field theories in such a way as to maintain their integrability. The boundary potential was determined by the conservation of the higher spin energy-like charges and the defect potential was similarly determined by the, perhaps unexpected, conservation of a defect momentum. Constructing the defect theory in the case of single scalar field theories gave constraints on which bulk theories are allowed on each side of the defect.

In the SG defect theory the defect conditions are exactly the BT. We found solitons can be both absorbed and emitted by a defect if they are travelling at specific rapidities. More general solitons scatter through the defect, either experiencing a time-delay or time-advance with the process being either flavour conserving or not. That is, depending on the rapidity of the scattering soliton, a kink solution can remain a kink or flip to an anti-kink solution. During all these processes energy, momentum and topological charge are transferred to and from the defect. The time-delay for soliton-defect scattering is found to be exactly half of that for soliton-soliton scattering and the SG particle is found to be purely transmitted by the defect.

In the defect ShG theory, we found the existence of a static defect bound state, but no higher bound states involving ShG breather solutions. We showed that the energy of this bound state is always higher than the vacuum in the parameter range where the bound state exists. We calculated the classical particle transmission factor through both the vacuum and bound state, again finding both states reflectionless. Analysis of the transmission factors backs up the conjecture that no more defect bound states exist and the transmission factors were checked to satisfy the classical defect bootstrap equation. In the literature there are two different suggestions for the quantum transmission matrix [25, 30], one which depends on the coupling constant and one that does not, and both of which agree with T_{vac} in the classical limit. The discovery of a previously unknown classical bound state provides an explanation for the pole that appears in T_{vac} and also the pole that appears in the candidate quantum transmission matrices.

We will now use the ideas presented in these introductory chapters in the analysis

of the more complicated complex sine-Gordon theory and compare and contrast the properties of the CSG theory with the properties of the SG and ShG theories.

Chapter 4

Complex sine-Gordon theory

This chapter starts the main section of work of this thesis on the complex sine-Gordon (CSG) theory. We begin with an overview of the bulk theory before in the subsequent chapters we introduce defects and dressed boundaries into the theory. The work in chapters 4, 5 and 6 covers the material in the paper *"Defects and dressed boundaries in complex sine-Gordon theory"* [1]. In chapter 7 we investigate quantum aspects of the CSG dressed boundary theory, the work appears in *"Quantum complex sine-Gordon dressed boundaries"* [2].

The complex sine-Gordon model, like the sine-Gordon and sinh-Gordon models covered in the introductory chapters 2 and 3, is an integrable field theory in 1+1 dimensions. Unlike the other two models where the fields are real, CSG is a theory of complex fields. The CSG theory has many properties in common with the SG and ShG theories due to their shared integrability. Like the SG model, we see that the CSG model admits soliton solutions. Whereas the SG solitons carry topological charge, CSG solitons carry a Noether charge due to the theory's $U(1)$ invariance. The multi-vacua of the SG theory leads to the topological nature of the SG soliton, this is absent in the CSG theory which has an unique vacuum.

The similarities and differences between the CSG and SG model provide strong motivation to undertake further analysis into the CSG model and in particular into defect and boundary theories. As we have seen the SG theory has been thoroughly analysed both with boundary and defect, which led to the discovery of many interesting phenomena. In these theories the soliton solutions are found to interact with

the boundary and defect in various ways. They can be absorbed or emitted by both boundary and defect, as well being reflected from the boundary and transmitted through the defect.

We find that it is possible to construct CSG defect and boundary theories that are classically integrable. Whether similar interactions to those in SG theory, between CSG solitons and CSG boundary and defect are observed is investigated. Will there be added sophistication due to the solitons holding a Noether charge? These are the questions that make the research presented here an interesting and worthwhile study. The CSG theory is the perfect extension to the SG theory to see whether certain properties are repeated and are therefore possibly traits of all integrable theories and to see whether new properties appear from the increased complexity.

After the introductory material of this chapter, in chapter 5 we investigate the possibility of introducing an integrable defect into the theory. We analyse the properties of the defect and investigate the nature of the interactions between solitons and the defect. In chapter 6 we use the integrable CSG defect to generate a wider class of boundary conditions which we similarly examine.

The CSG theory goes back to the mid 1970's when it was independently introduced by various people, arriving at the now standard CSG Lagrangian from very different starting points. Lund and Regge [31, 32] found that a model of relativistic vortices in a superfluid in 4D, where the strings/vortices interact through a massless scalar field, can be reinterpreted as a set of two coupled non-linear equations in 2D. These equations admit solitary wave solutions and are equivalent to today's CSG theory. The 4D Lagrangian they started with was the same as introduced by Kalb and Ramond [33] when generalising the classical action of a distance theory between point particles to include 1D strings in analogy with Feynman and Wheeler's [34] description of Maxwell's theory. Lund and Regge did not know whether the theory they had constructed was integrable.

The answer to this question was given by Pohlmeyer and Rehren [35, 36], who constructed the CSG Lagrangian as one of a series of relativistically invariant field theories in 1+1 D with a one parameter family of BT and an infinite number of integrals of motion. These were obtained by a dimensional reduction of the $O(n)$

non-linear σ-model, with the $O(3)$ and $O(4)$ σ-models corresponding to the SG and CSG models respectively.

Getmanov [37,38] constructed the CSG Lagrangian when writing down all "Lagrange Lorentz-invariant field theory models in 2 dimensional space-time for the complex scalar field with an infinite number of conserved currents". He found two non-trivial models which he called CSG I and II, with CSG I being the focus of the current theses.

Bakas [39] presented a Lagrangian description of the CSG model in terms of a $SU(2)/U(1)$ coset model perturbed by its first thermal operator. This work was built upon by Park and Chin, who in [40] demonstrated the duality between the positive and negative coupling sectors of the theory. In addition they wrote down the BT for the model using the WZW picture and complex field notation. Using the BT to construct one and two-soliton solutions, he showed that the two-soliton solution can describe either soliton-soliton scattering or a breather solution depending on the choice of the parameters in the BT. Fernandez-Pousa et al. [41,42] carried out further investigation into the class of homogeneous sine-Gordon theories of which the CSG model is the simplest.

The first investigations into the quantum regime of the theory were by de Vega and Maillet [43,44] who showed that the theory is renormalisable at 1-loop level with just a finite renormalisation of the coupling constant λ

$$\lambda^2 \to \lambda_R^2 = \frac{\lambda^2}{1 - \frac{\lambda^2}{4\pi}} \tag{4.0.1}$$

and calculated the 1-loop S-matrix. They continued to analyse the theory semi-classically, constructed soliton solutions by the inverse scattering method, calculated the semi-classical mass spectrum, using the method of Dashen et al. [45], and the semi-classical S-matrix. These results were built upon by Dorey and Hollowood [46] who used the Bohr-Sommerfeld quantisation rule to show that the charge of the CSG soliton is quantised, calculated the classical time-delay experienced by solitons during soliton-soliton scattering before conjecturing full S-matrices for soliton-soliton and meson-solitons scattering which were in full agreement to all the previous semi-classical computations.

Following on from work on other integrable field theories in restricted domains, the CSG model has been studied with a boundary by Bowcock and Tzamtzis [47]. They found a one parameter family of boundary conditions that preserve the integrability in the boundary theory and constructed conserved energy and charge. They analysed the CSG boundary model, calculating the soliton and particle classical reflection factors and found the existence of boundary bound states. Subsequently [48] they conjecture the form of the fully quantum reflection matrix using the bootstrap principle.

The CSG theory has been used in general relativity [49] and more widely in the area of optics. McCall and Hahn [50] used the SG theory to model the lossless propagation of light pulses, although this was a somewhat over-simplification of the the physical reality. Park and Chin [51, 52] used the extra phase degree of freedom present in the CSG model allowing them to account for frequency modulation effects.

Most recently the CSG model has attracted some attention in the context of magnons in string theory. The CSG equation is equivalent to the equations of motion of a string moving on an $\mathbb{R}$ x S^3 subspace of AdS_5 x S^5 [35, 53]. This equivalence is used in current work verifying the prediction of the $AdS/$CFT correspondence that the spectrum of operator dimensions in planar $\mathcal{N} = 4$ SUSY Yang-Mills and the spectrum of a free strings on AdS_5 x S^5 are the same [54]. Integrable boundaries have already been used in this context [55–57].

4.1 CSG Lagrangian description

The complex sine-Gordon theory is described by the Lagrangian

$$\mathcal{L}_{CSG} = \frac{\partial_t u\, \partial_t u^* - \partial_x u\, \partial_x u^*}{1 - \lambda^2 u u^*} - 4\beta u u^* \tag{4.1.1}$$

in 1+1 dimensions. Here u is a complex field, λ is the coupling constant and β is related to the mass parameter. The constant λ can be absorbed into u and u^* by scaling the field, in which case it appears as an overall factor multiplying the Lagrangian. Until chapter 7 we only consider the classical theory, so we can consistently set $\lambda = 1$.

The Lagrangian has a global $U(1)$ symmetry, i.e. it remains unchanged under the transformations $u \to e^{i\alpha}u$, $u^* \to e^{-i\alpha}u^*$, this leads to a conserved charge by Noether's theorem. The Lagrangian looks very similar to that of a massive free complex field. The interactions in the model can be thought of as arising when the denominator $1 - \lambda^2 uu^*$ is expanded in small fluctuations about the vacuum $u = 0$. We derive the CSG equation of motion (and its complex conjugate)

$$\partial_{tt}u - \partial_{xx}u + \frac{u^*((\partial_t u)^2 - (\partial_x u)^2)}{1 - uu^*} + 4\beta u(1 - uu^*) \;=\; 0\,, \tag{4.1.2}$$

by varying the action $S = \int dtL$ in the usual way. By considering small fluctuations we see that $\beta = \frac{m^2}{4}$.

The connection to the SG theory can be explicitly seen by a change of variables $u = \sin\phi\; e^{2i\eta}$. When η is taken to be a constant, the CSG equation becomes

$$\partial_{tt}\phi - \partial_{xx}\phi + 4\beta\cos\phi\sin\phi = 0\,, \tag{4.1.3}$$

which gives the familiar SG equation of motion

$$\partial_{tt}\phi - \partial_{xx}\phi + \sin\phi = 0\,, \tag{4.1.4}$$

after the rescalings $\phi \to \frac{\phi}{2}$, $\sqrt{\beta} \to \frac{1}{2}$. The energy has the form

$$E = \int dx\;\; \frac{\partial_t u\,\partial_t u^* + \partial_x u\,\partial_x u^*}{1 - uu^*} + 4\beta uu^* \tag{4.1.5}$$

and the momentum

$$P = -\int dx\;\; \frac{\partial_x u\,\partial_t u^* + \partial_x u^*\,\partial_t u}{1 - uu^*}\,. \tag{4.1.6}$$

Analogous to the SG theory, their conservation follows from the equations

$$\partial_t \mathcal{E} + \partial_x \mathcal{P} = 0\,, \qquad \partial_t \mathcal{P} + \partial_x \mathcal{E}^* = 0\,, \tag{4.1.7}$$

where $\mathcal{E}^* = \mathcal{E}(\beta \to -\beta)$. As in the SG theory and all integrable theories there are infinitely many higher spin charges that are conserved. In [47] a formula for some of the higher conserved charges are generated using the Lax pair method, in appendix A.1 we rewrite the next conserved energy-like and momentum-like charge

in notation consistent with the work in this thesis. The extra conserved charge due to the $U(1)$ symmetry by Noether's theorem takes the form

$$\begin{aligned} Q &= \int dx\, j^0 \\ &= \int dx\, \frac{\partial \mathcal{L}}{\partial(\partial_t u)} iu - \frac{\partial \mathcal{L}}{\partial(\partial_t u^*)} iu^* \\ &= i \int dx\, \frac{u\,\partial_t u^* - u^*\,\partial_t u}{1 - uu^*}\,. \end{aligned} \tag{4.1.8}$$

As with the Lagrangian the expressions for these conserved charges deviate from those of the free complex field by the denominator factor multiplying the derivative terms. The theory has two sectors corresponding to the sign of β, in these two sectors the vacuum field configurations are different. When $\beta > 0$ the vacuum is $u = 0$ and therefore topologically trivial, while when $\beta < 0$ the energy is minimised when $|u| = 1$, in this regime the vacuum spontaneously breaks the $U(1)$ symmetry of the theory.

4.2 CSG as a Wess-Zumino-Witten model

As first demonstrated by Bakas [39], the CSG model can be reformulated as a gauged Wess-Zumino-Witten (WZW) model [58,59] perturbed by a potential. Consider the action

$$S = S_{gWZW} + S_{pot}\,, \tag{4.2.1}$$

where S_{gWZW} is the standard gauged WZW action

$$\begin{aligned} S_{gWZW} &= -\frac{1}{4\pi}\int_\Sigma \mathrm{d}z\,\mathrm{d}\bar{z}\ \mathrm{Tr}(g^{-1}\partial g\, g^{-1}\bar{\partial} g) - \frac{1}{12\pi}\int_B \mathrm{Tr}(\tilde{g}^{-1}\mathrm{d}\tilde{g}\wedge\tilde{g}^{-1}\mathrm{d}\tilde{g}\wedge\tilde{g}^{-1}\mathrm{d}\tilde{g}) \\ &\quad + \frac{1}{2\pi}\int \mathrm{Tr}(-W\bar{\partial} g\, g^{-1} + \bar{W}g^{-1}\partial g + WgWg^{-1} - W\bar{W})\,, \end{aligned} \tag{4.2.2}$$

and S_{pot} is the perturbing potential

$$S_{pot} = \frac{\beta}{2\pi}\int \mathrm{Tr}(g\,\sigma_3 g^{-1}\sigma_3)\,. \tag{4.2.3}$$

The action is defined in a three-dimensional manifold B whose boundary is our normal compactified two-dimensional space Σ, g is a $SU(2)$ group element with $\tilde{g}$ its extension to the three-dimensional manifold. W and $\bar{W}$ are a connection that

gauge the anomaly free diagonal subgroup $U(1)$ of $SU(2)$. The perturbing potential breaks the conformal symmetry demonstrated by a WZW model and gives masses to the fields, with the mass parameter β.

Varying the action with respect to the field g gives the equation of motion

$$-\frac{1}{2\pi}\int \mathrm{Tr}\,[\partial+(g^{-1}\partial g+g^{-1}Wg+i\beta\lambda\sigma_3),\ \bar{\partial}+(\bar{W}-\frac{i}{\lambda}g^{-1}\sigma_3 g)]\,g_{-1}\,\delta g=0\,, \quad (4.2.4)$$

which takes zero curvature form [40]. Similarly the variation with respect to the gauge fields W and $\bar{W}$ lead to the following constraint equations

$$\begin{aligned} 0 &= -\frac{1}{2\pi}\int \mathrm{Tr}\left(\bar{\partial}g\,g^{-1}-g\bar{W}g^{-1}+\bar{W}\right)\delta W\,, \\ 0 &= \frac{1}{2\pi}\int \mathrm{Tr}\left(g^{-1}\partial g+g^{-1}Wg-W\right)\delta\bar{W}\,. \end{aligned} \quad (4.2.5)$$

Combining the constraint equations (4.2.5) and the diagonal part of the equation of motion (4.2.4) results in the flatness condition

$$\partial\bar{W}-\bar{\partial}W=0\,, \quad (4.2.6)$$

which allows the non-local gauge $W=\bar{W}=0$ to be chosen [60]. In this gauge the equation of motion (4.2.4) simplifies to

$$[\partial+(g^{-1}\partial g+i\beta\lambda\sigma_3),\ \bar{\partial}-\frac{i}{\lambda}g^{-1}\sigma_3 g]=0 \quad (4.2.7)$$

and the constraint equations (4.2.5), which are only valid for the diagonal component, to

$$\bar{\partial}g\,g^{-1}=0\,,\quad g^{-1}\partial g=0\,. \quad (4.2.8)$$

In this formulation the positive and negative β sectors of the CSG model in the complex field notation are treated simultaneously with the connection between the $SU(2)$ group element g and the complex fields u and v given by

$$g=\begin{pmatrix} u & -iv^* \\ -iv & u^* \end{pmatrix}\,, \quad (4.2.9)$$

where $v=-\sqrt{1-uu^*}e^{-i\theta}$ is the dual field to u. The diagonal components correspond to the $\beta>0$ sector, so u satisfies the CSG equation with $\beta>0$ and the off-diagonal to the $\beta<0$ sector with v satisfying the CSG equation with $\beta<0$.

θ is to be thought of as an auxiliary field and is defined up to a constant by the constraint equations (4.2.8), which in the complex field notation become

$$\begin{aligned} \partial_t\theta &= -\frac{i}{2}\left(\frac{u\partial_x u^* - u^*\partial_x u}{1-uu^*}\right), \\ \partial_x\theta &= -\frac{i}{2}\left(\frac{u\partial_t u^* - u^*\partial_t u}{1-uu^*}\right). \end{aligned} \tag{4.2.10}$$

The vacuum of the two sectors in complex field notation are respectively

$$u = 0\,, \quad v = -e^{i\Omega} \tag{4.2.11}$$

and in this notation

$$g_{vac} = \begin{pmatrix} 0 & ie^{-i\Omega} \\ ie^{i\Omega} & 0 \end{pmatrix}. \tag{4.2.12}$$

As shown previously for the SG theory, BT are extremely useful in the theory of integrable models. We used BT to create multi-soliton solutions and found that they were exactly the defect conditions required to formulate the integrable SG defect. BT exist in the WZW notation between two $SU(2)$ matrix variables f and g [40]

$$\begin{aligned} g^{-1}\partial g - f^{-1}\partial f - \delta\sqrt{\beta}\left[g^{-1}\sigma_3 f, \sigma_3\right] &= 0\,, \\ \bar{\partial}g\, g^{-1}\sigma_3 - \sigma_3\bar{\partial}f\, f^{-1} + \frac{\sqrt{\beta}}{\delta}\left[gf^{-1}, \sigma_3\right] &= 0\,. \end{aligned} \tag{4.2.13}$$

If the group elements f and g satisfy the BT then it can be checked that f and g both satisfy the gauged WZW equation of motion and the constraint equations.

We continue the introduction into the CSG theory by using the BT (4.2.13) as the starting point to analyse the soliton solutions in the complex field notation.

4.3 Complex sine-Gordon solitons I

We re-express the BT (4.2.13) in complex field notation

$$\begin{aligned} -\frac{\partial_t w - \partial_x w}{z^*} + \frac{\partial_t u - \partial_x u}{v^*} + 2\sqrt{\beta}\,\delta\,(wv + uz) &= 0\,, \\ \frac{\partial_t u + \partial_x u}{v} + \frac{\partial_t w + \partial_x w}{z} - \frac{2\sqrt{\beta}}{\delta}\,(uz^* - wv^*) &= 0\,, \end{aligned} \tag{4.3.1}$$

where $v = -\sqrt{1-uu^*}e^{-i\theta}$ and $z = -\sqrt{1-ww^*}e^{-i\psi}$ are the dual fields of u and w respectively. Each dual field introduces an auxiliary field which are determined up to a constant by constraint equations, θ by equations (4.2.10) and ψ by

$$\begin{aligned} \partial_t\psi &= -\frac{i}{2}\left(\frac{w\partial_x w^* - w^*\partial_x w}{1-ww^*}\right), \\ \partial_x\psi &= -\frac{i}{2}\left(\frac{w\partial_t w^* - w^*\partial_t w}{1-ww^*}\right). \end{aligned} \tag{4.3.2}$$

It can be checked that if u, v, w, z satisfy the BT then u and w satisfy the CSG equation with $\beta > 0$ and v and z satisfy the CSG equation with $\beta < 0$. Therefore by knowing one solution to the CSG equation, the BT allow a second solution to the CSG equation to be found. This new solution has a soliton-number one higher than the original solution. As with the SG model the CSG BT simplify the process of finding soliton solutions, since they are first order differential equations opposed to the second order CSG equation.

Explicitly from the vacuum $(u, v) = (0, -e^{i\Omega})$ we can find the one-soliton solution. Substituting these vacuum values into the BT (4.3.1) to give

$$\begin{aligned} 0 &= \partial_t w^* - \sqrt{\beta}\left(\delta\, e^{i(\Omega-\psi)} - \frac{e^{-i(\Omega-\psi)}}{\delta}\right) w^*\sqrt{1-ww^*}, \\ 0 &= \partial_x w^* + \sqrt{\beta}\left(\delta\, e^{i(\Omega-\psi)} + \frac{e^{-i(\Omega-\psi)}}{\delta}\right) w^*\sqrt{1-ww^*}, \end{aligned} \tag{4.3.3}$$

which can be rewritten in terms of solely the dual field

$$\begin{aligned} \partial_t z^* &= \sqrt{\beta}e^{i\Omega}\left(\delta - \frac{1}{\delta}\right)(1-zz^*), \\ \partial_x z^* &= -\sqrt{\beta}e^{i\Omega}\left(\delta + \frac{1}{\delta}\right)(1-zz^*). \end{aligned} \tag{4.3.4}$$

These are simultaneously solved by the following expressions for the one-soliton solutions in the two regimes of the theory

$$\begin{aligned} w = u_{1-sol} &= \frac{\cos(a)\exp(2i\sqrt{\beta}\sin(a)(t\cosh(\theta) - x\sinh(\theta)))}{\cosh(2\sqrt{\beta}\cos(a)(x\cosh(\theta) - t\sinh(\theta)))}, \\ z = v_{1-sol} &= -e^{i\Omega}\left(\cos(a)\tanh(2\sqrt{\beta}\cos(a)(x\cosh(\theta) - t\sinh(\theta))) - i\sin(a)\right), \end{aligned} \tag{4.3.5}$$

where the phase of the dual field z is given by

$$\psi = -\Omega + \arctan\left(\tan(a)\coth(2\sqrt{\beta}\cos(a)(x\cosh(\theta) - t\sinh(\theta)))\right), \tag{4.3.6}$$

a is associated to the charge of the solution and θ is the rapidity of the solution related to the parameter δ that appears in the BT by $\delta = e^{\theta}$. These solutions were originally derived by Getmanov [38] and Lund and Regge [31].

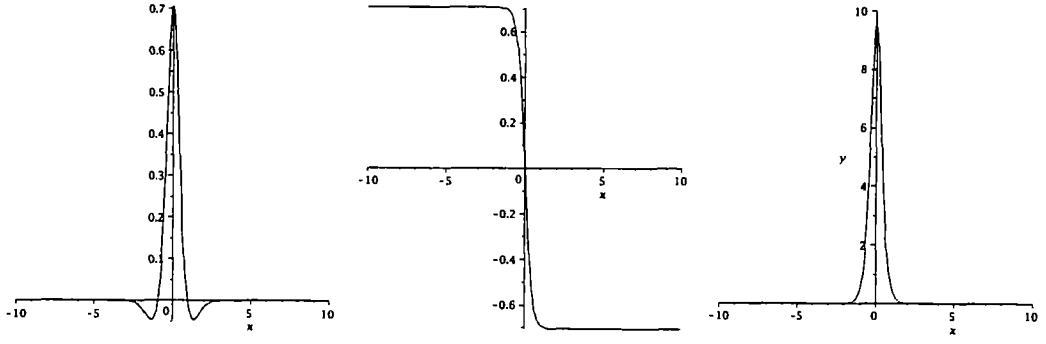

(a) Real part of u_{1-sol} (b) Real part of v_{1-sol} (c) Energy Density

Fig. 4.1: CSG one-soliton with $a = \frac{\pi}{4}$, $\Omega = 0$, $\theta = 1$ at time, $t = 0$.

Figure 4.1 graphically illustrated the CSG one-soliton solution, the energy plot shows that the solution is indeed a localised energy solution and figure 4.1(b) shows that the dual field v exhibits a SG kink-like nature.

4.4 Explicit formula for the auxiliary fields

In this section we present an explicit and general formula for the auxiliary fields, which in previous literature had only being defined up to a constant by constraint equations (4.2.10), (4.3.2). The realisation that this is possible facilitates the introduction of defects into the theory, which we discuss in chapter 5.

In Pohlmeyer and Rehren's 1979 paper *"Reduction of the two-dimensional O(n) non-linear σ-model"* [36] where the CSG theory is generated by reducing the $O(4)$ non-linear σ-model. They present an explicit formula for ω

$$\omega = \arcsin\left(\frac{\epsilon^{ab}\psi^a\psi'^b}{\sqrt{1-\psi^b\psi^b}\sqrt{1-\psi'^b\psi'^b}}\right), \tag{4.4.1}$$

where (ψ^0, ψ^1) are related to (u, w) in our notation and ω is related to the difference in the auxiliary fields θ and ψ. We denote this difference by $\alpha = \theta - \psi$.

This formula suggests that it might be possible to find an explicit formula for α in the CSG theory. As θ and ψ only appear in the combination $\alpha = \theta - \psi$ in the BT

(4.3.1) this could allow the theory to be fully determined by only considering the fields (u, w) of the new function α, as opposed to having to consider both sectors of the theory simultaneously. More explicitly the BT (4.3.1) can be written in terms of the u and w fields along with α as

$$\begin{aligned}\frac{u_t - u_x}{\sqrt{1-uu^*}} - \frac{w_t - w_x}{\sqrt{1-ww^*}}e^{i\alpha} &= -2\sqrt{\beta}\,\delta\left(w\sqrt{1-uu^*} + u\sqrt{1-ww^*}e^{i\alpha}\right), \\ \frac{u_t + u_x}{\sqrt{1-uu^*}}e^{i\alpha} + \frac{w_t + w_x}{\sqrt{1-ww^*}} &= \frac{2\sqrt{\beta}}{\delta}\left(u\sqrt{1-ww^*} - w\sqrt{1-uu^*}e^{i\alpha}\right). \end{aligned} \quad (4.4.2)$$

We continue by cross-differentiating these BT (4.4.2) and make the assumption that they imply that u and w satisfy the CSG equation. This allows differential equations in α to be produced

$$\begin{aligned} 0 &= \frac{\partial\alpha}{\partial u^*} - \frac{1}{2}\frac{u\sqrt{1-ww^*}\sin(\alpha) - i\sqrt{1-uu^*}w}{(1-uu^*)\sqrt{1-ww^*}\cos(\alpha)}, \\ 0 &= \frac{\partial\alpha}{\partial w^*} - \frac{1}{2}\frac{w\sqrt{1-uu^*}\sin(\alpha) + i\sqrt{1-ww^*}u}{(1-ww^*)\sqrt{1-uu^*}\cos(\alpha)} \end{aligned} \quad (4.4.3)$$

and similarly two differential equations for $\frac{\partial\alpha}{\partial u}$, $\frac{\partial\alpha}{\partial w}$. Equations (4.4.3) are respectively solved by

$$\begin{aligned} \alpha &= \arcsin\left[\frac{i}{2}\left(\frac{w\sqrt{1-uu^*}}{u\sqrt{1-ww^*}} + \frac{f(u,w,w^*)}{\sqrt{1-ww^*}\sqrt{1-uu^*}}\right)\right], \\ \alpha &= \arcsin\left[\frac{i}{2}\left(-\frac{u\sqrt{1-ww^*}}{w\sqrt{1-uu^*}} + \frac{g(u,u^*,w)}{\sqrt{1-ww^*}\sqrt{1-uu^*}}\right)\right]. \end{aligned} \quad (4.4.4)$$

For these solutions to be consistent it is necessary that

$$\begin{aligned} f(u,w,w^*) &= -\frac{u}{w}(1-ww^*) + h(u,w), \\ g(u,u^*,w) &= \frac{w}{u}(1-uu^*) + h(u,w). \end{aligned} \quad (4.4.5)$$

Substituting this ansatz for α into the aforementioned equations involving $\frac{\partial\alpha}{\partial u}$, $\frac{\partial\alpha}{\partial w}$, results in two simple differential equations for $h(u,w)$

$$\begin{aligned} \frac{\partial}{\partial u}h(u,w) &= \frac{w}{u^2} + \frac{1}{w}, \\ \frac{\partial}{\partial w}h(u,w) &= -\frac{u}{w^2} - \frac{1}{u}, \end{aligned} \quad (4.4.6)$$

which are solved by $h(u,v) = \frac{u}{w} - \frac{w}{u} + 2i\sin A$. This yields an explicit formula for alpha

$$\begin{aligned} \alpha &= \arcsin\left[\frac{i}{2}\left(\frac{w\sqrt{1-uu^*}}{u\sqrt{1-ww^*}} - \frac{u\sqrt{1-ww^*}}{w\sqrt{1-uu^*}} + \frac{\frac{u}{w} - \frac{w}{u} + 2i\sin A}{\sqrt{1-ww^*}\sqrt{1-uu^*}}\right)\right] \\ &= \arcsin\left[\frac{i}{2}\left(\frac{uw^* - wu^* + 2i\sin A}{\sqrt{1-ww^*}\sqrt{1-uu^*}}\right)\right]. \end{aligned} \quad (4.4.7)$$

This formula for α involves a new parameter A and reduces to the formula given by Pohlmeyer and Rehren (4.4.1) in the case when $A = 0$. Now the CSG BT (4.4.2) depend on two parameters δ and A. In the next section we use this new description to reanalyse the soliton solutions of the theory and generate a new formula for the two-soliton solution.

4.5 Complex sine-Gordon solitons II

The explicit formula for α, the difference in the auxiliary fields, presented in the previous section allow the BT to be rewritten without using the dual fields (4.4.2). As with the previous BT it can be checked that these BT imply that both u and w satisfy the CSG equation. As we have already shown BT are incredibly useful as they reduce the task of finding solutions to the CSG equation from solving 2nd order differential equations to solving 1st order differential equations. In fact by using the Theorem of Permutability, after the one-soliton solution is constructed, to generate multi-soliton solutions no more differential equations have to be solved. The BT can be thought of as a "soliton producing factory", starting with the vacuum solution $u = 0$ a one-soliton solution can be constructed then a two-soliton solution,... $u_{vac} \rightarrow u_{1-sol} \rightarrow u_{2-sol}$. To find the one-soliton solution, we substitute the simplified vacuum $u = 0$, $u^* = 0$ into the BT (4.4.2) giving

$$\begin{aligned} \frac{w_t - w_x}{\sqrt{1 - ww^*}} e^{i\alpha} &= -2\sqrt{\beta}\delta w\,, \\ \frac{w_t + w_x}{\sqrt{1 - ww^*}} &= -\frac{2\sqrt{\beta}}{\delta} w\, e^{i\alpha}\,, \end{aligned} \tag{4.5.1}$$

which are solved by

$$u_{1-sol} = \frac{\cos(a) e^{2i\sqrt{\beta}\sin(a)(t\cosh(\theta) - x\sinh(\theta))}}{\cosh(2\sqrt{\beta}\cos(a)(x\cosh(\theta) - t\sinh(\theta)))}\,. \tag{4.5.2}$$

We note that this is the same as the positive β sector soliton solution (4.3.5) presented earlier. The parameters in the soliton solution are related to the parameters in the BT by $a = A$, $e^{\theta} = \delta$. The one-soliton solution has the form of a wave packet with the phase velocity of the plane wave part $\coth(\theta)$ and group velocity (i.e. the velocity at which the localised energy moves) of $\tanh(\theta)$. The external $\cos(a)$ gives

the height of the solution. In the limits $\cos(a) \approx$ small the solution reduces to a plane wave solution and in the case where $\sin(a) = 0$ the solution becomes real. It is noted that due to the non-topological nature of the vacuum, the soliton is also non-topological. Recalling that in the dual field picture, the dual field soliton solution had a topological nature. The topological nature of the theory is now hidden away in the complicated behaviour of α. The energy

$$E_{sol} = 8\sqrt{\beta}\,|\cos(a)|\cosh(\theta) \tag{4.5.3}$$

of the soliton solution is always positive, while the momentum

$$P_{sol} = 8\sqrt{\beta}\,|\cos(a)|\sinh(\theta) \tag{4.5.4}$$

can be positive or negative. They both depend on the charge parameter a and the rapidity of the soliton θ. We illustrate the charge of the soliton in figure 4.2 showing that the charge Q is 2π periodic in a and is ill-defined at $a = 0$.

$0 < a < \frac{\pi}{2}$	$Q_{sol} = -4a + 2\pi$
$\frac{\pi}{2} < a < \pi$	$Q_{sol} = -2\pi + 4a$
$-\frac{\pi}{2} < a < 0$	$Q_{sol} = -4a - 2\pi$
$-\pi < a < -\frac{\pi}{2}$	$Q_{sol} = 4a + 2\pi$

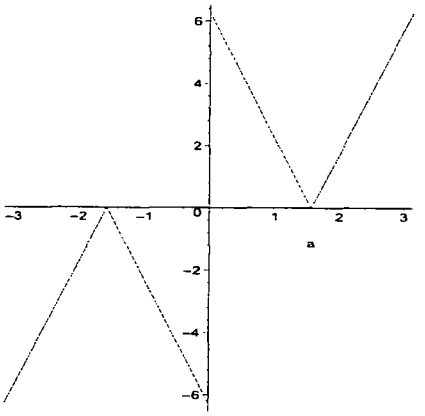

Fig. 4.2: Charge $Q(a)$ of the complex sine-Gordon soliton.

Section 2.1.4 showed that in the case of the SG theory the BT can be used again in conjunction with the Theorem of Permutability. We illustrate the ToP specifically for the CSG theory in figure 4.5. This provides an elegant way to generate the two-soliton solution from the one-soliton solution. The ToP states that the use of multiple BTs with different parameters is a commutative process. This allows the same two-soliton solution to be constructed by the two different routes in the ToP diamond. Combining the four different BTs in a particular way allows the two-soliton solution to be constructed by only solving algebraic equations. The

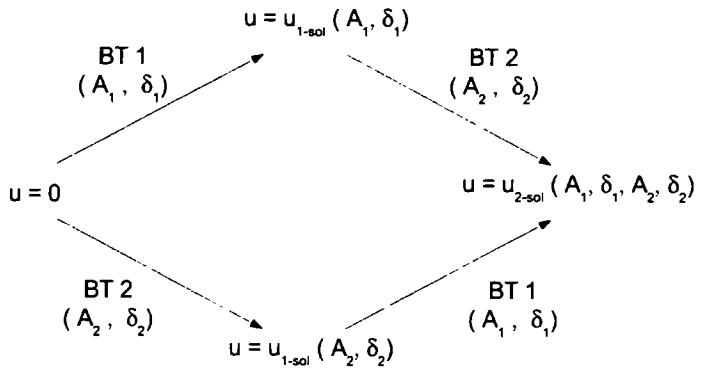

Fig. 4.3: Generating multi-soliton solutions via the Theorem of Permutability.

two-soliton solution generated

$$u_{2-sol} = \frac{(u_1\delta_1 - u_2\delta_2)(\sqrt{1-u_2u_2^*}e^{-i\alpha_2}\delta_1 - \sqrt{1-u_1u_1^*}e^{-i\alpha_1}\delta_2)}{\delta_1^2 - \delta_1\delta_2(u_1u_2^* + u_2u_1^* + 2\sqrt{1-u_1u_1^*}\sqrt{1-u_2u_2^*}\cos(\alpha_1-\alpha_2)) + \delta_2^2} + \frac{(u_1\delta_2 - u_2\delta_1)(\sqrt{1-u_1u_1^*}e^{i\alpha_1}\delta_1 - \sqrt{1-u_2u_2^*}e^{i\alpha_2}\delta_2)}{\delta_1^2 - \delta_1\delta_2(u_1u_2^* + u_2u_1^* + 2\sqrt{1-u_1u_1^*}\sqrt{1-u_2u_2^*}\cos(\alpha_1-\alpha_2)) + \delta_2^2} \tag{4.5.5}$$

is written in terms of the two constituent one-solitons in the intermediate steps in the ToP

$$u_i = \frac{N_i\cos(a_i)e^{2i\sqrt{\beta}\sin(a_i)(\cosh(\theta_i)\,t-\sinh(\theta_i)(x-c_i))}}{\cosh(2\sqrt{\beta}\cos(a_i)(\cosh(\theta_i)(x-c_i)-\sinh(\theta_i)\,t))},$$
$$u_i^* = \frac{N_i^*\cos(a_i)e^{-2i\sqrt{\beta}\sin(a_i)(\cosh(\theta_i)\,t-\sinh(\theta_i)(x-c_i))}}{\cosh(2\sqrt{\beta}\cos(a_i)(\cosh(\theta_i)(x-c_i)-\sinh(\theta_i)\,t))}, \tag{4.5.6}$$

where $N_1 = 1$, $N_2 = e^{i\psi}$. We set $N_1 = 1$ since it is only the relative phase which affects the solution. The solution also depends on the BT parameters where $a_i = A_i$, $e^{\theta_i} = \delta_i$ with the A_i dependence through

$$\alpha_i = \arcsin\left[\frac{-\sin A_i}{\sqrt{1-u_iu_i^*}}\right]. \tag{4.5.7}$$

This form of the two-soliton solution is different to the one previously written down [46] as it depends explicitly on the α parameters and is explicitly checked to satisfy the equation of motion. The two-soliton solution describes soliton-soliton scattering which we analyse in the next section.

4.6 Soliton-soliton scattering

The two-soliton solution (4.5.5) describes the totally elastic scattering process between two one-soliton solutions. That is no energy is dissipated during the interaction but the solitons do get affected in a subtle way. As in the SG theory the solitons are time-delayed or time-advanced by the scattering. In addition to this common property with the SG theory the CSG solitons are also phase shifted during the scattering. Unlike the SG kink and anti-kink, all CSG solitons are topologically trivial. There is no need differentiate between solitons and anti-solitons, although when the charge parameter is in the range $-\frac{\pi}{2} < a < 0$ the solution is sometimes referred to as an anti-soliton. In SG soliton scattering the relative signs of the parameters δ_i determines whether the scatting is soliton-soliton or soliton-anti-soliton. This terminology can be carried through to the CSG soliton scattering, however for any choice of the parameters δ_i the scattering is topologically the same and it has been shown that by the choice of the charge parameters a_i there is a duality between soliton-soliton and soliton-anti-soliton scattering [47]. Due to this, we always talk about soliton-soliton scattering.

The two-soliton solution is written in terms of its two constituent one-solitons, constituent as these are the solitons that are involved in the scattering process, albeit time and phase shifted, and constituent as these are the two one-solitons created by the intermediate steps in the ToP.

To calculate the time-delay and phase shift experienced by the two solitons during a scattering process, we analyse the two soliton solution in particular limits. Analogous to the SG calculation in section 2.1.5 we examine the solution along the line of both solitons in the far past and far future. For example to look at soliton u_1 in the far past we set $x = \tanh(\theta_1)t + x'$ and send $t \to -\infty$. This has the effect of setting $u_2 = 0$ and α_2 to one of its extremal values. We assume that $\theta_1 > \theta_2$ without loss of generality and specify $\cos(\alpha_1) = \cos(A_1)$ at $t \to -\infty$ where the u_1 soliton to the left of the u_2 soliton. For the choices of alpha to be consistent we need $\cos(\alpha_2) = -\cos(A_2)$ at $t \to -\infty$ and so $\alpha_2 = A_2 + \pi$. The other limits are shown in figure 4.4.

We calculate these four different limits of the two-soliton solution and compare

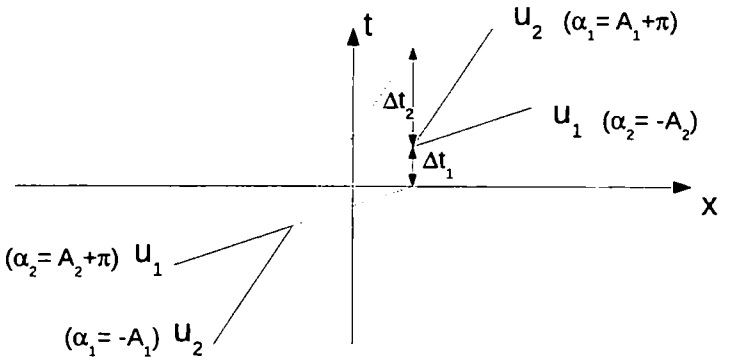

Fig. 4.4: CSG soliton-soliton scattering in general reference frame with $\theta_1 > \theta_2$.

them with the one-soliton solution

$$\begin{aligned} u_i &= \frac{e^{i\phi_i^{\pm}}\cos(a_i)e^{2i\sqrt{\beta}\sin(a_i)(\cosh(\theta_i)(t-\Delta t_i^{\pm})-\sinh(\theta_i)x)}}{\cosh(2\sqrt{\beta}\cos(a_i)(\cosh(\theta_i)x-\sinh(\theta_i)(t-\Delta t_i^{\pm})))}, \\ u_i^* &= \frac{e^{-i\phi_i^{\pm}}\cos(a_i)e^{-2i\sqrt{\beta}\sin(a_i)(\cosh(\theta_i)(t-\Delta t_i^{\pm})-\sinh(\theta_i)x)}}{\cosh(2\sqrt{\beta}\cos(a_i)(\cosh(\theta_i)x-\sinh(\theta_i)(t-\Delta t_i^{\pm})))}, \end{aligned} \tag{4.6.1}$$

which has its time shifted $t \longrightarrow t - \Delta t_i^{\pm}$ and allows a phase factor $e^{i\phi_i^{\pm}}$. Comparing the limits of the two-soliton scattering solution with the standard one-soliton solution allows the time-delays and phase shifts experienced by the solitons to be determined. Firstly in the limit of the two-soliton solution around u_1 in the far past gives

$$\begin{aligned} e^{i\phi_1^-} &= -e^{2\sqrt{\beta}\sinh(\theta_1+ia_1)\Delta t_1^-}\left(\frac{\delta_1 e^{ia_1}-\delta_2 e^{ia_2}}{\delta_2+\delta_1 e^{ia_1}e^{ia_2}}\right), \\ e^{4\sqrt{\beta}\cos(a_1)\sinh(\theta_1)\Delta t_1^-} &= \frac{(\delta_2+\delta_1 e^{ia_1}e^{ia_2})(\delta_1+\delta_2 e^{ia_1}e^{ia_2})}{(\delta_1 e^{ia_1}-\delta_2 e^{ia_2})(\delta_1 e^{ia_2}-\delta_2 e^{ia_1})}. \end{aligned} \tag{4.6.2}$$

These are the phase shift and time-delays between the actual physical incoming soliton and the mathematical entity inserted into the two-soliton solution. Similarly for the two-soliton solution around u_1 in the far future

$$\begin{aligned} e^{i\phi_1^+} &= e^{2\sqrt{\beta}\sinh(\theta_1+ia_1)\Delta t_1^+}\left(\frac{\delta_2+\delta_1 e^{ia_1}e^{ia_2}}{\delta_1 e^{ia_1}-\delta_2 e^{ia_2}}\right), \\ e^{4\sqrt{\beta}\cos(a_1)\sinh(\theta_1)\Delta t_1^+} &= \frac{(\delta_1 e^{ia_1}-\delta_2 e^{ia_2})(\delta_1 e^{ia_2}-\delta_2 e^{ia_1})}{(\delta_2+\delta_1 e^{ia_1}e^{ia_2})(\delta_1+\delta_2 e^{ia_1}e^{ia_2})}. \end{aligned} \tag{4.6.3}$$

We combine these to give the actual time-delay

$$\begin{aligned} \Delta t_1 &= \Delta t_1^+ - \Delta t_1^- \\ &= \frac{1}{2\sqrt{\beta}\cos(a_1)\sinh(\theta_1)}\ln\left(\frac{(\delta_1 e^{ia_1}-\delta_2 e^{ia_2})(\delta_1 e^{ia_2}-\delta_2 e^{ia_1})}{(\delta_2+\delta_1 e^{ia_1}e^{ia_2})(\delta_1+\delta_2 e^{ia_1}e^{ia_2})}\right) \end{aligned} \tag{4.6.4}$$

and phase shift

$$\begin{aligned} e^{i\phi_1} &= e^{i\phi_1^+}e^{-i\phi_1^-} \\ &= -e^{2\sqrt{\beta}\sinh(\theta_1+ia_1)\Delta t_1}\left(\frac{\delta_2+\delta_1 e^{ia_1}e^{ia_2}}{\delta_1 e^{ia_1}-\delta_2 e^{ia_2}}\right)^2, \end{aligned} \tag{4.6.5}$$

experienced by soliton u_1, the soliton moving with greater rapidity. Similarly for soliton u_2 in the far past gives

$$\begin{aligned} e^{i\phi_2^-} &= -e^{i\psi}e^{2\sqrt{\beta}\sinh(\theta_2+ia_2)\Delta t_2^-}\left(\frac{\delta_1+\delta_2 e^{ia_1}e^{ia_2}}{\delta_1 e^{ia_1}-\delta_2 e^{ia_2}}\right), \\ e^{4\sqrt{\beta}\cos(a_2)\sinh(\theta_2)\Delta t_2^-} &= \frac{(\delta_1 e^{ia_1}-\delta_2 e^{ia_2})(\delta_1 e^{ia_2}-\delta_2 e^{ia_1})}{(\delta_2+\delta_1 e^{ia_1}e^{ia_2})(\delta_1+\delta_2 e^{ia_1}e^{ia_2})} \end{aligned} \tag{4.6.6}$$

and in the far future

$$\begin{aligned} e^{i\phi_2^+} &= e^{i\psi}e^{2\sqrt{\beta}\sinh(\theta_2+ia_2)\Delta t_2^+}\left(\frac{\delta_1 e^{ia_1}-\delta_2 e^{ia_2}}{\delta_1+\delta_2 e^{ia_1}e^{ia_2}}\right), \\ e^{4\sqrt{\beta}\cos(a_2)\sinh(\theta_2)\Delta t_2^+} &= \frac{(\delta_2+\delta_1 e^{ia_1}e^{ia_2})(\delta_1+\delta_2 e^{ia_1}e^{ia_2})}{(\delta_1 e^{ia_1}-\delta_2 e^{ia_2})(\delta_1 e^{ia_2}-\delta_2 e^{ia_1})}. \end{aligned} \tag{4.6.7}$$

Again we combine these to obtain the time-delay

$$\begin{aligned} \Delta t_2 &= \Delta t_2^+ - \Delta t_2^- \\ &= \frac{1}{2\sqrt{\beta}\cos(a_2)\sinh(\theta_2)}\ln\left(\frac{(\delta_2+\delta_1 e^{ia_1}e^{ia_2})(\delta_1+\delta_2 e^{ia_1}e^{ia_2})}{(\delta_1 e^{ia_1}-\delta_2 e^{ia_2})(\delta_1 e^{ia_2}-\delta_2 e^{ia_1})}\right) \end{aligned} \tag{4.6.8}$$

and phase shift

$$\begin{aligned} e^{i\phi_2} &= e^{i\phi_2^+}e^{-i\phi_2^-} \\ &= -e^{2\sqrt{\beta}\sinh(\theta_2+ia_2)\Delta t_2}\left(\frac{\delta_1 e^{ia_1}-\delta_2 e^{ia_2}}{\delta_1+\delta_2 e^{ia_1}e^{ia_2}}\right)^2, \end{aligned} \tag{4.6.9}$$

experienced by the slower moving soliton. We rewrite the time-delays in a more elegant form

$$\begin{aligned} \Delta t_1 &= \frac{1}{\sqrt{\beta}\cos(a_1)\sinh(\theta_1)}\ln\left|\frac{\sinh\left(\frac{\theta_1-\theta_2}{2}+i\frac{a_1-a_2}{2}\right)}{\cosh\left(\frac{\theta_1-\theta_2}{2}+i\frac{a_1+a_2}{2}\right)}\right|, \\ \Delta t_2 &= \frac{1}{\sqrt{\beta}\cos(a_2)\sinh(\theta_2)}\ln\left|\frac{\cosh\left(\frac{\theta_1-\theta_2}{2}+i\frac{a_1+a_2}{2}\right)}{\sinh\left(\frac{\theta_1-\theta_2}{2}+i\frac{a_1-a_2}{2}\right)}\right|. \end{aligned} \tag{4.6.10}$$

There is a special frame of reference, the centre of momentum (COM) frame, where both solitons are delayed by the same amount $\Delta t_1 = \Delta t_2$, this is when

$$\sqrt{\beta}\cos(a_1)\sinh(\theta_1) + \sqrt{\beta}\cos(a_2)\sinh(\theta_2) = 0. \tag{4.6.11}$$

In this limit the time-delays agree with the formula presented in [46]. Scattering in the COM reference frame is shown in figure 4.5. In fact the figure shows a even more specialised situation, where $\theta_2 = -\theta_1$ and therefore $a_2 = a_1$ due to energy and charge conservation constraints.

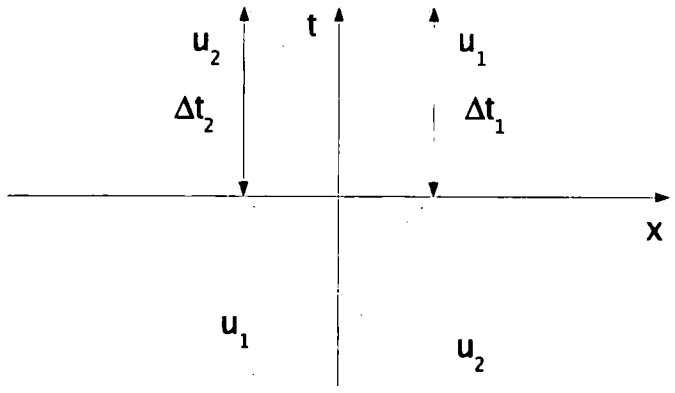

Fig. 4.5: CSG soliton-soliton scattering in COM frame, where both solitons experience the same time-delay.

4.7 Particle-soliton scattering

The CSG particle is taken to be a small fluctuation around the $u = 0$ vacuum solution and can also be thought of as a one-soliton solution in the small charge limit $a = \frac{\pi}{2} - \epsilon$. The anti-particle is similarly the one-soliton solution in a different small charge limit, one where the charge is small and negative namely $a = -\frac{\pi}{2} + \epsilon$. In these limits the soliton solution becomes

$$\begin{aligned} u_{particle} &= e^{2i\sqrt{\beta}(\cosh(\theta_p)\, t - \sinh(\theta_p)\, x)}\,, \\ u_{anti-particle} &= e^{-2i\sqrt{\beta}(\cosh(\theta_p)\, t - \sinh(\theta_p)\, x)}\,. \end{aligned} \tag{4.7.1}$$

The non-topological nature of the CSG soliton sector leads to this unusual dual description of the CSG particle. Unlike in the SG theory where the soliton and particle sectors are distinct.

We calculate the transmission factor for a particle scattering through a soliton, when the particle has greater rapidity than the soliton, by taking the $a_1 = \frac{\pi}{2}$ limit in the soliton-soliton time-delays and phase factors. This is the meson-soliton scattering described in [46]. We find that the time-delays vanish in these two limits and the phase factors reduce to the particle-soliton transmission factor

$$T_{particle/sol} = -\left(\frac{\delta + ie^{\theta_p}e^{ia}}{\delta e^{ai} - ie^{\theta_p}}\right)^2 , \tag{4.7.2}$$

which we rewrite as

$$T = \frac{\sinh\left(\frac{(\theta_p-\theta)}{2} + \frac{i}{2}(a-\frac{\pi}{2})\right)^2}{\sinh\left(\frac{(\theta_p-\theta)}{2} - \frac{i}{2}(a-\frac{\pi}{2})\right)^2} . \tag{4.7.3}$$

This limit also confirms that the soliton solution is unchanged during the particle-soliton scattering process. Similarly by taking the $a_2 = \frac{\pi}{2}$ limit in the soliton-soliton time-delays and phase factors gives the particle-soliton transmission factor for when the particle has less rapidity than the soliton

$$T_{sol/particle} = \frac{1}{T_{particle/sol}} . \tag{4.7.4}$$

These transmission factors can also be calculated by solving the linearised equations of motion around a one-soliton solution. We generate these linearised equations by substituting a one-soliton solution plus a small perturbation

$$u = u_{1-sol}(a,\theta) + \epsilon\, e(x,t) \tag{4.7.5}$$

into the CSG equation. This produces a differential equation that the small perturbation $e(x,t)$ must satisfy

$$\begin{aligned} 0 = {} & \frac{\partial^2}{\partial t^2}e(x,t) - \frac{\partial^2}{\partial x^2}e(x,t) + \frac{4i\sqrt{\beta}\cos^2(a)\sin(a)}{\cosh^2(2X)-\cos^2(a)}\frac{\partial}{\partial t}e(x,t) \\ & + \frac{4\sqrt{\beta}\cos^2(a)\tanh(2X)}{\cosh^2(2X)-\cos^2(a)}\frac{\partial}{\partial x}e(x,t) \\ & - \frac{4\beta\cos^2(a)(2\cosh^2(2X)-\cos^2(a))}{\cosh^2(2X)(\cosh^2(2X)-\cos^2(a))}e^{4i\sqrt{\beta}\sin(a)t}e^*(x,t) \\ & + \frac{4\beta(\cos^4(a)-3\cosh^2(2X)\cos^2(a)+\cosh^4(2X))}{\cosh^2(2X)(\cosh^2(2X)-\cos^2(a))}e(x,t) , \end{aligned} \tag{4.7.6}$$

where $X = \sqrt{\beta}\cos(a)(x\cosh(\theta) - t\sinh(\theta))$. We find that this is solved by

$$\begin{aligned} e(x,t) &= -i\frac{\delta e^{\theta_p} e^{ai}\cos^2(a)\, e^{4i\sqrt{\beta}\sin a(t\cosh(\theta)-x\sinh(\theta))}\, e^{-2i\sqrt{\beta}(t\cosh(\theta_p)-x\sinh(\theta_p))}}{\cosh^2(2X)(\delta + e^{ai}e^{\theta_p}i)(\delta e^{ai} - e^{\theta_p}i)} \\ &\quad + \frac{c_1\cosh^2(2X) + c_2\cosh(2X)\sinh(2X) + c_3}{\cosh^2(2X)} e^{2i\sqrt{\beta}(t\cosh(\theta_p)-x\sinh(\theta_p))}, \end{aligned} \tag{4.7.7}$$

where

$$\begin{aligned} c_1 &= \frac{-i(e^{\theta_p}e^{ai} + \delta e^{ai}i + e^{\theta_p} - \delta i)(e^{\theta_p}e^{ai} - e^{\theta_p} - \delta i - \delta e^{ai}i)}{2(-\delta i + e^{\theta_p}e^{ai})(-e^{\theta_p}i + \delta e^{ai})}, \\ c_2 &= \frac{ie^{ai}\cos(a)(e^{\theta_p} - \delta)(e^{\theta_p} + \delta)}{(-\delta i + e^{\theta_p}e^{ai})(-e^{\theta_p}i + \delta e^{ai})}, \\ c_3 &= \frac{e^{ai}e^{\theta_p}\delta\cos^2(a)}{(-\delta i + e^{\theta_p}e^{ai})(-e^{\theta_p}i + \delta e^{ai})}. \end{aligned} \tag{4.7.8}$$

To calculate the particle transmission matrix we examine the asymptotic limits of the full solution (4.7.7). In the case where the particle has greater rapidity than the soliton $\theta_p > \theta$, the limits we examine are the spatial infinities. Taking $\cos(a) > 0$ without loss of generality the solution becomes

$$\begin{aligned} e(x,t) &= (c_1 + c_2)\, e^{2i\sqrt{\beta}(t\cosh(\theta_p)-x\sinh(\theta_p))} \\ &= -\frac{\delta + ie^{\theta_p}e^{ia}}{\delta e^{ai} - ie^{\theta_p}} e^{2i\sqrt{\beta}(t\cosh(\theta_p)-x\sinh(\theta_p))}, \end{aligned} \tag{4.7.9}$$

as $x \to \infty$ and

$$\begin{aligned} e(x,t) &= (c_1 - c_2)e^{2i\sqrt{\beta}(t\cosh(\theta_p)-x\sinh(\theta_p))} \\ &= \frac{\delta e^{ai} - ie^{\theta_p}}{\delta + ie^{\theta_p}e^{ia}} e^{2i\sqrt{\beta}(t\cosh(\theta_p)-x\sinh(\theta_p))}, \end{aligned} \tag{4.7.10}$$

as $x \to -\infty$. We calculate the particle-soliton transmission matrix (where the particle's rapidity is greater) by combining the phase shifts appearing in the asymptotic limits

$$T_{particle/sol} = -\left(\frac{\delta + ie^{\theta_p}e^{ia}}{\delta e^{ai} - ie^{\theta_p}}\right)^2. \tag{4.7.11}$$

To generate the particle-soliton transmission matrix where the soliton has greater rapidity than the particle, it is the time infinities of the full solution that we examine. As $t \to \infty$ the solution becomes

$$\begin{aligned} e(x,t) &= c_1 - c_2 \\ &= \frac{\delta e^{ai} - ie^{\theta_p}}{\delta + ie^{\theta_p}e^{ia}} \end{aligned} \tag{4.7.12}$$

and as $t \to -\infty$

$$\begin{aligned} e(x,t) &= c_1 + c_2 \\ &= -\frac{\delta + ie^{\theta_p}e^{ia}}{\delta e^{ai} - ie^{\theta_p}}. \end{aligned} \tag{4.7.13}$$

Combining to give

$$T_{sol/particle} = \frac{1}{T_{particle/sol}}. \tag{4.7.14}$$

4.8 Summary

In this chapter we introduced the complex sine-Gordon theory starting with a historical overview of the development of the theory up to the present day. CSG theory can be described by either a Lagrangian of a single complex scalar filed in 1+1 D or as a perturbed WZW model. In both descriptions BT exist that allow the construction of soliton solutions. The theory has two sectors depending on the sign of β, the $SU(2)$ gauge field g in the WZW model treats both sectors of the theory together. We constructed the one-soliton solution where both the sectors are considered simultaneously, with the v field soliton solution exhibiting a kink-like nature.

We have found an explicit formula for α the difference in the auxiliary fields, where the auxiliary fields are introduced in the definition of the dual fields and appear in the BT. Previously only constraint equations on these fields were known. This allowed us to write the BT and soliton solutions without the need for the dual fields, therefore allowing the theory to be analysed using only the $\beta > 0$ sector fields and α.

The CSG soliton solution holds an additional charge due to the $U(1)$ invariance of the theory. We analysed the two-soliton solution, showing that it describes soliton-soliton scattering where the solitons experience a time-delay and a phase shift. We calculated the particle-soliton transmission factor directly and also noted that the particle is the low charge limit of the soliton solution. The non-topological nature of the soliton solution means that unlike in SG theory the soliton and particle sectors are not distinct. In the original description the dual field held the topological

information of the theory, this is now contained in the complicated definition of α. Namely that $\cos(\alpha)$ is defined by a square root, whose argument vanishes for certain values of the fields. This means at this point a different branch of the solution is needed to keep $\cos(\alpha)$ smooth. This behaviour appears in the examination of the two-soliton solution in the various temporal limits. The α description facilitates the introduction of defects into the CSG theory in the next chapter, where this behaviour of α needs to be carefully treated.

Chapter 5

CSG theory with defect

In chapter 3 we introduced the idea of separating two bulk field theories by an internal boundary or defect with the purpose of modelling an impurity or dis-continuity in the theory. We explicitly showed the construction of defect SG and ShG theories where classical integrability was maintained. Both theories were found to exhibit interesting but different properties, due to difference in the topological nature of the theories.

In the analysis of the SG defect it was discovered that it can store energy, momentum and topological charge which permits the emission and absorption of solitons. Solitons and particles can also scatter through the SG defect with the time-delay experienced by the soliton observed to be half of that experienced by a soliton scattering through another soliton.

The ShG defect has no 'solitons' solutions to emit or decay but there exists a classical bound state involving a static ShG 'solitons' on each side of the defect. We showed that there are a range of parameters where the 'solitons' infinities are "hidden behind" the defect, allowing the bound state to have finite energy.

The properties exhibited by these two theories make the construction of a CSG defect theory an interesting project. Like the SG theory the CSG has soliton solutions which suggest similar emission and absorption properties may be prevalent. The interaction between defect and solitons is expected to be more sophisticated due to the CSG solitons carrying a $U(1)$ Noether charge. Recall that they are described by a charge parameter a as well as their rapidity θ.

In this chapter first using the original 'two field' description of the CSG theory and secondly using the new description involving α we construct a CSG defect theory. The defect theory is constructed by restricting two separate CSG theories to the two halflines and by introducing a term in the Lagrangian at $x = 0$, to describe the defect. As in the case of previous studies into integrable field theories with defects despite being free to add any defect term, the term used here is carefully specified to maintain the classical integrability of the model. Although by this design no specific impurity is modelled by the defect, the defect introduced is done so as to retain the interesting mathematical properties displayed by the original bulk theory.

After constructing a classically integrable defect theory, we analyse the various solitons solutions permitted by the defect theory. To show that classical integrability is preserved we produce explicit formula for conserved defect energy and conserved defect momentum and show that the next higher spin charges can be similarly modified to be also conserved.

5.1 CSG defect in the 'two field' description

In this section we use the CSG theory described by the complex field u in the $\beta > 0$ sector and its dual field v in the $\beta < 0$ sector to construct an integrable defect theory. In this description the set up is as shown in figure 5.1, with the two CSG complex

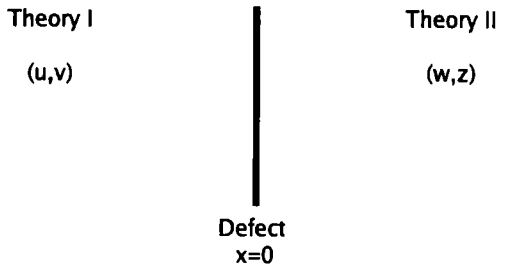

Fig. 5.1: The set up for the CSG defect theory in 'two field' description.

fields u and v restricted to the halfline $x < 0$ and the fields w and z restricted to the halfline $x > 0$. The different sector fields are related by introducing two auxiliary

fields θ and ψ

$$v = -\sqrt{1-uu^*}e^{-i\theta}\,, \qquad z = -\sqrt{1-ww^*}e^{-i\psi}\,, \tag{5.1.1}$$

recalling that the auxiliary fields θ, ψ satisfy the constraint equations (4.2.10), (4.3.2). The defect is described by terms in the Lagrangian restricted to $x = 0$, which along with contributions from the bulk create defect conditions that the left and right fields satisfy. Therefore the CSG defect Lagrangian has the form

$$L = \int_{-\infty}^{0} dx\ \mathcal{L}^{CSG}(u,v) + \int_{0}^{\infty} dx\ \mathcal{L}^{CSG}(w,z) + \left[\mathcal{L}_D(u,v,w,z)\right]\big|_{x=0}\,, \tag{5.1.2}$$

where the bulk Lagrangians $\mathcal{L}^{CSG}$ have the usual form (4.1.1) and the precise form of the defect term $\mathcal{L}_D$ is to be determined.

The CSG BT (4.3.1) can be expressed involving the $\beta > 0$ sector field and the auxiliary fields

$$\frac{e^{i\psi}\partial w^*}{\sqrt{1-ww^*}} - \frac{e^{i\theta}\partial u^*}{\sqrt{1-uu^*}} - 2\delta\sqrt{\beta}\left(e^{i\theta}w^*\sqrt{1-uu^*} + e^{i\psi}u^*\sqrt{1-ww^*}\right) = 0\,, \tag{5.1.3}$$

$$\frac{e^{-i\theta}\bar{\partial}u^*}{\sqrt{1-uu^*}} + \frac{e^{-i\psi}\bar{\partial}w^*}{\sqrt{1-ww^*}} - \frac{2\sqrt{\beta}}{\delta}\left(e^{-i\psi}u^*\sqrt{1-ww^*} - e^{-i\theta}w^*\sqrt{1-uu^*}\right) = 0\,, \tag{5.1.4}$$

recalling that $\partial \equiv \frac{\partial}{\partial z} = \frac{\partial}{\partial t} - \frac{\partial}{\partial x}$, $\bar{\partial} \equiv \frac{\partial}{\partial z} = \frac{\partial}{\partial t} + \frac{\partial}{\partial x}$. Following from the previous work on SG and ShG theories we expect that these BT are exactly the defect conditions required for classical integrability to be preserved. To check this claim, we convert the BT into equations that bare resemblance to the SG defect conditions. Taking the linear combinations

$$(5.1.3)e^{-i\psi} + (5.1.4)e^{i\psi} \qquad \text{and} \qquad (5.1.3)e^{-i\theta} + (5.1.4)e^{i\theta}\,, \tag{5.1.5}$$

give the equations

$$\begin{aligned}
\frac{\partial_x u^*}{1-uu^*} &= -\frac{\partial_t w^*}{\cos(\alpha)\sqrt{1-uu^*}\sqrt{1-ww^*}} + \frac{i\sin(\alpha)\,\partial_t u^*}{\cos(\alpha)(1-uu^*)} \\
&\quad + \frac{\delta\sqrt{\beta}}{\cos(\alpha)}\left(e^{i\alpha}w^* + u^*\frac{\sqrt{1-ww^*}}{\sqrt{1-uu^*}}\right) \\
&\quad + \frac{\sqrt{\beta}}{\cos(\alpha)\,\delta}\left(u^*\frac{\sqrt{1-ww^*}}{\sqrt{1-uu^*}} - e^{-i\alpha}w^*\right), \\
\frac{\partial_x w^*}{1-ww^*} &= -\frac{i\sin(\alpha)\,\partial_t w^*}{\cos(\alpha)(1-ww^*)} - \frac{\partial_t u^*}{\cos(\alpha)\sqrt{1-ww^*}\sqrt{1-uu^*}} \\
&\quad - \frac{\delta\sqrt{\beta}}{\cos(\alpha)}\left(w^*\frac{\sqrt{1-uu^*}}{\sqrt{1-ww^*}} + e^{-i\alpha}u^*\right) \\
&\quad + \frac{\sqrt{\beta}}{\cos(\alpha)\,\delta}\left(e^{i\alpha}u^* - w^*\frac{\sqrt{1-uu^*}}{\sqrt{1-ww^*}}\right),
\end{aligned} \tag{5.1.6}$$

where $\alpha = \theta - \psi$, as defined earlier, is the difference in the auxiliary fields and governed by the constraint equations

$$\begin{aligned}
\partial_t\alpha &= -\frac{i}{2}\left(\frac{u\partial_x u^* - u^*\partial_x u}{1-uu^*} - \frac{w\partial_x w^* - w^*\partial_x w}{1-ww^*}\right), \\
\partial_x\alpha &= -\frac{i}{2}\left(\frac{u\partial_t u^* - u^*\partial_t u}{1-uu^*} - \frac{w\partial_t w^* - w^*\partial_t w}{1-ww^*}\right).
\end{aligned} \tag{5.1.7}$$

If these (5.1.6) are the defect conditions, we should be able to generate them from the Lagrangian (5.1.2). By examining the form of the projected defect conditions and again with comparison with the SG theory, we conjecture a suitable ansatz for the defect term in the Lagrangian to be

$$\mathcal{L}_D = A_1 u_t + A_2 u_t^* + A_3 w_t + A_4 w_t^* - D(u, w, u^*, w^*, \alpha). \tag{5.1.8}$$

It has two kinds of term, one linear in the first time derivative of the fields, where the coefficients $A_i = A_i(u, w, u^*, w^*\alpha)$ are assumed to be functions of the fields and α, and the defect potential $D(u, w, u^*, w^*, \alpha)$, which is similarly a function of the fields and α.

Varying the action with respect to the fields gives the CSG equations (4.1.2) for

u and w in their respective bulk regions and the following conditions

$$\begin{aligned}\frac{\partial_x u^*}{1-uu^*} &= \frac{\partial \mathcal{L}_D}{\partial u} + \frac{\partial \mathcal{L}_D}{\partial \alpha}\frac{\partial \alpha}{\partial u} - \partial_t\left(\frac{\partial \mathcal{L}_D}{\partial u_t}\right), \\ -\frac{\partial_x w^*}{1-ww^*} &= \frac{\partial \mathcal{L}_D}{\partial w} + \frac{\partial \mathcal{L}_D}{\partial \alpha}\frac{\partial \alpha}{\partial w} - \partial_t\left(\frac{\partial \mathcal{L}_D}{\partial w_t}\right)\end{aligned} \tag{5.1.9}$$

and their complex conjugate conditions valid at $x = 0$. Using the ansatz form of $\mathcal{L}_D$ (5.1.8) we rewrite these conditions as

$$\begin{aligned}\frac{\partial_x u^*}{1-uu^*} &= (F_{21}u_t^* + F_{31}w_t + F_{41}w_t^*) - \frac{\partial D}{\partial u} - \frac{\partial D}{\partial \alpha}\frac{\partial \alpha}{\partial u}, \\ \frac{\partial_x w^*}{1-ww^*} &= -(F_{13}u_t + F_{23}u_t^* + F_{43}w_t^*) + \frac{\partial D}{\partial w} + \frac{\partial D}{\partial \alpha}\frac{\partial \alpha}{\partial w},\end{aligned} \tag{5.1.10}$$

where $F_{ij} = \frac{\partial A_i}{\partial \phi_j} - \frac{\partial A_j}{\partial \phi i}$ with $\phi = (u, u^*, w, w^*)$ and

$$\begin{aligned}\frac{\partial \alpha}{\partial u} &= \frac{i}{2}\left(-\frac{iu^*\sin(\alpha)}{\cos(\alpha)(1-uu^*)} + \frac{w^*}{\cos(\alpha)\sqrt{1-uu^*}\sqrt{1-ww^*}}\right), \\ \frac{\partial \alpha}{\partial u^*} &= \frac{i}{2}\left(-\frac{iu\sin(\alpha)}{\cos(\alpha)(1-uu^*)} - \frac{w}{\cos(\alpha)\sqrt{1-uu^*}\sqrt{1-ww^*}}\right), \\ \frac{\partial \alpha}{\partial w} &= \frac{i}{2}\left(-\frac{iw^*\sin(\alpha)}{\cos(\alpha)(1-ww^*)} - \frac{u^*}{\cos(\alpha)\sqrt{1-uu^*}\sqrt{1-ww^*}}\right), \\ \frac{\partial \alpha}{\partial w^*} &= \frac{i}{2}\left(-\frac{iw\sin(\alpha)}{\cos(\alpha)(1-ww^*)} + \frac{u}{\cos(\alpha)\sqrt{1-uu^*}\sqrt{1-ww^*}}\right).\end{aligned} \tag{5.1.11}$$

We obtain these formulae for the derivatives of α by comparing the constraint equation for $\partial_t\alpha$ (5.1.7) with $\partial_t\alpha$ expanded using the chain rule

$$\frac{\partial \alpha}{\partial t} = \frac{\partial \alpha}{\partial u}u_t + \frac{\partial \alpha}{\partial u^*}u_t^* + \frac{\partial \alpha}{\partial w}w_t + \frac{\partial \alpha}{\partial w^*}w_t^*. \tag{5.1.12}$$

In the constraint equations we eliminate the spatial derivatives of the fields by using the defect conditions (5.1.6), this leaves an expression linear in the time derivatives in the same form as (5.1.12). We compare the coefficients of the time derivatives in the two expressions to generate (5.1.11).

Comparing the different forms of the defect conditions (5.1.6) and (5.1.10) fur-

ther, gives the equations for the defect potential D

$$\begin{aligned}
\frac{\partial D}{\partial u} + \frac{\partial D}{\partial \alpha}\frac{\partial \alpha}{\partial u} = \\
-\frac{\delta\sqrt{\beta}}{\cos(\alpha)}\left(e^{i\alpha}w^* + u^*\frac{\sqrt{1-ww^*}}{\sqrt{1-uu^*}}\right) - \frac{\sqrt{\beta}}{\cos(\alpha)\delta}\left(u^*\frac{\sqrt{1-ww^*}}{\sqrt{1-uu^*}} - e^{-i\alpha}w^*\right), \\
\frac{\partial D}{\partial w} + \frac{\partial D}{\partial \alpha}\frac{\partial \alpha}{\partial w} = \\
-\frac{\delta\sqrt{\beta}}{\cos(\alpha)}\left(w^*\frac{\sqrt{1-uu^*}}{\sqrt{1-ww^*}} + e^{-i\alpha}u^*\right) + \frac{\sqrt{\beta}}{\cos(\alpha)\delta}\left(e^{i\alpha}u^* - w^*\frac{\sqrt{1-uu^*}}{\sqrt{1-ww^*}}\right)
\end{aligned} \tag{5.1.13}$$

and their complex conjugate equations and equations in F_{ij}

$$\begin{aligned}
F_{21}u_t^* + F_{31}w_t + F_{41}w_t^* &= -\frac{\partial_t w^*}{\cos(\alpha)\sqrt{1-uu^*}\sqrt{1-ww^*}} + \frac{i\sin(\alpha)\,\partial_t u^*}{\cos(\alpha)(1-uu^*)}, \\
F_{13}u_t + F_{23}u_t^* + F_{43}w_t^* &= -\frac{i\sin(\alpha)\,\partial_t w^*}{\cos(\alpha)(1-ww^*)} - \frac{\partial_t u^*}{\cos(\alpha)\sqrt{1-ww^*}\sqrt{1-uu^*}},
\end{aligned} \tag{5.1.14}$$

along with their complex conjugates. By inspection we solve (5.1.13)

$$\begin{aligned}
D &= \delta\sqrt{\beta}\left(\sqrt{1-uu^*}\sqrt{1-vv^*}(e^{i\alpha}+e^{-i\alpha}) - uw^* - u^*w\right) \\
&\quad + \frac{\sqrt{\beta}}{\delta}\left(\sqrt{1-uu^*}\sqrt{1-vv^*}(e^{i\alpha}+e^{-i\alpha}) + uw^* + u^*w\right),
\end{aligned} \tag{5.1.15}$$

which we rewrite in terms of the dual fields

$$D = \delta\sqrt{\beta}\,(v^*z + vz^* - uw^* - u^*w) + \frac{\sqrt{\beta}}{\delta}\,(v^*z + vz^* + uw^* + u^*w)\,. \tag{5.1.16}$$

It is more complicated to solve (5.1.14) for A_i, first we read off expressions for F_{ij} by matching coefficients, giving for example

$$\begin{aligned}
F_{21} &= \frac{i\sin(\alpha)}{\cos(\alpha)(1-uu^*)}, \qquad F_{31} = 0, \qquad F_{41} = -\frac{1}{\cos(\alpha)\sqrt{1-uu^*}\sqrt{1-ww^*}}, \\
F_{43} &= -\frac{i\sin(\alpha)}{\cos(\alpha)(1-ww^*)}, \qquad F_{13} = 0, \qquad F_{23} = -\frac{1}{\cos(\alpha)\sqrt{1-ww^*}\sqrt{1-uu^*}}.
\end{aligned} \tag{5.1.17}$$

It is observed that the F_{ij} are constructed to take the form of a non-abelian field strength tensor. They are automatically anti-symmetric $F_{ij} = -F_{ji}$ and satisfy the Bianchi identity

$$F_{[ij,k]} = \frac{\partial F_{ij}}{\partial \phi_k} + \frac{\partial F_{jk}}{\partial \phi_i} + \frac{\partial F_{ki}}{\partial \phi_j} = 0\,. \tag{5.1.18}$$

With this gauge theory interpretation it allows gauge choices to be made to help solve for A_i. We use two separate gauge choices $(i)A_1 = A_3 = 0$, $(ii)A_2 = A_4 = 0$ which simplify the differential equations allowing the components of the vector potential A_i to be solved for

$$\begin{aligned}
A_1 &= \frac{1}{u}\ln\left(2\sqrt{1-uu^*}\sqrt{1-ww^*}e^{-i\alpha} - 2(1-uu^*)\frac{w}{u}\right) - \frac{1}{2}\frac{\ln(w)}{u}, \\
A_2 &= \frac{1}{u^*}\ln\left(2\sqrt{1-uu^*}\sqrt{1-ww^*}e^{i\alpha} - 2(1-uu^*)\frac{w^*}{u^*}\right) - \frac{1}{2}\frac{\ln(w^*)}{u^*}, \\
A_3 &= -\frac{1}{w}\ln\left(2\sqrt{1-uu^*}\sqrt{1-ww^*}e^{i\alpha} - 2(1-ww^*)\frac{u}{w}\right) + \frac{1}{2}\frac{\ln(u)}{w}, \\
A_4 &= -\frac{1}{w^*}\ln\left(2\sqrt{1-uu^*}\sqrt{1-ww^*}e^{-i\alpha} - 2(1-ww^*)\frac{u^*}{w^*}\right) + \frac{1}{2}\frac{\ln(u^*)}{w^*},
\end{aligned} \tag{5.1.19}$$

which are rewritten in the dual fields notation

$$\begin{aligned}
A_1 &= \frac{1}{u}\ln\left(2vz^* - 2(1-uu^*)\frac{w}{u}\right) - \frac{1}{2}\frac{\ln(w)}{u}, \\
A_2 &= \frac{1}{u^*}\ln\left(2v^*z - 2(1-uu^*)\frac{w^*}{u^*}\right) - \frac{1}{2}\frac{\ln(w^*)}{u^*}, \\
A_3 &= -\frac{1}{w}\ln\left(2v^*z - 2(1-ww^*)\frac{u}{w}\right) + \frac{1}{2}\frac{\ln(u)}{w}, \\
A_4 &= -\frac{1}{w^*}\ln\left(2vz^* - 2(1-ww^*)\frac{u^*}{w^*}\right) + \frac{1}{2}\frac{\ln(u^*)}{w^*}.
\end{aligned} \tag{5.1.20}$$

We now have known formulae for the terms in the CSG defect Lagrangian D and A_i and therefore an explicit form of the CSG defect action in the 'two field' picture. This action generates the defect conditions (5.1.6) which by construction are the CSG BT (4.3.1).

Whether or not this defect theory constructed maintains the classical integrability of the bulk theory remains to be answered. For the theory to remain integrable there should be an infinite number of conserved charges, starting from the lowest spin charges, the energy and momentum as well as the Noether charge. We produce these three charges in the defect theory and show that they are conserved. The defect energy can be read straight from the Lagrangian to have the form

$$E_{def} = \int_{-\infty}^{0} dx\ \mathcal{E}^{CSG} + \int_{0}^{+\infty} dx\ \mathcal{E}^{CSG} + \left[D(u,w,u^*,w^*,v,z,v^*,z^*)\right]\Big|_{x=0}. \tag{5.1.21}$$

The conservation of the defect energy $\frac{\partial E_{def}}{\partial t} = 0$ is easily checked. The defect momentum and charge cannot be read directly from the Lagrangian and we determine

their form by asking what contribution needs to be added at the defect to ensure they are conserved. We conjecture the defect momentum and charge to have the form

$$\begin{aligned} P_{def} &= -\int_{-\infty}^{0} dx\ \frac{\partial_x u\,\partial_t u^* + \partial_x u^*\,\partial_t u}{1-uu^*} - \int_{0}^{\infty} dx\ \frac{\partial_x w\,\partial_t w^* + \partial_x w^*\,\partial_t w}{1-ww^*} + \left[\mathcal{P}_D\right]\big|_{x=0}\,, \\ Q_{def} &= i\int_{-\infty}^{0} dx\ \frac{u\,\partial_t u^* - u^*\,\partial_t u}{1-uu^*} + i\int_{0}^{\infty} dx\ \frac{w\,\partial_t w^* - w^*\,\partial_t w^*}{1-ww^*} + \left[\mathcal{Q}_D\right]\big|_{x=0}\,, \end{aligned} \tag{5.1.22}$$

where $\mathcal{P}_D$, $\mathcal{Q}_D$ are specifically chosen to make the expressions conserved. Demanding the conservation of defect momentum $\frac{\partial P_{def}}{\partial t} = 0$ leads to the following equations

$$\begin{aligned} \frac{\partial \mathcal{P}_D}{\partial u} &+ \frac{\partial \mathcal{P}_D}{\partial \alpha}\frac{\partial \alpha}{\partial u} = \\ &\frac{\delta\sqrt{\beta}}{\cos(\alpha)}\left(-e^{i\alpha}w^* - u^*\frac{\sqrt{1-ww^*}}{\sqrt{1-uu^*}}\right) + \frac{\sqrt{\beta}}{\cos(\alpha)\delta}\left(u^*\frac{\sqrt{1-ww^*}}{\sqrt{1-uu^*}} - e^{-i\alpha}w^*\right)\,, \\ \frac{\mathcal{P}_D}{\partial w} &+ \frac{\partial \mathcal{P}_D}{\partial \alpha}\frac{\partial \alpha}{\partial w} = \\ &\frac{\delta\sqrt{\beta}}{\cos(\alpha)}\left(-w^*\frac{\sqrt{1-uu^*}}{\sqrt{1-ww^*}} - e^{-i\alpha}u^*\right) + \frac{\sqrt{\beta}}{\cos(\alpha)\delta}\left(-e^{i\alpha}u^* + w^*\frac{\sqrt{1-uu^*}}{\sqrt{1-ww^*}}\right)\,, \end{aligned} \tag{5.1.23}$$

which are solved by

$$\mathcal{P}_D = -\delta\sqrt{\beta}\,(-v^*z - vz^* + u^*w + uw^*) - \frac{\sqrt{\beta}}{\delta}\,(v^*z + vz^* + u^*w + w^*u)\,. \tag{5.1.24}$$

Similarly charge conservation gives the equation

$$\frac{\partial \mathcal{Q}_D}{\partial t} = i\left(\frac{u^*\partial_x u - u\partial_x u^*}{1-uu^*} - \frac{w^*\partial_x w - w\partial_x w^*}{1-ww^*}\right)\,, \tag{5.1.25}$$

which is solved by

$$\mathcal{Q}_D = 2(\theta - \psi)\,. \tag{5.1.26}$$

We have formulated conserved defect energy, momentum and charge and in appendix A.3 we show that defect terms can be added to the next higher spin charges making them conserved, going along way to show that the CSG defect theory is classically integrable.

5.2 Soliton solutions in the 'two field' description

Having constructed a CSG defect theory, in this section we analyse the different solutions to the bulk CSG equations and defect conditions. We start with an analysis of the vacuum and then investigate how solitons interact with the defect. Placing the bulk vacuum on both sides of the defect

$$(u, v) = (0, e^{i\Omega_u}), \qquad (w, z) = (0, e^{i\Omega_w}), \tag{5.2.1}$$

trivially solves the CSG equations in the bulk regions and the defect conditions (4.3.1). The energy, momentum and charge for this configuration are

$$E = 2\sqrt{\beta}\left(\delta + \frac{1}{\delta}\right)\cos(\Omega_u - \Omega_w), \quad P = -2\sqrt{\beta}\left(\delta - \frac{1}{\delta}\right)\cos(\Omega_u - \Omega_w),$$
$$Q = -2(\Omega_u - \Omega_w). \tag{5.2.2}$$

The value of the dual field on each side of the defect affects the vacuum energy. The degenerate vacuum of the theory with $\delta > 0$ is when $(\Omega_v - \Omega_w) = \pi$, explicitly

$$(u, v) = (0, e^{i\Omega_u}), \qquad (w, z) = (0, -e^{i\Omega_u}), \tag{5.2.3}$$

with vacuum energy

$$E_{vac} = -2\sqrt{\beta}\left(\delta + \frac{1}{\delta}\right). \tag{5.2.4}$$

The energy is at its maximum with $\delta > 0$ when $(\Omega_v - \Omega_w) = 0$ with the difference between these two extremals of the energy being exactly the energy of a soliton with rapidity $e^{\theta} = \delta$ and maximum charge $a = 0$. These extremals swap roles if the defect rapidity is negative $\delta < 0$.

Following from the property of the SG defect that it can both emit and absorb soliton solutions, we investigate whether the same phenomena is allowed in the CSG defect theory. Naïvely it might be thought that defects are unable to absorb or emit solitons in the CSG model, since at early/late times the bulk configuration would look like the vacuum near the defect and the conserved charges carried by the absorbed or emitted soliton would still have to be accounted for. However the fact that the defect can have different energies depending on the phase of the dual fields, suggests that energy can be transferred to and from the defect and therefore allow the possibility of soliton absorption and emission.

5.2.1 Soliton emission from the defect

First we consider the situation where a defect possibly decays by emitting a soliton, this process is modelled by placing the null solution on the left hand side of the defect and a right-moving one-soliton solution on the right hand side. Explicitly the field configurations are

$$\begin{aligned} u &= 0, \\ v &= e^{i\Omega}, \\ w &= e^{di}\cos(a)\,\frac{\exp(2i\sqrt{\beta}\sin(a)(\cosh(\theta)\,t-(x-c)\sinh(\theta)))}{\cosh(2\sqrt{\beta}\cos(a)((x-c)\cosh(\theta)-t\sinh(\theta)))}, \\ z &= -e^{ie}\left(\cos(a)\tanh(2\sqrt{\beta}\cos(a)((x-c)\cosh(\theta)-t\sinh(\theta)))-i\sin(a)\right). \end{aligned} \tag{5.2.5}$$

The one-soliton solution has rapidity $\theta > 0$, charge parameter a and has freedom on the phase of the field, phase of the dual field and position of the soliton, governed respectively by the parameters c, d, e. The vacuum on the left of the defect is chosen with the dual phase Ω without loss of generality. In the far past the soliton is at left infinity hidden far behind the defect so the fields are in the vacuum configuration around the defect with some phase difference between the two dual fields. As time evolves the right-moving soliton passes through $x = 0$ and is emitted by the defect. The soliton continues to moves away to right infinity leaving a different vacuum configuration around the defect as time approaches positive infinity. The defect conditions put a constraint

$$\delta\, e^{ei} + e^{\theta}\, e^{\Omega i} = 0 \tag{5.2.6}$$

on the parameters in the solutions, generated by substituting the solutions into the defect conditions and simplifying the expressions. For a defect with $\delta > 1$ the constraint becomes

$$\delta = e^{\theta}, \qquad e^{ei} = e^{(\Omega\pm\pi)i} \tag{5.2.7}$$

and for $\delta < 1$

$$\delta = -e^{\theta}, \qquad e^{ei} = e^{\Omega i}. \tag{5.2.8}$$

Analysing the $\delta > 1$ case with $\cos(a) > 0$ then at $t \longrightarrow +\infty$ the field configuration is

$$(u, v) = (0,\ e^{i\Omega}), \qquad (w, z) = (0,\ e^{i(\Omega+a\pm\pi)}) \tag{5.2.9}$$

and at $t \to -\infty$

$$(u, v) = (0,\ e^{i\Omega}), \qquad (w, z) = (0,\ e^{i(\Omega - a)}). \tag{5.2.10}$$

This shows that the energy of defect before the emission is positive $E = 2\sqrt{\beta}(\delta + \delta^{-1})\cos(a)$ and after the soliton has been emitted the defect has negative energy $E = 2\sqrt{\beta}(\delta + \delta^{-1})\cos(\pi - a)$. The energy difference is $\Delta E = 4\sqrt{\beta}(\delta + \delta^{-1})\cos(a)$, which as needs to be the case for total energy conservation is the energy of the emitted soliton with rapidity $e^{\theta} = \delta$ and charge parameter a. The change in energy stored on the defect is due to the phase of the dual field of the one-soliton solution being different before and after the soliton has been emitted.

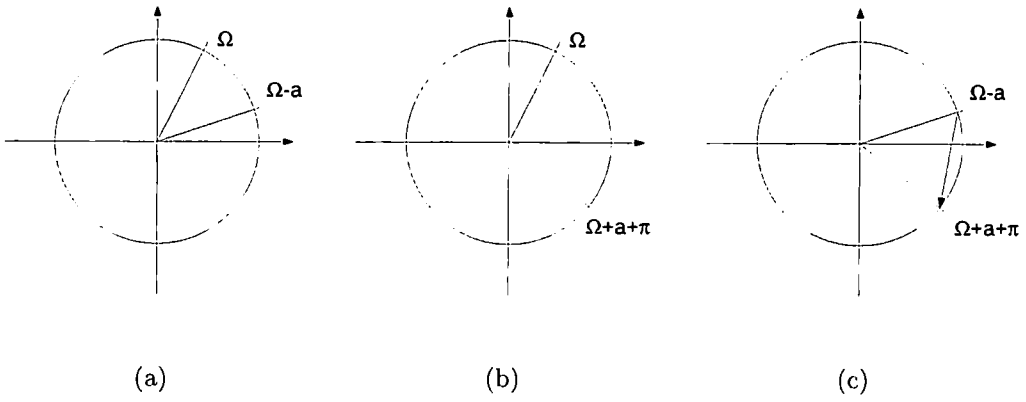

Fig. 5.2: The evolution of the dual field z during the emission of a soliton.

Figure 5.2 shows the change in the z-field during the process with the values $0 < a < \Omega < \frac{\pi}{2}$. Figure 5.2(a) shows the initial values of the dual fields either side of the defect, the v-field with phase Ω and the z-field with phase $\Omega - a$. The initial energy of the defect depends on the difference in these phases and is proportional to $\cos(\Omega - (\Omega - a)) = \cos(a) > 0$. Figure 5.2(b) shows the final values of the dual fields, with the v-field unaltered and the z-field now at the pure phase $a + \Omega + \pi$. Again the energy depends on the difference now proportional to $\cos(\Omega - (\Omega + a + \pi)) = \cos(\pi + a) < 0$. The arrow in figure 5.2(c) indicates the path along which the z-field evolves. The modulus of the field does not remain unitary for all time and the path it follows is a chord across the unit circle. This is easier to see with the case $\Omega = 0$, the z-field simplifies to

$$z = \cos(a)\tanh(2\sqrt{\beta}\cos(a)((x - c)\cosh(\theta) - t\,\sinh(\theta))) - i\sin(a)\,, \tag{5.2.11}$$

where only the real part is now time dependent. Figure 5.3(c) shows the evolution

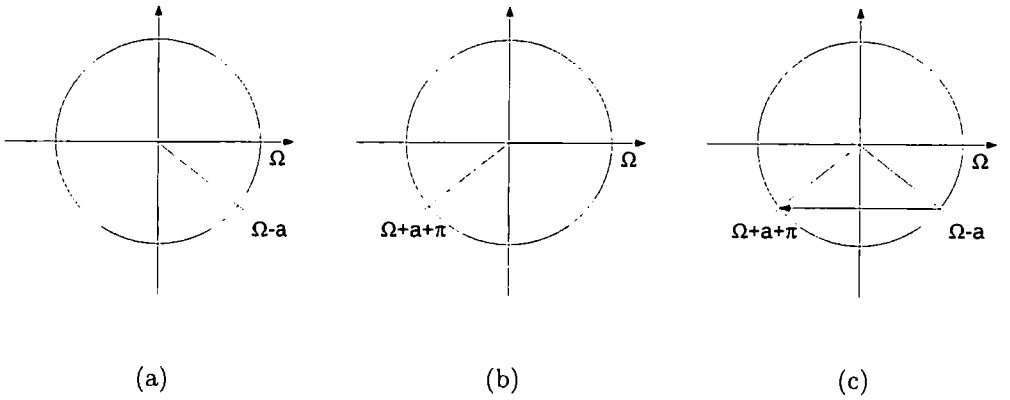

(a) (b) (c)

Fig. 5.3: The evolution of the dual field z during the emission of a soliton, $\Omega = 0$.

of z with $\Omega = 0$. Since the imaginary part does not change, the path it evolves along is a horizontal chord from one side of the unit circle to the other. The change in the dual fields at the defect is also shown in figure 5.4, which plots the real parts of the dual field v and z with time evolving from the figure 5.4(a) to 5.4(d). They

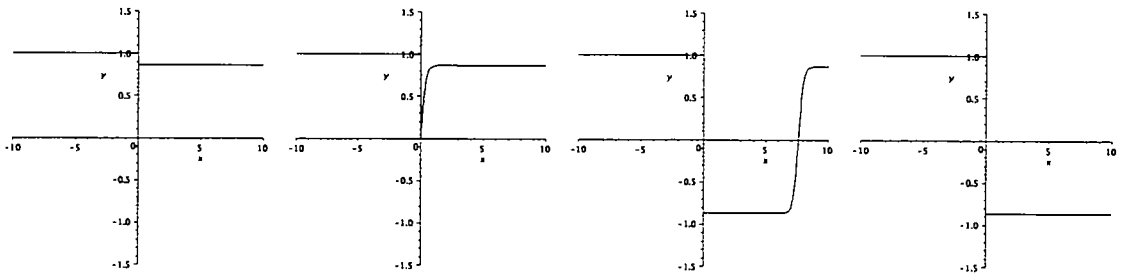

(a) (b) (c) (d)

Fig. 5.4: The evolution of the real parts of the dual fields v and z during the emission of a soliton with $\Omega = 0$, $a = \frac{\pi}{6}$, time flowing (a) - (d).

show the kink-like nature of the CSG soliton's dual field which displays the theory's topological nature. Before the emission the real part of the z-field at the defect has the value $\cos(a) = \frac{\sqrt{3}}{2}$ and afterwards $\cos(\pi - a) = -\frac{\sqrt{3}}{2}$, in between it changes smoothly between these two values as the soliton is emitted from the defect. Figure 5.5 also illustrates this emission process by plotting the real part of the fields u and w, showing the oscillating nature of the CSG soliton moving away from the defect leaving the fields at the defect the same $u = 0$, $w = 0$ before and after the emission.

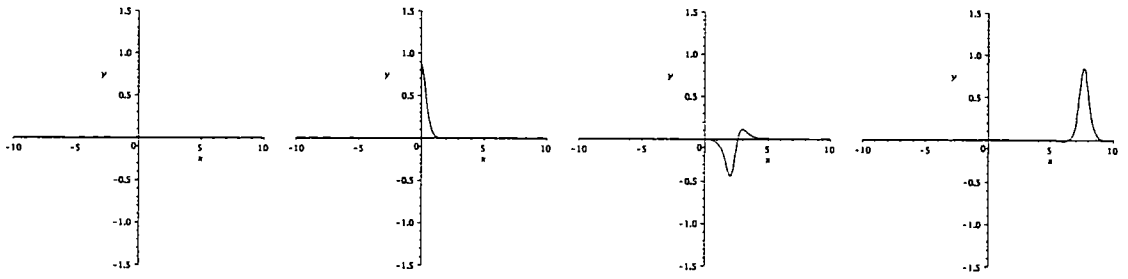

(a) (b) (c) (d)

Fig. 5.5: The evolution of the real parts of the fields u and w during the emission of a soliton with $\Omega = 0$, $a = \frac{\pi}{6}$, time flowing (a) - (d).

The defect that emits a maximally charged soliton $a = 0$ is the defect which initially has the maximum energy. For this the dual fields initially have the same phase

$$\Omega_u = \Omega_w = \Omega \tag{5.2.12}$$

and after the soliton has been emitted the dual fields are at anti-podal points across the unit circle. In the case when $\Omega = 0$ and $a = 0$ the path of the z-field is along the real axis from 1 to -1.

As with the energy it is easy to check the conservation of momentum and charge during these emission processes, before the emission the defect has the charges

$$E_{before} = 2\sqrt{\beta}\left(\delta + \frac{1}{\delta}\right)\cos(a), \quad P_{before} = 2\sqrt{\beta}\left(\delta - \frac{1}{\delta}\right)\cos(a),$$
$$Q_{before} = -2a \tag{5.2.13}$$

and after

$$E_{after} = -2\sqrt{\beta}\left(\delta + \frac{1}{\delta}\right)\cos(a), \quad P_{after} = -2\sqrt{\beta}\left(\delta - \frac{1}{\delta}\right)\cos(a),$$
$$Q_{after} = 2a - 2\pi \tag{5.2.14}$$

with the emitted soliton having

$$E_{sol} = 8\sqrt{\beta}\cosh(\theta)\cos(a), \quad P_{sol} = 8\sqrt{\beta}\sinh(\theta)\cos(a),$$
$$Q_{sol} = 2\pi - 4a. \tag{5.2.15}$$

We have shown that the defect with maximum energy can decay to the vacuum defect by emitting a maximally charged soliton $a = 0$ and that any other defect with positive energy can decay to a defect with equal and opposite negative energy. The constraints from the defect conditions show that for a defect to emit a right-moving soliton it has to be described by $|\delta| > 1$ and this value determines the rapidity of the soliton emitted, but what charge does the emitted soliton have? The charge of the soliton that is emitted depends on the difference between the phases of the dual fields at the defect, explicitly $a = \Omega_u - \Omega_w$. There is no restriction on the charge of the solitons that can be emitted by a defect as long as the previous relationship holds.

The vacuum defect is a stable object by definition and in fact only positive energy defects can emit a soliton. Therefore all negative energy defects are stable. This is a consequence of the property that each positive energy defect only decays into a defect with the equal and opposite negative energy and therefore the energy of the emitted soliton is always twice that of original defect. The zero energy defect with $\Omega_u - \Omega_w = \frac{\pi}{2}$ is also stable as the soliton it emits has zero charge and in this limit the solution collapses to a null solution.

5.2.2 Soliton absorption by the defect

Having thoroughly analysed the emission of a CSG soliton, we now examine the possibility of defects absorbing a soliton. The set up to model the absorption is a right-moving one-soliton solution on the left side of the defect and the vacuum solution on the right

$$\begin{aligned} u &= e^{di}\cos(a)\,\frac{\exp(2i\sqrt{\beta}\sin(a)(\cosh(\theta)\,t-(x-c)\sinh(\theta)))}{\cosh(2\sqrt{\beta}\cos(a)((x-c)\cosh(\theta)-t\sinh(\theta)))}\,, \\ v &= -e^{ie}\left(\cos(a)\tanh(2\sqrt{\beta}\cos(a)((x-c)\cosh(\theta)-t\sinh(\theta)))-i\sin(a)\right)\,, \\ w &= 0\,, \\ z &= e^{i\Omega}\,, \end{aligned} \tag{5.2.16}$$

with freedom on the positions and phases of the one-soliton solution given by c, d, e. We substitute these solutions into the defect conditions and generate the constraint

$$\delta\, e^{ei} - e^{\theta}\, e^{\Omega i} = 0\,, \tag{5.2.17}$$

which as for the the emission case does not put any restriction on the initial position of the soliton c and the relative phase of the u-field d. This is expected as the initial position of the soliton solution can be absorbed into a redefinition of time and it is the phase difference between the left and right fields that matters and since $w = 0$ it has no phase, d is unrestrained. The constraint separates, if $\delta > 1$ then

$$\delta = e^{\theta}, \quad e = \Omega, \tag{5.2.18}$$

while if $\delta < 1$ then

$$\delta = -e^{\theta}, \quad e = \Omega \pm \pi. \tag{5.2.19}$$

The constraint again shows that rapidity of the soliton that can be absorbed is determined by the defect rapidity parameter and the phase of the dual field of the soliton must be related to the phase of the dual field of the vacuum. Analysing the situation with $\delta > 1$, then the fields at the defect initially have the values

$$(u,\ v) = (0,\ e^{i(\Omega - a + \pi)})\,, \quad (w, z) = (0, e^{i\Omega}) \tag{5.2.20}$$

and after the absorption

$$(u,\ v) = (0,\ e^{i(\Omega + a)})\,, \quad (w, z) = (0, e^{i\Omega})\,. \tag{5.2.21}$$

The evolution of the the dual field v for $0 < a \approx \Omega < \frac{\pi}{2}$ is shown in figure 5.6(c). Figure 5.7 shows the evolution of the real part of dual fields v and z for the values $\Omega = a = \frac{\pi}{3}$ with time progressing from figure 5.7(a) to 5.7(d). Figure 5.7 again shows the kink-like nature of the dual field of the one-soliton solution. It illustrates the soliton moving towards the defect before being absorbed by the defect, with the value of the field at the defect changing during the process. The real part of the v-field evolves smoothly from its initial value of -1 to its final value of $-\frac{1}{2}$, with the field taking the approximate path of the chord shown in figure 5.6(c). For $\delta > 1$ and $0 < a < \frac{\pi}{2}$ the defect before absorption has

$$E_{before} = -2\sqrt{\beta}\left(\delta + \frac{1}{\delta}\right)\cos(a)\,, \quad P_{before} = -2\sqrt{\beta}\left(\delta - \frac{1}{\delta}\right)\cos(a)\,,$$

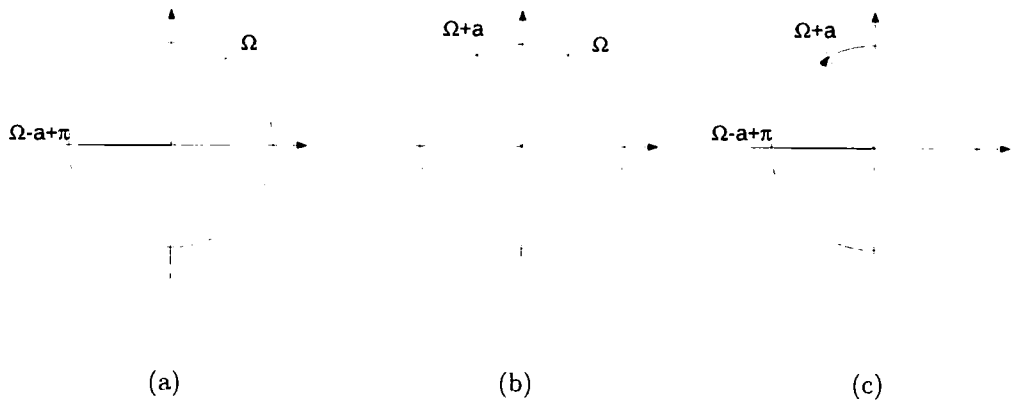

Fig. 5.6: The evolution of the dual field v during the absorption of a soliton.

$$Q_{before} = 2a - 2\pi \tag{5.2.22}$$

and after

$$E_{after} = 2\sqrt{\beta}\left(\delta + \frac{1}{\delta}\right)\cos(a)\,, \quad P_{after} = 2\sqrt{\beta}\left(\delta - \frac{1}{\delta}\right)\cos(a)\,, \quad Q_{after} = -2a, \tag{5.2.23}$$

with the absorbed soliton having

$$E_{sol} = 8\sqrt{\beta}\cosh(\theta)\cos(a)\,, \quad P_{sol} = 8\sqrt{\beta}\sinh(\theta)\cos(a)\,, \quad Q_{sol} = 2\pi - 4a. \tag{5.2.24}$$

These formulae show explicitly the energy, momentum and charge conservation during the soliton absorption, with for example $E_{before} + E_{sol} = E_{after}$ when the constraint (5.2.18) is used.

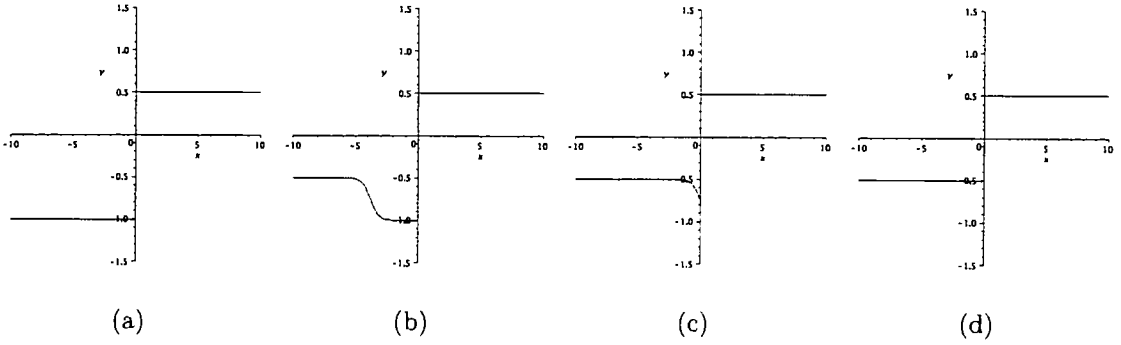

Fig. 5.7: The evolution of the real parts of the dual fields v and z during the absorption of a soliton with $\Omega = \frac{\pi}{3}$, $a = \frac{\pi}{3}$.

Analysing these processes has shown that the defect has different amounts of energy, momentum and charge when the dual fields take different values, this allows

the CSG defect to absorb and emit solitons. For a defect to emit a soliton the initial energy had to be positive and likewise for a defect to be able to absorb a soliton it has to have negative energy. That completes the analysis of the soliton absorption and emission. The next question we investigate is what happens to solitons approaching a defect that are not absorbed?

5.2.3 Soliton scattering with the defect

To analyse the situation of a soliton scattering through the defect, we consider the field configurations of a one-soliton solution on both sides of the defect

$$\begin{aligned}
u &= \frac{\cos(a)\, e^{2i\sqrt{\beta}\sin(a)(\cosh(\theta)\, t-\sinh(\theta)(x-c))}}{\cosh(2\sqrt{\beta}\cos(a)((x-c)\cosh(\theta)-t\sinh(\theta)))}\,, \\
v &= -\Big(\cos(a)\tanh(2\sqrt{\beta}\cos(a)((x-c)\cosh(\theta)-t\sinh(\theta)))-i\sin(a)\Big)\,, \\
w &= \frac{e^{fi}\cos(a)\, e^{2i\sqrt{\beta}\sin(a)(\cosh(\theta)\, t-\sinh(\theta)(x-d))}}{\cosh(2\sqrt{\beta}\cos(a)((x-d)\cosh(\theta)-t\sinh(\theta)))}\,, \\
z &= -e^{ei}\Big(\cos(a)\tanh(2\sqrt{\beta}\cos(a)((x-d)\cosh(\theta)-t\sinh(\theta)))-i\sin(a)\Big)\,.
\end{aligned} \tag{5.2.25}$$

These are not the most general choices of solution as we have set the rapidity and charge parameter to be the same on each side of the defect. We make this choice to allow the possibility that energy and charge can be conserved. There is freedom in the solutions given by the parameters c, d, e, f, which allow phase and spatial shifts between the left and right solutions. Substituting these solutions into the defect conditions and expanding as a time series, we generate the constraints

$$\begin{aligned}
e^{2\sqrt{\beta}\, c\cosh(\theta-ia)} &= -e^{2\sqrt{\beta}\, d\cosh(\theta-ia)}\frac{e^{-fi}(\delta e^{ia}e^{ie}-e^{\theta})}{\delta e^{ia}+e^{ei}e^{\theta}}\,, \\
e^{2\sqrt{\beta}\, c\cosh(\theta+ia)} &= -e^{2\sqrt{\beta}\, d\cosh(\theta+ia)}\frac{e^{fi}(\delta-e^{ai}e^{\theta}e^{ei})}{\delta e^{ei}+e^{ai}e^{\theta}}\,.
\end{aligned} \tag{5.2.26}$$

We combine these two constraints

$$e^{4\sqrt{\beta}\, c\cosh(\theta)\cos(a)} = e^{4\sqrt{\beta}\, d\cosh(\theta)\cos(a)}\frac{(\delta e^{ia}e^{ie}-e^{\theta})(\delta-e^{ai}e^{\theta}e^{ei})}{(\delta e^{ia}+e^{ei}e^{\theta})(\delta e^{ei}+e^{ai}e^{\theta})} \tag{5.2.27}$$

and reinterpret as a time-delay

$$\Delta t = \frac{1}{4\sqrt{\beta}\,\sinh(\theta)\cos(a)}\ln\left[\frac{(\delta e^{ia}e^{ie}-e^{\theta})(\delta-e^{ai}e^{\theta}e^{ei})}{(\delta e^{ia}+e^{ei}e^{\theta})(\delta e^{ei}+e^{ai}e^{\theta})}\right] \tag{5.2.28}$$

and phase shift

$$e^{i\phi} = e^{2\sqrt{\beta}\sinh(\theta+ia)\Delta t}\frac{\delta e^{ei}+e^{\theta}e^{ai}}{e^{\theta}e^{ai}e^{ei}-\delta} \tag{5.2.29}$$

on the right hand side soliton. Therefore a soliton that does not get absorbed by the defect scatters through the defect experiencing a time-delay and phase shift. This is analogous to the SG theory where a scattering SG soliton experienced a time-delay. The extra phase freedom means that a phase shift as well as time-delay is experienced by a scattering CSG soliton. In SG theory the soliton-defect scattering can be flavour changing, as with the soliton-soliton scattering all CSG soliton-defect scattering are topologically the same.

This scattering process limits to the previously studied absorption and emission cases where the poles and zeroes occur inside the logarithm. Absorption is the limit where the time-delay $\Delta t \to +\infty$, which corresponds to where the poles occur, for example for $\delta > 1$ when $\delta = e^{\theta}$ and $a = e \pm \pi$. Similarly emission is the limit when the time-delay $\Delta t \to -\infty$, which corresponds to where the zeroes occur, for example for $\delta > 1$ when $\delta = e^{\theta}$ and $a = -e$. Around these particular values the soliton experiences the largest time-delays, positive or negative. Figure 5.8 shows

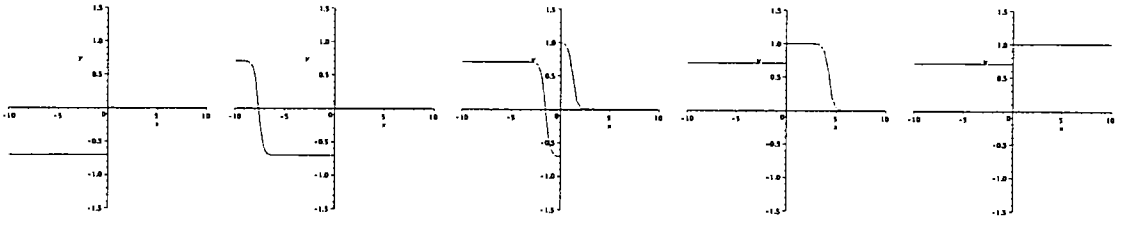

(a) (b) (c) (d) (e)

Fig. 5.8: The evolution of the real parts of the dual fields v and z during the scattering of a soliton with $\theta = 1$, $\delta = e^{\theta} + 0.01$, $a = -e = \frac{\pi}{4}$.

the real parts of the dual fields with the parameters slightly perturbed away from the emission scenario, with time progressing from figure 5.8(a) to 5.8(e). It shows the initial set up with the real parts of the dual fields at $v_R = -\frac{1}{\sqrt{2}}$ and $z_R = 0$ with a soliton with charge $a = \frac{\pi}{4}$ and rapidity $\theta = 1$ moving in from left infinity. The left kink moves towards the defect and the right kink bridging different vacua is emitted by the defect before the left kink has fully reached the defect. This is an example of

scattering with a negative time-delay or equivalently the soliton experiences a time-advance. The right kink then moves away to right infinity leaving the real part of the dual fields at $v_R = \frac{1}{\sqrt{2}}$ and $z_R = 1$. The difference in the real part of the dual fields at the defect is different before and after the scattering. This is compatible with the initial and final defect energies been equal as the phase difference between the dual fields at the defect is the same before and after. In this example $\Omega_u - \Omega_w = \frac{\pi}{4}$. The defects initial and final energy have to be the same for energy to be conserved, since the time-delayed and phase shifted soliton has the same energy as the original soliton $E_{sol} = 8\sqrt{\beta}\cosh(\theta)\cos(a)$. The total energy of the whole system in this process is

$$E = 8\sqrt{\beta}\cos(a)\cosh(\theta) + 2\sqrt{\beta}\cos(e)\left(\delta + \frac{1}{\delta}\right), \tag{5.2.30}$$

which we calculate by substituting the values of the fields (5.2.25) in the energy formula (5.1.21) and simplify using (5.2.26). A less computationally extensive method to derive this energy formula is to use the fact that the energy is conserved. This allows either the simplified situation of the initial or final state to be used to calculate the energy. This reduces the calculation to adding the energy of the soliton and the energy of the defect, since the soliton and defect are infinitely separated at $t \to \pm\infty$. By inspection (5.2.30) can be seen to have this form. The total momentum and charge for the system of a soliton scattering through a defect are similarly calculated for $0 < a < \frac{\pi}{2}$ to be

$$P = 8\sqrt{\beta}\cos(a)\sinh(\theta) + 2\sqrt{\beta}\cos(e)\left(\delta - \frac{1}{\delta}\right), \qquad Q = -4a + 2\pi + 2e\,. \tag{5.2.31}$$

Figure 5.9 shows an example of a scattering process where the parameters are set near to the absorption limit of $\delta = e^{\theta}$ and $a = e \pm \pi$. This produces a scattering process where the outgoing soliton experiences a positive time-delay. Time evolves from figure 5.9(a) to 5.9(e). It shows the initial state where the real part of the dual fields are $v_R = -\frac{1}{\sqrt{2}}$ and $z_R = 1$. A kink solution comes in from left infinity and is totally absorbed before the kink on the right is emitted from the defect. This moves away to right infinity, leaving the fields $v_R = \frac{1}{\sqrt{2}}$ and $z_R = 0$ in the final state. The phase difference between the dual fields at the defect is the same before and after the scattering $\Omega_u - \Omega_w = \frac{3\pi}{4}$. Again this is not in conflict with figure 5.9 that shows

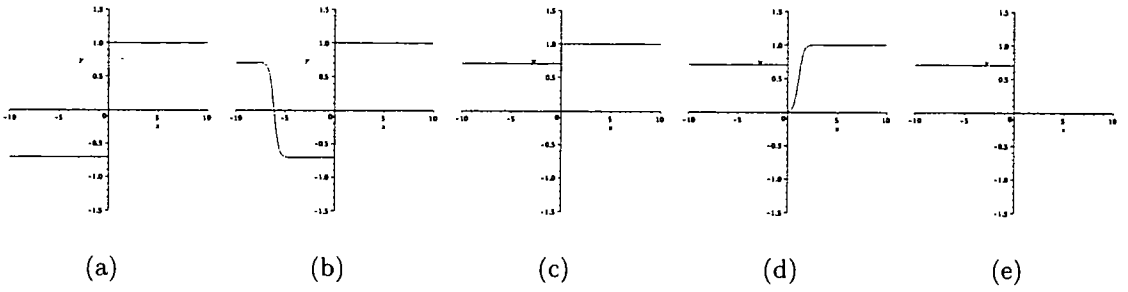

(a) (b) (c) (d) (e)

Fig. 5.9: The evolution of the real parts of the dual fields v and z during the scattering of a soliton with $\theta = 1$, $\delta = e^{\theta} + 0.01$, $a = e + \pi = \frac{\pi}{4}$.

the difference in the real parts of the dual field to be different before and after the scattering.

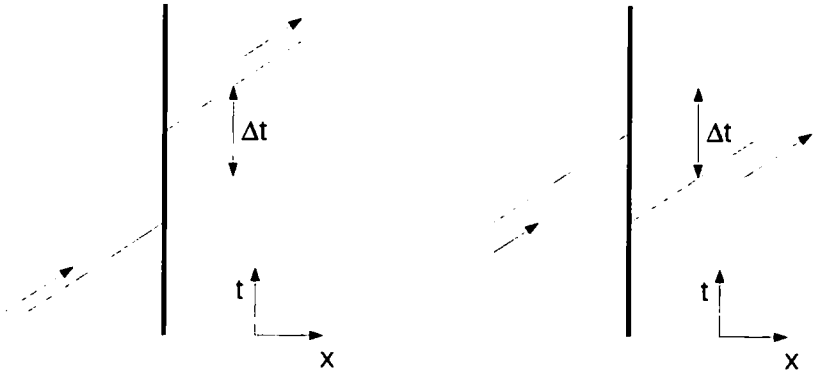

(a) (b)

Fig. 5.10: World line of a soliton experiencing a (a) time-delay (b) time-advance.

Figure 5.10 illustrates the paths in space-time the soliton takes when experiencing a time-delay or time-advance and figure 5.11 displays the progress of the energy profile of the soliton, where time flowing from 5.11(a) to 5.11(d). It shows that the energy of the soliton remains the same before and after the scattering with the defect and that the soliton experiences a time-delay, since the incoming soliton reaches the defect before the outgoing soliton leaves the defect.

Whether the soliton experiences a time-delay or time-advance is determined by the energy of the initial defect. If the energy of the defect is positive, as in the case shown in figure 5.8 where $E \sim \cos(e) = \cos(\frac{\pi}{4}) > 0$, then the soliton experiences a

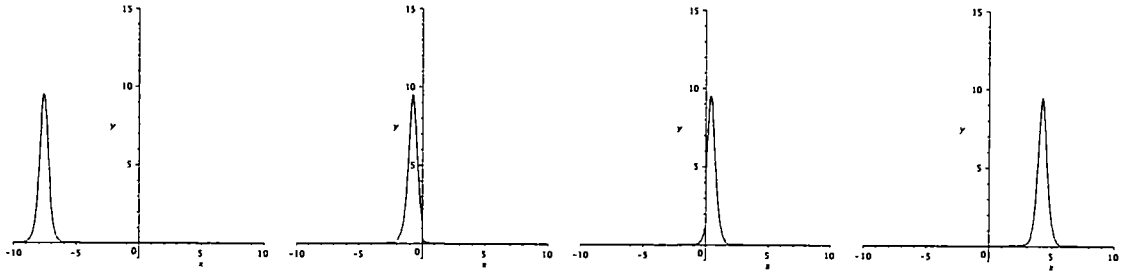

(a) (b) (c) (d)

Fig. 5.11: The evolution of the energy density during the soliton-defect scattering when the soliton experiences a time-delay.

time-advance. Whereas if the energy of the defect is negative, as in the case shown in figure 5.9 where $E \sim \cos(e) = \cos(\frac{3\pi}{4}) < 0$, then the soliton is time-delayed. A positive energy defect can time-advance an incoming soliton because it has energy to transfer to the outgoing soliton before it receives energy from the incoming soliton. Likewise a negative energy defect needs to receive energy from the incoming soliton before the outgoing soliton can be released, therefore it is time-delayed.

Another limit of the soliton-defect scattering process is the stationary soliton or $\theta = 0$ limit. This simplifies the constraint on the solitons position relative to each other to

$$e^{4\sqrt{\beta}\cos(a)\,c} = e^{4\sqrt{\beta}\cos(a)\,d}\frac{(\delta e^{ai}e^{ei}-1)(\delta - e^{ei}e^{ai})}{(\delta e^{ei}+e^{ai})(\delta e^{ai}+e^{ei})} \tag{5.2.32}$$

and the energy, momentum and charge of this configuration become

$$E = 8\sqrt{\beta}\cos(a) + 2\sqrt{\beta}\cos(e)\left(\delta + \frac{1}{\delta}\right), \quad P = 2\sqrt{\beta}\cos(e)\left(\delta - \frac{1}{\delta}\right),$$
$$Q = -4a + 2\pi + 2e, \tag{5.2.33}$$

for $0 < a < \frac{\pi}{2}$. The energy does not depend on the position of the solitons so it exhibits zero mode behaviour and is not a bound state. The solitons can be moved away from the defect with no change in the energy.

We commented earlier that the energy of the defect depends on the difference in the phases of the dual fields at the defect. The way in which we have set up this scattering process, this is exactly the phase e on the dual field of the right soliton solution. Along with the incoming soliton parameters θ, a and the defect parameter

δ it is this phase e that determines how the soliton scatters, i.e. the time-delay and phase shift it experiences. The phase e is a property of the outgoing soliton and we suggest that it would be a nicer situation if the scattering process was totally determined by the incoming soliton and the defect it is advancing towards. Although a different viewpoint is that to describe the initial defect then one needs the value of the defect parameter δ and the phase difference in the dual fields at the defect and it is this initial description that determines the form of the outgoing soliton.

This complexity in the description of the soliton-defect scattering in the 'two field' picture provides the motivation to find a new description of the CSG defect theory. This led us to the realisation that the difference in the auxiliary fields are defined by an explicit formula (see section 4.4) and the development of a CSG defect theory using α, which we introduce in the next section.

5.3 CSG defect in alpha description

In chapter 4 we presented an explicit formula for $\alpha = \theta - \psi$ the difference in the left and right auxiliary fields (4.4.7)

$$\alpha = \arcsin\left[\frac{i}{2}\left(\frac{uw^* - wu^* + 2i\sin A}{\sqrt{1-ww^*}\sqrt{1-uu^*}}\right)\right]. \tag{5.3.1}$$

This allowed the CSG BT (4.4.2) and two-soliton solution (4.5.5) to be rewritten in terms of α instead of the dual fields. The discovery of this explicit form of α was prompted by the aim to find a tidier interpretation of the CSG defect theory.

In this section we use α to reconstruct the CSG defect. The set up has the u-field on the left side of the defect and the w-field on the right side of the defect with the defect now described by parameters δ and A, via α.

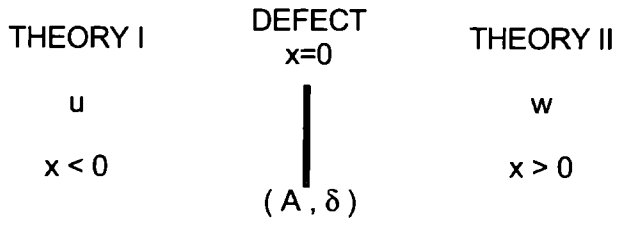

Fig. 5.12: The set up for CSG defect theory in alpha description.

We follow the same method as before to construct the various quantities that describe the CSG defect model. Unsurprisingly the quantities have the same form as in the 'two field' description with the definition of α substituted into them. The Lagrangian has the form (5.1.2) with the defect potential

$$\begin{aligned} D &= \delta\sqrt{\beta}\left(2\cos(\alpha)\sqrt{1-uu^*}\sqrt{1-ww^*} - uw^* - u^*w\right) \\ &\quad + \frac{\sqrt{\beta}}{\delta}\left(2\cos(\alpha)\sqrt{1-uu^*}\sqrt{1-ww^*} + uw^* + u^*w\right) \end{aligned} \tag{5.3.2}$$

and the coefficients of the time derivative terms

$$\begin{aligned} A_1 = A_2^* &= \frac{1}{u}\ln\left(2\sqrt{1-uu^*}\sqrt{1-ww^*}e^{-i\alpha} - 2(1-uu^*)\frac{w}{u}\right) - \frac{1}{2}\frac{\ln(w)}{u}, \\ A_3 = A_4^* &= -\frac{1}{w}\ln\left(2\sqrt{1-uu^*}\sqrt{1-ww^*}e^{i\alpha} - 2(1-ww^*)\frac{u}{w}\right) + \frac{1}{2}\frac{\ln(u)}{w}. \end{aligned} \tag{5.3.3}$$

Varying the action gives the defect conditions

$$\begin{aligned}\frac{u_t - u_x}{\sqrt{1-uu^*}} - \frac{w_t - w_x}{\sqrt{1-ww^*}}e^{i\alpha} &= -2\sqrt{\beta}\,\delta\left(w\sqrt{1-uu^*} + u\sqrt{1-ww^*}e^{i\alpha}\right), \\ \frac{u_t + u_x}{\sqrt{1-uu^*}}e^{i\alpha} + \frac{w_t + w_x}{\sqrt{1-ww^*}} &= \frac{2\sqrt{\beta}}{\delta}\left(u\sqrt{1-ww^*} - w\sqrt{1-uu^*}e^{i\alpha}\right), \quad (5.3.4)\end{aligned}$$

which as expected are exactly the BT (4.4.2). The conserved defect energy (5.1.21), momentum and charge (5.1.22) take the same form as in the previous description with the defect momentum term

$$\begin{aligned}\mathcal{P}_D &= -\delta\sqrt{\beta}\left(-2\cos(\alpha)\sqrt{1-uu^*}\sqrt{1-ww^*} + u^*w + uw^*\right) \\ &\quad -\frac{\sqrt{\beta}}{\delta}\left(2\cos(\alpha)\sqrt{1-uu^*}\sqrt{1-ww^*} + u^*w + w^*u\right) \quad (5.3.5)\end{aligned}$$

and charge defect term

$$\mathcal{Q}_D = 2\alpha\,. \quad (5.3.6)$$

5.4 Soliton solutions in alpha description

Using the new description of the CSG defect, in this section we similarly analyse the soliton solutions. The previous analysis showed that the CSG defect theory exhibits interesting soliton solutions. We repeat all of the solutions covered in the 'two field' description and note comparisons and contrasts between the two descriptions.

Starting as before, we place the bulk vacuum on each side of the defect

$$u = 0, \quad w = 0, \quad (5.4.1)$$

which now involves setting the only field on each side of the defect to zero. This choice is unique unlike in the 'two field' description. It trivially solves the CSG equation and the defect conditions (5.3.4). It has energy, momentum and charge

$$E = 2\sqrt{\beta}\,(\delta + \frac{1}{\delta})\cos(\alpha'')\,, \quad P = 2\sqrt{\beta}\,(\delta - \frac{1}{\delta})\cos(\alpha'')\,, \quad Q = 2\alpha''\,, \quad (5.4.2)$$

where

$$\alpha'' = \alpha(u=0, w=0) = \arcsin\big(-\sin(A)\big). \quad (5.4.3)$$

As before the energy, momentum and charge receive no contribution from the bulk but a non-zero contribution at $x = 0$, which is attributed to the defect. Their values

depend on the two defect parameters δ and A, with the A dependence through the definition of α''. The non-trivial way in which α'' is related to A

$$\sin(\alpha'') = -\sin(A)\,, \tag{5.4.4}$$

leads to the interesting property that the energy, momentum and charge can take different values despite the bulk fields remaining in the vacuum and the defect parameters taking the same values. Explicitly (5.4.4) has the solutions

$$\alpha'' = -A\,,\ A \pm \pi\,, \tag{5.4.5}$$

where the two solutions give different values to $\cos(\alpha'')$ and therefore to the energy and momentum. In particular, depending on which solution is taken the energy, momentum and charge become either

$$E = 2\sqrt{\beta}\,(\delta + \frac{1}{\delta})\cos(A)\,, \quad P = 2\sqrt{\beta}\,(\delta - \frac{1}{\delta})\cos(A)\,, \quad Q = -2A \tag{5.4.6}$$

or

$$E = -2\sqrt{\beta}\,(\delta + \frac{1}{\delta})\cos(A)\,, \quad P = -2\sqrt{\beta}\,(\delta - \frac{1}{\delta})\cos(A)\,, \quad Q = 2(A \pm \pi)\,. \tag{5.4.7}$$

Therefore to fully determine the defect, as well as the values of δ and A, the solution to (5.4.4) used needs to be specified. The lowest energy defect for a fixed $\delta > 0$ is when $\cos(A) = -1$ in (5.4.6) or $\cos(A) = 1$ in (5.4.7), which has energy

$$E_{vac} = -2\sqrt{\beta}\left(\delta + \frac{1}{\delta}\right) \tag{5.4.8}$$

and charge

$$Q_{vac} = \pm 2\pi. \tag{5.4.9}$$

This corresponds with the lowest energy defect in the 'two field' description (5.2.4). The defect has maximum energy

$$E = 2\sqrt{\beta}\left(\delta + \frac{1}{\delta}\right)\,, \tag{5.4.10}$$

when $\cos(\alpha'') = 1$ with charge $Q = 0$. When $\delta < 0$ the energies of these extremal defects are swapped but the charges stay the same.

In contrast to the 'two field' description of the defect theory, the introduction of α has got rid of the need to consider the dual fields. Specifically the roles that

the phase of the dual fields played in determining the defect properties has been simplified by the use of the extra charge parameter A on the defect. However the method by which the defect transfers the conserved charges is now through the non-trivial definition of α and its time dependence.

Through the choice of δ and α'' there exists defects with positive energy and defects with negative energy (with either positive or negative momentum). From the properties discovered in the 'two field' description, we refer to defects with positive energy as excited defects and defects with negative energy as unexcited defects.

We consider the choice $\alpha'' = -A$ and examining (5.4.6) shows there are different regions of parameters that give excited defects, namely

$$\delta > 0, \quad \cos(A) > 0 \quad \text{and} \quad \delta < 0, \quad \cos(A) < 0. \tag{5.4.11}$$

If we also consider the momentum of the defect then the two cases above are further split in two. Explicitly if $\delta > 1$ and $\cos(A) > 0$ then the defect is excited with positive momentum, whereas if $0 < \delta < 1$ and $\cos(A) > 0$ then the defect's momentum is negative. There is a similar splitting for the second parameter range. Taking into account the charge of the defect we find there are in fact four defects with the same positive energy and positive momentum but with different charge.

These excited defects are displayed in table 5.1. It lists four defects with energy

$0 < A < \frac{\pi}{2}$	$A = A'$	$\delta = \delta' > 1$	$Q = -2A' \in \{0, -\pi\}$
$-\frac{\pi}{2} < A < 0$	$A = -A'$	$\delta = \delta' > 1$	$Q = 2A' \in \{\pi, 0\}$
$\frac{\pi}{2} < A < \pi$	$A = \pi - A'$	$\delta = -\delta' < -1$	$Q = 2A' - 2\pi \in \{-\pi, -2\pi\}$
$-\pi < A < -\frac{\pi}{2}$	$A = -\pi + A'$	$\delta = -\delta' < -1$	$Q = 2\pi - 2A' \in \{2\pi, \pi\}$

Table 5.1: Four excited defects with the same energy and momentum.

$E = 2\sqrt{\beta}|(\delta' + \frac{1}{\delta'})\cos(A')|$ and momentum $P = 2\sqrt{\beta}|(\delta' - \frac{1}{\delta'})\cos(A')|$ each with different charge.

The specific example when $A' = \frac{\pi}{3}$, $\delta' = 2$ is shown in table 5.2, where the defects have energy $E_{def} = \frac{5\sqrt{\beta}}{2}$ and momentum $P_{def} = \frac{3\sqrt{\beta}}{2}$. The table shows explicitly that the defects have different charge.

$A = \frac{\pi}{3}$	$\delta = 2$	$Q = -\frac{2\pi}{3}$
$A = -\frac{\pi}{3}$	$\delta = 2$	$Q = \frac{2\pi}{3}$
$A = \frac{2\pi}{3}$	$\delta = -2$	$Q = -\frac{4\pi}{3}$
$A = -\frac{2\pi}{3}$	$\delta = -2$	$Q = \frac{4\pi}{3}$

Table 5.2: Four defects with the energy $E_{def} = \frac{5\sqrt{\beta}}{2}$ and momentum $P_{def} = \frac{3\sqrt{\beta}}{2}$.

Recalling that the other solution to (5.4.4) gave (5.4.7), we consider the defects with positive energy and momentum that this choice describes. These are shown in table 5.3. The parameter choice $A' = \frac{\pi}{3}$, $\delta' = -2$ gives defects with the same energy

$0 <$	A	$< \frac{\pi}{2}$	$A = A'$	$\delta = \delta'$	< -1	$Q = 2A' - 2\pi$	$\in \{-\pi, -2\pi\}$
$-\frac{\pi}{2} <$	A	< 0	$A = -A'$	$\delta = \delta'$	< -1	$Q = 2\pi - 2A'$	$\in \{2\pi, \pi\}$
$\frac{\pi}{2} <$	A	$< \pi$	$A = \pi - A'$	$\delta = -\delta'$	> 1	$Q = -2A'$	$\in \{0, -\pi\}$
$-\pi <$	A	$< -\frac{\pi}{2}$	$A = -\pi + A'$	$\delta = -\delta'$	> 1	$Q = 2A'$	$\in \{\pi, 0\}$

Table 5.3: Four excited defects with the same energy and momentum.

$E_{def} = \frac{5\sqrt{\beta}}{2}$ and momentum $P_{def} = \frac{3\sqrt{\beta}}{2}$ as before. The charge of the defects are shown in table 5.4. Comparison between tables 5.4 and 5.2 show that using either

$A = \frac{\pi}{3}$	$\delta = -2$	$Q = -\frac{2\pi}{3}$
$A = -\frac{\pi}{3}$	$\delta = -2$	$Q = \frac{2\pi}{3}$
$A = \frac{2\pi}{3}$	$\delta = 2$	$Q = -\frac{4\pi}{3}$
$A = -\frac{2\pi}{3}$	$\delta = 2$	$Q = \frac{4\pi}{3}$

Table 5.4: Four defects with the energy $E_{def} = \frac{5\sqrt{\beta}}{2}$ and momentum $P_{def} = \frac{3\sqrt{\beta}}{2}$.

solution to (5.4.4) gives the same four defects.

Therefore to give a list of the possible CSG defects only one of the solutions (5.4.5) has to be considered, as the other simply gives another cover of the same defects. From now on we use $\cos(\alpha'') = \cos(A)$ without loss of generality. Similarly we find that there are four unexcited defects with the same negative energy and

positive momentum but with different charge. These are shown in table 5.5.

$0 <$	A	$< \frac{\pi}{2}$	$A = A'$	$\delta = \delta'$	< -1	$Q = -2A'$	$\in \{0, -\pi\}$
$-\frac{\pi}{2} <$	A	< 0	$A = -A'$	$\delta = \delta'$	< -1	$Q = 2A'$	$\in \{\pi, 0\}$
$\frac{\pi}{2} <$	A	$< \pi$	$A = \pi - A'$	$\delta = -\delta'$	> 1	$Q = 2A' - 2\pi$	$\in \{-\pi, -2\pi\}$
$-\pi <$	A	$< -\frac{\pi}{2}$	$A = -\pi + A'$	$\delta = -\delta'$	> 1	$Q = 2\pi - 2A'$	$\in \{2\pi, \pi\}$

Table 5.5: Four unexcited defects with the same energy and momentum.

Taking the specific parameter choice $A' = \frac{\pi}{3}$, $\delta' = -2$ gives four defects with energy $E_{def} = -\frac{5\sqrt{\beta}}{2}$ and momentum $P_{def} = \frac{3\sqrt{\beta}}{2}$ and charge listed in table 5.6.

$A = \frac{\pi}{3}$	$\delta = -2$	$Q = -\frac{2\pi}{3}$
$A = -\frac{\pi}{3}$	$\delta = -2$	$Q = \frac{2\pi}{3}$
$A = \frac{2\pi}{3}$	$\delta = 2$	$Q = -\frac{4\pi}{3}$
$A = -\frac{2\pi}{3}$	$\delta = 2$	$Q = \frac{4\pi}{3}$

Table 5.6: Four defects with the energy $E_{def} = -\frac{5\sqrt{\beta}}{2}$ and momentum $P_{def} = \frac{3\sqrt{\beta}}{2}$.

The excited and unexcited defects we have listed in the tables above all have positive momentum. There are also excited and unexcited defects with negative momentum when $|\delta| < 1$. Similarly there are four defects with the same energy and negative momentum which have four different values of charge.

This concludes the classification of the different CSG defects. We have shown that to fully determine the defect, as well as the two defect parameters the value of α'' has to be specified. However the choice of α'' only creates a second cover of all the defects, if we consider the full range of values of the parameters. We have shown that defects with the same energy and momentum can actually hold four different values of charge. The defects can have either positive or negative energy and momentum, which we will show determines the way the defect can interact with CSG solitons.

5.4.1 Soliton emission from the defect

As in the 'two field' description, we analyse soliton emission and absorption in the α description. That the CSG defect can hold different amounts of the conserved charges, supports the previous results that soliton emission and absorption are possible. Namely, an unexcited defect can absorb a soliton, thus exciting it and an excited defect can decay into an unexcited defect by emitting a soliton. This is further suggested by the fact that the energy of a soliton (4.5.3) is exactly twice the energy of a defect (5.4.2), when the relevant parameters are matched and defects with positive and negative energy of the same magnitude are linked by the solutions to equation (5.4.4). Since the defect conditions and BT are one and the same thing the properties of the BT also provide evidence for the absorption and emission of solitons by the defect. The BT provide a means of generating a one-soliton solution from the vacuum, the emission of a soliton from the defect is exactly this situation with the process occurring dynamically.

To examine the emission of a soliton, we analyse the field configurations to replicate a right-moving soliton being emitted from the right hand side of the defect. The set up required is the vacuum on the left hand side of the defect and a right-moving one-soliton solution on the right. In this situation α becomes

$$\alpha' = \arcsin\left(\frac{-\sin(A)}{\sqrt{1-ww^*}}\right), \tag{5.4.12}$$

where $w = w_{1-sol}$ is the specified one-soliton solution. Substituting these into the defect conditions (5.3.4), we find that they are satisfied when

$$\begin{aligned} a &= A\,, \quad & e^{\theta} &= \delta\,, \\ a &= A \pm \pi\,, \quad & e^{\theta} &= -\delta\,. \end{aligned} \tag{5.4.13}$$

In order to generate these constraint conditions between the defect and soliton parameters we must make a choice on the starting value of α'. At both time infinities the fields at the defect becomes zero so α' reduces to α'', this has two solutions (5.4.5). We take the solution $\cos(\alpha') = \cos(A)$ at $t \to -\infty$ without loss of generality to generate the constraints. We can equally use the other solution $\cos(\alpha') = -\cos(A)$, it generates slightly different constraints but when we analyse the emission processes they are found to be identical to what we now describe.

We have set up the problem so the emitted soliton is right-moving $\theta > 0$. The constraints (5.4.13) show that for a defect to emit a right-moving soliton then we require $|\delta| > 1$. This is explained by a right-moving soliton having positive energy and momentum, therefore for total energy and total momentum to be conserved the initial excited defect has to have positive energy and momentum, thus $|\delta| > 1$.

To analyse in more detail the process of the CSG defect emitting a soliton, we examine the decays of two of the four excited defects listed in table 5.1. Table 5.7 shows the decay of excited defect I which is described by $0 < A < \frac{\pi}{2}$ and $\delta > 1$ and has charge in the region $-\pi < Q_{def} < 0$. This defect decays by emitting a positively

Excited Defect I	$\rightarrow$	Unexcited Defect I
$(0 < A < \frac{\pi}{2}\ ,\ \delta > 1)$	Emitted Soliton	$(\frac{\pi}{2} < A' < \pi\ ,\ \delta' > 1)$
$\alpha = -A$	$(a = A, e^{\theta} = \delta)$	$\alpha = A - \pi$
$E = 2\sqrt{\beta}\cos(A)(\delta + \frac{1}{\delta})$	$E_{sol} = 4\sqrt{\beta}\cos(A)(\delta + \frac{1}{\delta})$	$E' = -E$
$P = 2\sqrt{\beta}\cos(A)(\delta - \frac{1}{\delta})$	$P_{sol} = 4\sqrt{\beta}\cos(A)(\delta - \frac{1}{\delta})$	$P' = -P$
$Q = -2A$	$Q_{sol} = 2\pi - 4A$	$Q' = 2A - 2\pi$

Table 5.7: The decay process of excited defect I.

charged soliton and the resulting defect has negative energy and momentum, the same magnitude as the initial defect, and charge $-2\pi < Q_{def} < -\pi$. Similarly table 5.8 shows excited defect II described by $-\pi < A < -\frac{\pi}{2}$ and $\delta < -1$ with charge $\pi < Q_{def} < 2\pi$ decaying, by emitting a positively charged soliton, into an unexcited defect with equal and opposite energy and momentum.

The two decays illustrate that each defect with positive energy and momentum emits precisely one right-moving soliton. During any emission process the value of α' changes with time from one solution of (5.4.4) to the other. It is the non-trivial way that α is defined and its time dependence that means the value of α' is different before and after the emission process. This property allows the defect to transfer energy, momentum and charge to and from soliton solutions and therefore make soliton emission possible.

In the analysis of the vacuum we showed that the solutions of (5.4.4) allowed

Excited Defect II	$\rightarrow$	Unexcited Defect II
$(-\pi < A < -\frac{\pi}{2}\ ,\ \delta < -1)$	Emitted Soliton	$(0 > A' > -\frac{\pi}{2}\ ,\ \delta' < -1)$
$\alpha = -A$	$(A-\pi, -\delta)$	$\alpha = A + \pi$
$E = 2\sqrt{\beta}\cos(A)(\delta + \frac{1}{\delta})$	$E_{sol} = 4\sqrt{\beta}\cos(A)(\delta + \frac{1}{\delta})$	$E' = -E$
$P = 2\sqrt{\beta}\cos(A)(\delta - \frac{1}{\delta})$	$P_{sol} = 4\sqrt{\beta}\cos(A)(\delta - \frac{1}{\delta})$	$P' = -P$
$Q = -2A$	$Q_{sol} = -2\pi - 4A$	$Q' = 2A + 2\pi$

Table 5.8: The decay process of excited defect II.

defects with either positive and negative energy to be described by the same δ and A. The evolution of α' during the emission is what allows the defect to change from the initial defect with positive energy to the final negative energy defect. To investigate precisely what is happening during an emission process, we note that due to the definition of α (4.4.7), $\cos(\alpha')$ is defined

$$\cos(\alpha') = \sqrt{1 - \sin^2(\alpha')} = \frac{\sqrt{1 - ww^* - \sin^2(A)}}{\sqrt{1 - ww^*}} \tag{5.4.14}$$

using a square root. During the emission process

$$1 - ww^* = 1 - \cos^2(a)\mathrm{sech}^2(2\sqrt{\beta}\cos(a)(-\sinh(\theta)t)) \tag{5.4.15}$$

becomes equal to $\sin^2(A)$. At this moment the argument in the square root in the numerator of $\cos(\alpha')$ becomes equal to zero and we need to choose the opposite branch of this square root in order to keep the function smooth. It is this prescription that means by the end of the process α' is equal to the other solution of (5.4.4), namely $\alpha' = A \pm \pi$.

This evolution of $e^{i\alpha'}$ in the complex plane is shown in figure 5.13 for the two decays illustrated in tables 5.7 and 5.8. It shows $e^{i\alpha'}$ changing during both emissions from $\alpha' = -A$ to $\alpha' = A \pm \pi$. Figure 5.13(a) shows the evolution for $e^{i\alpha'}$ during the decay of excited defect I where $0 < A < \frac{\pi}{2}$ and figure 5.13(b) illustrates the progress of $e^{i\alpha'}$ during the decay of excited defect II where $-\pi < A < -\frac{\pi}{2}$. We note that in both cases the value of $\sin(\alpha')$ is the same at the beginning and the end of the process, while the value of $\cos(\alpha')$ is different.

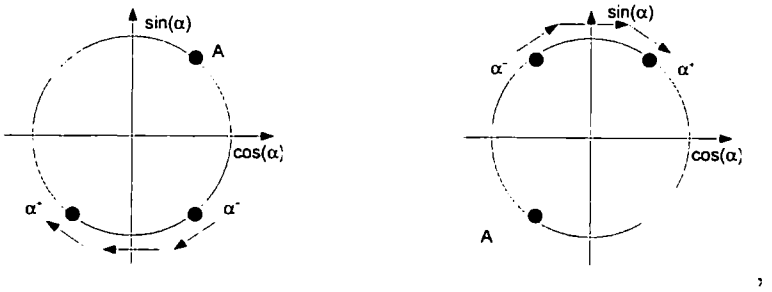

Fig. 5.13: The evolution of $e^{i\alpha'}$ during two emission processes, decay of (a) excited defect I, (b) excited defect II.

As mentioned earlier a specific defect emits just one type of soliton but there is the interesting phenomena that there are two defects that emit the same soliton. The decay of two such defects are shown in tables 5.9 and 5.10. The two excited defects E_A and E_B have the same energy and momentum but different charge, $Q = -\frac{2\pi}{3}$ and $Q = \frac{4\pi}{3}$ respectively. They emit the same soliton, specifically a soliton with energy $E_{sol} = 5\sqrt{\beta}$, momentum $P_{sol} = 3\sqrt{\beta}$ and charge $Q_{sol} = \frac{2\pi}{3}$. The change

E_A	$\rightarrow$	U_A
$(A = \frac{\pi}{3}\ ,\ \delta = 2)$	Emitted Soliton	$(A' = \frac{2\pi}{3}\ ,\ \delta' = 2)$
$\alpha = -A$	$(a = A, e^{\theta} = \delta)$	$\alpha = A - \pi$
$E = \frac{5\sqrt{\beta}}{2}$	$E_{sol} = 5\sqrt{\beta}$	$E' = -E$
$P = \frac{3\sqrt{\beta}}{2}$	$P_{sol} = 3\sqrt{\beta}$	$P' = -P$
$Q = -\frac{2\pi}{3}$	$Q_{sol} = \frac{2\pi}{3}$	$Q' = -\frac{4\pi}{3}$

Table 5.9: The decay of excited defect E_A.

in charge from the initial excited defect to the final unexcited defect for the two processes are graphically illustrated in figure 5.14. It shows that the initial and final charge of the defects are symmetrically spaced about $Q = \pm\pi$. We find this to be the case for any emission. The maximally charged soliton $Q_{sol} = 2\pi$ is emitted by defects with charge 2π or 0, while the defects with charge $\pm\pi$ are stable and do not emit any soliton. For any emission the charge of the unexcited defect is never the

E_B	$\rightarrow$	U_B
$(A = -\frac{2\pi}{3}\ ,\ \delta = -2)$	Emitted Soliton	$(A' = -\frac{\pi}{3}\ ,\ \delta' = -2)$
$\alpha = -A$	$(A - \pi, -\delta)$	$\alpha = A + \pi$
$E = \frac{5\sqrt{\beta}}{2}$	$E_{sol} = 5\sqrt{\beta}$	$E' = -E$
$P = \frac{3\sqrt{\beta}}{2}$	$P_{sol} = 3\sqrt{\beta}$	$P' = -P$
$Q = \frac{4\pi}{3}$	$Q_{sol} = \frac{2\pi}{3}$	$Q' = \frac{2\pi}{3}$

Table 5.10: The decay of excited defect E_B.

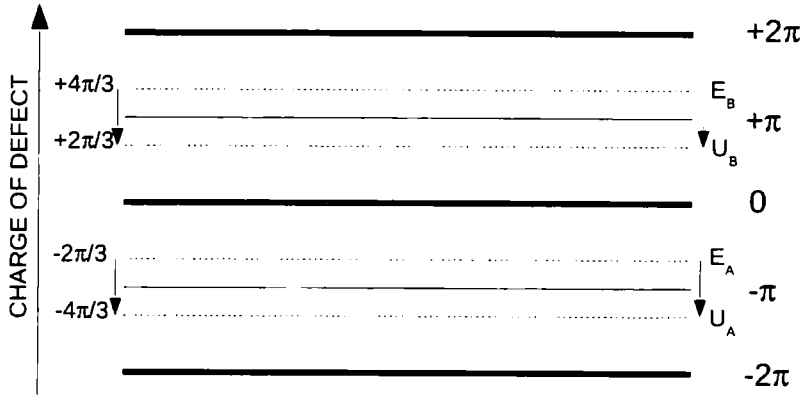

Fig. 5.14: Charge of defects E_A and E_B that emit a $Q = \frac{2\pi}{3}$ soliton.

opposite of the initial charge.

Considering the pair of defects that emit the same soliton (for example E_A and E_B) then the unexcited defect, that the other excited defect of the pair decays into, does has the opposite charge of the first excited defect, as well as energy and momentum. For example U_B has the opposite charge to E_A, as do U_A and E_B. We call this its anti-defect, for example U_B is the anti-defect of E_A and vice-versa.

5.4.2 Soliton absorption by the defect

The opposite process to a soliton being emitted from the defect is for a soliton to be absorbed by an unexcited defect. The field configuration we need to describe this process is a right-moving one-soliton solution on the left hand side of the defect and the vacuum on the right. In this situation α becomes

$$\alpha' = \arcsin\left(\frac{\sin(A)}{\sqrt{1-uu^*}}\right), \tag{5.4.16}$$

where $u = u_{1-sol}$ is the right-moving one-soliton. We find that the defect conditions (5.3.4) are satisfied, again we use $\cos(\alpha') = \cos(A)$ as $t \to -\infty$, when

$$\begin{aligned} a &= -A\,, \qquad e^{\theta} = -\delta\,, \\ a &= -A \pm \pi\,, \qquad e^{\theta} = \delta\,. \end{aligned} \tag{5.4.17}$$

These conditions show that it is required that $|\delta| > 1$ for a defect to absorb a right-moving soliton. This can be explained by noticing that for an unexcited defect to absorb a right moving soliton it has to have negative energy and momentum, which requires $|\delta| > 1$.

Unexcited Defect I	$\to$	Excited Defect I
$(\frac{\pi}{2} < A < \pi\ ,\ \delta > 1)$	Absorbed Soliton	$(0 < A' < \frac{\pi}{2},\ \delta' > 1)$
$\alpha = -A$	$(a = -A + \pi, e^{\theta} = \delta)$	$\alpha = A - \pi$
$E = 2\sqrt{\beta}\cos(A)(\delta + \frac{1}{\delta})$	$E_{sol} = -4\sqrt{\beta}\cos(A)(\delta + \frac{1}{\delta})$	$E' = -E$
$P = 2\sqrt{\beta}\cos(A)(\delta - \frac{1}{\delta})$	$P_{sol} = -4\sqrt{\beta}\cos(A)(\delta - \frac{1}{\delta})$	$P' = -P$
$Q = -2A$	$Q_{sol} = -2\pi + 4A$	$Q' = 2A - 2\pi$

Table 5.11: Showing unexcited defect I absorbing a soliton.

In table 5.11 we show that unexcited defect I described by $\frac{\pi}{2} < A < \pi$ with $Q \in \{-\pi, -2\pi\}$ absorbs a positively charged soliton becoming excited defect I. Similarly table 5.12 shows that unexcited defect II described by $-\frac{\pi}{2} < A < 0$ with $Q \in \{0, \pi\}$ absorbs a positively charged soliton becoming excited defect II. In both absorption processes we check that the total energy, momentum and charge of the

Unexcited Defect II	→	Excited Defect II
$(-\frac{\pi}{2} < A < 0\ ,\ \delta < -1)$	Absorbed Soliton	$(-\pi < A' < -\frac{\pi}{2}\ ,\ \delta' < -1)$
$\alpha = -A$	$(-A, -\delta)$	$\alpha = A + \pi$
$E = 2\sqrt{\beta}\cos(A)(\delta + \frac{1}{\delta})$	$E_{sol} = -4\sqrt{\beta}\cos(A)(\delta + \frac{1}{\delta})$	$E' = -E$
$P = 2\sqrt{\beta}\cos(A)(\delta - \frac{1}{\delta})$	$P_{sol} = -4\sqrt{\beta}\cos(A)(\delta - \frac{1}{\delta})$	$P' = -P$
$Q = -2A$	$Q_{sol} = 2\pi + 4A$	$Q' = 2A + 2\pi$

Table 5.12: Showing unexcited defect II absorbing a soliton.

system are conserved. For example, the energy of the unexcited defect plus the energy of the absorbed soliton is equal to the energy of the excited defect.

As in the emission process α' varies with time during absorption. As the fields at the defect change there is a moment when

$$1 - uu^* = \sin^2(A)\,. \tag{5.4.18}$$

In order to keep $\cos(\alpha')$ smooth, at this point, we take the other branch of the square root in the definition of $\cos(\alpha')$. This means that α' changes from $-A$ in the far past to $A \pm \pi$ in the far future. Figure 5.15 shows the evolution of $e^{i\alpha'}$ for the two absorption processes, figure 5.15(a) shows the evolution of $e^{i\alpha'}$ when unexcited defect I absorbs a soliton and figure 5.15(b) for unexcited defect II similarly.

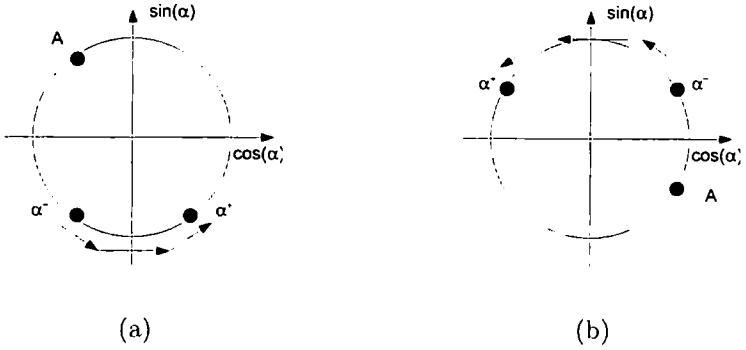

Fig. 5.15: The evolution of $e^{i\alpha'}$ during two absorption processes involving (a) unexcited defect I and (b) unexcited defect II.

Tables 5.13 and 5.14 show that there are two unexcited defects that absorb the same soliton. The two unexcited defects U_A and U_B have the same energy and

momentum but different charge, $Q = -\frac{4\pi}{3}$ and $Q = \frac{2\pi}{3}$ respectively. They absorb the soliton with $E_{sol} = 5\sqrt{\beta}$, $P_{sol} = 3\sqrt{\beta}$ and $Q_{sol} = \frac{2\pi}{3}$. With comparison with the emission tables 5.9 and 5.10, we find that defect E_A emits a soliton to decay to U_A and defect U_A absorbs the same soliton to become E_A.

U_A	$\rightarrow$	E_A
$(A = \frac{2\pi}{3}\ ,\ \delta = 2)$	Absorbed Soliton	$(A' = \frac{\pi}{3},\ \delta' = 2)$
$\alpha = -A$	$(a = -A + \pi, e^{\theta} = \delta)$	$\alpha = A - \pi$
$E = -\frac{5\sqrt{\beta}}{2}$	$E_{sol} = 5\sqrt{\beta}$	$E' = -E$
$P = -\frac{3\sqrt{\beta}}{2}$	$P_{sol} = 3\sqrt{\beta}$	$P' = -P$
$Q = -\frac{4\pi}{3}$	$Q_{sol} = \frac{2\pi}{3}$	$Q' = -\frac{2\pi}{3}$

Table 5.13: Showing unexcited defect U_A absorbing a soliton with charge $Q_{sol} = \frac{2\pi}{3}$.

U_B	$\rightarrow$	E_B
$(A = -\frac{\pi}{3}\ ,\ \delta = -2)$	Emitted Soliton	$(A' = -\frac{2\pi}{3}\ ,\ \delta' = -2)$
$\alpha = -A$	$(-A, -\delta)$	$\alpha = A + \pi$
$E = -\frac{5\sqrt{\beta}}{2}$	$E_{sol} = 5\sqrt{\beta}$	$E' = -E$
$P = -\frac{3\sqrt{\beta}}{2}$	$P_{sol} = 3\sqrt{\beta}$	$P' = -P$
$Q = \frac{2\pi}{3}$	$Q_{sol} = \frac{2\pi}{3}$	$Q' = \frac{4\pi}{3}$

Table 5.14: Showing unexcited defect U_B absorbing a soliton with charge $Q_{sol} = \frac{2\pi}{3}$.

In this analysis into defects absorbing and emitting solitons, we have only considered right-moving soliton solutions, or at least we have only interpreted them as such. In fact when solving the defect conditions no restrictions on θ were used so the solutions describe both right- and left-moving solitons. We have solely studied solutions involving right-moving solitons, but there are similarly solutions when left-moving solitons are emitted and absorbed. The energy and momentum of the initial defect control what process can occur. The sign of the defect energy determines

whether a soliton can be absorbed or emitted and the sign of the defect momentum determines whether the soliton is left- or right-moving.

In figures 5.16, 5.17 we show explicitly that the energy and momentum of the defect determines whether it absorbs or emits a soliton and whether the soliton is right- or left-moving. We consider the defect with its charge parameter in the range $-\frac{\pi}{2} < A < \frac{\pi}{2}$ with α initially chosen such that $\cos(\alpha) = \cos(A)$. For the four different regions of δ we illustrate how the defect interacts with the soliton.

In figure 5.16(a) $\delta < -1$ so the energy and momentum of the defect are negative. Considering only that the total energy and momentum is conserved, we can deduce that this defect can absorb a right-moving soliton. Similarly in figure 5.16(b) with $-1 < \delta < 0$ the energy of the defect is negative and the momentum is positive, therefore the defect can absorb a left-moving soliton.

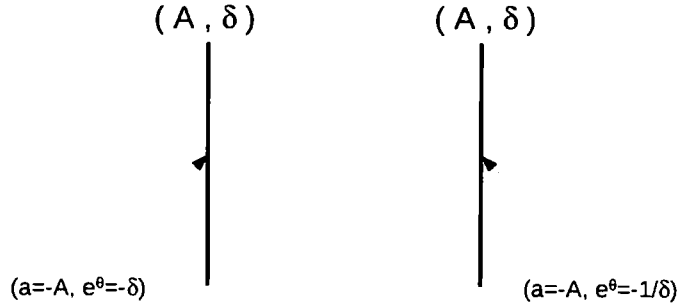

(a) E_- P_- (b) E_- P_+

Fig. 5.16: Defects able to absorb a soliton, $-\frac{\pi}{2} < A < \frac{\pi}{2}$, (a) $\delta < -1$, (b) $-1 < \delta < 0$.

In figure 5.17(a) $0 < \delta < 1$ the defect has positive energy and negative momentum and the defect can emit a left-moving soliton. Finally if $\delta > 1$ as in figure 5.17(b) then both the defect energy and momentum are positive and the defect can emit a right-moving soliton. The annotation in each of the figures shows the condition between the soliton parameters and defect parameters for the defect conditions to be satisfied for the particular process illustrated. This concludes the analysis on the specific soliton solutions that different defects can emit and absorb. We continue to analyse soliton and particle scattering with the CSG defect.

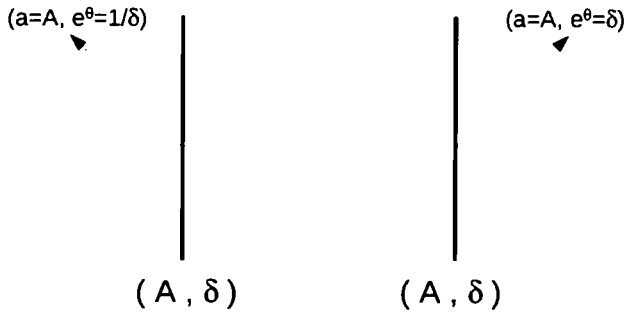

(a) E_+ P_- (b) E_+ P_+

Fig. 5.17: Defects able to emit a soliton, $-\frac{\pi}{2} < A < \frac{\pi}{2}$, (a) $0 < \delta < 1$, (b) $\delta > 1$.

5.4.3 Soliton scattering with the defect

As in the first description of the defect theory, we place a one-soliton solution on each side of the defect

$$\begin{aligned} u &= \frac{\cos(a)\, e^{2i\sqrt{\beta}\sin(a)(\cosh(\theta)\, t - \sinh(\theta)\, x)}}{\cosh(2\sqrt{\beta}\cos(a)(t\sinh(\theta) - x\cosh(\theta)))}, \\ w &= e^{i\phi}\frac{e^{2i\sqrt{\beta}\sin(a)(\cosh(\theta)(t-\Delta t) - \sinh(\theta)\, x)}}{\cosh(2\sqrt{\beta}\cos(a)((t-\Delta t)\sinh(\theta) - x\cosh(\theta)))}, \end{aligned} \tag{5.4.19}$$

to model the process of a one-soliton scattering with the defect. The soliton solutions are not the most general that could be chosen, with the charge parameter a and rapidity θ taken to be the same in the left and right solitons. In fact if we start with general soliton solutions, then the defect conditions force the choices made above. We interpret that the solitons are right-moving $\theta > 0$ but again the following calculations hold for any θ. Note that we are allowing the outgoing soliton w to differ from the incoming soliton u by a time-delay Δt and a phase shift $e^{i\phi}$. This fits with the result of the analogous calculation in the 'two field' description.

To calculate how a soliton is affected by travelling through a defect, we solve the defect conditions in this situation. The expressions for the defect conditions become extremely complicated and are made manageable by expanding the individual terms as a power series in the exponentiated time $e^{2\sqrt{\beta}\cos(a)\sinh(\theta)t}$. We then solve the terms

of the power series for the time-delay

$$\Delta t = \frac{1}{2\sqrt{\beta}\cos(a)\sinh(\theta)}\ln\left|\frac{\sinh\left(\frac{\theta-\chi}{2}+i\frac{a-A}{2}\right)}{\cosh\left(\frac{\theta-\chi}{2}+i\frac{a+A}{2}\right)}\right|, \tag{5.4.20}$$

and phase shift

$$e^{i\phi} = e^{2\sqrt{\beta}\sinh(\theta+ia)\Delta t}\frac{\delta+e^{\theta}e^{ia}e^{iA}}{e^{\theta}e^{ia}-\delta e^{iA}}, \tag{5.4.21}$$

where $e^{\chi}=\delta$ and again without loss of generality $\alpha=-A$ at $t\to-\infty$. We note that this time-delay is very similar to the time-delay experienced by a soliton in soliton-soliton scattering. If the parameters are matched between the defect and one of the solitons then the time-delay experienced by a soliton scattering through the defect is exactly half of the time-delay experienced when scattering through a soliton (4.6.4). This is the same relation as found in the SG model.

As we found during the analysis in the 'two field' description both the emission and absorption processes should appear as limits in the soliton-defect scattering time-delay. To check that the poles and zeros that appear in the logarithm in the time-delay are the exact conditions for soliton absorption and emission it is useful to rewrite the time-delay

$$\Delta t = \frac{1}{2\sqrt{\beta}\cos(a)\sinh(\theta)}\ln\left|\frac{\sinh\left(\frac{\theta-\chi}{2}+i\frac{a-A}{2}\right)}{\sinh\left(\frac{\theta-\chi}{2}+i\frac{a+A\pm\pi}{2}\right)}\right|, \tag{5.4.22}$$

with only hyperbolic sines inside the logarithm. The emission limit is when the time-delay tends to negative infinity, this coincides with the argument of the logarithm tending to zero which occurs when the hyperbolic sine in the numerator goes to zero. Thus

$$\theta=\chi, \quad a=A, \tag{5.4.23}$$

which agrees with the $\delta>0$ condition (5.4.13). Similarly the absorption limit is when the time-delay tends to positive infinity, so when

$$\theta=\chi, \quad a=-A\pm\pi, \tag{5.4.24}$$

which agrees with (5.4.17).

In this description it is obvious that the soliton before and after scattering has the same energy, momentum and charge, since a time or phase shift does not affect

any of these charges. Therefore for the conservation laws to hold the initial and final defect must hold the same charges. In this scenario α depends on both one-soliton solutions and $\cos(\alpha)$ has the form

$$\cos(\alpha) = \frac{\sqrt{4(1-uu^*)(1-ww^*)+(uw^*-wu^*+2i\sin(A))^2}}{2\sqrt{1-uu^*}\sqrt{1-ww^*}}. \tag{5.4.25}$$

Unlike in the emission and absorption processes $\cos(\alpha)$ never becomes zero during the soliton-defect scattering process. In figure 5.18 we show this explicitly for two choices of the parameters. Since the square root never reaches the branch point, the solution remains on the same branch and the value of α is initially and finally the same.

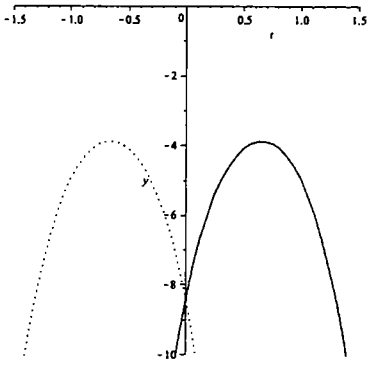

Fig. 5.18: Evolution of $\cos(\alpha)$ in soliton-defect scattering with $a = \frac{\pi}{3}$, $\theta = 1$, $\chi = 1$, $A = \frac{3\pi}{4}$(line)/$\frac{\pi}{4}$(dots).

As we commented in the previous analysis the sign of time-delay depends on the energy of the initial defect. We illustrate this in figure 5.19. Figure 5.19(a) shows the case when the initial defect has positive energy and the time-delay is negative for all values of a. This implies that a soliton scattering through a positive energy defect always experiences a time-advance. The stalactitic divergences show where the emission limits occur. Figure 5.19(b) shows the positive time-delay always experienced by a soliton scattering through a negative energy defect, with the stalagmitic divergences showing the absorption limits.

We could continue to analyse more complicated scenarios. For example we could study the situation with two incoming solitons and one outgoing soliton but essentially this is just a combination of soliton scattering and a soliton being absorbed.

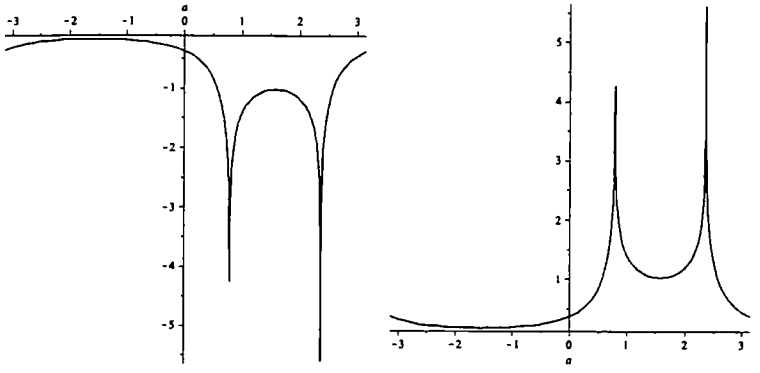

(a) $\theta = 1$, $A = \frac{\pi}{4}$, $\chi = 1$ (b) $\theta = 1$, $A = \frac{3\pi}{4}$, $\chi = 1$

Fig. 5.19: Time-delay experienced by soliton in soliton-defect scattering, against the charge parameter a of the soliton.

It is possible for the behaviour of the solitons in such a system to be calculated from the building blocks of emission, absorption and scattering we have presented here.

5.4.4 Particle scattering with the defect

The CSG particle $u_{particle}$ is described by (4.7.1) which we generate either by considering a small perturbation around the vacuum or the $a = \frac{\pi}{2}$ limit in the CSG soliton solution. To analyse what happens to a particle travelling towards a defect, we need to calculate the particle-defect reflection and transmission factors. To compute these factors we solve the linearised defect conditions

$$\begin{aligned} 0 &= -\left(\frac{\partial u_\epsilon}{\partial t} - \frac{\partial u_\epsilon}{\partial x}\right) + \left(\frac{\partial w_\epsilon}{\partial t} - \frac{\partial w_\epsilon}{\partial x}\right) e^{i\alpha} - 2\sqrt{\beta}\,\delta(w_\epsilon + u_\epsilon e^{i\alpha})\,, \\ 0 &= -\left(\frac{\partial u_\epsilon}{\partial t} + \frac{\partial u_\epsilon}{\partial x}\right) e^{i\alpha} - \left(\frac{\partial w_\epsilon}{\partial t} + \frac{\partial w_\epsilon}{\partial x}\right) + \frac{2\sqrt{\beta}}{\delta}(u_\epsilon - w_\epsilon e^{i\alpha})\,, \end{aligned} \quad (5.4.26)$$

which result from substituting $u = \epsilon\, u_\epsilon$, $w = \epsilon\, w_\epsilon$ into the defect conditions (5.3.4) and looking at the terms linear in ϵ. The ansatz to which these are solved

$$\begin{aligned} u_\epsilon &= u_{particle}(\theta) + R\, u_{particle}(-\theta)\,, \\ w_\epsilon &= T\, u_{particle}(\theta)\,, \end{aligned} \quad (5.4.27)$$

is a right-moving particle reflected and/or transmitted by the defect. We substitute the ansatz into the linearised defect conditions (5.4.26) and find that there is no

reflection and the transmission factor is

$$T_{particle/defect} = \frac{e^{\theta} - i\delta e^{i\alpha}}{e^{i\alpha}e^{\theta} + i\delta}. \tag{5.4.28}$$

This shows that like the SG and ShG defects, the CSG defect is reflectionless. We also compute this transmission factor by substituting the particle limit $a = \frac{\pi}{2}$ into the soliton-defect phase factor (5.4.21). In this limit the soliton-defect time-delay (5.4.20) vanishes.

5.4.5 Soliton equal to two defects?

We stated earlier that the soliton-defect time-delay (5.4.20) is half the soliton-soliton time-delay (4.6.4) if we match the relevant defect and soliton parameters. We check

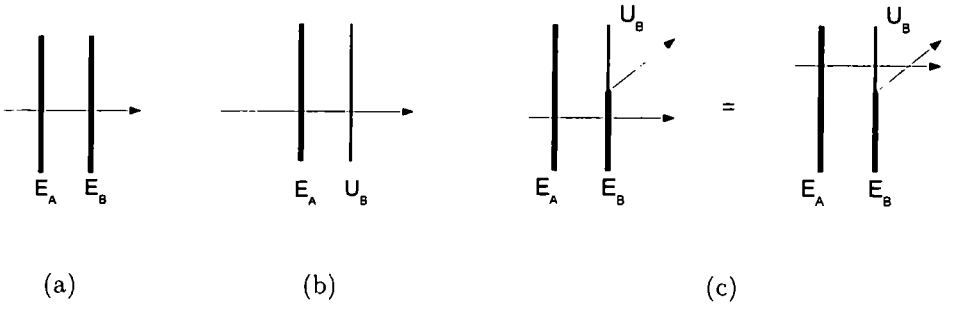

Fig. 5.20: (a) Soliton scattering through two excited defects. (b) Soliton scattering through an excited and an unexcited defect. (c) Soliton scattering through a defect and decaying defect.

the specific example that if a soliton or particle scatters through defects E_A and E_B (introduced in tables 5.9, 5.10) then the combined time-delay and phase shift are the same than if a soliton or particle scatters through a soliton with charge parameter $a = \frac{\pi}{3}$ and rapidity $e^{\theta} = 2$. That is the following relations hold

$$\Delta_t(E_A) + \Delta_t(E_B) = \Delta_t(\text{sol}), \quad e^{i\phi(E_A)}e^{i\phi(E_B)} = e^{i\phi(\text{sol})}, \quad T_{E_A}\,T_{E_B} = T_{sol}. \tag{5.4.29}$$

The summed total of the energy, momentum and charge of the two excited defects exactly matches the energy, momentum and charge of the soliton. These observations suggest that the integrable defects could be the fundamental objects of the theory, with two defects combined to give the solitons of the theory.

If as in figure 5.20(b) two defects are placed together whose quantities sum to zero, for example defects E_A and U_B, then the scattering soliton or particle experiences no overall time-delay or phase shift.

$$\Delta_t(E_A) + \Delta_t(U_B) = 0\,, \qquad e^{i\phi(E_A)}e^{i\phi(U_B)} = 1\,, \qquad T_{E_A}\,T_{U_B} = 1\,. \tag{5.4.30}$$

Figure 5.20(c) shows the decay of defect E_B when placed next to defect E_A, the integrability of the model ensures that the scattering of a soliton or particle through such a configuration should not be affected by the time that the scattering takes place. Therefore scattering through defects E_A and E_B should be the same as scattering through defects E_A and U_B and the emitted soliton, using the two previous results (5.4.29), (5.4.30) we see that this is the case. In appendix B.1 we show the relations (5.4.29), (5.4.30) explicitly. In appendix B.2 we show the consistency of the classical soliton-soliton and soliton-defect scattering properties, by examining explicitly a decay and absorption process.

5.5 Summary

In this section we have constructed a CSG defect theory that maintains the classical integrability of the bulk CSG theory. In fact, we have derived the CSG defect theory using two different descriptions. First, we constructed an integrable defect using the original 'two field' description, where on each side of the defect the field and its dual have to be simultaneously considered. In this description, the defect is described by one parameter δ. We showed that the energy, momentum and charge of the defect depends on the difference in the dual fields at the defect and that a positive energy defect can emit a soliton, while a negative energy defect can absorb a soliton. The difference in the initial and final dual fields at the defect allows for energy, momentum and charge to be transferred either to or from the defect during these processes. We found that solitons scatter through the defect experiencing a time-delay or time-advance, depending on the initial energy of the defect, and a phase shift.

Using the α formula derived in section 4.4 we re-derived the integrable CSG defect. This allows us to have to consider only the the $\beta > 0$ sector fields on each

side of the defect. The defect is now described by two parameters A and δ. The energy, momentum and charge of the defect now depend on these two parameters and also the choice of how α is related to A. We showed that there are four defects with the same energy and momentum but different charge. As in the first description we found that excited defects can emit a soliton and solitons can be absorbed by unexcited defects. The transfer of the conserved charges is now described by the value of $\cos(\alpha)$ being different at the beginning and end of the process, this is explicitly realised by the branch of the square root changing at a point during the process to keep the evolution of $\cos(\alpha)$ smooth. We found that each defect can absorb or emit one specific soliton, but there are two defects that can absorb or emit the same soliton. The change in charge during emission and absorption is found to be symmetric around $Q = \pm\pi$ and a defect never decays into its anti-defect.

We showed that solitons scatter through the defect experiencing a time-delay and phase shift and that the CSG particle is purely transmitted through the defect. As in the SG theory we have found that the time-delay for soliton-defect scattering is exactly half that of soliton-soliton scattering, suggesting that defects may be the fundamental objects of integrable field theories.

All the results in both descriptions agree with each other. Despite the complexity of the definition and behaviour of α we find this description better for the CSG defect. The fact that the defect is described by a rapidity parameter δ and charge parameter A which are directly related to the rapidity and charge of the absorbed or emitted soliton is a nice feature. In the next section we use this description of the CSG defect to construct a CSG boundary theory by "dressing the boundary".

Chapter 6

Complex sine-Gordon with dressed boundary

In this chapter we introduce a new integrable complex sine-Gordon boundary theory, by restricting the bulk theory to the halfline $x < 0$ and introducing boundary conditions at $x = 0$. As throughout this thesis the boundary conditions are constructed to maintain the integrability of the theory. As commented on in chapter 3 many different 1+1 dimensional integrable field theories on the halfline have been studied.

In previous work [47] an integrable complex sine-Gordon boundary theory was constructed with the Lagrangian

$$L = \int_{-\infty}^{0} dx \quad \mathcal{L}_{CSG} + \left[2C\sqrt{1-uu^*}\right]\Big|_{x=0} , \tag{6.0.1}$$

where the boundary term has no derivative pieces unlike the CSG defect Lagrangian (5.1.2) introduced in this thesis. The boundary conditions resulting from varying this action are

$$\partial_x u = -Cu\sqrt{1-uu^*}\,, \qquad \partial_x u^* = -Cu^*\sqrt{1-uu^*}\,. \tag{6.0.2}$$

Soliton solutions in this theory were analysed including the computation of the soliton-boundary reflection factor. The very specific phenomena exhibited by this model points towards a more general boundary theory with more generic behaviour. For example this boundary allows the emission and absorption of only the maximally charged soliton. Why should one charge of soliton be treated uniquely in this

way? It leads to the question of whether there are integrable boundaries described by different boundary conditions that allow the emission and absorption of other charged solitons? This observation about the original boundary theory provides the motivation to go on and investigate whether more general boundary conditions exist.

Inspired by the idea [61] that a wider class of boundary conditions can be generated by placing a defect in front of an existing boundary, in this chapter we construct new dressed boundary conditions for the CSG model by placing an integrable CSG defect, using the α description, in front of the most basic integrable boundary, the Dirichlet boundary. This idea of dressing the boundary is a recent advance, apart from the work described here the same method has been recently used for the sinh-Gordon theory [30]. Similar techniques have been used in spin chains [20] and conformal field theories [21], while the connection between defects and boundaries has previously been commented on [22].

In the next section we construct the dressed boundary theory, before analysing the new theory in later sections. A review of the original boundary theory [47] is not used as a starting point. Instead throughout the chapter the previous results are shown to be a specific case of the new dressed boundary.

6.1 Constructing the dressed boundary theory

First we recall that one of the simplest integrable boundaries is the Dirichlet boundary which is described by the boundary conditions $w = 0$, $w^* = 0$. This appears as the limit $C \to \infty$ in the original CSG boundary conditions (6.0.2). To construct the dressed boundary theory we start with the Dirichlet boundary at $x = 0$ and place an integrable defect in front of boundary at $x = -\delta x$. Therefore we have two bulk regions where distinct CSG fields live, one to left of the defect and one between the boundary and defect. The integrability of the bulk and defect theory allows the defect to be moved up to the boundary. By taking the limit $\delta x \to 0$ we create the dressed boundary, illustrated in figure 6.1. We are left with the single bulk region to the left of the dressed boundary.

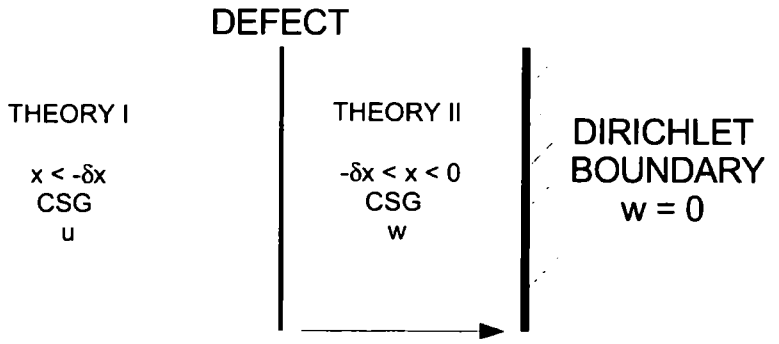

Fig. 6.1: Dressed boundary model set up.

To formulate the dressed boundary conditions, we substitute the Dirichlet boundary conditions (and $\partial_t w = 0$, $\partial_t w^* = 0$ since the boundary conditions hold for all time) into the CSG defect conditions (5.3.4) to give

$$\begin{aligned} \frac{u_t - u_x}{\sqrt{1-uu^*}} + w_x e^{i\alpha'} &= -2\sqrt{\beta}\,\delta\, u\, e^{i\alpha'}\,, \\ \frac{u_t + u_x}{\sqrt{1-uu^*}} e^{i\alpha'} + w_x &= \frac{2\sqrt{\beta}}{\delta} u\,, \end{aligned} \tag{6.1.1}$$

where

$$\alpha' = \arcsin\left(-\frac{\sin(A)}{\sqrt{1-uu^*}}\right)\,. \tag{6.1.2}$$

Combining these two conditions in a particular linear combination allows us to eliminate $\partial_x w$, producing the dressed boundary condition and its complex conjugate

$$\begin{aligned} \partial_x u &= -\partial_t u\; i\,\tan(\alpha') + \frac{\sqrt{\beta}}{\cos(\alpha')}\left(\delta + \frac{1}{\delta}\right) u\sqrt{1-uu^*}\,, \\ \partial_x u^* &= \partial_t u^*\; i\,\tan(\alpha') + \frac{\sqrt{\beta}}{\cos(\alpha')}\left(\delta + \frac{1}{\delta}\right) u^*\sqrt{1-uu^*}\,. \end{aligned} \tag{6.1.3}$$

The dressed boundary conditions (6.1.3) depend on the two parameters δ and A that appear in the CSG BT. They have first order time derivative terms inherited from the defect conditions, indicating that the dressed boundary will exhibit more general properties than the originally studied CSG boundary. The original boundary conditions appear as a specific case of the dressed boundary conditions when $A = 0$. This eliminates the first order time derivative term and the boundary conditions are

reduced to

$$\begin{aligned} \partial_x u &= \frac{\sqrt{\beta}}{\cos(\alpha^0)}\left(\delta+\frac{1}{\delta}\right) u\sqrt{1-uu^*}\,, \\ \partial_x u^* &= \frac{\sqrt{\beta}}{\cos(\alpha^0)}\left(\delta+\frac{1}{\delta}\right) u^*\sqrt{1-uu^*}\,, \end{aligned} \tag{6.1.4}$$

where $\alpha^0 = \{0, \pm\pi\}$. This is the boundary condition previously studied (6.0.2) with the identification

$$C = -\frac{\sqrt{\beta}}{\cos(\alpha^0)}\left(\delta+\frac{1}{\delta}\right)\,. \tag{6.1.5}$$

The multi-valued nature of α^0 alters the interpretation a little from the earlier analysis and allows easier understanding of the properties of the model, which we comment on later in the chapter.

From the dressed boundary conditions the aim, in a similar way to the defect model, is to formulate an expression for the Lagrangian and check that the dressed boundary conditions derived by this method, placing a defect in front of the Dirichlet boundary, does produce a theory that is classically integrable. Firstly to formulate the Lagrangian we hypothesise the general form

$$L = \int_{-\infty}^{0} dx\ \frac{\partial_t u\,\partial_t u^* - \partial_x u\,\partial_x u^*}{1-uu^*} - 4\beta\, uu^* + \left[A_1\,\partial_t u + A_2\,\partial_t u^* - \mathcal{L}_{db}\right]\Big|_{x=0}\,, \tag{6.1.6}$$

to include the standard bulk piece and boundary terms at $x = 0$. The form chosen is not the most general that can be written down. Using the defect Lagrangian as a guide, we have restricted the dressed boundary term in the Lagrangian to a dressed boundary potential term and terms linear in the first time derivative of the fields. Varying the action produces the CSG equation (4.1.2) in the bulk region $x < 0$ and the following conditions on the boundary $x = 0$

$$\begin{aligned} \frac{\partial_x u}{1-uu^*} &= \frac{\partial \mathcal{L}_B}{\partial u^*} - \partial_t\left(\frac{\partial \mathcal{L}_{DB}}{\partial(\partial_t u^*)}\right)\,, \\ \frac{\partial_x u^*}{1-uu^*} &= \frac{\partial \mathcal{L}_B}{\partial u} - \partial_t\left(\frac{\partial \mathcal{L}_{DB}}{\partial(\partial_t u)}\right)\,, \end{aligned} \tag{6.1.7}$$

where

$$\mathcal{L}_{DB} = A_1\,\partial_t u + A_2\,\partial_t u^* + \mathcal{L}_{db}\,. \tag{6.1.8}$$

We find the quantities in the Lagrangian

$$\begin{aligned} \mathcal{L}_{db} &= 2\sqrt{\beta}\left(\delta+\frac{1}{\delta}\right)\cos(\alpha')\sqrt{1-uu^*}\,, \\ A_1 &= -\frac{i}{u}\alpha'\,, \\ A_2 &= \frac{i}{u^*}\alpha'\,, \end{aligned} \tag{6.1.9}$$

by comparing the dressed boundary conditions (6.1.3) with the Euler-Lagrange equations (6.1.7). As with the defect theory the dressed boundary energy

$$\begin{aligned} E_{db} = \int_{-\infty}^{0} dx\ & \frac{\partial_t u\,\partial_t u^* + \partial_x u\,\partial_x u^*}{1-uu^*} + 4\beta\, uu^* \\ & + \left[2\sqrt{\beta}\left(\delta+\frac{1}{\delta}\right)\cos(\alpha')\sqrt{1-uu^*}\right]\Big|_{x=0}\,, \end{aligned} \tag{6.1.10}$$

is read directly from the Lagrangian and its conservation $\partial_t E_{db} = 0$ is easily verified. We formulate the conserved dressed boundary charge

$$Q_{db} = i\int_{x=-\infty}^{0} dx\ \frac{u\,\partial_t u^* - u^*\partial_t u}{1-uu^*} + \left[2\alpha'\right]\Big|_{x=0}\,, \tag{6.1.11}$$

by using the dressed boundary conditions to specify the boundary term needed to be added to the bulk charge to maintain its conservation in the dressed boundary theory.

In the dressed boundary theory there is no conserved dressed boundary momentum. This is expected as the dressed boundary breaks the translational invariance, the symmetry responsible for momentum conservation. This argument also applies to the defect theory, but the property that the BT and therefore defect conditions are true for all x means that in the defect theory it is possible to construct a conserved defect momentum. The lack of conserved momentum does not stop the theory from being classically integrable. There are infinite number of higher spin energy-like conserved charges which can be assumed to follow due to the construction of the dressed boundary, from the constituent integrable boundary and integrable defect. To support this conjecture in appendix A.2 we explicitly construct the form of the next energy-like charge and show its conservation.

There is a connection between the dressed boundary quantities and their defect counterparts. In fact the dressed boundary Lagrangian and quantities are retrieved from the defect ones by substituting $w = 0, \quad \partial_t w = 0$ into the defect quantities. This indicates that the dressed boundary theory can be constructed directly in the Lagrangian picture, as an alternative to the process used here where we found the dressed boundary conditions first and then the Lagrangian. In the work of Bajnok and Simon [30] they construct the dressed boundary sinh-Gordon theory in the Lagrangian form.

In this section we have constructed the CSG dressed boundary theory; formulating boundary conditions, the Lagrangian and conserved energy and charge. The various quantities of the theory have increased complexity over the quantities of the original CSG boundary theory, due to the presence of time derivative terms in the boundary conditions and Lagrangian. We have shown that the original theory is just one specific case of the dressed theory, the case when $A = 0$. The aim of producing a more general CSG boundary theory has been achieved. In the next section we analyse solutions to the dressed boundary theory to investigate whether the boundary exhibits any new properties.

6.2 Soliton solutions

In this section we investigate the different soliton solutions that solve the field equations, the equations of motion and dressed boundary conditions. We start by examining the vacuum of the theory before investigating whether the dressed boundary can absorb or emit solitons. We go on and ask whether dressed boundary bound states exist and examine how solitons and particles scatter from the dressed boundary.

The obvious candidate for the vacuum of the dressed boundary theory is when the bulk fields are in vacuum $u = 0$. This configuration has energy and charge

$$\begin{aligned} E &= 2\sqrt{\beta}\left(\delta + \frac{1}{\delta}\right)\cos(\alpha_0)\,, \\ Q &= 2\alpha_0\,, \end{aligned} \tag{6.2.1}$$

where $\alpha_0 = \alpha'(u = 0)$. As with the defect theory there is no contribution to the

energy and charge from the bulk but a non-zero contribution from the boundary. The contribution at the boundary depends on the two parameters that appear in the BT and dressed boundary conditions, with an explicit dependence on α_0 through which A appears. This α_0 dependence means that the dressed boundary can have different values of energy and charge for the same values of δ and A. Analogous to the defect we expect this behaviour to allow the boundary to emit and absorb solitons. The minimum energy solution for fixed $\delta > 0$ is when $\cos(\alpha_0) = -1$ with energy and charge

$$\begin{aligned} E &= -2\sqrt{\beta}\left(\delta + \frac{1}{\delta}\right), \\ Q &= 2\pi. \end{aligned} \tag{6.2.2}$$

As in the defect theory whether the energy of the dressed boundary is positive or negative determines its properties. We expect that a boundary with positive energy to be able to emit a soliton, while a boundary of negative energy to be able to absorb a soliton. We analyse these scenarios in the next section. From now on we will label a boundary with negative energy as an unexcited boundary and a boundary with positive energy an excited boundary.

It is natural to split the excited boundaries into eight types, meaning that there are eight boundaries with the same positive energy but different charges. As in the defect theory we need to make a choice on the solution of $\cos(\alpha_0)$, without loss of generality we use $\cos(\alpha_0) = \cos(A)$. In fact pairs of the boundaries have the same charge, but we list them separately as they are described by different δ and A. The excited boundaries listed in table 6.1 have energy $E = 2\sqrt{\beta}\left|\left(\delta + \frac{1}{\delta}\right)\cos(A)\right|$. For the specific case where $A' = \frac{\pi}{3}$ and $\delta' = 2$ then the eight boundaries have energy $E = \frac{5\sqrt{\beta}}{2}$ and charge $Q \in \left\{\pm\frac{2\pi}{3}, \pm\frac{4\pi}{3}\right\}$. Similarly we display the eight unexcited boundaries with energy $E = -2\sqrt{\beta}\left|\left(\delta + \frac{1}{\delta}\right)\cos(A)\right|$ in table 6.2. The specific case when $A' = \frac{\pi}{3}$ and $\delta' = -2$ gives boundaries with $E = -\frac{5\sqrt{\beta}}{2}$ and $Q \in \left\{\pm\frac{2\pi}{3}, \pm\frac{4\pi}{3}\right\}$.

6.2.1 Soliton absorption by the boundary

To analyse whether a soliton can be absorbed by the dressed boundary, we solve the field equations for a right-moving one-soliton solution moving from left infinity

$0 < A < \frac{\pi}{2}$	$A = A'$	$\delta > 1$	$\delta = \delta'$	$Q = -2A'$	$\in \{0, -\pi\}$
$-\frac{\pi}{2} < A < 0$	$A = -A'$	$\delta > 1$	$\delta = \delta'$	$Q = 2A'$	$\in \{\pi, 0\}$
$\frac{\pi}{2} < A < \pi$	$A = \pi - A'$	$\delta < -1$	$\delta = -\delta'$	$Q = 2(A' - \pi)$	$\in \{-\pi, -2\pi\}$
$-\pi < A < -\frac{\pi}{2}$	$A = -\pi + A'$	$\delta < -1$	$\delta = -\delta'$	$Q = 2(\pi - A')$	$\in \{2\pi, \pi\}$
$0 < A < \frac{\pi}{2}$	$A = A'$	$0 < \delta < 1$	$\delta = \frac{1}{\delta'}$	$Q = -2A'$	$\in \{0, -\pi\}$
$-\frac{\pi}{2} < A < 0$	$A = -A'$	$0 < \delta < 1$	$\delta = \frac{1}{\delta'}$	$Q = 2A'$	$\in \{\pi, 0\}$
$\frac{\pi}{2} < A < \pi$	$A = \pi - A'$	$-1 < \delta < 0$	$\delta = -\frac{1}{\delta'}$	$Q = 2(A' - \pi)$	$\in \{-\pi, -2\pi\}$
$-\pi < A < -\frac{\pi}{2}$	$A = -\pi + A'$	$-1 < \delta < 0$	$\delta = -\frac{1}{\delta'}$	$Q = 2(\pi - A')$	$\in \{2\pi, \pi\}$

Table 6.1: 8 excited boundaries with the same positive energy.

$0 < A < \frac{\pi}{2}$	$A = A'$	$\delta < -1$	$\delta = \delta'$	$Q = -2A'$	$\in \{0, -\pi\}$
$-\frac{\pi}{2} < A < 0$	$A = -A'$	$\delta < -1$	$\delta = \delta'$	$Q = 2A'$	$\in \{\pi, 0\}$
$\frac{\pi}{2} < A < \pi$	$A = \pi - A'$	$\delta > 1$	$\delta = -\delta'$	$Q = 2(A' - \pi)$	$\in \{-\pi, -2\pi\}$
$-\pi < A < -\frac{\pi}{2}$	$A = A' - \pi$	$\delta > 1$	$\delta = -\delta'$	$Q = 2(\pi - A')$	$\in \{2\pi, \pi\}$
$0 < A < \frac{\pi}{2}$	$A = A'$	$-1 < \delta < 0$	$\delta = \frac{1}{\delta'}$	$Q = -2A'$	$\in \{0, -\pi\}$
$-\frac{\pi}{2} < A < 0$	$A = -A'$	$-1 < \delta < 0$	$\delta = \frac{1}{\delta'}$	$Q = 2A'$	$\in \{\pi, 0\}$
$\frac{\pi}{2} < A < \pi$	$A = \pi - A'$	$0 < \delta < 1$	$\delta = -\frac{1}{\delta'}$	$Q = 2(A' - \pi)$	$\in \{-\pi, -2\pi\}$
$-\pi < A < -\frac{\pi}{2}$	$A = A' - \pi$	$0 < \delta < 1$	$\delta = -\frac{1}{\delta'}$	$Q = 2(\pi - A')$	$\in \{2\pi, \pi\}$

Table 6.2: 8 unexcited boundaries with the same negative energy.

towards the boundary. As with the defect computations, we have to make a choice on the initial value of α'. Using $\cos(\alpha') = \cos(A)$ at the past temporal infinity without loss of generality, we find the dressed boundary conditions are satisfied when

$$\begin{aligned} \delta &= e^{\theta},\ e^{-\theta} \qquad a = -A + \pi\,, \\ \delta &= -e^{\theta},\ -e^{-\theta} \qquad a = -A\,. \end{aligned} \tag{6.2.3}$$

Since the boundary conditions can be satisfied in this set up there are boundaries that do absorb a soliton. This is expected knowing the behaviour of the defect, which also absorbs solitons and remembering that the dressed boundary is constructed by placing a defect in front of a Dirichlet boundary. Recall that the defect could only absorb a right-moving soliton if the defect rapidity was $|\delta| > 1$, but a boundary described by any δ can absorb a soliton due to the four separate choices (6.2.3) that satisfy the boundary conditions.

Thinking of the dressed boundary as a construction of its constituent defect and boundary, we can explain these extra absorption processes by noting that there are two ways that a boundary can absorb a soliton. Figure 6.2(a) shows the soliton

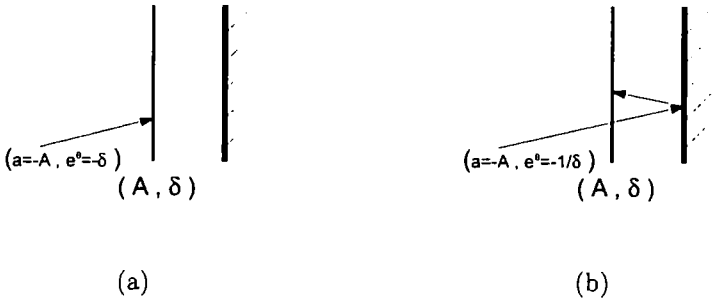

Fig. 6.2: The two methods of soliton absorption by the dressed boundary.

being absorbed directly by the defect and figure 6.2(b) shows the second method of absorption where the soliton is absorbed after reflecting back from the Dirichlet boundary. This second method allows boundaries with rapidity $|\delta| < 1$ to absorb solitons, as well as the usual defect absorption by boundaries with rapidity $|\delta| > 1$.

We find that each boundary absorbs exactly one soliton but there are four unexcited boundaries that absorb a soliton of the same energy and charge. In tables 6.3 and 6.4 we show two such boundaries absorbing a charge $Q_{sol} = \frac{2\pi}{3}$ soliton with energy $E_{sol} = 5\sqrt{\beta}$. The other two boundaries that absorb the same soliton are related by $\delta \to \frac{1}{\delta}$. In absorption I we have an unexcited boundary described by $A = \frac{2\pi}{3}$ and $\delta = 2$ being excited by the absorption of the described soliton and similarly in II an unexcited boundary with $A = -\frac{\pi}{3}$ and $\delta = -2$. Analogous to the defect case, α' changes in time allowing the boundary to change energy and charge which makes this absorption process possible.

6.2.2 Soliton emission by the boundary

We have seen that the dressed boundary can absorb a soliton solution if the initial energy of the boundary is negative. We now analyse whether the reversal of this process is possible, i.e. can an excited boundary emit a soliton? To examine whether the boundary can emit a soliton we solve the field equations for a left-moving soliton,

Unexcited Boundary I	$\rightarrow$	Excited Boundary I
$(A = \frac{2\pi}{3}\ ,\ \delta = 2)$	Absorbed Soliton	$(A' = \frac{\pi}{3},\ \delta' = 2)$
$\alpha = -A$	$(a = -A + \pi, e^{\theta} = \delta)$	$\alpha = A - \pi$
$E = -\frac{5\sqrt{\beta}}{2}$	$E_{sol} = 5\sqrt{\beta}$	$E' = -E$
$Q = -\frac{4\pi}{3}$	$Q_{sol} = \frac{2\pi}{3}$	$Q' = -\frac{2\pi}{3}$

Table 6.3: Unexcited boundary I absorbing a soliton with $E_{sol} = 5\sqrt{\beta}$ and $Q_{sol} = \frac{2\pi}{3}$.

Unexcited Boundary II	$\rightarrow$	Excited Boundary II
$(A = -\frac{\pi}{3}\ ,\ \delta = -2)$	Absorbed Soliton	$(A' = -\frac{2\pi}{3}\ ,\ \delta' = -2)$
$\alpha = -A$	$(a = -A, e^{\theta} = -\delta)$	$\alpha = A + \pi$
$E = -\frac{5\sqrt{\beta}}{2}$	$E_{sol} = 5\sqrt{\beta}$	$E' = -E$
$Q = \frac{2\pi}{3}$	$Q_{sol} = \frac{2\pi}{3}$	$Q' = \frac{4\pi}{3}$

Table 6.4: Unexcited boundary II absorbing a soliton with $E_{sol} = 5\sqrt{\beta}$ and $Q_{sol} = \frac{2\pi}{3}$.

once again we make the choice $\cos(\alpha') = \cos(A)$ at $t \rightarrow -\infty$. We find the dressed boundary conditions are satisfied when

$$\begin{aligned} \delta &= e^{\theta},\ e^{-\theta} \qquad a = A, \\ \delta &= -e^{\theta},\ -e^{-\theta} \qquad a = A + \pi\,. \end{aligned} \tag{6.2.4}$$

As with the absorption process we explain the property that boundaries of all $\delta \in \mathbb{R}$ can emit a soliton by splitting the emission processes into two types. The soliton can be emitted, either directly from the defect shown in figure 6.3(a) or emitted to the right before reflecting back from the Dirichlet boundary illustrated in figure 6.3(b).

Again we find that each boundary emits just one type of soliton but there are four boundaries that emit a soliton with the same energy and charge. In tables 6.5 and 6.6 we show two boundaries that emit a soliton with energy $E_{sol} = 5\sqrt{\beta}$ and charge $Q_{sol} = \frac{2\pi}{3}$. These two boundaries, excited boundary I described by $A = \frac{\pi}{3}$ and $\delta = 2$ and excited boundary II with $A = -\frac{2\pi}{3}$ and $\delta = -2$, are joined by two

(a) (b)

Fig. 6.3: The two methods of soliton emission by the dressed boundary.

other boundaries related by $\delta \longrightarrow \frac{1}{\delta}$ that emit the same soliton.

Excited Boundary I	$\longrightarrow$	Unexcited Boundary I
$(A = \frac{\pi}{3}\ ,\ \delta = 2)$	Emitted Soliton	$(A' = \frac{2\pi}{3}\ ,\ \delta' = 2)$
$\alpha = -A$	$(a = A, e^{\theta} = \delta)$	$\alpha = A - \pi$
$E = \frac{5\sqrt{\beta}}{2}$	$E_{sol} = 5\sqrt{\beta}$	E' = -E
$Q = -\frac{2\pi}{3}$	$Q_{sol} = \frac{2\pi}{3}$	$Q' = -\frac{4\pi}{3}$

Table 6.5: Excited boundary I emitting a soliton with $E_{sol} = 5\sqrt{\beta}$ and $Q_{sol} = \frac{2\pi}{3}$.

As with the defect we find that the change in charge during emission and absorption is once again symmetric around $Q = \pm\pi$. For example, during the emission process described in table 6.6 the charge of the boundary before is $Q = \frac{4\pi}{3}$ and after $Q = \frac{2\pi}{3}$, symmetric around $Q = +\pi$.

The CSG boundary theory previously studied only allowed the emission and absorption of the maximally charged soliton, although the authors did not explicitly state that the boundary could have $Q = \pm 2\pi$ as well as zero charge. Explicitly the restriction from the dressed boundary to the theory with no time derivatives in the boundary term of the Lagrangian is by setting $A = 0$, which actually amounts to setting $\alpha' = \alpha^{A=0} = \{0,\ \pm\pi\}$. This restricted theory is different to the one originally studied, with the conserved charge of this theory having the form

$$Q^{A=0} \;=\; i\int_{-\infty}^{0} dx\ \frac{u\,\partial_t u^* - u^*\partial_t u}{1 - uu^*} + \left[2\,\alpha^{A=0}\right]\Big|_{x=0}\,, \qquad (6.2.5)$$

Excited Boundary II	→	Unexcited Boundary II
$(A = -\frac{2\pi}{3}\ ,\ \delta = -2)$	Emitted Soliton	$(A' = -\frac{\pi}{3}\ ,\ \delta' = -2)$
$\alpha = -A$	$(a = A + \pi, -e^{\theta} = \delta)$	$\alpha = A + \pi$
$E = \frac{5\sqrt{\beta}}{2}$	$E_{sol} = 5\sqrt{\beta}$	E' = -E
$Q = \frac{4\pi}{3}$	$Q_{sol} = \frac{2\pi}{3}$	$Q' = \frac{2\pi}{3}$

Table 6.6: Excited boundary II emitting a soliton with $E_{sol} = 5\sqrt{\beta}$ and $Q_{sol} = \frac{2\pi}{3}$.

allowing the boundary to have charge $Q^{A=0} = \{0,\ \pm 2\pi\}$, not just zero charge. This theory does permit soliton emission and absorption, with the maximally charged soliton emitted from the excited defect and absorbed by the unexcited defect.

We have shown that dressed boundary can store both energy and charge and due to the definition of α' can transfer the charges to and from soliton solutions allowing the absorption and emission of solitons. Each excited boundary can emit a soliton solution, with the soliton charge related to the initial charge of the boundary and similarly all boundaries with negative energy can absorb a specific soliton.

6.2.3 Dressed boundary bound states

Following on from analysing soliton absorption and emission, we go on a ask whether there exists any dressed boundary bound states. Mathematically constructed by solving the boundary conditions with a stationary soliton solution, (4.5.2) with $\theta = 0$, in the bulk with its position shifted $x \longrightarrow x - c$. We find that the boundary conditions are satisfied when

$$\left(\delta + \frac{1}{\delta}\right) = 2\frac{\cos(a)\sinh(C)\sqrt{\cos^2(A)\cosh(C)^2 - \cos^2(a)} + \sin(a)\sin(A)\cosh(C)^2}{\cosh(C)^2 - \cos^2(a)}, \tag{6.2.6}$$

where $C = 2\sqrt{\beta}\cos(a)c$. This constraint is only valid when the argument in the square root is greater than zero and

$$\frac{1}{2}\left(\delta + \frac{1}{\delta}\right) \in \left[\min\left\{-\cos(A+a), \cos(A-a)\right\},\ \max\left\{-\cos(A+a), \cos(A-a)\right\}\right], \tag{6.2.7}$$

which implies that δ is a pure phase within the range specified. We can solve the constraint (6.2.6) to find

$$\tanh(2\sqrt{\beta}\cos(a)c) = \pm\frac{(\cos(b)\,\sin(a) - \sin(A))}{\cos(a)\,\sin(b)}\,, \quad \pm i\tan(a)\,, \tag{6.2.8}$$

with the last two solutions discounted as they infer c is complex. Here we have defined b through the relation $\frac{1}{2}(\delta + \frac{1}{\delta}) = \cos(b)$. There are therefore two positions where the bound soliton can be placed for the boundary conditions to be satisfied, and these are related by the parity transformation $x \longrightarrow -x$. To understand these solutions, it is useful to rewrite the boundary conditions (6.1.3) in the form

$$\sqrt{\cos(A)^2 - uu^*}\,\partial_x u \;=\; \partial_t u\; i\;\sin(A) + \sqrt{\beta}\left(\delta + \frac{1}{\delta}\right)u(1 - uu^*)\,. \tag{6.2.9}$$

Using the expression (6.2.8) for $\tanh(2\sqrt{\beta}\cos(a)c)$, it is easy to show that

$$\sqrt{\cos(A)^2 - uu^*} = \pm\frac{(\cos(b)\,\sin(a)\, - \sin(A))}{\sin(b)} \tag{6.2.10}$$

and for the boundary condition (6.2.9) to be satisfied, the signs in (6.2.8) and (6.2.10) must be correlated. Thus the two solutions for the position of the soliton correspond to different choices of the sign of the square root in the boundary conditions (6.2.9). The same square root appears in the boundary Lagrangian, and thus the two different solutions correspond to bound states of different boundaries. We calculate the energy and charge of the bound state by substituting the stationary soliton solution into the total energy (6.1.10) and charge (6.1.11) respectively and simplify using the two valid solutions for $\tanh(2\sqrt{\beta}\cos(a)c)$ to give

$$\begin{aligned} E_{bs}^{\pm} &= 4\sqrt{\beta}\,(|\cos(a)| \pm \sin(A)\sin(b))\,, \\ Q_{bs}^{\pm} &= Q_{bulk} \pm 2\left(b - \frac{\pi}{2}\right)\,, \end{aligned} \tag{6.2.11}$$

where

$$Q_{bulk} = \left\{ \begin{array}{lcl} 2a - \pi & ; & \frac{\pi}{2} < a < \pi \\ \pi - 2a & ; & 0 < a < \frac{\pi}{2} \\ -2a - \pi & ; & -\frac{\pi}{2} < a < 0 \\ 2a + \pi & ; & -\pi < a < -\frac{\pi}{2} \end{array} \right\}. \tag{6.2.12}$$

These dressed boundary bound states include the bound states found in the original boundary theory, with all the above quantities in the case when $A = 0$

agreeing to the previous quantities [47]. The way the charge is written above suggests that it does not change in the $A = 0$ limit, this is not the case due to the A dependence in (6.2.6).

6.2.4 Soliton reflection from the boundary

We continue the analysis of the classical solutions by calculating the classical time-delay for a soliton reflecting from the dressed boundary. We model the reflection using a two-soliton solution and demanding it satisfies the boundary conditions. By specifying that one of the constituent solitons is left-moving and the other right-moving, the idea is to make the right-moving soliton represent the soliton before it reflects from the boundary and the left-moving one model the soliton after reflection. To ensure that energy and charge conservation are satisfied we make the parameter choices $a_1 = a_2 = a$ and $\theta_1 = -\theta_2 = \theta$. These choices mean that the two solitons involved in the soliton-soliton scattering carry the same charge and equal and opposite rapidity. Therefore we are modelling the soliton reflection where the the incoming and outgoing solitons have the same energy and charge.

Substituting the expression for a two-soliton solution (4.5.5), along with the constituent one-soliton solutions (4.5.2) u_1, u_2 with $N_1 = 1$, $N_2 = e^{if}$, $c_1 = c$, $c_2 = d$ (we can set $N_1 = 1$, since it is only the phase difference between the two solitons that affects the scattering properties) into the boundary condition creates a long and complicated expression. To simplify the computation we expand each element of the boundary condition in a power series for an exponentiated time parameter. As the boundary conditions hold for all time we can use the individual terms of the power series to solve for constraint conditions. We solve for $(\delta + \delta^{-1})$ and use the fact that this is real to give two constraints. The first by specifying the imaginary part of the whole expression vanishes

$$i\left(e^{\theta}\sin(\zeta + A) + e^{-\theta}\sin(\zeta - A)\right) = \frac{\sinh(\theta)}{\cos(a)}\left(e^{-ia}\sinh(\lambda - iA) - e^{ia}\sinh(\lambda + iA)\right), \tag{6.2.13}$$

and the remaining real equation

$$\delta + \frac{1}{\delta} = \frac{\sin(a)\left(e^{\theta}\sin(\zeta + A) - e^{-\theta}\sin(\zeta - A)\right)}{\cosh(\lambda) + \cos(\zeta)} - \frac{\cosh(\theta)\left(e^{ia}\sinh(\lambda + iA) + e^{-ia}\sinh(\lambda - iA)\right)}{\cosh(\lambda) + \cos(\zeta)}, \tag{6.2.14}$$

where

$$e^{\lambda} = e^{2\sqrt{\beta}\cos(a)\cosh(\theta)(c+d)}, \qquad e^{i\zeta} = e^{2i\sqrt{\beta}\sin(a)\sinh(\theta)(c+d)}\, e^{-i\phi}. \tag{6.2.15}$$

We expand the constraint equations and solve for $\cosh(\lambda)$, $\sinh(\lambda)$, $\cos(\zeta)$, $\sin(\zeta)$ allowing quadratics in $\cosh(\chi)$ in terms of either λ or ζ to be found by eliminating the other

$$0 = \cosh^2(\chi) + \frac{\cosh(\theta)}{\sinh(\lambda)}\left(e^{ia}\cosh(\lambda + iA) + e^{-ia}\cosh(\lambda - iA)\right)\cosh(\chi) + \frac{2\sinh(\lambda)\cosh(\theta) + e^{2ia}\sinh(\lambda + 2iA) + e^{-2ia}\sinh(\lambda - 2iA)}{4\sinh(\lambda)}, \tag{6.2.16}$$

$$0 = \cosh^2(\chi) + \frac{\sin(a)}{\sin(\zeta)}\left(e^{\theta}\cos(\zeta + A) - e^{-\theta}\cos(\zeta - A)\right)\cosh(\chi) - \frac{\left(2\cos(2a)\sin(\zeta) + e^{2\theta}\sin(\zeta + 2A) + e^{-2\theta}\sin(\zeta - 2A)\right)}{4\sin(\zeta)}. \tag{6.2.17}$$

We solve these quadratics for $e^{2\lambda}$ and $e^{2i\zeta}$ respectively and re-express using

$$e^{\lambda} = e^{2\sqrt{\beta}\cos(a)\sinh(\theta)\Delta t}, \qquad e^{i\zeta} = e^{-i\phi}\, e^{2i\sqrt{\beta}\sin(a)\cosh(\theta)\Delta t}, \tag{6.2.18}$$

as a time-delay

$$\Delta t = \frac{1}{2\sqrt{\beta}\cos(a)\sinh(\theta)} \ln\left|\frac{\sinh\left(\frac{\theta-\chi}{2} + i\frac{a-A}{2}\right)\sinh\left(\frac{\theta+\chi}{2} + i\frac{a-A}{2}\right)}{\cosh\left(\frac{\theta-\chi}{2} + i\frac{a+A}{2}\right)\cosh\left(\frac{\theta+\chi}{2} + i\frac{a+A}{2}\right)}\right| \tag{6.2.19}$$

and phase shift

$$e^{i\phi} = -\left(\frac{\delta + e^{\theta}e^{iA}e^{ia}}{e^{\theta}e^{ia} - \delta e^{iA}}\right)\left(\frac{1 + \delta e^{iA}e^{ia}e^{\theta}}{e^{iA} - \delta e^{\theta}e^{ia}}\right) e^{2\sqrt{\beta}\sinh(\theta + ia)\Delta t}, \tag{6.2.20}$$

experienced by the soliton reflecting from the dressed boundary.

Figure 6.4 shows that the time-delay experienced by the reflected soliton is due to two effects, the standard time-delay from the soliton-soliton scattering and the

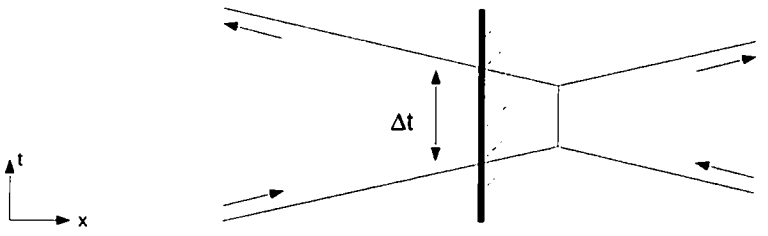

Fig. 6.4: Soliton reflection from dressed the boundary.

position behind the boundary where this scattering takes place. These two effects both arise because of the mathematical construction used to describe the soliton scattering from the boundary, in reality the time-delay experienced by the soliton is due to a non-zero time scattering with the boundary. As with the defect time-delay, soliton emission and absorption appear as special limits of the soliton-boundary time-delay.

6.2.5 Particle reflection from the boundary

To complete the analysis of solutions interacting with the boundary we investigate how the CSG particle interacts with the dressed CSG boundary. First we consider the reflection from the dressed boundary and then from the dressed boundary bound state. To calculate the particle reflection matrix, we linearise the dressed boundary conditions giving

$$\begin{aligned} \frac{\partial u_\epsilon}{\partial x} - i\tan(A)\frac{\partial u_\epsilon}{\partial t} - \frac{\sqrt{\beta}}{\cos(A)}\left(\delta + \frac{1}{\delta}\right)u_\epsilon &= 0, \\ \frac{\partial u_\epsilon^*}{\partial x} + i\tan(A)\frac{\partial u_\epsilon^*}{\partial t} - \frac{\sqrt{\beta}}{\cos(A)}\left(\delta + \frac{1}{\delta}\right)u_\epsilon^* &= 0. \end{aligned} \tag{6.2.21}$$

These linearised equations are then solved with an incoming and outgoing particle (4.7.1)

$$u_\epsilon = u_{particle}(\theta) + R_{particle}\, u_{particle}(-\theta), \tag{6.2.22}$$

which gives the particle reflection factor

$$R_{particle} = \frac{2i\sinh(\theta + iA) + (\delta + \frac{1}{\delta})}{2i\sinh(\theta - iA) - (\delta + \frac{1}{\delta})}. \tag{6.2.23}$$

We can also obtain this particle reflection factor by taking the $a = \frac{\pi}{2}$ limit of the soliton reflection phase factor (6.2.20).

The calculation to find the particle reflection factor from the dressed boundary bound state is more involved. First we need the solution for a small perturbation around a stationary soliton solution (4.7.7). We rewrite the solution for a right-moving plane wave

$$e_R(x,t) = f(x)\, e^{-2i\sqrt{\beta}(\cosh(\theta)\, t - \sinh(\theta)\, x)} e^{4i\sqrt{\beta}\sin(a)\, t} + g_R(x)\, e^{2i\sqrt{\beta}(\cosh(\theta)\, t - \sinh(\theta)\, x)}\,, \tag{6.2.24}$$

where

$$\begin{aligned} f(x) &= \frac{1}{\cosh^2(2\sqrt{\beta}\cos(a)\, x)}\,, \\ g_R(x) &= c_1 + c_2 \tanh(2\sqrt{\beta}\cos(a)\, x) + \frac{1}{\cosh^2(2\sqrt{\beta}\cos(a)\, x)} \end{aligned} \tag{6.2.25}$$

and

$$\begin{aligned} c_1 &= -\frac{2i(e^{\theta}e^{ia} - e^{\theta} - ie^{ia} - i)(e^{\theta}e^{ia} + e^{\theta} - i + ie^{ia})e^{ia}}{e^{\theta}(e^{ia} - i)^2(e^{ia} + i)^2}\,, \\ c_2 &= -\frac{2i(e^{\theta} + 1)(e^{\theta} - 1)e^{ia}}{e^{\theta}(e^{ia} - i)(e^{ia} + i)}\,. \end{aligned} \tag{6.2.26}$$

Similarly for a left-moving plane wave

$$e_L(x,t) = f(x)\, e^{-2i\sqrt{\beta}(\cosh(\theta)\, t + \sinh(\theta)\, x)} e^{4i\sqrt{\beta}\sin(a)\, t} + g_L(x)\, e^{2i\sqrt{\beta}(\cosh(\theta)\, t + \sinh(\theta)\, x)}\,, \tag{6.2.27}$$

where

$$g_L(x) = c_1 - c_2 \tanh(2\sqrt{\beta}\cos(a)x) + \frac{1}{\cosh^2(2\sqrt{\beta}\cos(a)x)}\,. \tag{6.2.28}$$

By substituting a small perturbation around the stationary soliton into the boundary conditions we find the linearised boundary conditions around the bound state. This is a differential equation in the linearised bulk solution involving the one-soliton solution bound to the boundary. The linearised solution to represent a particle reflecting from the boundary bound state is

$$E(x,t) = e_R(x - c, t) + \rho\, e_L(x - c, t)\,, \tag{6.2.29}$$

where c is the position of the bound soliton (6.2.8). ρ is a constant which can be found by demanding that the perturbation $E(x,t)$ satisfies the linearised boundary conditions. By inspecting the $x \to -\infty$ limit of the resultant plane wave solution, the classical particle-bound-state reflection factor is identified to be

$$R_{bs} = \frac{(e^{\theta} + ie^{ib}e^{iA})(e^{iA}e^{\theta} - ie^{ib})(e^{\theta}e^{ia} - i)^2}{(e^{ib}e^{\theta}e^{iA} - i)(ie^{iA} + e^{ib}e^{\theta})(ie^{ia} + e^{\theta})^2}\,. \tag{6.2.30}$$

6.2.6 Descriptions of charged boundaries

We begin our examination of the spectrum of boundaries by comparing the two descriptions for charged boundaries. For the CSG dressed boundary, both unexcited boundary with the properties (6.2.1) and the boundary bound states with the properties (6.2.11) can carry charge. One idea is that these might provide two alternative descriptions for a single tower of charged boundary states. However this turns out not to be the case. Despite having the freedom to set the charge and energies to agree, we find that the particle reflection factors do not equate. We conclude that the unexcited boundary and bound state are not the same object, expect in particular cases.

For example the unexcited boundary with charge Q is described by the charge parameter $A = -\frac{Q}{2}$ and if we consider a bound state (using E^{+}_{bs} and Q^{+}_{bs} (6.2.11)) described by the same A with $0 < a < \frac{\pi}{2}$ then the bound state has charge Q when $a = b + A$ and the energy

$$E^{+} = 4\sqrt{\beta}\,(\cos(b+A) + \sin(A)\sin(b)) = 4\sqrt{\beta}\cos(A)\cos(b)\,, \tag{6.2.31}$$

equals the energy of the unexcited boundary. We find that the particle reflection factors also agree in this limit. Therefore the bound state and unexcited boundary are the same object when the charge parameter of the bound soliton is the specific value $a = A + b$. There is a similar limit when using E^{-}_{bs} and Q^{-}_{bs} (6.2.11), in this case to bound state reduces to the unexcited boundary when $a = A - b$.

To understand these limits we analyse the bound state solutions. We reinterpret the allowed range of values for $\cos(b)$ (6.2.7) as a constraint on the charge parameter a of the bound soliton. Figure 6.5 illustrates the values of a for two boundaries, with the dotted line on the figures $\cos(b)$ and the two solid curves $\cos(A - a)$ and

$-\cos(A+a)$. Classical bound states exist for the values of a when the two curves

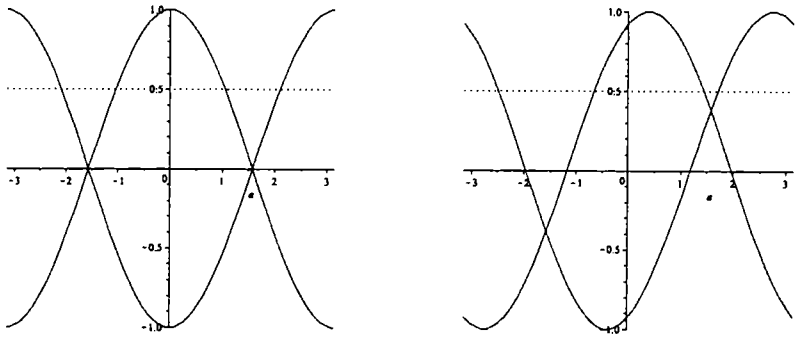

(a) (b)

Fig. 6.5: Plots of $\cos(b)$, $\cos(A-a)$, $-\cos(A+a)$, for (a) $A=0$, $b=\frac{\pi}{3}$, (b) $A=\frac{\pi}{8}$, $b=\frac{\pi}{3}$.

lie either side the dotted line. For both boundaries there are two separate regions, we concentrate on the region that includes $a=0$. Figure 6.5(a) shows that there exists bound states if $-\frac{\pi}{3} < a < \frac{\pi}{3}$ for the boundary described by $A=0$, $b=\frac{\pi}{3}$. Similarly, figure 6.5(b) shows that there exists bound states if $-\frac{\pi}{3}+\frac{\pi}{8} < a < \frac{\pi}{3}+\frac{\pi}{8}$ for the boundary described by $A=\frac{\pi}{8}$, $b=\frac{\pi}{3}$. We note that both ranges are between $A+b$ and $A-b$, which are precisely the values where the bound state reduces to the unexcited boundary.

Figure 6.6 shows that for both boundaries on the right end of the region $a=A+b$ the bound soliton is positioned away at positive infinity $c \to +\infty$ and at the left extreme away $a=A-b$ at negative infinity when the plus solution for $\tanh(2\sqrt{\beta}\cos(a)c)$ (6.2.8) is used. While figure 6.7 shows that for both boundaries when $a=A+b$ the bound soliton is positioned away at negative infinity $c \to -\infty$ and when $a=A-b$ positioned at positive infinity when the minus solution for $\tanh(2\sqrt{\beta}\cos(a)c)$ (6.2.8) is used. These figures illustrate that in both charge limits where the bound state reduces to the unexcited boundary the bound soliton is positioned at right infinity behind the boundary. As the charge parameter moves away from the unexcited boundary limit, either decreasing from $a=A+b$ or increasing from $a=A-b$, the bound soliton moves from right infinity to left infinity when it reaches the other end of the range. The soliton being positioned at right infinity and hidden behind the boundary fits with the fact that the bound state reduces to

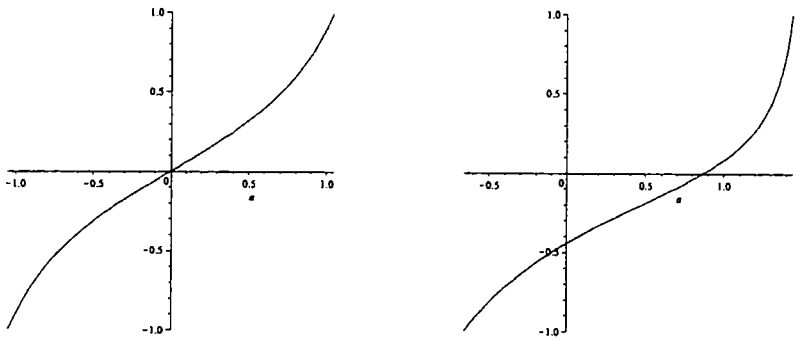

(a) (b)

Fig. 6.6: Plots of $\tanh(2\sqrt{\beta}\cos(a)c)$ using plus sign with $\beta = 1$ for (a) $A = 0$, $b = \frac{\pi}{3}$, (b) $A = \frac{\pi}{8}$, $b = \frac{\pi}{3}$.

the unexcited boundary when the soliton is in this position. In figures 6.8 and 6.9

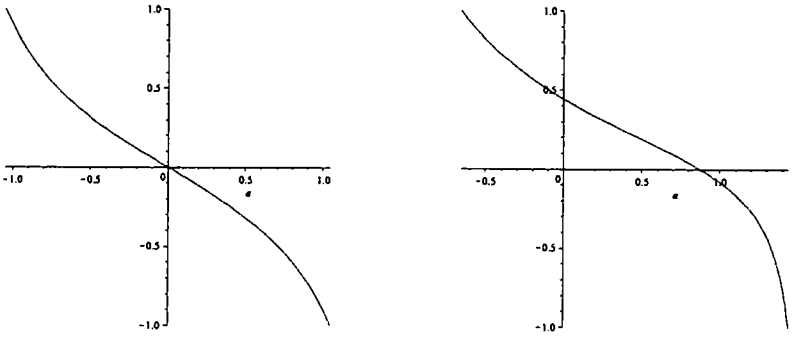

(a) (b)

Fig. 6.7: Plots of $\tanh(2\sqrt{\beta}\cos(a)c)$ using minus sign with $\beta = 1$ for (a) $A = 0$, $b = \frac{\pi}{3}$, (b) $A = \frac{\pi}{8}$, $b = \frac{\pi}{3}$.

we graph the energy and charge for the bound states in the range of a where the constraint is satisfied, using both forms of the energy and charge. They show that the energy and charge are simply shifted by a constant between the different energy and charge formulae. In both examples the maximum energy is when $a = 0$.

To complete the analysis of the classical bound states we examine one further example with $A = \frac{\pi}{4}$, $b = \frac{\pi}{8}$. In figure 6.10 the energy and charge are plotted for the two different energy and charge formulae. We note that in figure 6.10(b) that as the bound soliton moves out from right infinity, this corresponds to the charge parameter increasing from $A - b$, the energy of the bound state decreases. We come

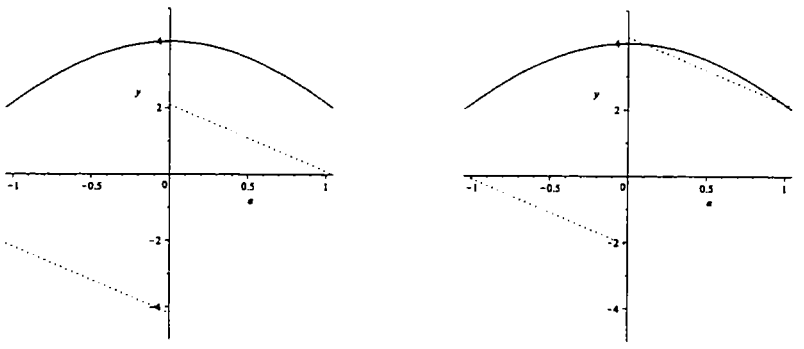

(a) (b)

Fig. 6.8: Charge (dotted) and energy (solid) of bound states with $\beta = 1$ for $A = 0$, $b = \frac{\pi}{3}$ using (a) E^+, Q^+ (b) E^-, Q^-.

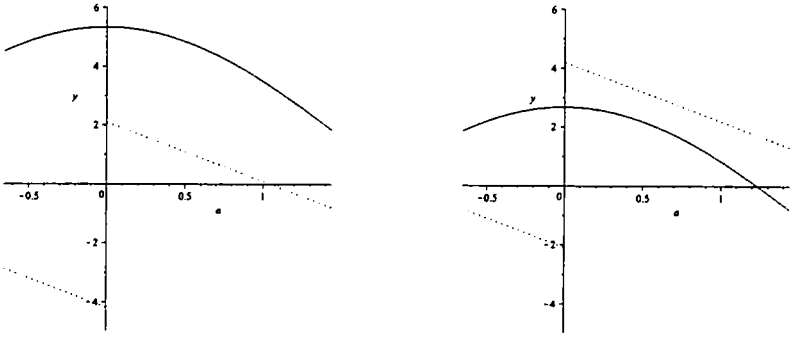

(a) (b)

Fig. 6.9: Charge (dotted) and energy (solid) of bound states with $\beta = 1$ for $A = \frac{\pi}{8}$, $b = \frac{\pi}{3}$ using (a) E^+, Q^+ (b) E^-, Q^-.

back to this point in the analysis of the quantum theory.

Analysis of the particle reflection factor (6.2.23) shows that it has two poles at

$$\theta = A + b - \frac{\pi}{2}, \quad A - b - \frac{\pi}{2}, \tag{6.2.32}$$

which correspond respectively to the field taking the values

$$u = e^{-2i\sqrt{\beta}\sin(A-b)t}\, e^{2\sqrt{\beta}\cos(A-b)x}, \quad e^{-2i\sqrt{\beta}\sin(A+b)t}\, e^{2\sqrt{\beta}\cos(A+b)x}. \tag{6.2.33}$$

These suggest the existence of bound states when the bound soliton has either charge parameter $a = A + b$ or $a = A - b$. This is in agreement with what we discovered when considering the bound states with the soliton hidden far behind the boundary at right infinity.

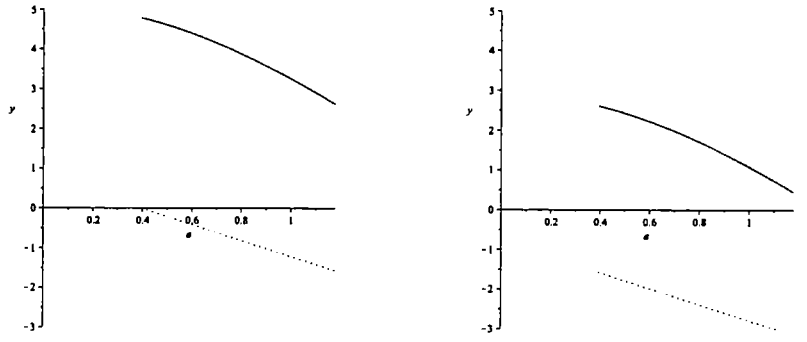

(a) (b)

Fig. 6.10: Charge (dotted) and energy (solid) of bound states with $\beta = 1$ for $A = \frac{\pi}{4}$, $b = \frac{\pi}{8}$ using (a) E^+, Q^+ (b) E^-, Q^-

The bound states found here are an extra solution not found in the defect theory. In the defect theory it is possible to satisfy the defect conditions with a stationary soliton on each side of the defect, but there is no constraint on the positions of the solitons. It exhibits zero mode type behaviour and the solitons are not bound to the defect. In the introduction we commented that the ShG boundary admits breather bound state solutions. They are similar to the CSG bound states found here in that they are both time dependent solutions, due to the nature of the ShG breather solution and the rotating phase in the CSG soliton solution.

6.2.7 Dressed boundary consistency check

In this section we check the consistency of the soliton time-delay when reflecting from the dressed boundary in relation to the soliton-defect time-delay and reflection time-delay from the Dirichlet boundary. Figure 6.11 shows the check in diagrammatic form.

We find that the following relations do hold

$$\Delta_{DB} = \Delta t_L + \Delta_{Dir} + \Delta t_R\,, \quad e^{i\phi_{DB}} = e^{i\phi_L} e^{i\phi_{Dir}} e^{i\phi_R}\,, \quad R_{DB} = T_L\, R_{Dir}\, T_R\,, \tag{6.2.34}$$

leaving the details to appendix B.3. Therefore the quantities that describe the classical scattering with defect and boundary are consistent. In appendix B.4 we

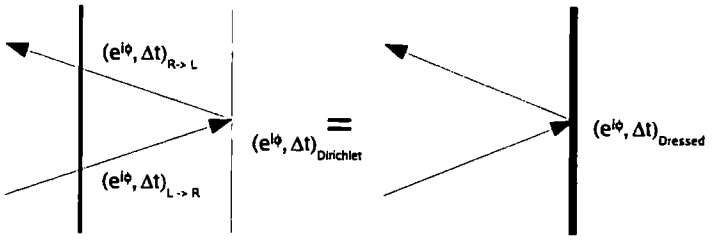

Fig. 6.11: Soliton or particle reflection from the dressed boundary.

show the consistency of the classical soliton-soliton and soliton-boundary scattering properties, by examining explicitly a decay and absorption process.

6.3 Summary

This concludes the classical analysis of the CSG dressed boundary theory. We have shown that it is possible to construct a classically integrable boundary theory by dressing a Dirichlet boundary with the CSG defect. The boundary produced takes a more general form to the CSG boundary theory studied previously.

We have constructed a boundary theory described by a Lagrangian with two types of boundary terms. The terms linear in the time derivatives of the fields lead to more interesting properties over the original boundary. The dressed boundary can store the Noether charge of the CSG theory and due to the definition of α' this charge can be transferred to and from the boundary. This property allows every boundary to be able to absorb or emit a soliton with charge related to the charge of the boundary. As with the defect the energy of boundary determines whether it is excited or not and therefore whether it can absorb or emit a soliton.

We have shown the existence of a boundary bound state where a stationary soliton solution is bound to the boundary. The two descriptions of charged boundaries, namely the unexcited boundary and the boundary bound state, have been shown to be distinct apart from specific choices of the parameters. Depending on the branch of the solution to $\cos(\alpha)$ used in the boundary conditions the bound state limits

to the unexcited boundary with either $a = A + b$ or $a = A - b$ and the soliton positioned at right infinity. For particular examples we illustrated how the energy and the charge of the bound states varies as the value of a changes across the allowed range. These bound states play an important role in the determination of the quantum reflection matrices in the next chapter. Solitons that are not absorbed by the boundary are found to be reflected experiencing a time-delay and phase shift. This is similar to the behaviour of a CSG soliton scattering through the CSG defect. The CSG particle also reflects from the boundary and we calculated the reflection factor from the bare boundary and also from the boundary bound state.

In the next section we build on the classical properties of the dressed boundary theory presented here to explore the quantum theory and ultimately conjecture a quantum reflection matrix.

Chapter 7

Quantum complex sine-Gordon theory

The previous chapters have given a thorough analysis of the classical CSG theory, from the original bulk theory to the newly presented CSG with defect and dressed boundary. In this chapter we move away from the classical theory, first providing a review of quantum aspects of the CSG theory. We go on to semi-classically analyse the quantum spectrum of dressed boundary bound states, before conjecturing a fully quantum reflection matrix. The bootstrap method is used to generate quantum reflection matrices to describe any charged soliton reflecting from any excited boundary. A preliminary physical pole analysis is performed, with their existence explained by the formation of bound states or Coleman-Thun processes. This builds on [48] where the quantum reflection matrix for the originally studied CSG boundary was conjectured. We start with a review on general S-matrix theory.

7.1 Quantum S-matrix theory review

In 1+1 dimensions the scattering in the theory is totally determined once the S-matrix governing the $2 \to 2$ scattering is known, illustrated in figure 7.1 [10]. The S-matrix is constrained by various algebraic relations. One such relation is the Yang-Baxter relation (1.0.1), however in the CSG theory where the scattering is diagonal this relation is trivially satisfied. The following discussion is restricted to theories

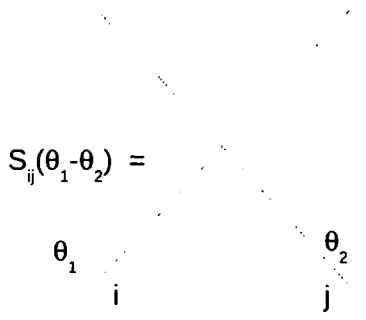

Fig. 7.1: The $2 \to 2$ scattering matrix.

where the scattering is diagonal. In these theories the S-matrix is constrained by the following relations

- real analyticity: $S(\theta)$ real for purely imaginary θ
- unitarity: $S_{ij}(\theta)\, S_{ij}(-\theta) = 1$
- crossing: $S_{ij}(\theta) = S_{i\bar{j}}(i\pi - \theta)$.

If there exists a bound state k formed by particles of type i and j fusing at specific relative rapidities as shown in figure 7.2(a), then the S-matrices satisfy the bulk bootstrap equation (see figure 7.2(b))

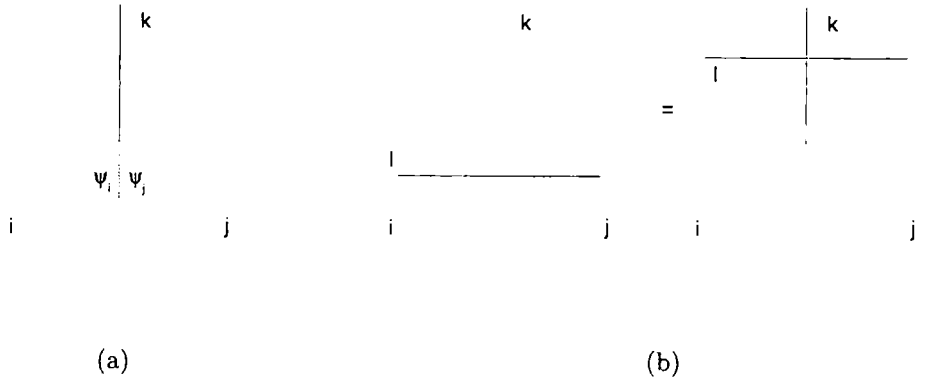

Fig. 7.2: Formation of a bound state and the bulk bootstrap relation.

$$S_{lk}(\theta) = S_{li}(\theta - i\psi_i)\, S_{lj}(\theta + i\psi_j)\,. \tag{7.1.1}$$

When the theory has a boundary the scattering of a particle with the boundary is governed by the reflection matrix R, illustrated in figure 7.3. We again restrict the discussion to diagonal scattering which means the boundary Yang-Baxter equation is trivially satisfied. Similarly to the S-matrix, the R-matrix is constrained by the

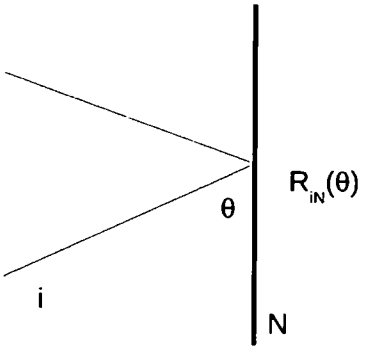

Fig. 7.3: The reflection matrix.

following relations [4]

- real analyticity: $R(\theta)$ real for purely imaginary θ
- unitarity: $R_i(\theta)\, R_i(-\theta) = 1$
- crossing: $R_i(\theta - \frac{i\pi}{2})\, R_{\bar{i}}(\theta + \frac{i\pi}{2})\, S_{\bar{i}i}(2\theta) = 1$

and the boundary bootstrap relation, shown in figure 7.4,

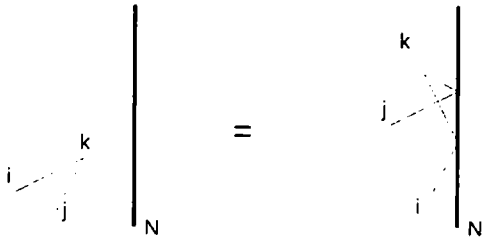

Fig. 7.4: The boundary bootstrap relation.

$$R_{kN}(\theta) = R_{jN}(\theta + i\psi_j)\, S_{ij}(2\theta)\, R_{iN}(\theta - i\psi_i)\,. \tag{7.1.2}$$

If there exists boundary bound states formed by a particle fusing with a boundary at a specific rapidity as illustrated in figure 7.5(a), then the scattering from the bound state is given by the reflection bootstrap equation

$$R_{kM}(\theta) = S_{ik}(\theta - i\psi_{iN})\, R_{kN}(\theta)\, S_{ik}(\theta + i\psi_{iN})\,, \tag{7.1.3}$$

illustrated in 7.5(b). When we conjecture the reflection matrix for a charge $Q = +1$

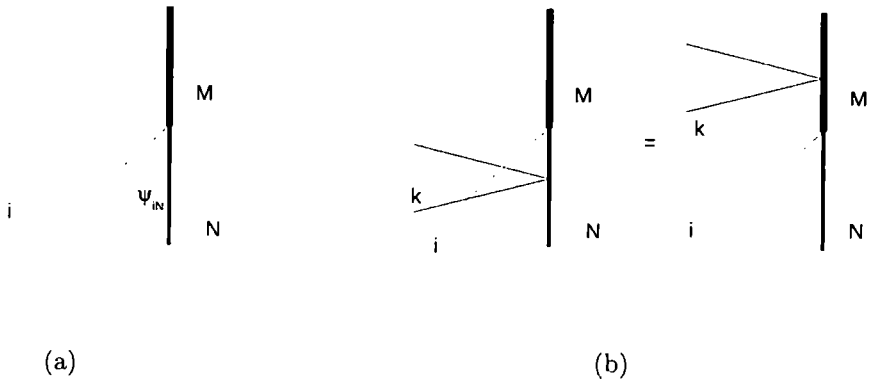

Fig. 7.5: Formation of a boundary bound state and the boundary reflection bootstrap relation.

CSG particle from a charged unexcited boundary, we check that they satisfy these constraints and use the bootstrap relations to generate the reflection matrices for any charged CSG particle from any charged excited boundary.

7.2 Quantum CSG bulk theory

We return to the CSG theory by reviewing quantum aspects of the bulk theory. The quantised bulk theory was first considered by Maillet and de Vega [44], with the results reviewed and expanded on by Dorey and Hollowood [46] to the point where they conjecture a S-matrix to describe the quantum scattering of charged solitons in CSG theory. The next section deals with the semi-classical results, with the S-matrix introduced in the following section.

7.2.1 Semi-classical quantisation

To begin the discussion a few properties of the CSG soliton (4.5.2) are noted. As already commented on the CSG soliton rotates in the internal $U(1)$ space with the constant angular velocity $w = 2\sqrt{\beta}\sin(a)$. We re-express the energy

$$E(w) = \frac{8\sqrt{\beta}}{\lambda^2}\sqrt{1-\frac{w^2}{4\beta}}\cosh(\theta) = E(0)\sqrt{1-\frac{w^2}{4\beta}}, \tag{7.2.1}$$

and charge

$$Q(w) = \frac{4}{\lambda^2}\arccos\left(\frac{w}{2\sqrt{\beta}}\right), \tag{7.2.2}$$

of the soliton in terms of its angular velocity, where λ is the coupling constant which was set equal to one in the previous work on the classical theory (see equation (4.1.1)). These expressions highlight the unusual property that the energy and charge of the soliton decreases as the angular velocity in the internal space increases. The limit of this property is when the angular velocity reaches its maximum $w = 2\sqrt{\beta}$, where the energy and charge vanish but also in this limit the soliton is damped to zero by the $\cos(a)$ factor. Due to the periodic time-dependent nature of the stationary soliton solution

$$u^{stat}_{1-sol} = \frac{\cos(a)e^{2i\sqrt{\beta}\sin(a)t}}{\cosh(2\sqrt{\beta}\cos(a)x)}, \tag{7.2.3}$$

the Bohr-Sommerfeld quantisation (B-S) condition

$$S[u] + E[u]\tau = 2\pi n, \tag{7.2.4}$$

can be applied [62,63]. Where $n \in \mathbb{Z}$, S is the action functional, E the energy and $\tau = \frac{2\pi}{w}$ the period of the solution u. Using the explicit form of the stationary soliton (7.2.3) the left hand side of the B-S condition becomes

$$8\beta\sin^2(a)\,\frac{\pi}{\sqrt{\beta}\sin(a)}\int_{-\infty}^{0} dx\,\frac{uu^*}{1-uu^*}, \tag{7.2.5}$$

which is proportional to the charge of the stationary soliton (4.2) and the B-S condition reduces to

$$2\pi Q = 2\pi n. \tag{7.2.6}$$

Hence the charge is restricted to integer values $Q = \pm 1, \pm 2, \ldots, \pm N = \pm\lfloor\frac{2\pi}{\lambda^2}\rfloor$. The classical charge formula, illustrated in figure 4.2, shows the multi-valued nature of

the charge when $a = 0$. Dorey and Hollowood [46] resolve this issue by stating that the charge should be identified mod $2N$. More generally only specific values of the coupling constant should be considered $\lambda^2 = \frac{4\pi}{k}$, where $k \in \mathbb{Z} > 1$ and the charge is now identified mod k. The spectrum of the charge becomes

$$\begin{aligned} Q &= 0,\ \pm 1,\ \pm 2, \ldots,\ \pm\frac{k}{2} \qquad k \text{ even}, \\ Q &= 0,\ \pm 1,\ \pm 2, \ldots,\ \pm\frac{k-1}{2} \qquad k \text{ odd}. \end{aligned} \tag{7.2.7}$$

If k is even then the solitons with charge $Q = \pm\frac{k}{2}$ are identified, but if k is odd then no solitons are identified. However when incrementing up from $Q = +1$ in single units of charge the step from $Q = \frac{k-1}{2}$ leads to $Q = -\frac{k-1}{2}$, from where it continues up to the $Q = -1$. Figure 7.6(a) shows the case when k is even and figure 7.6(b) when k is odd. These two cases illustrate why the coupling constant λ is restricted in the way it is.

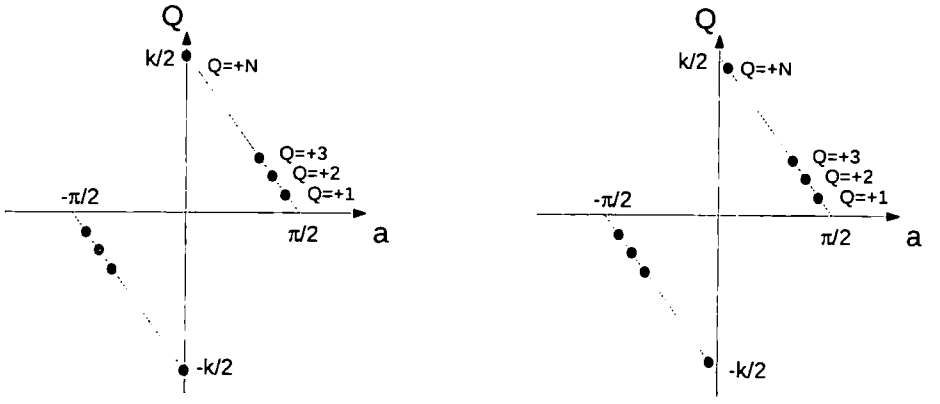

(a) k even (b) k odd

Fig. 7.6: The quantisation of the charge of a CSG soliton.

The quantisation of the charge can be equivalently described as the quantisation of the soliton charge parameter

$$a = \frac{\pi}{2} - \frac{n\pi}{k}, \tag{7.2.8}$$

where n is the charge of the soliton. This gives the semi-classical energy spectrum of the stationary soliton with the charge n soliton having the energy

$$E_n = \frac{2\sqrt{\beta}k}{\pi} \sin\left(\frac{n\pi}{k}\right). \tag{7.2.9}$$

Maillet and de Vega [44] computed the one-loop corrections to this energy spectrum. They found these corrections were obtained by a renormalisation of the coupling constant

$$\lambda^2 \to \lambda_R^2 = \frac{4\pi\lambda^2}{4\pi - \lambda^2}, \qquad k \to k_R = k - 1. \tag{7.2.10}$$

7.2.2 Quantum CSG S-matrix

In this section we review the conjectured exact form for the CSG S-matrix by Dorey and Hollowood [46]. From this point the coupling constant k will be taken as the renormalised version k_R. The S-matrix to describe the scattering of two charged solitons is presented to be

$$S_{Q_1,Q_2}(\theta) = F_{Q_1-Q_2}(\theta)\left[\prod_{n=1}^{Q_2-1} F_{Q_1+Q_2-2n}(\theta)\right]^2 F_{Q_1+Q_2}(\theta), \tag{7.2.11}$$

where

$$F_x(\theta) = \frac{\sinh\left(\frac{\theta}{2} + i\frac{\pi x}{2k}\right)}{\sinh\left(\frac{\theta}{2} - i\frac{\pi x}{2k}\right)}. \tag{7.2.12}$$

It is constructed from products of F factors so it automatically satisfies the unitarity $F_x(\theta)\ F_x(-\theta) = 1$ and analyticity constraints. Each of the F factors has a pole at $\theta = i\frac{\pi x}{k}$. This S-matrix is the minimal choice which has the correct pole structure, explicitly poles are expected at the rapidities where the scattering solitons form bound states. Charge conservation suggests that two solitons with charge Q_1 and Q_2 bind to form solitons with charge $Q_1 \pm Q_2$ in the forward and crossed channels respectively. Other poles are expected to coincide with processes introduced by Coleman and Thun [64].

CSG solitons only form bound states when they have very specific relative rapidity. For example, two charge $Q = +1$ solitons bind together to form a charge $Q = +2$ soliton when they have the relative rapidity $\frac{2i\pi}{k}$. Figure 7.7(a) shows two such $Q = +1$ solitons with rapidities $\pm\frac{i\pi}{k}$ joining to become a stationary $Q = +2$ soliton. In this figure and all the ones to follow time flows up the diagram. We substitute the required charge parameters into the energy formula for the soliton, namely $a = \frac{\pi}{2} - \frac{\pi}{k}$ for the charge $Q = +1$ solitons and $a = \frac{\pi}{2} - \frac{2\pi}{k}$ for the charge $Q = +2$ soliton and use the double angle formula to show that energy is conserved

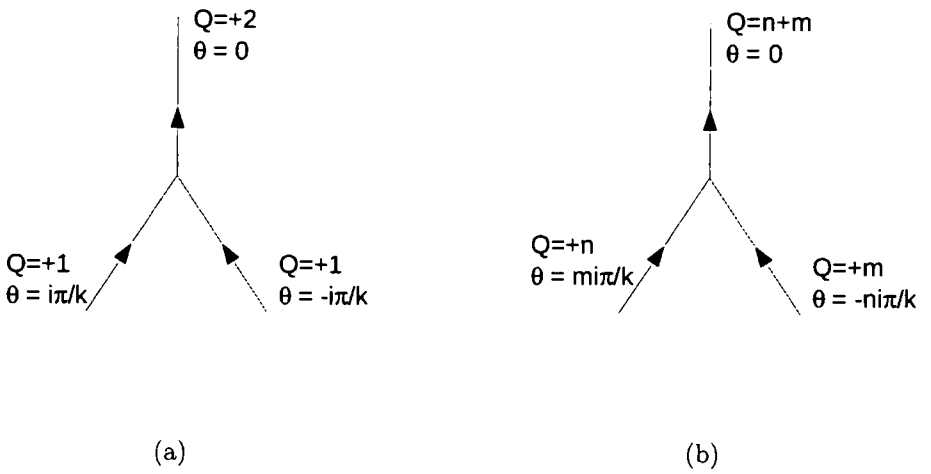

Fig. 7.7: The fusing of (a) two $Q = +1$ solitons, (b) a $Q = +n$ and $Q = +m$ soliton.

for these rapidities

$$8\sqrt{\beta}\cos\left(\frac{\pi}{2}-\frac{\pi}{k}\right)\left(\cosh\left(\frac{i\pi}{k}\right)+\cosh\left(\frac{-i\pi}{k}\right)\right)=8\sqrt{\beta}\cos\left(\frac{\pi}{2}-\frac{2\pi}{k}\right)\cosh(0)\,. \tag{7.2.13}$$

Similarly as shown in figure 7.7(b), two solitons of charge $Q = +n$ and $Q = +m$ fuse to form a bound state of charge $Q = n+m$ at the relative rapidity $\frac{i(n+m)\pi}{k}$. Note that the relative rapidity is always imaginary and in the physical strip $0 < \mathcal{I}m(\theta) < \pi$. The rapidities of the scattering solitons can be given non-zero real parts, but they must be equal. For example two $Q = +1$ solitons with rapidities $\psi \pm \frac{i\pi}{k}$ fuse to form charge $Q = +2$ soliton travelling with real rapidity ψ.

The S-matrix (7.2.11) describing the scattering of two charge $Q = +1$ solitons is

$$S_{1,1}(\theta) = F_0(\theta)\ F_2(\theta) = F_2(\theta)\,. \tag{7.2.14}$$

The $F_2(\theta)$ factor has a pole at $\theta = \frac{2i\pi}{k}$ which corresponds to the formation of a charge $Q = +2$ soliton in the forward channel, illustrated in Figure 7.8(a). Similarly the scattering of charge $Q = +1$ and $Q = +n$ soliton is governed by the S-matrix

$$S_{n,1}(\theta) = F_{n-1}(\theta)\ F_{n+1}(\theta)\,, \tag{7.2.15}$$

where both of the F factors have poles which correspond to the formation of bound states. As before in the forward channel process, illustrated in figure 7.8(b) and also in the cross channel shown in figure 7.8(c).

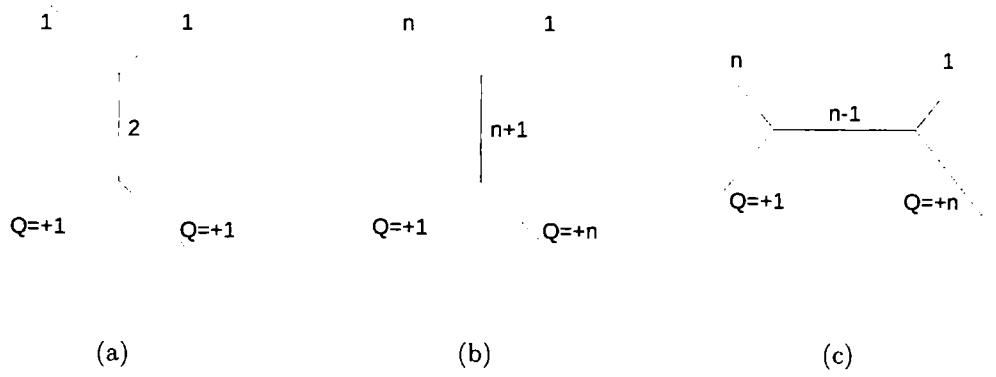

Fig. 7.8: Formation of (a) $Q = +2$ soliton in forward channel, (b) $Q = n + 1$ soliton in forward channel, (c) $Q = n - 1$ soliton in cross channel.

The general S-matrix governing the scattering between two solitons of charge $Q = Q_1$ and $Q = Q_2$, where $Q_1 \geq Q_2$, has simple poles in the forward and cross channels, shows in figures 7.9(a) and 7.9(b) and extra double poles due to Coleman-

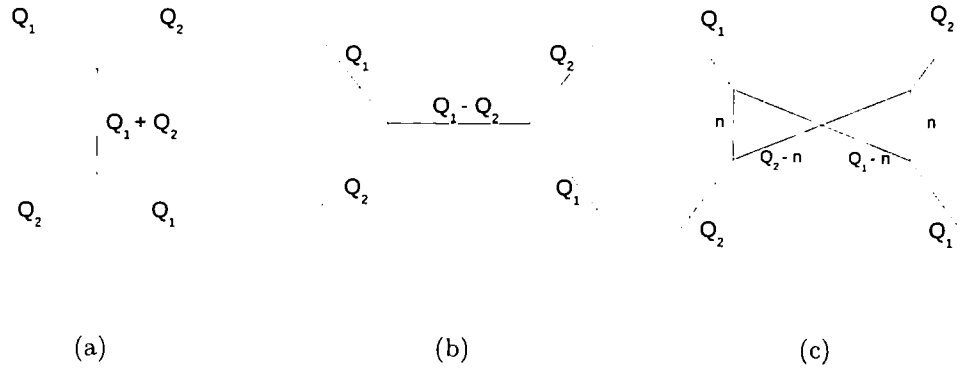

Fig. 7.9: Formation of (a) $Q = Q_1 + Q_2$ soliton in forward channel, (b) $Q = Q_1 - Q_2$ soliton in cross channel, (c) Process with intermediate states of charge $Q_1 - n$ and $Q_2 - n$, which results in a double pole due to the two on-shell internal loops.

Thun processes illustrated in figure 7.9(c). There are $Q_2 - 1$ such processes as the stationary intermediate soliton can have charge $Q = n = 1 \rightarrow Q_2 - 1$. In two-dimensions these processes result in double poles due to the two on-shell internal loops.

This concludes the review of the quantum CSG theory in the bulk, we use the

techniques and some of the results in the following sections to assist in the investigation into quantum aspects of the CSG dressed boundary theory.

7.3 Quantum CSG dressed boundary

We start this section by applying a semi-classical method on the bound state to investigate the spectrum of boundaries. The classical bound state solution is periodic therefore, as for the periodic soliton solution, the Bohr-Sommerfeld quantisation condition (7.2.4) can be applied. Using the form of the dressed boundary action (6.1.6) and energy (6.1.10) the left hand side of the B-S condition becomes

$$S + E\tau = \int_{t=0}^{\tau} dt \int_{-\infty}^{0} dx \, \frac{2\,\partial_t u\,\partial_t u^*}{1-uu^*} + \left[A_1 u_t + A_2 u_t^*\right]\Big|_{x=0} . \tag{7.3.1}$$

The computation on the bulk part of this expression works in identical fashion to the calculation for the soliton solution. The boundary term becomes

$$\int_{t=0}^{\tau} dt \; 4\sqrt{\beta}\sin(a)\alpha' = 4\pi\alpha' , \tag{7.3.2}$$

using that the period is $\tau = \frac{\pi}{\sqrt{\beta}\sin(a)}$ and that α' has no time-dependence when u is the stationary soliton solution. As for the bulk piece we find this boundary term to be equal to 2π times the boundary term of the charge. Therefore the B-S condition for the dressed boundary bound state becomes

$$S_{cl}[u_{cl}] + E_{cl}[u_{cl}]\tau = 2\pi Q_{bs} = 2\pi n , \tag{7.3.3}$$

implying that the charge of the bound states is quantised $Q_{bs} = n$. We recall that there are two formulae for the energy and charge of the bound states (6.2.11), in this initial analysis we use E_{bs}^{+} and Q_{bs}^{+} which limits to the unexcited boundary when $a = A + b$. We can reinterpret this quantisation of the bound state charge as a quantisation condition on the charge parameter a of the bound soliton, when $\cos(a) > 0$

$$a = b - \frac{2\pi n}{k} , \tag{7.3.4}$$

giving an approximation to the energy spectrum

$$E_n^{+} = \frac{k\sqrt{\beta}}{\pi}\left(\cos\left(b - \frac{2\pi n}{k}\right) + \sin(A)\sin(b)\right) . \tag{7.3.5}$$

The energy difference between consecutive states becomes

$$E^+_{n+1} - E^+_n = \frac{k\sqrt{\beta}}{\pi}\left(\cos\left(b - \frac{2\pi(n+1)}{k}\right) - \cos\left(b - \frac{2\pi n}{k}\right)\right), \tag{7.3.6}$$

which we rewrite as

$$E^+_{n+1} - E^+_n = \frac{2k\sqrt{\beta}}{\pi}\cos\left(\frac{\pi}{2} - \frac{\pi}{k}\right)\cos\left(\frac{\pi}{k}(2n+1) + \frac{\pi}{2} - b\right). \tag{7.3.7}$$

We note that this the same as the energy formula for a charge $Q = +1$ soliton

$$E_{sol}(Q = +1) = \frac{2k\sqrt{\beta}}{\pi}\cos\left(\frac{\pi}{2} - \frac{\pi}{k}\right)\cosh(\theta), \tag{7.3.8}$$

with the imaginary rapidity

$$\theta = i\left(b - \frac{\pi}{k}(2n+1) - \frac{\pi}{2}\right). \tag{7.3.9}$$

This suggests that the charge $Q_{bs} = n+1$ bound state can be generated by a $Q = +1$ soliton fusing with the charge $Q_{bs} = n$ bound state at this specific rapidity. This semi-classical energy difference agrees with the classical energy curves in figures 6.8(a), 6.9(a), 6.10(a), where the energy increases as the charge increases with a decreasing from $A + b$.

In section 6.2.6 we found that the unexcited boundary of $Q = +N$ appears as the limit of the bound state where the bound soliton is pushed away to right infinity and has the charge parameter $a = A + b$. The unexcited boundary is described by the charge parameter $A = -\frac{2N\pi}{k}$ and since the bound state charge is quantised and the unexcited boundary can be thought of as a bound state, a quantisation condition on A is implied. Therefore the unexcited boundaries can have charge $Q = N \in \mathbb{Z}$ where $\frac{-k}{2} \leq N \leq \frac{k}{2}$. For the analysis to come, we denote an unexcited boundary with charge $Q = N$ as $N(0)$.

Since the unexcited boundary can be described as a particular limit of the bound state, the energy difference formula (7.3.6) should hold between the unexcited boundary and the first excited bound state. This first step from the unexcited boundary is a step up the energy curve from the right hand edge of the allowed classical region, see figure 6.8(a) for an example. We denote the first excited state above a $Q = N$ unexcited boundary as $N(1)$, similarly $N(m)$ for the m^{th} excited.

We consider the process where a charge $Q = +1$ soliton fuses with an unexcited boundary of charge $Q = +N$ to form the first excited bound state with charge $Q = N + 1$. The process is shown in figure 7.10(a). A soliton with charge $Q = +1$

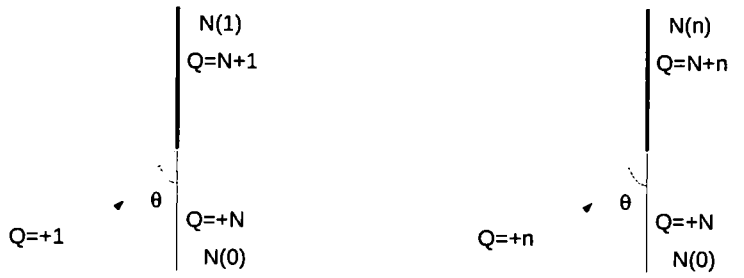

(a) (b)

Fig. 7.10: (a) Charge $Q = +1$ soliton fusing to charge $Q = +N$ boundary, (b) Charge $Q = +n$ soliton fusing to charge $Q = +N$ boundary.

is described by $a_{sol} = \frac{\pi}{2} - \frac{\pi}{k}$ and therefore has energy

$$E_{sol} = \frac{2k\sqrt{\beta}}{\pi} \cosh(\theta) \sin\left(\frac{\pi}{k}\right) . \tag{7.3.10}$$

The charge $Q = +N$ unexcited boundary has energy

$$E = \frac{k\sqrt{\beta}}{\pi} \cos(b) \cos\left(\frac{2\pi N}{k}\right) . \tag{7.3.11}$$

while the bound state with charge $Q = N + 1$ implies that the bound soliton is described by

$$a = b + A - \frac{2\pi}{k} \tag{7.3.12}$$

and the bound state has the energy

$$E_{bs}^{+} = \frac{k\sqrt{\beta}}{\pi} \left(\cos\left(b - \frac{2\pi}{k}(1+N) \right) + \sin(A) \sin(b) \right) . \tag{7.3.13}$$

This fusion process is set up so that charge conservation is automatically satisfied, while energy conservation requires the fusing soliton to have the rapidity

$$\theta = i \left(b - \frac{\pi}{k}(1+2N) - \frac{\pi}{2} \right) . \tag{7.3.14}$$

This fusing rapidity agrees with the rapidity from the semi-classical energy difference (7.3.9) with $n = N$. The fusion of a charge $Q = +1$ soliton then has the effect of shifting the charge parameter of the stationary soliton in the bound state from

$$a_0 = b + A \longrightarrow a_1 = a_0 - \frac{2\pi}{k} . \tag{7.3.15}$$

The quantisation of the bound soliton's charge parameter (7.3.4) shows that this sequence continues with $a_{n+1} = a_n - \frac{2\pi}{k}$. The semi-classical energy spectrum suggests that the fusion process can be repeated. Namely a $Q = +1$ soliton can fuse with the first excited boundary with charge $Q = N + 1$ at the rapidity

$$\theta = i\left(b - \frac{\pi}{k}(3 + 2N) - \frac{\pi}{2}\right) . \tag{7.3.16}$$

Continuing the process a $Q = +1$ soliton can fuse with the m^{th} excited boundary with charge $Q = N + m$ at the rapidity

$$\theta = i\left(b - \frac{\pi}{k}(1 + 2m + 2N) - \frac{\pi}{2}\right) , \tag{7.3.17}$$

to form a higher bound state with charge $Q = N + m + 1$.

As a generalisation to the process in figure 7.10(a), the fusion of a charge $Q = n$ can be considered shown in figure 7.10(b). We find that the rapidity at which this process occurs is

$$\theta = i\left(b - \frac{\pi}{k}(n + 2N) - \frac{\pi}{2}\right) , \tag{7.3.18}$$

resulting in the same excited boundary than if n $Q = +1$ solitons had been consecutively fused, or in fact any combination of solitons whose charge sum to n. The analysis of these fusion processes show that when using E^+_{bs}, Q^+_{bs} the fusion of a soliton steps the bound soliton charge parameter a down from $a = A + b$ in quantum steps and the energy and charge of the bound states increase up the curves illustrated in figures 6.8(a), 6.9(a), 6.10(a). Closer inspection shows that the energy only increases up to $a = 0$, we come back to this point later in the chapter.

Similarly we can repeat the analysis using E^-_{bs}, Q^-_{bs} (6.2.11), starting by applying the B-S condition to the charge formula Q^-_{bs} which implies the quantisation condition on a, for $\cos(a) > 0$

$$a = -b - \frac{2\pi n}{k} , \tag{7.3.19}$$

giving the energy of the charge n state to be

$$E_n^- = \frac{k\sqrt{\beta}}{\pi}\left(\cos\left(b+\frac{2\pi n}{k}\right) - \sin(A)\,\sin(b)\right) \tag{7.3.20}$$

and the semi-classical energy difference

$$\begin{aligned} E_{n-1}^- - E_n^- &= \frac{k\sqrt{\beta}}{\pi}\left(\cos\left(b+\frac{2\pi(n-1)}{k}\right) - \cos\left(b+\frac{2\pi n}{k}\right)\right) \\ &= -\frac{2k\sqrt{\beta}}{\pi}\cos\left(\frac{\pi}{2}-\frac{\pi}{k}\right)\cos\left(\frac{\pi}{k}(2n-1)+\frac{\pi}{2}+b\right), \end{aligned} \tag{7.3.21}$$

which corresponds to the negative of the energy of a $Q=+1$ soliton with rapidity

$$\theta = i\left(\frac{\pi}{k}(2n-1)+\frac{\pi}{2}+b\right). \tag{7.3.22}$$

For this choice of energy and charge formulae the bound state reduces to the unexcited boundary when $a = A - b$, which is at the left hand edge of the allowed classical region. Therefore to step into the allowed region the charge parameter has to increase and this coincides with a decrease in the charge, shown in figures 6.8(b), 6.9(b), 6.10(b), the energy can increase or decrease.

For a choice of parameters (A, b) such as in figure 6.10(b), increasing the value of a from $A-b$ to $A-b+\frac{2\pi}{k}$ decreases the charge and energy of the boundary state whilst moving the bound soliton away from right infinity. This can be interpreted as the emission of a charge $Q=+1$ soliton (or particle) from the unexcited boundary at rapidity given by (7.3.22). This is illustrated in figure 7.3. This process is also possible for higher charged solitons at the rapidity

$$\theta = i\left(\frac{\pi}{k}(2N-n)+\frac{\pi}{2}+b\right). \tag{7.3.23}$$

This behaviour is the opposite the the fusion processes described earlier, the difference is due to the bound state charge increasing when a decreases from $A+b$ and decreasing when a increases from $A-b$. In the next section we use the semi-classical energy spectrum (7.3.6) and fusing angles (7.3.17) to help determine the fully quantum reflection matrices.

7.3.1 Dressed boundary bootstrap

The procedure to generate quantum reflection matrices for charged CSG solitons from the dressed boundary is to first conjecture the reflection matrix for the charge

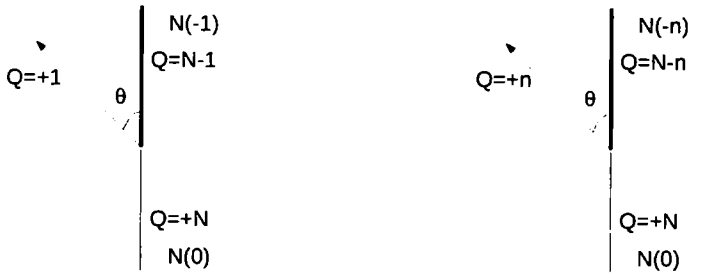

(a) (b)

Fig. 7.11: (a) Charge $Q = +1$ soliton emitting from charge $Q = +N$ boundary, (b) Charge $Q = +n$ soliton emitting from charge $Q = +N$ boundary.

$Q = +1$ soliton or particle from a charge $Q = +N$ unexcited boundary. From this reflection matrix we use the reflection bootstrap and boundary bootstrap procedures to generate the general quantum reflection matrix for a charge $Q = +n$ soliton from an excited charge $Q = N+m$ boundary [4,65,66]. We make various checks to ensure that the original conjecture makes sense.

As in the previous work on the quantum CSG boundary theory [48], which covers the subsection of dressed boundaries with $A = 0$, it is assumed that the reflection matrices are constructed out of F factors (7.2.12). The CSG S-matrix (7.2.11) is defined as a product of these F factors and since the boundary Yang-Baxter equation relates the reflection matrices and the S-matrix this assumption has foundation. Since we generate the reflection matrices from F factors they automatically satisfy analyticity, unitarity and $2\pi i$ periodicity constraints.

The CSG S-matrix is identically the minimal a_{k-1} S-matrix which is recovered from the $a_{k-1}^{(1)}$ Affine Toda field theory (ATFT) when the parts with the coupling constant are omitted. Therefore as in the previous work on the CSG boundary theory we use the terms of the reflection matrix of the $a_{k-1}^{(1)}$ ATFT [67,68], which do not include the coupling constant, as a starting point for the CSG dressed boundary reflection matrix. Using the block notation $(x) = F_x(\theta)$ the terms in the charge $Q = +n$ soliton reflection matrix are

$$R_n^{\text{base}} = \prod_{c=1}^{n} (c-1)(c-k). \tag{7.3.24}$$

The matrix for the reflection of a charge $Q = +1$ soliton from a charge $Q = +N$ unexcited dressed boundary, which we denote by $R_1^{N(0)}$, should therefore include the factor $(1 - k)$. This cannot be the whole expression as it does not contain a factor that corresponds to the known formation of a bound state discussed in the previous section, where a charge $Q = +1$ soliton fuses with an unexcited boundary of charge $Q = +N$. This process occurs when the incoming soliton has the rapidity $\theta = \frac{i\pi}{k}(1 + 2N - B)$ where $B = \frac{kb}{\pi} - \frac{k}{2}$. This fusion process indicates the need for block factor $(1 + 2N - B)$ in the minimal choice for $R_1^{N(0)}$.

Delius and Gandenberger [68] showed that when block factors appear in the pairs $(x)(k-x)$ then the bootstrap is guaranteed to close. In the previous work [48] charge conjugation invariance, i.e. $R_1^0 = R_{-1}^0$ was needed. However, in the case of the charged dressed boundary we do not expect invariance under charge conjugation. It is therefore not required for the reflection matrix to have its F factors appear in these pairs. In fact they cannot appear in this way for the charge conjugation symmetry to be broken.

The way forward in this case is to assume that a similar factor to $(k-1-2N+B)$ does accompany $(1 + 2N - B)$ in $R_1^{N(0)}$ and to find the correct factor we check that the classical limit $k \to \infty$ is correct, by examining the classical reflection factors for a particle and anti-particle reflecting from the dressed boundary

$$\begin{aligned} R_{particle} &= -\frac{(\delta e^{\theta} + ie^{iA})(\delta e^{iA} - ie^{\theta})}{(\delta + ie^{iA}e^{\theta})(\delta e^{iA}e^{\theta} - i)}, \\ R_{anti-particle} &= -\frac{(\delta - ie^{\theta}e^{iA})(\delta e^{iA}e^{\theta} + i)}{(\delta e^{iA} + ie^{\theta})(\delta e^{\theta} - ie^{iA})}. \end{aligned} \tag{7.3.25}$$

These formulae differ from the ones presented in section 6.2.5 due to a difference in the prescription in the signs of k and ω. We note that in the $A = 0$ limit $R_{particle} = R_{anti-particle}$, which confirms the charge conjugation symmetry in this case. Similarly the particle reflection factor from the bound state with these prescriptions is

$$R^{bs}_{particle} = \frac{(1 + ie^{ib}e^{iA}e^{\theta})(e^{iA} - ie^{ib}e^{\theta})(e^{ia} - ie^{\theta})^2}{(e^{ib}e^{iA} - ie^{\theta})(ie^{iA}e^{\theta} + e^{ib})(ie^{ia}e^{\theta} + 1)^2}. \tag{7.3.26}$$

We find that a conjecture for $R_1^{N(0)}$ which has the correct classical limit and includes

the pole that corresponds to the known bound state is

$$\begin{aligned} R_1^{N(0)}(\theta) &= R_1^{\text{base}}(1+2N-B)(k+B-1+2N) \\ &= (1-k)(1+2N-B)(k+B-1+2N)\,. \end{aligned} \tag{7.3.27}$$

7.3.2 Reflection bootstrap

We use the reflection bootstrap mechanism from $R_1^{N(0)}$ to generate the reflection matrices for higher charged solitons reflecting from the unexcited boundary, denoted by $R_n^{N(0)}$. The reflection bootstrap uses the integrability of the model to equate the fusion of two solitons before and after reflection from the boundary. It allows the reflection matrix for the higher charged soliton to be calculated from known lower charge soliton reflection matrices and S-matrices. We illustrate the first step in the reflection bootstrap procedure in figure 7.12, which gives the relation between

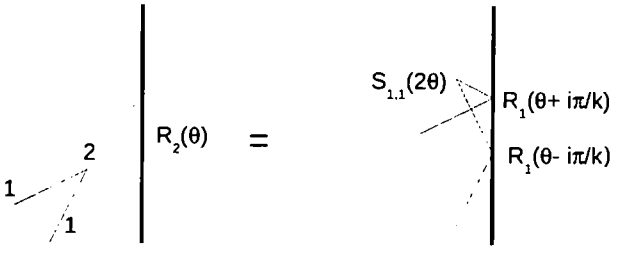

Fig. 7.12: Reflection bootstrap for two $Q = +1$ solitons fusing into a $Q = +2$ soliton.

a charge $Q = +2$ and charge $Q = +1$ CSG soliton reflecting from the unexcited boundary

$$R_2^{N(0)}(\theta) = R_1^{N(0)}\left(\theta - \frac{i\pi}{k}\right) R_1^{N(0)}\left(\theta + \frac{i\pi}{k}\right) S_{1,1}(2\theta)\,. \tag{7.3.28}$$

It uses the property illustrated in figure 7.7(a) that the two $Q = +1$ solitons fuse at the relative imaginary rapidity $\frac{2i\pi}{k}$. Explicitly writing the F factors that appear in the two $R_1^{N(0)}$

$$F_x\left(\theta - i\frac{\pi}{k}\right) = \frac{\sinh\left(\frac{\theta}{2} + \frac{i\pi}{2k}(x-1)\right)}{\sinh\left(\frac{\theta}{2} - \frac{i\pi}{2k}(x+1)\right)}, \quad F_x\left(\theta + i\frac{\pi}{k}\right) = \frac{\sinh\left(\frac{\theta}{2} + \frac{i\pi}{2k}(x+1)\right)}{\sinh\left(\frac{\theta}{2} - \frac{i\pi}{2k}(x-1)\right)}, \tag{7.3.29}$$

shows that we can combine them using

$$F_x\left(\theta - i\frac{\pi}{k}\right)\ F_x\left(\theta + i\frac{\pi}{k}\right) = F_{x+1}(\theta)\ F_{x-1}(\theta)\,. \tag{7.3.30}$$

Along with the form of the S-matrix

$$S_{1,1}(2\theta) = F_0(2\theta)F_2(2\theta) = -(1)(1-k)\,, \tag{7.3.31}$$

this gives

$$R_2^{N(0)}(\theta) = (1-k)(1)(2-k)(2+2N-B)(2N-B)(k+B+2N)(k+B-2+2N)\,. \tag{7.3.32}$$

It is noticed the base factor R_2^{base} appears, allowing it to be rewritten as

$$R_2^{N(0)}(\theta) = R_2^{\text{base}} \prod_{j=0}^{1} (2N-B+2j)(k+B+2N-2j)\,. \tag{7.3.33}$$

To find the reflection factors for higher charged solitons we use the fusion process between higher charged solitons and a charge $Q = +1$ soliton. For example for the next step to generate $R_3^{N(0)}$ we use the fusion process between a charge $Q = +1$ and $Q = +2$ soliton, illustrated in figure 7.13. This gives the relation

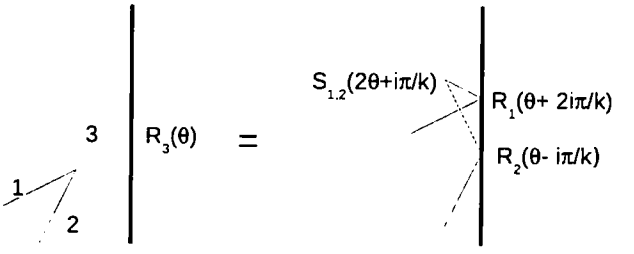

Fig. 7.13: Reflection bootstrap for a $Q = +1$ and $Q = +2$ soliton fusing into a $Q = +3$ soliton.

$$R_3^{N(0)}(\theta) = R_1^{N(0)}\left(\theta + \frac{2i\pi}{k}\right)\ R_2^{N(0)}\left(\theta - \frac{i\pi}{k}\right)\ S_{1,2}\left(2\theta + \frac{i\pi}{k}\right)\,. \tag{7.3.34}$$

To find the explicit form of $R_3^{N(0)}(\theta)$ we use the reflection bootstrap iteratively, namely we use the equation for $R_2^{N(0)}$

$$R_2^{N(0)}\left(\theta - \frac{i\pi}{k}\right) = R_1^{N(0)}\left(\theta - \frac{2i\pi}{k}\right)\ R_1^{N(0)}(\theta)\ S_{1,1}\left(2\theta - \frac{2i\pi}{k}\right) \tag{7.3.35}$$

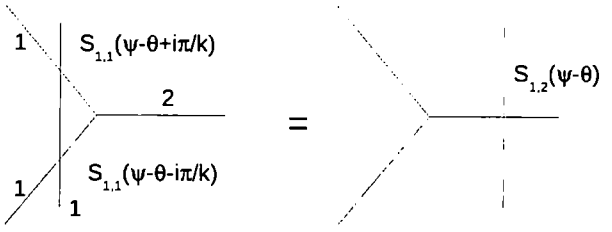

Fig. 7.14: Bulk bootstrap relation allowing the S-matrix between charge $Q = +1$ and $Q = +2$ solitons to be related to the S-matrix between two $Q = +1$ solitons.

and the bulk bootstrap relation, shown in figure 7.14, which gives the relation

$$S_{1,2}\left(2\theta + \frac{i\pi}{k}\right) = S_{1,1}\left(2\theta + \frac{2i\pi}{k}\right) S_{1,1}(2\theta)\,. \tag{7.3.36}$$

We simplify the block factors that appear in $R_1^{N(0)}\left(\theta - \frac{2i\pi}{k}\right) R_1^{N(0)}\left(\theta + \frac{2i\pi}{k}\right)$ using

$$F_x\left(\theta - i\frac{2\pi}{k}\right) F_x\left(\theta + i\frac{2\pi}{k}\right) = F_{x+2}(\theta)\, F_{x-2}(\theta)\,, \tag{7.3.37}$$

to give the form of $R_3^{N(0)}(\theta)$

$$R_3^{N(0)}(\theta) = R_3^{\text{base}} \prod_{j=0}^{2} (2N - B + 2j - 1)(k + B + 2N - 2j + 1)\,. \tag{7.3.38}$$

We continue this procedure to generate the reflection matrix for a charge $Q = +n$ soliton reflecting from an unexcited boundary with charge $Q = +N$

$$R_n^{N(0)}(\theta) = R_n^{\text{base}} \prod_{j=0}^{n-1} (2N - B + 2j + 2 - n)(k + B + 2N - 2j - 2 + n)\,. \tag{7.3.39}$$

We check that the bootstrap closes, namely that

$$R_1^{N(0)}(\theta) = R_{k+1}^{N(0)}(\theta)\,. \tag{7.3.40}$$

This equation is true only for k even, so we shall restrict ourselves to these values of k. Also as expected, the charge conjugation symmetry is broken

$$R_{k-1}^{N(0)}(\theta) = (1-k)(-2N + B - k - 1)(1 - 2N - B) = R_{-1}^{N(0)}(\theta)\,. \tag{7.3.41}$$

In the classical limit this agrees with the reflection factor for the anti-particle (7.3.25) and along with $R_1^{N(0)}$ satisfies the crossing relation which we can rewrite as

$$R_1(\theta)\, R_{-1}(\theta + i\pi) = S_{1,1}(2\theta)\,. \tag{7.3.42}$$

We leave the details of these checks to appendix C.

7.3.3 Boundary bootstrap

Using the reflection bootstrap we have constructed the quantum reflection matrices for any charged soliton from the unexcited boundary. Now using the boundary bootstrap mechanism we generate the reflection matrices which describe the reflection from excited boundaries. The first step of this process is illustrated in figure 7.15, which gives the relation between a charge $Q = +1$ CSG soliton reflecting from the

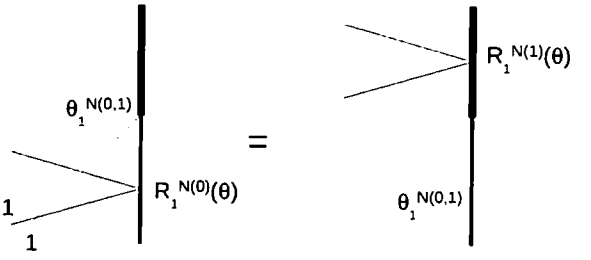

Fig. 7.15: Boundary bootstrap giving a relation for the reflection factor from the first excited boundary.

unexcited boundary and the charge $Q = +1$ soliton reflecting from the first excited bound state. Namely

$$S_{1,1}(\theta - \theta_1^{N(0,1)})\; R_1^{N(0)}(\theta)\; S_{1,1}(\theta + \theta_1^{N(0,1)}) = R_1^{N(1)}(\theta)\,, \tag{7.3.43}$$

where

$$\theta_1^{N(0,1)} = \frac{i\pi}{k}(1 + 2N - B)\,, \tag{7.3.44}$$

is the imaginary rapidity at which a charge $Q = +1$ soliton fuses with an unexcited boundary of charge $Q = +N$ (7.3.14). Noticing that the product of S-matrices can

be simplified

$$S_{1,1}\left(\theta+\frac{i\pi}{k}\psi\right)\ S_{1,1}\left(\theta-\frac{i\pi}{k}\psi\right)=(2+\psi)(2-\psi)\,, \tag{7.3.45}$$

then the reflection matrix from the excited boundary is

$$R_1^{N(1)}(\theta)=(1-k)(1-2N+B)(k+B-1+2N)(1+2N-B)(3+2N-B)\,. \tag{7.3.46}$$

In the classical limit this agrees with the particle reflection factor from the bound state (6.2.30). In $R_1^{N(1)}$ there is a new pole which appears in the similar factor $(3+2N-B)$ at

$$\theta_1^{N(1,2)}=\frac{i\pi}{k}(3+2N-B)\,, \tag{7.3.47}$$

this agrees with the rapidity required for the next bound state to be formed (7.3.16) and therefore we can use this pole to repeat the boundary bootstrap process, illustrated in figure 7.16. This gives the relation

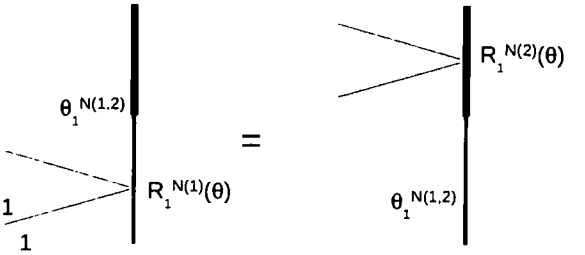

Fig. 7.16: Boundary bootstrap giving a relation for the reflection factor from the second excited boundary.

$$S_{1,1}(\theta-\theta_1^{N(1,2)})\ R_1^{N(1)}(\theta)\ S_{1,1}(\theta+\theta_1^{N(1,2)})=R_1^{N(2)}(\theta)\,, \tag{7.3.48}$$

which can be solved for the quantum reflection matrix for the $Q=+1$ soliton from the second excited bound state

$$R_1^{N(2)}(\theta)=(1-k)(1-2N+B)(k+B-1+2N)(3+2N-B)(5+2N-B)\,. \tag{7.3.49}$$

This again has a new pole, this time in the factor $(5+2N-B)$, which again agrees with the fusion factor (7.3.16). At every step a similar new pole appears and we use

it to iteratively apply the boundary bootstrap process. This results in the general reflection factor

$$R_1^{N(m)}(\theta) = (1-k)(1-2N+B)(k+B-1+2N)(2m-1+2N-B)(2m+1+2N-B)\,, \tag{7.3.50}$$

which describes the scattering of a charge $Q = +1$ soliton from the charge $Q = N+m$ m^{th} excited bound state. The charge of the boundary has Z_k symmetry which is exhibited by this formula since

$$R_1^{N(k)}(\theta) = R_1^{N(0)}(\theta)\,. \tag{7.3.51}$$

The final stage of the bootstrap process to complete the reflection matrices for all possible soliton-boundary reflections is to repeat the reflection bootstrap process starting with $R_1^{N(m)}$ (7.3.50) for any m. The first step is the relation

$$R_2^{N(m)}(\theta) = R_1^{N(m)}\left(\theta - \frac{i\pi}{k}\right)\, R_1^{N(m)}\left(\theta + \frac{i\pi}{k}\right)\, S_{1,1}(2\theta)\,, \tag{7.3.52}$$

which gives

$$R_2^{N(m)}(\theta) = R_2^{\text{base}}\, A_2^{N(m)}\, B_2^{N(m)}\, C_2^{N(m)}\,, \tag{7.3.53}$$

where

$$\begin{aligned} A_2^{N(m)} &= (k+B+2N)(k+B+2N-2)\,, \\ B_2^{N(m)} &= (2-2N+B)(-2N+B)\,, \\ C_2^{N(m)} &= (2m+2N-B-2)(2m+2N-B)^2(2m+2N-B+2)\,. \end{aligned} \tag{7.3.54}$$

Iteratively using the bootstrap gives

$$R_3^{N(m)}(\theta) = R_3^{\text{base}}\, A_3^{N(m)}\, B_3^{N(m)}\, C_3^{N(m)}\,, \tag{7.3.55}$$

where

$$\begin{aligned} A_3^{N(m)} &= (k+B+2N+1)(k+B+2N-1)(k+B+2N-3)\,, \\ B_3^{N(m)} &= (3-2N+B)(1-2N+B)(-1-2N+B)\,, \\ C_3^{N(m)} &= (2m+2N-B-3)(2m+2N-B-1)^2 \\ &\quad \text{x}\ (2m+2N-B+1)^2(2m+2N-B+3)\,. \end{aligned} \tag{7.3.56}$$

We continue this process to give the final general formula for the the quantum reflection matrix for a charge $Q = +n$ soliton from the m^{th} excited boundary with charge $Q = N + m$

$$\begin{aligned} R_n^{N(m)}(\theta) &= R_n^{\text{base}} \prod_{j=0}^{n-1}(n-2j-2N+B)(k+B+2N-n+2j) \\ &\text{x } (2m-n+2N-B)(2m+n+2N-B) \\ &\text{x } \prod_{j=1}^{n-1}(2m-n+2j+2N-B)^2 . \end{aligned} \tag{7.3.57}$$

From a conjectured form of $R_1^{N(0)}$, the reflection factor for the CSG particle from a charge $Q = +N$ unexcited boundary, we have used the bootstrap program to generate the general $R_n^{N(m)}$, the reflection factor for a charge $Q = +n$ soliton from the m^{th} excited boundary with charge $Q = N + m$. We have checked that our results agree with known classical formulae and that the bootstrap closes both on the charge of the reflecting soliton and the charge of the boundary.

7.4 Physical strip pole analysis

In this section we perform a preliminary analysis of the poles in the physical strip that appear in the dressed boundary reflection matrices. We first study some specific examples to find out which poles lie in the physical strip $0 < \mathcal{I}m(\theta) < \frac{\pi}{2}$. The examples we use are for values of A and b that we analysed the classical bound state solution in section 6.2.3, namely $A = 0$, $b = \frac{\pi}{3}$ and $A = \frac{\pi}{8}$, $b = \frac{\pi}{3}$. We use $k = 100$ and $k = 96$ respectively, chosen so that the charge of the boundary obeys the quantisation condition and high enough to show the existence of bound states.

7.4.1 Example I: $A = 0$, $b = \frac{\pi}{3}$, $k = 100$

The unexcited boundary has charge $Q = 0$ and the poles in $R_1^{N(0)}$ (7.3.27) appear at the rapidities

$$\begin{aligned} (1-k) \quad & -99\pi i \\ (1+2N-B) \quad & \frac{53}{300}\pi i \\ (k+B-1+2N) \quad & \frac{247}{300}\pi i . \end{aligned} \tag{7.4.1}$$

There is one physical pole associated with the factor $(1 + 2N - B)$, which is the pole we implemented the bootstrap procedure on. The excited boundaries generated by fusing particles to this unexcited boundary have the reflection matrices $R_1^{N(m)}$ (7.3.50), which has poles at the rapidities

$$\begin{aligned} (1-k) \quad & -99\pi i \\ (1-2N+B) \quad & -\frac{47}{300}\pi i \\ (k+B-1+2N) \quad & \frac{247}{300}\pi i \\ (2m+1+2N-B) \quad & \frac{53+6m}{300}\pi i \\ (2m-1+2N-B) \quad & \frac{47+6m}{300}\pi i\,. \end{aligned} \tag{7.4.2}$$

The pole associated with the factor $(2m+1+2N-B)$ remains in the physical strip until $m = 17$, where the pole is at the rapidity $\frac{155}{300}\pi i$. The pole that is used for the bootstrap $(2m-1+2N-B)$ remains in the next higher charge boundary reflection factor, in the next section we show that the existence of this physical pole can be explained by a Coleman-Thun process. Recalling that

$$a_0 = A + b = \frac{\pi}{3}\,, \quad a_m = A + b - \frac{2\pi m}{k} = \frac{\pi}{3} - \frac{m\pi}{50}\,, \tag{7.4.3}$$

then explicitly $a_{16} = \frac{2\pi}{150}$, $a_{17} = -\frac{\pi}{150}$. Therefore the charge parameter of the bound soliton for the final bound state actually lies past the maximum of the energy of the bound states at $a = 0$ shown in figure 6.8(a). However due to the quantisation of a the energy of boundary $N(17)$ is higher than $N(16)$

$$E_{N(16)} = \frac{k\sqrt{\beta}}{\pi}\cos\left(\frac{2\pi}{150}\right)\,, \quad E_{N(17)} = \frac{k\sqrt{\beta}}{\pi}\cos\left(\frac{\pi}{150}\right)\,. \tag{7.4.4}$$

We note that if the pole in $R_1^{N(17)}$ was still physical then the next bound state would have reduced energy, so the bootstrap procedure is halted when the highest energy bound state is reached.

7.4.2 Example II: $A = \frac{\pi}{8}$, $b = \frac{\pi}{3}$, $k = 96$

The unexcited boundary has charge $Q = -6$ and the poles in $R_1^{N(0)}$ (7.3.27) appear at the rapidities

$$\begin{aligned} (1-k) \quad & -95\pi i \\ (1+2N-B) \quad & \frac{5}{96}\pi i \\ (k+B-1+2N) \quad & \frac{67}{96}\pi i\,, \end{aligned} \tag{7.4.5}$$

so again there is one physical pole in the factor $(1+2N-B)$. The excited boundaries generated by fusing particles to this unexcited boundary have the reflection matrices $R_1^{N(m)}$ (7.3.50), which has poles at the rapidities

$$\begin{aligned} (1-k) \quad & -95\pi i \\ (1-2N+B) \quad & -\frac{3}{96}\pi i \\ (k+B-1+2N) \quad & \frac{67}{96}\pi i \\ (2m+1+2N-B) \quad & \frac{5+2m}{96}\pi i \\ (2m-1+2N-B) \quad & \frac{3+2m}{96}\pi i\,. \end{aligned} \tag{7.4.6}$$

The pole associated with the factor $(2m+1+2N-B)$ remains in the physical strip until $m = 22$, where the pole is at the rapidity $\frac{49}{96}\pi i$. Recalling that

$$a_0 = A + b = \frac{11\pi}{24}\,, \quad a_m = A + b - \frac{2\pi m}{k} = \frac{11\pi}{24} - \frac{m\pi}{48}\,, \tag{7.4.7}$$

then explicitly $a_{21} = \frac{\pi}{48}\,, a_{22} = 0$. This time the charge parameter of the bound soliton for the final bound state coincides with the maximum of the energy of the bound states at $a = 0$ shown in figure 6.9(a). Again the bootstrap procedure is halted when the highest energy bound state is reached. These two examples show for parameter choices such as these we correctly implemented the bootstrap methods, albeit for a finite number of steps. In the next section we explain the processes behind the physical poles.

7.4.3 Coleman-Thun processes

In this section we present the Coleman-Thun type processes [64] that explain the physical poles in the reflection matrices. Coleman-Thun processes were first used

in the case of boundary reflection matrices by Dorey et al. [69] and subsequently in [68, 70–73]. We limit ourselves to ranges of the parameters where the factors of the form $(x + 2N - B)$ and the base factors are the only ones in the physical strip, as in the examples shown above. We note that these are the poles that were used in the bootstrap, and are related to the rapidity of the fusing soliton needed to step up the E^{+}_{bs} energy curve, while a decreases from $A + b$. At the end of the section we comment on the range of parameters this is the case for and also whether any of the other poles can be physical.

Let us begin our analysis with the pole in the physical strip that appears in $R_1^{N(0)}$, namely $(1 + 2N - B)$. As already discussed this pole corresponds to the fusion of an incoming particle with the unexcited boundary. Figure 7.17 shows the reflection process where the bound state forms and then decays re-emitting the $Q = +1$ soliton. The label $\frac{i\pi}{k}(1 + 2N - B)$ indicates the incoming rapidity at which

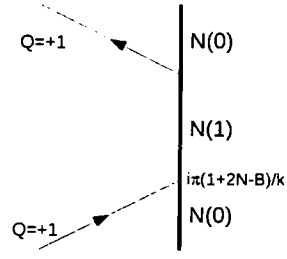

Fig. 7.17: Process that explains the physical pole $(1 + 2N - B)$ in $R_1^{N(0)}$.

the pole is present.

The reflection factor for a $Q = +2$ soliton reflecting from an unexcited boundary (7.3.32) has three such poles which for certain parameter choices are in the physical strip

$$(1)(2 + 2N - B)(2N - B)\,. \tag{7.4.8}$$

These poles correspond to the processes shown in figure 7.18. The pole in factor $(2 + 2N - B)$ is due to diagram 7.18(a) where the incoming soliton fuses with the boundary, forming a bound state before this excited state decays. The pole in (1) which is in the base factor, in this case R_2^{base}, is due to a process in which a

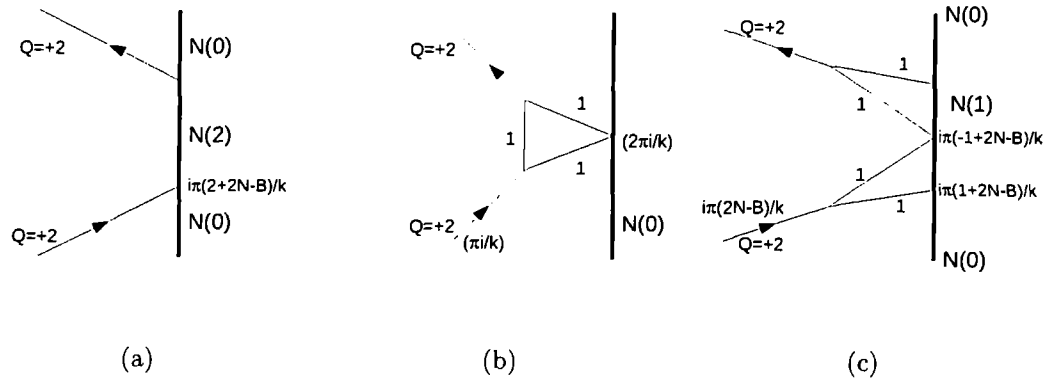

(a) (b) (c)

Fig. 7.18: Processes that explain the three physical poles in $R_2^{N(0)}$.

boundary bound state is not formed. This is a fixed pole as it does not depend on the boundary parameters and arises from the triangular diagram shown in 7.18(b) where the internal lines are on shell. It shows the incoming $Q = +2$ soliton decaying and recombining after one of the resultant charge $Q = +1$ solitons has reflected from the boundary. The final pole is from the factor $(2N - B)$ which is due to the process shown in figure 7.18(c), this is a mixture of the two previous processes. The incoming soliton decays before one of the resultant $Q = +1$ solitons fuses with the boundary to form the boundary bound state $N(1)$, the other resultant soliton reflects from the boundary before the bound state decays re-emitting the soliton which fuses with the reflected soliton.

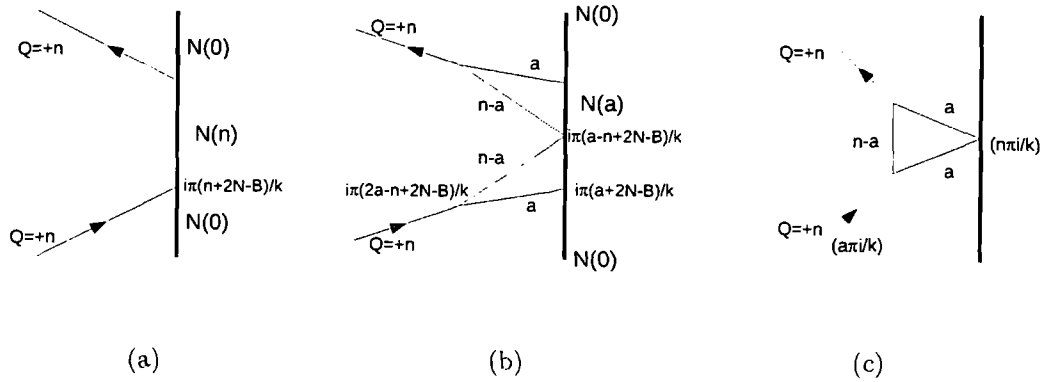

(a) (b) (c)

Fig. 7.19: Processes that explain the three physical poles in $R_n^{N(0)}$.

Increasing the incoming soliton to any charge $Q = +n$ the poles of the considered

form that could be in the physical strip in $R_n^{N(0)}$ (7.3.39) arise from diagrams of the same structure as just described. The pole in the factor $(n + 2N - B)$ comes from the process in figure 7.19(a) and the poles in $(2a - n + 2N - B)$ for $a = 1 \rightarrow n - 1$ are associated with the process in figure 7.19(b). There are $n - 1$ physical poles in R_n^{base} which arise due to triangular diagrams shown in figure 7.19(c) with $a = 1 \rightarrow n - 1$.

The three types of diagrams described above are all that is needed to explain the poles in the reflection matrix for any charged soliton reflecting from a charge $Q = +N$ unexcited dressed boundary. We find that is not the case for the reflection from excited boundaries and more diagrams are needed.

Considering the reflection matrix $R_1^{N(m)}$ for the reflection of a charge $Q = +1$ soliton from an excited boundary with charge $Q = N + m$ (7.3.50), we find that it has poles in the factors $(2m - 1 + 2N - B)$, $(2m + 1 + 2N - B)$. The pole in $(2m + 1 + 2N - B)$ arises because of the formation of the usual higher bound state, shown in figure 7.20(a). While the pole in $(2m - 1 + 2N - B)$ is because the excited defect decays before it becomes re-excited, shown in 7.20(b). For this process to occur the excitation state of the original boundary has to be greater or equal to the charge of the scattering soliton, in this example for a $Q = +1$ soliton we need $m > 0$.

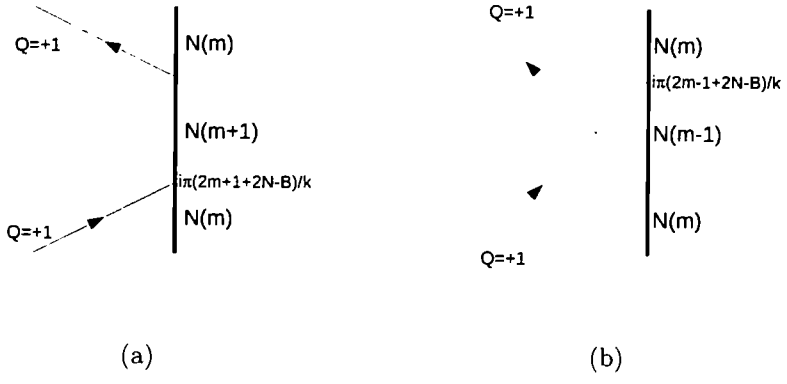

Fig. 7.20: Processes that explain the three physical poles in $R_1^{N(m)}$.

We continue to analyse the reflection factor for any charged soliton $Q = +n$ reflecting from an excited boundary $R_n^{N(m)}$ (7.3.57). It has $n - 1$ poles that appear in the R_n^{base} factor which are due to the triangular diagrams, shown in figure 7.19(c)

with $a = 1 \rightarrow n-1$. The pole in the factor $(2m+n+2N-B)$ comes from the standard process of the formation of a higher bound state illustrated in figure 7.21(a). While figure 7.21(b) shows the process that corresponds to the pole in $(2m-n+2N-B)$, where the boundary decays before fusing with the incoming soliton to reform the original excited boundary. We note that this process only occurs for $n \leq m$.

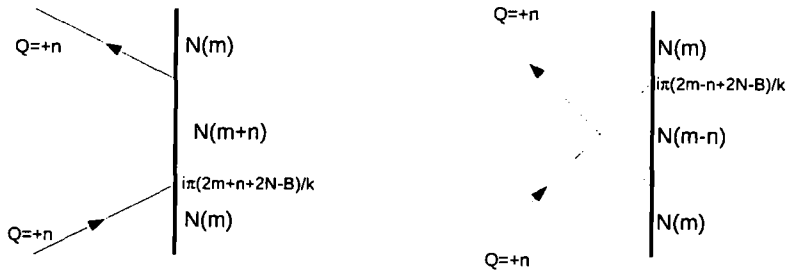

(a) (b)

Fig. 7.21: Processes that explain two of the physical poles in $R_n^{N(m)}$, namely the poles in the factors $(2m+n+2N-B)$ and $(2m-n+2N-B)$.

The double poles from the factors $(2m-n+2j+2N-B)^2$ correspond to two different processes. All $n-1$ poles arise due to the process shown in figure 7.22(a) with $a = 1 \rightarrow n-1$ as long as $n \geq 1$. Whereas r poles arise due to the new process shown in figure 7.22(b) where $a = 1 \rightarrow r$ and r is the lower value of m and $n-1$. In this process the excited boundary decays by emitting a charged soliton which fuses with the reflected soliton, a remnant of the decayed incoming soliton. We note that only when $m > n-1$ is there the maximum number of poles. For $m \leq n-1$ the poles that are not explained by the restrictions on processes in figures 7.21(a), 7.22(b) cancel with zeroes in the product $\prod_{j=0}^{n-1}(n-2j-2N+B)$.

We have described Coleman-Thun processes that explain all the poles of the form $(x+2N-B)$ that appear the various reflection matrices. As we saw with examples I and II the poles that we bootstrapped on do not stay in the physical strip and become unphysical when the bound state with maximum energy has been reached. At this point the bootstrap procedure is halted after a finite number of steps, $m = 17$ in

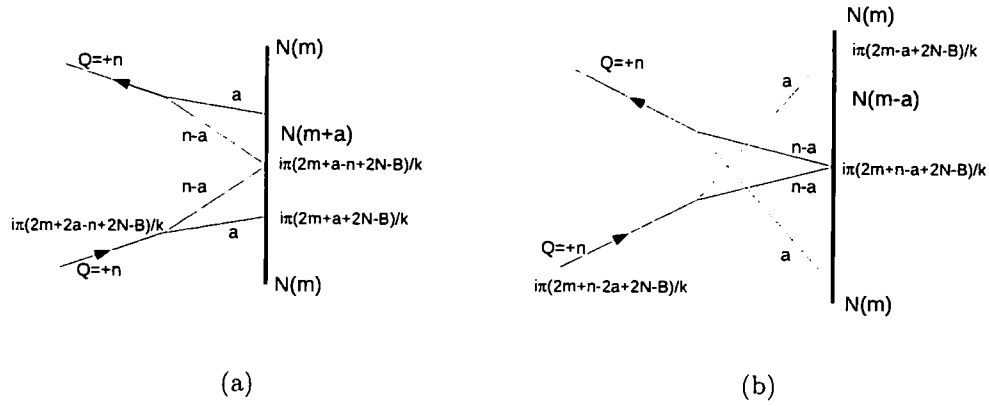

Fig. 7.22: Processes that explain the remaining physical poles in $R_n^{N(m)}$, namely the double poles in the factor $(2m - n + 2j + 2N - B)^2$.

example I. In the examples only the reflection matrix for a $Q = +1$ soliton reflecting from the boundary was considered, we revisit example I to investigate whether a similar pattern exists for higher charged solitons.

7.4.4 Example Ia: $A = 0$, $b = \frac{\pi}{3}$, $k = 100$

The pole that we bootstrapped on in the reflection matrix for a $Q = n$ soliton from an unexcited boundary (7.3.39) appears in the factor $(2N - B + n)$, this corresponds to the formation of a charge $Q = N + n$ bound state and has the value

$$\theta = \frac{i\pi}{300}(3n + 50)\,, \tag{7.4.9}$$

which is physical for $1 \leq n \leq 33$. Therefore a soliton with charge greater than $Q = 33$ cannot fuse with this unexcited boundary to form a bound state. Continuing to the reflection matrices (7.3.57) which describe a charge $Q = n$ soliton scattering with an excited boundary of charge $Q = N + m$, the pole we bootstrapped on appears in the factor $(2N - B + 2m + n)$ which corresponds to the formation of a higher bound state with charge $Q = N + m + n$ and has the value

$$\theta = \frac{i\pi}{300}(3n + 6m + 50)\,, \tag{7.4.10}$$

which is physical for $6m \leq 100 - 3n$. This limits to the original example I with $n = 1$ and the pole is physical until $m = 17$. For the scattering of the charge $Q = 2$

soliton the last boundary it can fuse to is the 15^{th} excited state, since from the 16^{th} excited state the resultant boundary has lower energy. Similarly a charge $Q = +3$ soliton can fuse to the 15^{th} excited state also. These can be deduced by looking at the charge parameter for excited boundaries with different charges and determining whether the fusion of a certain charged soliton will create a higher or lower energy state.

We have shown for this example the bootstrap procedure that we implemented is valid for a finite number of steps depending on the charge of the scattering soliton. In fact the pole we started the bootstrap procedure on in (7.3.27) is the only physical pole in this reflection matrix when

$$\frac{\pi}{k} \leq A+b \leq \frac{\pi}{2} - \frac{\pi}{k}, \qquad A < b - \frac{\pi}{k}, \qquad k \geq 4. \tag{7.4.11}$$

For these range of parameters the bootstrap procedure we implemented and pole analysis is valid for a finite number of steps. The bound states accessed by the bootstrap procedure are all related to the E_{bs}^{+} energy curve created by fusing solitons to the unexcited boundary with $a = A+b$. We will now briefly examine an example which falls outside of these parameter constraints.

7.4.5 Example III: $A = \frac{\pi}{4}$, $b = \frac{\pi}{8}$, $k = 96$

The unexcited boundary has charge $Q = -12$ and the poles in $R_1^{N(0)}$ (7.3.27) appear at the rapidities

$$\begin{aligned} (1-k) \quad & -95\pi i \\ (1+2N-B) \quad & \frac{13}{96}\pi i \\ (k+B-1+2N) \quad & \frac{35}{96}\pi i, \end{aligned} \tag{7.4.12}$$

where two poles lie in the physical strip associated with the factors $(1+2N-B)$ and $(k+B-1+2N)$. This circumstance lies outside all the previous analysis. The residues of these poles have the different sign, the pole in the factor $(1+2N-B)$ has the residue $1.65\,i$ and the pole in $(k-1+2N+B)$, residue $-3.58\,i$. This second physical pole is at the rapidity for the emission process, shown in figure 7.11(a), and possibly is explained by a crossed process because it is a remnant pole from the

lower energy boundary reflection matrix $R_1^{N(-1)}$. This would however suggest that the unexcited boundary is itself a bound state.

If we consider our bootstrap procedure then the excited boundaries generated have the reflection matrices $R_1^{N(m)}$ (7.3.50), which has poles at the rapidities

$$\begin{aligned}
(1-k) \quad & -95\pi i \\
(1-2N+B) \quad & -\frac{11}{96}\pi i \\
(k+B-1+2N) \quad & \frac{35}{96}\pi i \\
(2m+1+2N-B) \quad & \frac{11+2m}{96}\pi i \\
(2m-1+2N-B) \quad & \frac{13+2m}{96}\pi i\,.
\end{aligned} \tag{7.4.13}$$

where the pole from the factor $(2m-1+2N-B)$ stays in the physical strip until $m=18$. This seems similar to the other examples but the charge parameter of the bound soliton has the value $a_m = 0$, which lies outside of the classical region where bound states exist $\left[\frac{\pi}{8}, \frac{3\pi}{8}\right]$. In fact a_m moves outside the classical region at $m=13$. This property where the pole stays physical outside the allowed classical region is not explained by our analysis. Examining the residues of the poles we find that there are positive imaginary for $m = 0 \to 11$ but becomes negative imaginary for $m=12$ the exact value which if bootstrapped on would take a outside the classical range. We have therefore found that the physical poles we have not been able to explain both have the feature that their residue is negative imaginary, while all the poles we have explained by the formation of bound states or Coleman-Thun processes have a positive imaginary residue.

7.5 Summary

This chapter has moved away from the classical theory and started the investigation into the quantum CSG dressed boundary theory. We reviewed aspects of the quantum CSG theory, showing that the charge of the CSG soliton is quantised. The quantum S-matrix was presented and the existence of poles in the S-matrix explained due to the formation of higher charge bound states and Coleman-Thun processes.

Using the Bohr-Sommerfeld quantisation condition we showed that the charge of the boundary bound states is quantised and through the fact that the unexcited boundary appears as a limit of the bound states, all the boundaries in the quantum theory have integer charge. Using the charge quantisation condition we calculated the semi-classical energy difference between states differing by one unit of charge and showed that the energy difference is exactly that of a soliton with specific rapidity. This discovery prompted the analysis of soliton-boundary fusion processes and we found that a charge $Q = +1$ soliton can fuse with an unexcited boundary to form a excited bound state at the rapidity in agreement with the semi-classical energy difference. This fusion process can be repeated with the effect on the bound soliton of altering its charge parameter $a \longrightarrow a - \frac{2\pi}{k}$.

Using the existence of these bound states we conjectured the form of the quantum reflection matrix for a charge $Q = +1$ soliton from the unexcited boundary $R_1^{N(0)}$, checking that the conjectured form is in agreement with the classical limit. From $R_1^{N(0)}$ we used the reflection bootstrap procedure to generate reflection matrices for any charged soliton from the unexcited boundary $R_n^{N(0)}$, checking the classical limit for the anti-particle and that it displayed the charge periodicity property of the soliton. We note that we found that this was only possible for k even. To construct the reflection matrices which describe the scattering of a $Q = +1$ soliton from an excited boundary we used the boundary bootstrap and then to generalise to any charged soliton repeated the reflection bootstrap. The matrices were checked to be in agreement with the classical reflection factor from the bound state and checked that they preserve the periodicity of the boundary charge.

Finally we completed a preliminary analysis of the physical poles that appear in the various matrices. For some choices of the parameters we explain the physical poles either by the formation of higher bound states by the fusion process described above or by Coleman-Thun processes. In the examples we studied, they showed that the bootstrap method is valid for a finite number of steps until the bound state of highest energy is reached, at this point the pole we bootstrapped on becomes unphysical. A counter example showed that for certain parameter values there exists physical poles with negative residues that do not fit into the explanations

provided in this chapter. Further analysis is required to complete the picture and to better understand the bound states present on the E_{bs}^{-} energy curve, which goes to energies lower than the unexcited boundary suggesting that it itself is a bound state.

Chapter 8

Conclusion and discussion

In this thesis we have successfully constructed integrable CSG defect and CSG dressed boundary theories, thoroughly analysed their classical properties and conjectured a quantum reflection matrix for the boundary theory.

Inspired by the previous research into the SG theory with defect and boundary, the richness of the CSG theory made it a perfect candidate to further the study of 1+1 dimensional integrable field theories on restricted domains. As in the SG theory there exists CSG soliton solutions which, unlike the SG solitons that carry topological charge, carry a continuous Noether charge due to the $U(1)$ invariance of the theory. The CSG two-soliton solution models soliton-soliton scattering in the theory. As in all integrable theories the scattering is totally elastic and the solitons experience a time-delay or time-advance and a phase shift. Unlike the SG theory the CSG soliton and particle sectors are topologically the same, meaning that the CSG particle can be thought of as a perturbation around the vacuum or a soliton in a particular charge limit.

Previously, the CSG theory in complex field notation had to be analysed using both sectors of the theory, with an auxiliary field introduced in the relation between the fields of the different sectors. Solving the differential equations for the difference in the auxiliary fields α that appear in the BT, we were able to find an explicit formula α. This dispenses with the need to consider the fields and dual fields simultaneously and enabled us to rewrite both the Bäcklund transformation and two-soliton solution in terms of only the $\beta > 0$ fields. The formula for α introduces

a new parameter A into the theory and the BT now depend on this extra parameter, along with δ.

In the original description the dual field held the topological information of the theory, which is displayed by the dual field soliton solution exhibiting a kink-like nature. This topological nature seems to be lost in the new α description, it is however hidden away in the complicated definition of α. The square root in $\cos(\alpha)$ has to be carefully treated and branch cuts changed when the argument becomes zero, we have seen this to be the case during soliton-soliton scattering, soliton emission and absorption by both defect and boundary and the variation of the boundary bound states with respect to the charge parameter of the bound soliton a.

We constructed and analysed the CSG defect theory in both descriptions. By construction, the defect conditions at $x = 0$ are identical to the BT, following the pattern of defects in previously studied integrable theories. To show the integrability of these conditions, explicit formulae for the conserved energy, momentum and charge and next higher spin charges in the presence of a defect were constructed. Like the SG theory the CSG defect can be excited or unexcited which enables the defect to absorb and emit solitons when the soliton and defect parameters are particularly related. In SG these processes are possible because the defect can store the discrete topological charge, whereas in CSG the defect can store the continuous $U(1)$ Noether charge. In both theories there are two different defects that can absorb the same soliton, one defect with $\delta > 0$ and the other with $\delta < 0$. In SG these two defects have different topological charges and the CSG defects different charge Q. In all emission and absorption processes we find that the change in charge is symmetric around $Q = \pm\pi$ and a defect does not decay into its anti-defect.

CSG solitons that are not absorbed by the defect, scatter through the defect experiencing a time-delay or time-advance along with a phase shift. This is very similar to what happens in soliton-soliton scattering and in fact the time-delay experienced in soliton-defect scattering is exactly half of that experienced in soliton-soliton scattering, when the parameters are appropriately matched. This same phenomena is also witnessed for SG defects and solitons and suggests that defects maybe more

fundamental objects than solitons. The CSG particle scatters through the defect with no reflection. This purely transmitting nature of the defect is so far a universal property of integrable defects.

Both descriptions of the CSG defect theory illustrate the same properties, which is expected as they are two descriptions of the same theory. However there are differences in the way the properties are explained. In the α description the defect is described by two parameters δ and A, whereas in the 'two field' description it is only described by δ. The defect charge parameter A and its definition through α replace the need to consider the values of the dual fields at the defect. The difference in the dual fields or the value of A and the solution of α used, determines the energy, momentum and charge stored on the defect. The transfer of the conserved charges required for soliton emission or absorption to occur is facilitated by different means in the two descriptions. In the 'two field' description the dual field soliton solution connects different vacua and therefore the difference in the dual fields at the defect is different before and after emission or absorption. While in the α description the branch of the solution for $\cos(\alpha)$ has to be swapped mid-process, meaning the final defect has the opposite energy and momentum to the initial defect.

The new α description is preferred despite the complications the definition of α causes. Only having to consider a single field on each side of the defect and the direct correspondence between the charge parameter of the defect and the charge parameter of the soliton it can emit or absorb are advantages. For these reasons we used this description to construct the dressed boundary theory.

With the aim to generate a CSG boundary theory that has more generic properties to the model previously studied, we used the technique of dressing a boundary. This allows new boundary conditions to be created by placing a defect in front of a known boundary. In our case we dressed the CSG Dirichlet boundary with the CSG defect to create the CSG dressed boundary. The dressed boundary conditions are a wider class of boundary conditions, like the defect conditions they include time-derivative terms. We found the previously studied boundary to be the particular example of the dressed boundary where the coefficients of these time-derivatives terms vanish, achieved by setting the boundary charge parameter to zero.

As expected by its construction, the dressed boundary maintains classical integrability. We check this explicitly by generating a higher spin conserved energy-like charge. The dressed boundary inherits properties from its constituent defect, namely the absorption and emission of particular solitons. Analogous to the defect the charge and energy of the soliton that a specific boundary can absorb or emit is determined by the energy and charge of the boundary. Unlike the defect, a boundary described by all $\delta \in \mathbb{R}$ can for example absorb a right-moving soliton. This is explained from the construction of the boundary allowing two methods of absorption and emission, either straight to or from the defect and after reflecting from the Dirichlet boundary. Solitons that are not absorbed are reflected experiencing a time-delay and phase shift. The formula for classical soliton-defect and soliton-boundary scattering are shown to be consistent with the construction of the boundary.

There exist classical bound states in the boundary theory which are not present in the defect theory. A stationary soliton can be bound to the boundary when the boundary rapidity is a pure phase, within a certain range. This gives two descriptions of charged boundaries which we show are not equivalent apart from when the bound soliton is described by two particular values of the charge parameter and is positioned far behind the boundary at right infinity. There are two limits to the unexcited boundary due to the two formulae for the energy of the bound state. The two values of the charge parameter which limit to the unexcited boundary are at the two extremes of the allowed range for bound states to exist, while the opposite extreme of the allowed range corresponds to the soliton being at left infinity. The highest energy bound state is when $a = 0$.

Repeating the construction of the dressed boundary, another boundary could be produced by putting two defects in front of the Dirichlet boundary. To explicitly write down the boundary conditions of such a doubly dressed boundary is computationally tricky. However the properties of such a boundary are expected to include the ability to absorb solitons when the parameters match either of the defects. It is interesting to ponder whether two defects with the same parameters are allowed to placed alongside each other unlike the exclusion principle which does not allow

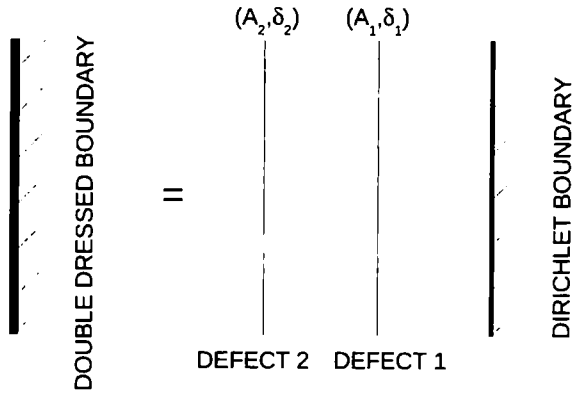

Fig. 8.1: The construction of a double dressed boundary.

either identical SG or CSG solitons to be placed alongside one another.

Placing defects in front of the boundary act like a soliton filter; it is possible to create an arbitrary absorption spectrum by placing appropriate defects in front of the boundary. In fact, one might speculate that there is the hypothetical limit where by placing an infinite number of different defects in front of the boundary one could create a boundary that was fully absorbing.

In the quantum theory the charge of the CSG soliton is quantised and the value of the coupling constant is restricted. Using the Bohr-Sommerfeld quantisation condition we found that the charge of the boundary bound states is quantised and since the unexcited boundary appears as a limit of the bound states this implies that all boundaries in the theory have quantised charge. Using the semi-classical energy spectrum as a guide we analysed the fusion of the CSG particle to an unexcited boundary, resulting in an excited boundary modelled by the classical bound state. The fusion process results in the bound soliton charge parameter being shifted $a_m = a_{m-1} - \frac{2\pi}{k}$, we note that this is quantised but can take different values to the charge parameter of a normal soliton.

Using these fusion processes a quantum reflection matrix is conjectured to describe the scattering of a $Q = +1$ soliton from an unexcited boundary. It is constructed to have a pole at the rapidity to coincide with the formation of the known bound state and checked to agree with the particle reflection factor in the classi-

cal limit. Using the reflection bootstrap the reflection matrix for the scattering of any charged soliton from the unexcited boundary is generated, closure and agreement with the anti-particle reflection factor are verified. The boundary bootstrap is employed to generalise to the reflection matrix for any charged soliton from any excited CSG boundary. The formula is seen to preserve the periodicity of the boundary charge and limits to the reflection matrix found for the original boundary theory.

We completed a preliminary analysis of the physical poles that appear in the various matrices. For a range of the parameters we explain the physical poles either by the formation of higher bound states by the fusion process described above or by Coleman-Thun processes. The examples we studied showed that the bootstrap method is valid for a finite number of steps until the bound state of highest energy is reached, at this point the pole we bootstrapped on becomes unphysical. For certain values of the parameters, when $A - b > 0$, there exists physical poles with negative residues that do not fit into the explanations provided here.

As well as the open questions to describe more completely the processes responsible for the physical poles in the boundary reflection matrix, the study of the quantum CSG defect theory is the obvious extension to the work presented here. Unlike the boundary theory there exists no bound states in the defect theory which means the same methods cannot be implemented. One handle is the assumption that the real emission and absorption processes should appear as poles of the quantum transmission matrix.

The production of the CSG defect and dressed boundary theory and their subsequent analysis has shown them to be interesting theories. The soliton interactions with defect and boundary confirm and build on the analysis of the SG theory, with the ability of a defect and boundary to store and transfer a continuous charge being a new phenomena. The properties discovered could be useful in the study of impurities in condensed matter systems and the control of solitons in optical communications.

Appendix A

CSG higher conserved charges

A.1 Bulk theory

The formula for the next conserved energy-like charge is

$$\begin{aligned}\mathcal{E}_2 \;=\; & \frac{1}{1-uu^*}\left[\frac{\partial u^*}{\partial t}\left(\frac{\partial^2 u}{\partial t^2}+\frac{\partial^2 u}{\partial x^2}\right)-\frac{\partial u}{\partial t}\left(\frac{\partial^2 u^*}{\partial t^2}+\frac{\partial^2 u^*}{\partial x^2}\right)+2\frac{\partial u^*}{\partial x}\frac{\partial^2 u}{\partial x\partial t}-2\frac{\partial u}{\partial x}\frac{\partial^2 u^*}{\partial x\partial t}\right] \\ & -\frac{1}{(1-uu^*)^2}\left[u^*\frac{\partial u^*}{\partial t}\left(\left(\frac{\partial u}{\partial t}\right)^2+\left(\frac{\partial u}{\partial x}\right)^2\right)-u\frac{\partial u}{\partial t}\left(\left(\frac{\partial u^*}{\partial t}\right)^2+\left(\frac{\partial u^*}{\partial x}\right)^2\right)\right. \\ & \qquad \left.+2\frac{\partial u}{\partial x}\frac{\partial u^*}{\partial x}\left(u^*\frac{\partial u}{\partial t}-u\frac{\partial u^*}{\partial t}\right)\right] \\ & -4\beta\left(u\frac{\partial u^*}{\partial t}-u^*\frac{\partial u}{\partial t}\right) \end{aligned} \tag{A.1.1}$$

and the next momentum-like charge

$$\begin{aligned}\mathcal{P}_2 \;=\; & \frac{1}{1-uu^*}\left[\frac{\partial u^*}{\partial x}\left(\frac{\partial^2 u}{\partial t^2}+\frac{\partial^2 u}{\partial x^2}\right)-\frac{\partial u}{\partial x}\left(\frac{\partial^2 u^*}{\partial t^2}+\frac{\partial^2 u^*}{\partial x^2}\right)+2\frac{\partial u^*}{\partial t}\frac{\partial^2 u}{\partial x\partial t}-2\frac{\partial u}{\partial t}\frac{\partial^2 u^*}{\partial x\partial t}\right] \\ & -\frac{1}{(1-uu^*)^2}\left[u^*\frac{\partial u^*}{\partial x}\left(\left(\frac{\partial u}{\partial t}\right)^2+\left(\frac{\partial u}{\partial x}\right)^2\right)-u\frac{\partial u}{\partial x}\left(\left(\frac{\partial u^*}{\partial t}\right)^2+\left(\frac{\partial u^*}{\partial x}\right)^2\right)\right. \\ & \qquad \left.+2\frac{\partial u}{\partial t}\frac{\partial u^*}{\partial t}\left(u^*\frac{\partial u}{\partial x}-u\frac{\partial u^*}{\partial x}\right)\right] \\ & -4\beta\left(u\frac{\partial u^*}{\partial x}-u^*\frac{\partial u}{\partial x}\right)\,. \end{aligned} \tag{A.1.2}$$

Their conservation is checked using that they satisfy

$$\frac{\partial \mathcal{E}_2}{\partial t} = \frac{\partial \mathcal{P}_2^*}{\partial x}, \quad \frac{\partial \mathcal{P}_2}{\partial t} = \frac{\partial \mathcal{E}_2^*}{\partial x}, \tag{A.1.3}$$

where $\mathcal{E}_2^* = \mathcal{E}_2(\beta \to -\beta)$, $\mathcal{P}_2^* = \mathcal{P}_2(\beta \to -\beta)$.

A.2 Dressed boundary theory

The contribution needed to be added the the next highest energy-like conserved charge is

$$\begin{aligned} \mathcal{B}_2 &= \frac{2\sqrt{\beta}}{\sqrt{\cos^2(A) - uu^*}} \left(u \frac{\partial u^*}{\partial t} - u^* \frac{\partial u}{\partial t} \right) \left(\delta + \frac{1}{\delta} \right) \\ &+ \frac{8i\sqrt{\beta}\sin(A)\cos(A)^2}{\sqrt{\cos(A)^2 - uu^*}} \left(\delta^2 + \frac{1}{\delta^2} \right) - \frac{4i\sqrt{\beta}\sin(A)uu^*}{\sqrt{\cos(A)^2 - uu^*}} \left(\delta - \frac{1}{\delta} \right)^2 . \end{aligned} \tag{A.2.1}$$

This is generated by writing $\mathcal{P}_2^*$ on the boundary as a total time derivative, since

$$E_2 = \int_{-\infty}^{0} dx \; \mathcal{E}_2 + \left[\mathcal{B}_2 \right]\Big|_{x=0} \tag{A.2.2}$$

and therefore

$$\begin{aligned} \frac{\partial E_2}{\partial t} &= \int_{-\infty}^{0} dx \; \frac{\partial \mathcal{E}_2}{\partial t} + \left[\frac{\partial \mathcal{B}_2}{\partial t} \right]\Big|_{x=0} \\ &= \left[\mathcal{P}_2^* + \frac{\partial \mathcal{B}_2}{\partial t} \right]\Big|_{x=0} \end{aligned} \tag{A.2.3}$$

A.3 Defect theory

The next energy-like charge has the form

$$E_2 = \int_{-\infty}^{0} dx \; \mathcal{E}_2(u) + \int_{0}^{+\infty} dx \; \mathcal{E}_2(w) + \left[\mathcal{D}_2 \right]\Big|_{x=0} \tag{A.3.1}$$

and the next momentum-like charge

$$P_2 = \int_{-\infty}^{0} dx \; \mathcal{P}_2(u) + \int_{0}^{+\infty} dx \; \mathcal{P}_2(w) + \left[\mathcal{P}_2^{def} \right]\Big|_{x=0} . \tag{A.3.2}$$

Therefore

$$\begin{aligned}\frac{\partial E_2}{\partial t} &= \int_{-\infty}^{0} dx\, \frac{\partial \mathcal{E}_2(u)}{\partial t} + \int_{0}^{\infty} dx\, \frac{\partial \mathcal{E}_2(w)}{\partial t} + \left[\frac{\partial \mathcal{D}_2}{\partial t}\right]\Big|_{x=0} \\ &= \left[\mathcal{P}_2^*(u) - \mathcal{P}_2^*(w) + \frac{\partial \mathcal{D}_2}{\partial t}\right]\Big|_{x=0} \end{aligned} \tag{A.3.3}$$

and

$$\begin{aligned}\frac{\partial P_2}{\partial t} &= \int_{-\infty}^{0} dx\, \frac{\partial \mathcal{P}_2(u)}{\partial t} + \int_{0}^{\infty} dx\, \frac{\partial \mathcal{P}_2(w)}{\partial t} + \left[\frac{\partial \mathcal{P}_2^{def}}{\partial t}\right]\Big|_{x=0} \\ &= \left[\mathcal{E}_2^*(u) - \mathcal{E}_2^*(w) + \frac{\partial \mathcal{P}_2^{def}}{\partial t}\right]\Big|_{x=0} . \end{aligned} \tag{A.3.4}$$

To show that these are conserved, we need be able to write

$$\mathcal{P}_2^*(u) - \mathcal{P}_2^*(w) \tag{A.3.5}$$

and

$$\mathcal{E}_2^*(u) - \mathcal{E}_2^*(w) \tag{A.3.6}$$

as total time derivatives. We find that $\mathcal{D}_2$ includes the terms

$$\begin{aligned}&-\frac{4\sqrt{\beta}}{\sqrt{1-ww^*}(1-uu^*)(1+e^{-2i\alpha})}\frac{\partial u}{\partial t}\left[u^*\sqrt{1-uu^*}(1-ww^*)e^{-i\alpha}\left(\delta+\frac{1}{\delta}\right)\right. \\ &\qquad\left.+w^*\sqrt{1-ww^*}(1-uu^*)\left(\delta-\frac{e^{-2i\alpha}}{\delta}\right)\right] \\ &+\frac{4\sqrt{\beta}}{\sqrt{1-ww^*}(1-uu^*)(1+e^{2i\alpha})}\frac{\partial u^*}{\partial t}\left[u^*\sqrt{1-uu^*}(1-ww^*)e^{i\alpha}\left(\delta+\frac{1}{\delta}\right)\right. \\ &\qquad\left.+w\sqrt{1-ww^*}(1-uu^*)\left(\delta-\frac{e^{2i\alpha}}{\delta}\right)\right] \\ &-\frac{4\sqrt{\beta}}{\sqrt{1-uu^*}(1-ww^*)(1+e^{-2i\alpha})}\frac{\partial w}{\partial t}\left[w^*\sqrt{1-ww^*}(1-uu^*)e^{-2i\alpha}\left(\delta+\frac{1}{\delta}\right)\right. \\ &\qquad\left.+u^*\sqrt{1-uu^*}(1-ww^*)\left(\delta e^{-2i\alpha}-\frac{1}{\delta}\right)\right] \\ &+\frac{4\sqrt{\beta}}{\sqrt{1-uu^*}(1-ww^*)(1+e^{2i\alpha})}\frac{\partial w^*}{\partial t}\left[w\sqrt{1-ww^*}(1-uu^*)e^{2i\alpha}\left(\delta+\frac{1}{\delta}\right)\right. \\ &\qquad\left.+u\sqrt{1-uu^*}(1-ww^*)\left(\delta e^{2i\alpha}-\frac{1}{\delta}\right)\right] ; \end{aligned} \tag{A.3.7}$$

these are checked to limit to the boundary terms involving time-derivatives (A.2.1). The remainder of $\mathcal{P}_2^*(u) - \mathcal{P}_2^*(w)$ after the time-derivative of the above terms have been subtracted has the form

$$\frac{\partial u}{\partial t}A_u + \frac{\partial u^*}{\partial t}A_{u^*} + \frac{\partial w}{\partial t}A_w + \frac{\partial w^*}{\partial t}A_{w^*} ; \tag{A.3.8}$$

which is a total time-derivative if

$$(A_u\,,A_{u^*}\,,A_w\,,A_{w^*}) = \left(\frac{\partial\mathcal{A}}{\partial u}\,,\frac{\partial\mathcal{A}}{\partial u^*}\,,\frac{\partial\mathcal{A}}{\partial w}\,,\frac{\partial\mathcal{A}}{\partial w^*}\,,\right) \tag{A.3.9}$$

for some $\mathcal{A}$. We check that this is the case by showing that the cross derivatives vanish, for example

$$\frac{\partial A_u}{\partial u^*} - \frac{\partial A_{u^*}}{\partial u} = 0\,, \qquad \frac{\partial A_u}{\partial w} - \frac{\partial A_w}{\partial u} = 0\,,\ldots \tag{A.3.10}$$

Similar reasoning is used to show that the next higher-spin momentum-like charge can be modified to be conserved in the defect theory.

Appendix B

Classical scattering processes

B.1 Soliton equal to two defects?

In this section equations (5.4.29)

$$\Delta_t(E_A)+\Delta_t(E_B) = \Delta_t(\text{sol})\,, \qquad e^{i\phi(E_A)}e^{i\phi(E_B)} = e^{i\phi(\text{sol})}\,, \qquad T_{E_A}\,T_{E_B} = T_{sol}\,, \quad \text{(B.1.1)}$$

which equate the time-delay and phase factor experienced by a soliton (or particle) scattering through two specific excited defects to the time-delay experienced by a soliton scattering through another soliton are explicitly confirmed. Similarly equations

$$\Delta_t(E_A) + \Delta_t(U_B) = 0\,, \qquad e^{i\phi(E_A)}e^{i\phi(U_B)} = 1\,, \qquad T_{E_A}\,T_{U_B} = 1\,, \qquad \text{(B.1.2)}$$

which state that the effects of scattering through a specific excited defect and unexcited defect cancel each other out, are verified. They are graphically illustrated in figure B.1. In tables 5.9 and 5.10 we introduced defects E_A, E_B, U_A and U_B, using $\alpha = -A$ the defects are described by the parameters in table B.1.

Firstly for the particle using (5.4.28) then the different transmission factors are

$$T_{E_A} = \frac{e^{\theta}e^{iA'} - i\delta'}{e^{\theta} + i\delta' e^{iA'}}\,, \qquad T_{E_B} = \frac{-e^{\theta}e^{iA'} + i\delta'}{e^{\theta} + ie^{iA'}\delta'}\,, \qquad T_{U_B} = \frac{e^{\theta} + ie^{iA'}\delta'}{e^{\theta}e^{iA'} - i\delta'}\,, \qquad \text{(B.1.3)}$$

which satisfy

$$T_{E_A}\,T_{U_B} = \left(\frac{e^{\theta}e^{iA'} - i\delta'}{e^{\theta} + i\delta' e^{iA'}}\right)\left(\frac{e^{\theta} + ie^{iA'}\delta'}{e^{\theta}e^{iA'} - i\delta'}\right) = 1 \qquad \text{(B.1.4)}$$

(a) (b)

Fig. B.1: (a) Soliton scattering through two excited defects. (b) Soliton scattering through an excited and an unexcited defect.

E_A	A	$= A'$	$= \frac{\pi}{3}$	δ	$= \delta'$	$= 2$
U_A	A	$= \pi - A'$	$= \frac{2\pi}{3}$	δ	$= \delta'$	$= 2$
E_B	A	$= A' - \pi$	$= \frac{-2\pi}{3}$	δ	$= -\delta'$	$= -2$
U_B	A	$= -A'$	$= \frac{-\pi}{3}$	δ	$= -\delta'$	$= -2$

Table B.1: The parameters that describe defects E_A, E_B, U_A and U_B.

and

$$T_{E_A}T_{E_B} = \left(\frac{e^{\theta}e^{iA'} - i\delta'}{e^{\theta} + i\delta' e^{iA'}}\right)\left(\frac{-e^{\theta}e^{iA'} + i\delta'}{e^{\theta} + ie^{iA'}\delta'}\right) = -\left(\frac{e^{\theta}e^{iA'} - i\delta'}{e^{\theta} + i\delta' e^{iA'}}\right)^2 . \tag{B.1.5}$$

Comparing with (4.7.2)

$$T_{particle/sol} = -\left(\frac{\delta_{sol} + ie^{\theta}e^{ia_{sol}}}{\delta_{sol}e^{ia_{sol}} - ie^{\theta}}\right)^2 , \tag{B.1.6}$$

shows that a particle scattering through excited defects E_A and E_B is affected in the same way as scattering through a soliton described by $a_{sol} = A'$ and $\delta_{sol} = \delta'$.

The soliton experiences the following time-delays through the different defects (5.4.20)

$$\Delta t(E_A) = \Delta t(E_B) = \frac{1}{4\sqrt{\beta}\cos(a)\sinh(\theta)} \ln\left(\frac{(e^{\theta}e^{ia} - \delta' e^{iA'})(e^{\theta}e^{iA'} - \delta' e^{ia})}{(\delta' + e^{ia}e^{iA'}e^{\theta})(e^{\theta} + e^{ia}e^{iA'}\delta')}\right) , \tag{B.1.7}$$

$$\Delta t(U_B) = \frac{1}{4\sqrt{\beta}\cos(a)\sinh(\theta)} \ln\left(\frac{(e^{\theta}e^{ia}e^{iA'} + \delta')(e^{\theta} + \delta' e^{iA'}e^{ia})}{(e^{ia}e^{\theta} - \delta' e^{iA'})(e^{\theta}e^{iA'} - e^{ia}\delta')}\right) , \tag{B.1.8}$$

which satisfy

$$\Delta t(E_A) + \Delta t(U_B) = 1 \tag{B.1.9}$$

and

$$\Delta t(E_A) + \Delta t(E_B) = \frac{1}{2\sqrt{\beta}\cos(a)\sinh(\theta)} \ln\left(\frac{(e^{\theta}e^{ia} - \delta' e^{iA'})(e^{\theta}e^{iA'} - \delta' e^{ia})}{(\delta' + e^{ia}e^{iA'}e^{\theta})(e^{\theta} + e^{ia}e^{iA'}\delta')}\right). \tag{B.1.10}$$

Comparing this with (4.6.4)

$$\Delta t(sol) = \frac{1}{2\sqrt{\beta}\cos(a)\sinh(\theta)} \ln\left(\frac{(e^{\theta}e^{ia} - \delta_{sol}e^{ia_{sol}})(e^{\theta}e^{ia_{sol}} - \delta_{sol}e^{ia})}{(\delta_{sol} + e^{\theta}e^{ia}e^{ia_{sol}})(e^{\theta} + \delta_{sol}e^{ia}e^{ia_{sol}})}\right), \tag{B.1.11}$$

shows that a soliton scattering through excited defects E_A and E_B is affected in the same way as scattering through a soliton described by $a_{sol} = A'$ and $\delta_{sol} = \delta'$. A soliton scattering through excited defect E_A and unexcited defect U_B experiences no overall time-delay.

A soliton scattering through a defect also experiences a phase shift (5.4.21)

$$e^{i\phi(E_A)} = -e^{i\phi(E_B)} = e^{2\sqrt{\beta}\sinh(\theta+ia)\Delta t(E_A)} \frac{\delta' + e^{\theta}e^{ia}e^{iA'}}{e^{\theta}e^{ia} - \delta' e^{iA'}}, \tag{B.1.12}$$

$$e^{i\phi(U_B)} = e^{2\sqrt{\beta}\sinh(\theta+ia)\Delta t(U_B)} \frac{e^{\theta}e^{ia} - \delta' e^{iA'}}{e^{\theta}e^{ia}e^{iA'} + \delta'}, \tag{B.1.13}$$

Which satisfy

$$e^{i\phi(E_A)}\ e^{i\phi(U_B)} = 1 \tag{B.1.14}$$

and

$$e^{i\phi(E_A)}\ e^{i\phi(E_B)} = -e^{2\sqrt{\beta}\sinh(\theta+ia)(\Delta t(E_A)+\Delta t(E_A))} \left(\frac{\delta' + e^{\theta}e^{ia}e^{iA'}}{e^{\theta}e^{ia} - \delta' e^{iA'}}\right)^2. \tag{B.1.15}$$

Comparing with (4.6.5)

$$e^{i\phi(sol)} = -e^{2\sqrt{\beta}\sinh(\theta+ia)\Delta t(sol)} \left(\frac{\delta_{sol} + e^{\theta}e^{ia}e^{ia_{sol}}}{e^{\theta}e^{ia} - \delta_{sol}e^{ia_{sol}}}\right)^2, \tag{B.1.16}$$

shows that the phase factors do satisfy (B.1.1).

The pair of excited defects needed to replicate the behaviour of a soliton have to be specifically chosen, they have to be a pair of defects that emit the same soliton. In fact the soliton that they replicate the behaviour of is exactly the soliton that they emit during a classical decay process. Shown in table B.2 are the energy and charges of the defects. Therefore

$$E(E_A) + E(E_B) = 4\sqrt{\beta}\left(\delta' + \frac{1}{\delta'}\right)\cos(A') \tag{B.1.17}$$

E_A	E	$= 2\sqrt{\beta}\left(\delta' + \frac{1}{\delta'}\right)\cos(A')$	Q	$= -2A'$
E_B	E	$= 2\sqrt{\beta}\left(-\delta' - \frac{1}{\delta'}\right)\cos(A' - \pi)$	Q	$= -2A' + 2\pi$
U_B	E	$= 2\sqrt{\beta}\left(-\delta' - \frac{1}{\delta'}\right)\cos(-A')$	Q	$= 2A'$

Table B.2: Energy and charge of defects E_A, E_B and U_B.

and

$$Q(E_A) + Q(E_B) = 2\pi - 4A', \tag{B.1.18}$$

which are exactly the energy and charge of a soliton with $a_{sol} = A'$ and $\delta_{sol} = \delta'$. So the two defects exhibit the same scattering properties and have the same conserved charges as the soliton. Similarly

$$E(E_A) + E(U_B) = 0, \quad Q(E_A) + Q(U_B) = 0, \tag{B.1.19}$$

so the energy and charge of the excited and unexcited defect cancel each other out. As with the two excited defects, the excited and unexcited also have to be carefully chosen, for the scattering behaviour to cancel an excited defect and its anti-defect are needed.

B.2 Defect processes

In this section we show explicitly the consistency of the classical scattering properties of CSG solitons and particles by considering the scattering through a decaying defect and through a defect absorbing a soliton.

B.2.1 Defect decay process

First we consider the process where an excited defect decays by emitting a right-moving soliton. The integrability of the theory says that the time of the scattering should not affect the time-delay and phase factor experienced by the soliton. Figure B.2 shows this process for the case when the scattering soliton has greater rapidity than the emitted soliton. The time-delay for a soliton scattering (5.4.20) through

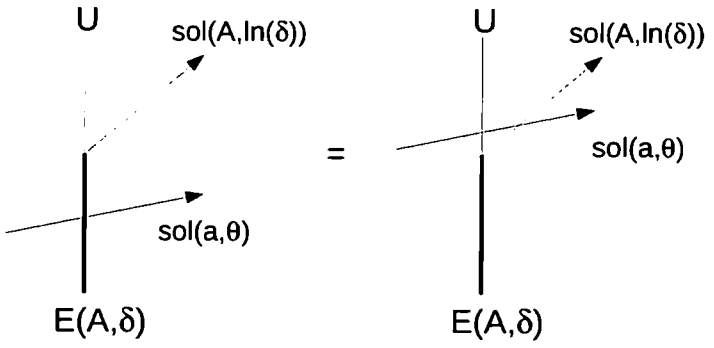

Fig. B.2: Soliton scattering through a decaying defect.

excited defect E_A is (B.1.7) and through U_A

$$\Delta t(U_A) = \frac{1}{4\sqrt{\beta}\cos(a)\sinh(\theta)} \ln\left(\frac{(e^{\theta}e^{ia}e^{iA'}+\delta')(e^{\theta}+e^{iA'}\delta' e^{ia})}{(e^{ia}e^{\theta}-\delta' e^{iA'})(e^{\theta}e^{iA'}-e^{ia}\delta')}\right) \tag{B.2.1}$$

and they experience the phase shifts (B.1.12),

$$e^{i\phi(U_A)} = e^{2\sqrt{\beta}\sinh(\theta+ia)\Delta t(U_A)} \frac{\delta' e^{iA'} - e^{\theta}e^{ia}}{e^{\theta}e^{ia}e^{iA'}+\delta'} . \tag{B.2.2}$$

The soliton emitted when defect E_A decays is described by $a_{sol} = A'$ and $e^{\theta_{sol}} = \delta_{sol} = \delta'$ through which the scattering soliton experiences the time-delay (B.1.11) and phase-factor (B.1.16). We check that these time-delays satisfy

$$\Delta t(U_A)+\Delta t(sol) = \frac{1}{4\sqrt{\beta}\cos(a)\sinh(\theta)} \ln\left(\frac{(e^{\theta}e^{ia}-\delta' e^{iA'})(e^{\theta}e^{iA'}-\delta' e^{ia})}{(\delta'+e^{ia}e^{iA'}e^{\theta})(e^{\theta}+e^{ia}e^{iA'}\delta')}\right) = \Delta t(E_A) \tag{B.2.3}$$

and the phase-factors

$$e^{i\phi(U_A)}\ e^{i\phi(sol)} = e^{2\sqrt{\beta}\sinh(\theta+ia)\Delta t(E_A)} \frac{\delta' + e^{\theta}e^{ia}e^{iA'}}{e^{\theta}e^{ia}-\delta' e^{iA'}} = e^{i\phi(E_A)} . \tag{B.2.4}$$

Therefore the time of scattering does not affect the scattering experienced by the soliton. This should also be true for the particle, which experiences the transmission factor (B.1.3) through E_A and

$$T_{U_A} = \frac{e^{\theta}+i\delta' e^{iA'}}{i\delta' - e^{\theta}e^{iA'}} , \tag{B.2.5}$$

through U_A. The particle-soliton scattering factor given by (B.1.6). Again we check these satisfy

$$T_{U_A}T_{sol} = \frac{\delta' + ie^{\theta}e^{iA'}}{ie^{\theta}-\delta' e^{iA'}} = T_{E_A} . \tag{B.2.6}$$

B.2.2 Defect absorption process

Figure B.3 shows an unexcited defect absorbing a soliton, becoming excited, with the defect conditions providing the relations $a_{sol} = -A'$ and $\delta_{sol} = -\delta'$. The soliton (or particle) scattering through the absorption process has greater rapidity than the absorbed soliton. The defect conditions are solved using the prescription that

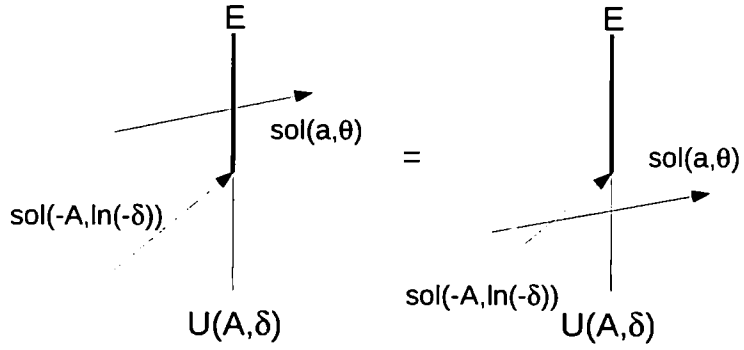

Fig. B.3: Soliton scattering through a defect absorbing a soliton.

$\alpha = -A$ as $t \to -\infty$, so in this set-up the time-delay, phase-factor for the soliton scattering through the excited defect is actually the one previously written down for the unexcited defect (B.2.1) and (B.2.2) and vice-versa. These new quantities we denote with a star.

$$\Delta t(E_A)^* = \Delta t(U_A)\,,\ \Delta t(U_A)^* = \Delta t(E_A)\,, \quad e^{i\phi(E_A)*} = e^{i\phi(U_A)}\,,\ e^{i\phi(U_A)*} = e^{i\phi(E_A)} \tag{B.2.7}$$

The soliton scattering through the slower rapidity absorbed soliton experiences the time-delay (B.1.11) and phase shift (B.1.16). These quantities with the defect condition relations applied do satisfy

$$\Delta t(E_A)^* = \Delta t(U_A)^* + \Delta t(sol)\,, \quad e^{i\phi(E_A)*} = e^{i\phi(U_A)*}\, e^{i\phi(sol)}\,. \tag{B.2.8}$$

Similarly for the particle we check the following holds

$$T^*_{E_A} = T_{particle/sol}\, T^*_{U_A}\,. \tag{B.2.9}$$

B.3 Dressed boundary consistency check

In this section the consistency check, due to the construction of the dressed boundary, on the classical soliton time-delay when reflecting from the dressed boundary and the classical soliton-defect time-delay and reflection time-delay from the Dirichlet boundary is verified. Figure B.4 shows the check in diagram form.

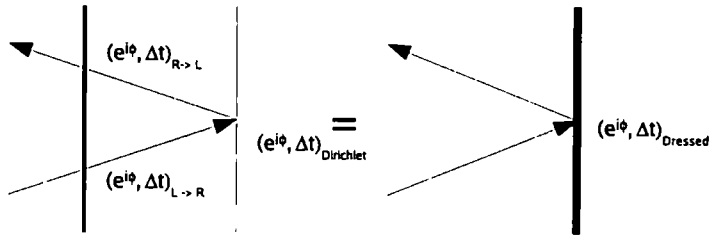

Fig. B.4: Soliton or particle reflection from the dressed boundary

Firstly considering the reflection of the CSG particle, from (4.7.2) the transmission for a left-moving particle scattering through the defect is

$$T_L = \frac{e^\theta - i\delta e^{i\alpha}}{e^{i\alpha}e^\theta + i\delta}, \tag{B.3.1}$$

and for a right-moving particle

$$T_R = 1/T_L(\theta \to -\theta). \tag{B.3.2}$$

The final factor which is needed is the reflection factor from the Dirichlet boundary which is $R_{Dir} = -1$. Therefore the particle-dressed boundary reflection factor should be

$$R_{DB} = T_L\ R_{Dir}\ T_R = -\frac{(e^\theta - i\delta e^{i\alpha})(e^{i\alpha} + i\delta e^\theta)}{(e^{i\alpha}e^\theta + i\delta)(1 - i\delta e^\theta e^{i\alpha})}, \tag{B.3.3}$$

which agrees with (6.2.23).

Similarly for the soliton scattering, from (5.4.20) the time-delay for a left-moving soliton scattering through the defect is

$$\Delta t_L = \frac{1}{2\sqrt{\beta}\cos(a)\sinh(\theta)} \ln \left| \frac{\sinh\left(\frac{\theta - X}{2} + i\frac{a+\alpha}{2}\right)}{\cosh\left(\frac{\theta - X}{2} + i\frac{a-\alpha}{2}\right)} \right| \tag{B.3.4}$$

where $\delta = e^{\chi}$ and from (5.4.21) the phase-factor

$$e^{i\phi_L} = e^{2\sqrt{\beta}\sinh(\theta+ia)\Delta t_L}\frac{\delta e^{i\alpha}+e^{\theta}e^{ia}}{e^{\theta}e^{ia}e^{i\alpha}-\delta}. \tag{B.3.5}$$

The right-moving soliton-defect scattering properties are related to the left-moving ones by

$$\Delta t_R = -\Delta t_L(\theta \to -\theta), \qquad e^{i\phi_R} = 1/e^{i\phi_L}(\theta \to -\theta). \tag{B.3.6}$$

Explicitly written

$$\Delta t_R = \frac{1}{2\sqrt{\beta}\cos(a)\sinh(\theta)}\ln\left|\frac{\sinh\left(\frac{\theta+\chi}{2}+i\frac{a+\alpha}{2}\right)}{\cosh\left(\frac{\theta+\chi}{2}+i\frac{a-\alpha}{2}\right)}\right|, \tag{B.3.7}$$

$$\begin{aligned} e^{i\phi_R} &= e^{2\sqrt{\beta}\sinh(-\theta+ia)\Delta t_R}\frac{e^{ia}e^{i\alpha}-\delta e^{\theta}}{\delta e^{i\alpha}e^{\theta}+e^{ia}} \\ &= e^{2\sqrt{\beta}\sinh(\theta+ia)\Delta t_R}\frac{e^{i\alpha}+\delta e^{ia}e^{\theta}}{1-\delta e^{i\alpha}e^{\theta}e^{ia}}. \end{aligned} \tag{B.3.8}$$

While the soliton scatters from the Dirichlet boundary with

$$\Delta t_{Dir} = 0, \qquad e^{i\phi_{Dir}} = -1. \tag{B.3.9}$$

We calculate

$$\Delta_{DB} = \Delta t_L + \Delta t_R = \frac{1}{2\sqrt{\beta}\cos(a)\sinh(\theta)}\ln\left|\frac{\sinh\left(\frac{\theta-\chi}{2}+i\frac{a+\alpha}{2}\right)\sinh\left(\frac{\theta+\chi}{2}+i\frac{a+\alpha}{2}\right)}{\cosh\left(\frac{\theta-\chi}{2}+i\frac{a-\alpha}{2}\right)\cosh\left(\frac{\theta+\chi}{2}+i\frac{a-\alpha}{2}\right)}\right|, \tag{B.3.10}$$

which agrees with (6.2.19) and

$$e^{i\phi_{DB}} = -e^{i\phi_L}e^{i\phi_R} = -e^{2\sqrt{\beta}\sinh(\theta+ia)(\Delta t_L+\Delta t_R)}\left(\frac{\delta e^{i\alpha}+e^{\theta}e^{ia}}{e^{\theta}e^{ia}e^{i\alpha}-\delta}\right)\left(\frac{e^{i\alpha}+\delta e^{ia}e^{\theta}}{1-\delta e^{i\alpha}e^{\theta}e^{ia}}\right) \tag{B.3.11}$$

which agrees with (6.2.20).

B.4 Dressed boundary processes

Similarly for the dressed boundary, the scattering of solitons and particles through boundary decay and absorption processes are explicitly verified.

B.4.1 Boundary decay process

Figure B.5 shows an excited boundary decaying, emitting a soliton with less rapidity than the scattering soliton or particle. The figure shows graphically the relationship the reflection and transmission factors should satisfy, as the time of the scattering should not affect how the soliton (or particle) reflects. The excited boundary is

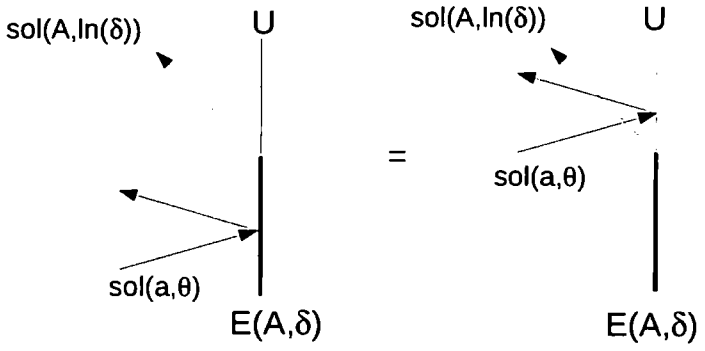

Fig. B.5: Soliton scattering through a decaying boundary.

taken to be excited boundary I from table 6.5, so the boundary conditions impose the conditions $a_{sol} = A$ and $e^{\theta_{sol}} = \delta$ on the soliton parameters. The time-delay for a soliton reflecting from the excited boundary is given by (6.2.19)

$$\Delta t(E) = \frac{1}{2\sqrt{\beta}\cos(a)\sinh(\theta)} \ln \left| \frac{\sinh\left(\frac{\theta-\chi}{2} + i\frac{a-A}{2}\right)\sinh\left(\frac{\theta+\chi}{2} + i\frac{a-A}{2}\right)}{\cosh\left(\frac{\theta-\chi}{2} + i\frac{a+A}{2}\right)\cosh\left(\frac{\theta+\chi}{2} + i\frac{a+A}{2}\right)} \right| , \tag{B.4.1}$$

and the phase shift by (6.2.20)

$$e^{i\phi(E)} = -\left(\frac{\delta + e^{\theta}e^{iA}e^{ia}}{e^{\theta}e^{ia} - e^{iA}\delta}\right)\left(\frac{1 + \delta e^{ia}e^{iA}e^{\theta}}{e^{iA} - \delta e^{\theta}e^{ia}}\right) e^{2\sqrt{\beta}(\sinh(\theta+ia)\Delta t(E)} , \tag{B.4.2}$$

and from the unexcited boundary

$$\Delta t(U) = -\Delta t(E) , \quad e^{i\phi(U)} = 1/e^{i\phi(E)} . \tag{B.4.3}$$

The incoming soliton experiences the time-delay and phase-factor given by

$$\Delta t(sol(-\theta)) = \Delta t(sol)\left(\delta_{sol} \to \frac{1}{\delta_{sol}}\right) , \quad e^{i\phi(sol(-\theta))} = e^{i\phi(sol)}\left(\delta_{sol} \to \frac{1}{\delta_{sol}}\right) . \tag{B.4.4}$$

when it scatters with the emitted soliton.

$$\Delta t(sol_{IN}) = \Delta t(sol(-\theta)), \quad e^{i\phi(sol_{IN})} = e^{i\phi(sol(-\theta))}. \tag{B.4.5}$$

While the outgoing soliton experiences the time-delay given by (B.1.11) and phase-factor (B.1.16).

$$\Delta t(sol_{OUT}) = \Delta t(sol), \quad e^{i\phi(sol_{OUT})} = e^{i\phi(sol)}. \tag{B.4.6}$$

It can be checked that these expressions satisfy

$$\Delta t(E) = \Delta t(sol_{IN}) + \Delta t(U) + \Delta t(sol_{OUT}) \tag{B.4.7}$$

and

$$e^{i\phi(E)} = e^{i\phi(sol_{IN})}\, e^{i\phi(U)}\, e^{i\phi(sol_{OUT})}. \tag{B.4.8}$$

Similarly for the particle, its reflection factor from the excited boundary is

$$R_E = -\frac{(e^{\theta}e^{iA} - i\delta)(1 + ie^{iA}\delta e^{\theta})}{(e^{\theta} + ie^{iA}\delta)(e^{iA} - i\delta e^{\theta})} \tag{B.4.9}$$

and from the unexcited boundary

$$R_U = -\frac{(e^{\theta} + ie^{iA}\delta)(e^{iA} - i\delta e^{\theta})}{(e^{iA}e^{\theta} - i\delta)(1 + ie^{iA}\delta e^{\theta})} \tag{B.4.10}$$

The incoming particle scatters through the emitted soliton with the transmission factor

$$T_{particle/sol(-\theta)} = T_{particle/sol}\left(\delta_{sol} \to \frac{1}{\delta_{sol}}\right) \tag{B.4.11}$$

and the outgoing particle with (B.1.6)

$$T_{sol}^{IN} = T_{particle/sol(-\theta)}, \quad T_{sol}^{OUT} = T_{particle/sol} \tag{B.4.12}$$

Which we check to satisfy

$$T_{sol}^{IN}\, R_U\, T_{sol}^{OUT} = R_E. \tag{B.4.13}$$

B.4.2 Boundary absorption process

Figure B.6 shows an unexcited boundary absorbing a soliton while a soliton (or particle) with greater rapidity scatters from the boundary, before and after the absorption. The unexcited boundary used to check the relation displayed in the figure is unexcited boundary II from table 6.4, so the boundary conditions give the constraints $a_{sol} = -A$ and $e^{\theta_{sol}} = -\delta$. As the usual prescription of $\alpha' = -A$ as

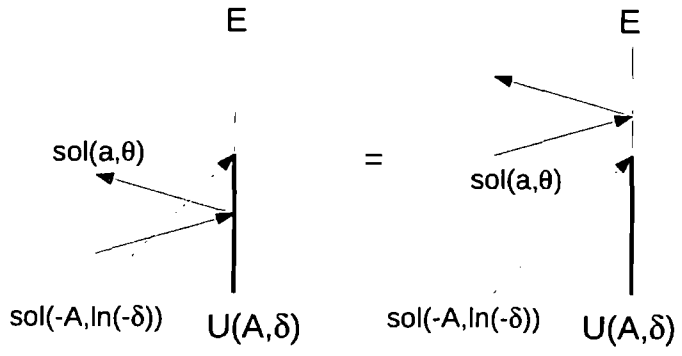

Fig. B.6: Soliton scattering through a boundary absorbing a soliton.

$t \to -\infty$ is used to solve the boundary conditions which means as in the defect computations the expressions for the excited and unexcited boundary swap round. For the particle

$$R_E^* = R_U, \quad R_U^* = R_E, \tag{B.4.14}$$

and for the soliton

$$\Delta t(E)^* = \Delta t(U), \ \Delta t(U)^* = \Delta t(E), \quad e^{i\phi(E)*} = e^{i\phi(U)}, \ e^{i\phi(U)*} = e^{i\phi(E)} \tag{B.4.15}$$

Considering the particle

$$T_{sol}^{IN} = T_{particle/sol}, \quad T_{sol}^{OUT} = T_{particle/sol(-\theta)}, \tag{B.4.16}$$

which using the constraints from the boundary conditions $a_{sol} = -A$ and $e^{\theta_{sol}} = -\delta$, can be checked to satisfy

$$T_{sol}^{IN} \ R_U^* \ T_{sol}^{OUT} = R_E^* \tag{B.4.17}$$

Similarly for the soliton which reflects from the different boundaries with the following time-delays and phase-factors

$$\Delta t(E)^* = \Delta t(U)\,,\ \Delta t(U)^* = \Delta t(E)\,,\quad e^{i\phi(E)*} = e^{i\phi(U)}\,,\ e^{i\phi(U)*} = e^{i\phi(E)}\,. \tag{B.4.18}$$

The incoming soliton experiences the scattering

$$\Delta t(sol_{IN}) = \Delta t(sol),\quad e^{i\phi(sol_{IN})} = e^{i\phi(sol)} \tag{B.4.19}$$

and the outgoing soliton

$$\Delta t(sol_{OUT}) = \Delta t(sol(-\theta)),\quad e^{i\phi(sol_{OUT})} = e^{i\phi(sol(-\theta))}\,, \tag{B.4.20}$$

which we check satisfy

$$\Delta t(sol_{IN}) + \Delta t(U)^* + \Delta t(sol_{OUT}) = \Delta t(E)^* \tag{B.4.21}$$

and

$$e^{i\phi(sol_{IN})}\ e^{i\phi(U)*}\ e^{i\phi(sol_{OUT})} = e^{i\phi(E)*}\,. \tag{B.4.22}$$

Appendix C

Closure of reflection bootstrap

In this appendix we check the closure of the reflection bootstrap procedure implemented in section 7.3.2. We found the reflection factor for a charge $Q = n$ soliton from a charge $Q = N$ unexcited boundary to be

$$R_n^{N(0)}(\theta) = R_n^{\text{base}} \prod_{j=0}^{n-1} (2N - B + 2j + 2 - n)(k + B + 2N - 2j - 2 + n)\,. \quad \text{(C.0.1)}$$

To check that this formula closes means to check that

$$R_1^{N(0)}(\theta) = R_{k+1}^{(N(0))}(\theta)\,, \quad \text{(C.0.2)}$$

which is checking that the reflection factors show the property that the soliton's charge is periodic. First using the crossing symmetry relation

$$R_1(\theta)\; R_{-1}(\theta + i\pi) = S_{1,1}(2\theta)\,, \quad \text{(C.0.3)}$$

implies

$$R_{-1}(\theta + i\pi) = -(1)(1-k)(k-1)(-1-2N+B)(1-2N-k-B)\,, \quad \text{(C.0.4)}$$

which becomes

$$R_{-1}(\theta) = (1-k)(k-1-2N+B)(1-2N-B)\,. \quad \text{(C.0.5)}$$

This is promising, as it has the correct pole $(1-2N-B)$ for the known bound state and limits to the classical reflection factor for the anti-particle. To show closure we need $R_{k-1}(\theta)$ to give the same result. First recall $R_1^{\text{base}} = (1-k)$ and

$$R_{k-1}^{\text{base}} = (1-k)(2)(2-k)(3)(3-k)...(k-3)(-2)(k-2)(-1), \quad \text{(C.0.6)}$$

using $(x)(-x) = 1$ shows for k even $R_{k-1}^{\text{base}} = (1-k)$. To check the other factors in

$$R_{k-1}^{N(0)}(\theta) = R_{k-1}^{\text{base}} \prod_{j=0}^{k-2} (2N - B + 2j + 3 - k)(B + 2N - 2j - 3), \tag{C.0.7}$$

we write out terms in the product

j	factor	j	factor
0	$(2N-B+3-k)(B+2N-3)$	$k-2$	$(2N-B+k-1)(B+2N+1)$
1	$(2N-B+5-k)(B+2N-5)$	$k-3$	$(2N-B+k-3)(B+2N+2)$
$\vdots$		$\vdots$	
$\frac{k}{2}-3$	$(2N-B-3)(-k+B+2N+3)$	$\frac{k}{2}+1$	$(2N-B+5)(-k+B+2N-5)$
$\frac{k}{2}-2$	$(2N-B-1)(-k+B+2N+1)$	$\frac{k}{2}$	$(2N-B+3)(-k+B+N-3)$
$\frac{k}{2}-1$	$(2N-B+1)(-k+B+2N-1)$		

reordering these terms

factor	factor
$(2N+B-3)(2N-B+3)$	$(2N-B+1)$
$(2N+B-5)(2N-B+5)$	$(2N+B+1)(2N-B-1)$
$(2N+B-7)(2N-B+7)$	$(2N+B+3)(2N-B-3)$
$\vdots$	$\vdots$
$(2N+B-k+3)(2N-B+k-3)$	$(2N+B+k-7)(2N-B-k+7)$
$(2N+B-k+1)(2N-B+k-1)$	$(2N+B+k-5)(2N-B-k+5)$
$(2N+B-k-1)$	$(2N+B+k-3)(2N-B-k+3)$

shows that the terms appear in pairs expect for two terms, using $(x)(-x) = 1$ allows the array of terms to be completed and $R_{k-1}^{N(0)}$ rewritten

$$\begin{aligned} R_{k-1}^{N(0)}(\theta) &= (1-k)(-2N+B-k-1)(1-2N-B) \\ &\qquad \times \prod_{j=0}^{k-1} (2N+B+1+2j)(2N-B+1+2j) \\ &= (1-k)(-2N+B-k-1)(1-2N-B) \\ &= R_{-1}^{N(0)}(\theta)\,. \end{aligned} \tag{C.0.8}$$

The terms in the product cancel as $2N$ is an even integer and therefore the product as the form

$$\prod_{j=0}^{k-1} (B+1+2j)(-B-1-2j) = 1\,. \tag{C.0.9}$$

We have shown that the reflection bootstrap close for k even.

Bibliography

[1] Peter Bowcock and James Umpleby. Defects and Dressed Boundaries in Complex Sine-Gordon Theory. *JHEP*, 01:008, 2009, 0805.3668.

[2] Peter Bowcock and James Umpleby. Quantum complex sine-Gordon dressed boundaries. *JHEP*, 11:038, 2008, 0809.0661.

[3] Bill Bryson. Notes from a Small Island. 1996.

[4] Subir Ghoshal and Alexander B. Zamolodchikov. Boundary S matrix and boundary state in two-dimensional integrable quantum field theory. *Int. J. Mod. Phys.*, A9:3841–3886, 1994, hep-th/9306002.

[5] Subir Ghoshal. Bound state boundary S matrix of the Sine-Gordon model. *Int. J. Mod. Phys.*, A9:4801–4810, 1994, hep-th/9310188.

[6] P. Bowcock, E. Corrigan, P. E. Dorey, and R. H. Rietdijk. Classically integrable boundary conditions for affine Toda field theories. *Nucl. Phys.*, B445:469–500, 1995, hep-th/9501098.

[7] G. Delfino, G. Mussardo, and P. Simonetti. Scattering theory and correlation functions in statistical models with a line of defect. *Nucl. Phys.*, B432:518–550, 1994, hep-th/9409076.

[8] P. Bowcock, E. Corrigan, and C. Zambon. Classically integrable field theories with defects. *Int. J. Mod. Phys.*, A19S2:82–91, 2004, hep-th/0305022.

[9] John Scott Russell. Report on Waves. *British Association for the Advancement of Science*, 120:311–390, 1844.

[10] Alexander B. Zamolodchikov and Alexei B. Zamolodchikov. Factorized S-matrices in two dimensions as the exact solutions of certain relativistic quantum field models. *Annals Phys.*, 120:253–291, 1979.

[11] P. Dorey. Exact S matrices. 1996, hep-th/9810026.

[12] L. Bianchi. Lezioni di geometria differenziale Vol 1 and 2. 1922.

[13] G.L. Lamb. Elements of soliton theory. *Wiley*, 1980.

[14] H. Saleur, S. Skorik, and N. P. Warner. The Boundary sine-Gordon theory: Classical and semiclassical analysis. *Nucl. Phys.*, B441:421–436, 1995, hep-th/9408004.

[15] A. MacIntyre. Integrable boundary conditions for classical sine-Gordon theory. *J. Phys.*, A28:1089–1100, 1995, hep-th/9410026.

[16] E. Corrigan and G. W. Delius. Boundary breathers in the sinh-Gordon model. *J. Phys.*, A32:8601–8614, 1999, hep-th/9909145.

[17] E. Corrigan and A. Taormina. Reflection factors and a two-parameter family of boundary bound states in the sinh-Gordon model. *J. Phys.*, A33:8739–8754, 2000, hep-th/0008237.

[18] Olalla Castro-Alvaredo and Andreas Fring. From integrability to conductance, impurity systems. *Nucl. Phys.*, B649:449–490, 2003, hep-th/0205076.

[19] M. Mintchev, E. Ragoucy, and P. Sorba. Scattering in the presence of a reflecting and transmitting impurity. *Phys. Lett.*, B547:313–320, 2002, hep-th/0209052.

[20] Roger E. Behrend and Paul A. Pearce. Integrable and conformal boundary conditions for sl(2) A- D-E lattice models and unitary minimal conformal field theories. 2000, hep-th/0006094.

[21] K. Graham and G. M. T. Watts. Defect lines and boundary flows. *JHEP*, 04:019, 2004, hep-th/0306167.

[22] Z. Bajnok and A. George. From defects to boundaries. *Int. J. Mod. Phys.*, A21:1063–1078, 2006, hep-th/0404199.

[23] Ismagil Habibullin and Anjan Kundu. Quantum and classical integrable sine-Gordon model with defect. *Nucl. Phys.*, B795:549–568, 2008, 0709.4611.

[24] P. Bowcock, E. Corrigan, and C. Zambon. Affine Toda field theories with defects. *JHEP*, 01:056, 2004, hep-th/0401020.

[25] P. Bowcock, E. Corrigan, and C. Zambon. Some aspects of jump-defects in the quantum sine-Gordon model. *JHEP*, 08:023, 2005, hep-th/0506169.

[26] E. Corrigan and C. Zambon. Aspects of sine-Gordon solitons, defects and gates. *J. Phys.*, A37:L471, 2004, hep-th/0407199.

[27] V. Caudrelier, M. Mintchev, and E. Ragoucy. Solving the quantum non-linear Schrodinger equation with delta-type impurity. *J. Math. Phys.*, 46:042703, 2005, math-ph/0404047.

[28] V. Caudrelier, M. Mintchev, and E. Ragoucy. The quantum non-linear Schroedinger model with point-like defect. *J. Phys.*, A37:L367–L376, 2004, hep-th/0404144.

[29] J. F. Gomes, L. H. Ymai, and A. H. Zimerman. The super mKdV and sinh-Gordon hierarchy: Solitons and Backlund defects. *J. Phys.*, A39:7471–7483, 2006, hep-th/0601014.

[30] Z. Bajnok and Zs. Simon. Solving topological defects via fusion. 2007, arXiv:0712.4292 [hep-th].

[31] Fernando Lund and Tullio Regge. Unified Approach to Strings and Vortices with Soliton Solutions. *Phys. Rev.*, D14:1524, 1976.

[32] Fernando Lund. Example of a Relativistic, Completely Integrable, Hamiltonian System. *Phys. Rev. Lett.*, 38:1175, 1977.

[33] Michael Kalb and Pierre Ramond. Classical direct interstring action. *Phys. Rev.*, D9:2273, 1974.

[34] John Archibald Wheeler and Richard Phillips Feynman. Classical Electrodynamics in Terms of Direct Interparticle Action. *Rev. Mod. Phys.*, 21(3):425–433, Jul 1949.

[35] K. Pohlmeyer. Integrable Hamiltonian Systems and Interactions Through Quadratic Constraints. *Commun. Math. Phys.*, 46:207–221, 1976.

[36] K. Pohlmeyer and Karl-Henning Rehren. Reduction of the two-dimensional O(n) nonlinear sigma model. *J. Math. Phys.*, 20:2628, 1979.

[37] B. S. Getmanov. Two-dimensional Lorentz invariant field theory models with higher integrals of motion: comples scalar fields. *Zvenigorod, Proceedings, Group Theoretical Methods*, 1:385–397, 1982.

[38] B. S. Getmanov. New Lorentz Invariant Systems with Exact Multi-Soliton Solutions. *Pisma Zh. Eksp. Teor. Fiz.*, 25:132–136, 1977.

[39] Ioannis Bakas. Conservation laws and geometry of perturbed coset models. *Int. J. Mod. Phys.*, A9:3443–3472, 1994, hep-th/9310122.

[40] Q-Han Park and H. J. Shin. Duality in complex sine-Gordon theory. *Phys. Lett.*, B359:125–132, 1995, hep-th/9506087.

[41] Carlos R. Fernandez-Pousa, Manuel V. Gallas, Timothy J. Hollowood, and J. Luis Miramontes. The symmetric space and homogeneous sine-Gordon theories. *Nucl. Phys.*, B484:609–630, 1997, hep-th/9606032.

[42] Carlos R. Fernandez-Pousa and J. Luis Miramontes. Semi-classical spectrum of the homogeneous sine-Gordon theories. *Nucl. Phys.*, B518:745–769, 1998, hep-th/9706203.

[43] H. J. de Vega and J. M. Maillet. Renormalization character and quantum S-matrix for a classically integrable theory. *Phys. Lett.*, B101:302, 1981.

[44] H. J. de Vega and J. M. Maillet. Semiclassical quantization of the complex sine-Gordon field theory. *Phys. Rev.*, D28:1441, 1983.

[45] Roger F. Dashen, Brosl Hasslacher, and André Neveu. Particle spectrum in model field theories from semiclassical functional integral techniques. *Phys. Rev. D*, 11(12):3424–3450, Jun 1975.

[46] Nicholas Dorey and Timothy J. Hollowood. Quantum scattering of charged solitons in the complex sine-Gordon model. *Nucl. Phys.*, B440:215–236, 1995, hep-th/9410140.

[47] P. Bowcock and G. Tzamtzis. The complex sine-Gordon model on a half line. *JHEP*, 03:047, 2007, hep-th/0203139.

[48] Peter Bowcock and Georgios Tzamtzis. Quantum complex sine-Gordon model on a half line. *JHEP*, 11:018, 2007, hep-th/0612120.

[49] H. J. de Vega, J. Ramirez Mittelbrunn, M. Ramon Medrano, and Norma G. Sanchez. The General solution of the 2-D sigma model stringy black hole and the massless complex Sine-Gordon model. *Phys. Lett.*, B323:133–138, 1994, hep-th/9312085.

[50] S. L. McCall and E. L. Hahn. Self-Induced Transparency. *Phys. Rev.*, 183(2):457–485, Jul 1969.

[51] Q-Han Park and H. J. Shin. Effective Field Theory for Coherent Optical Pulse Propagation. 1996, hep-th/9605052.

[52] Q-Han Park and H. J. Shin. Field theory for coherent optical pulse propagation. *Phys. Rev. A*, 57(6):4621–4642, Jun 1998.

[53] Heng-Yu Chen, Nick Dorey, and Keisuke Okamura. On the scattering of magnon boundstates. *JHEP*, 11:035, 2006, hep-th/0608047.

[54] Heng-Yu Chen, Nick Dorey, and Keisuke Okamura. Dyonic giant magnons. *JHEP*, 09:024, 2006, hep-th/0605155.

[55] Diego M. Hofman and Juan Martin Maldacena. Reflecting magnons. *JHEP*, 11:063, 2007, 0708.2272.

[56] Heng-Yu Chen and Diego H. Correa. Comments on the Boundary Scattering Phase. *JHEP*, 02:028, 2008, 0712.1361.

[57] Changrim Ahn, Dongsu Bak, and Soo-Jong Rey. Reflecting Magnon Bound States. *JHEP*, 04:050, 2008, 0712.4144.

[58] J. Wess and B. Zumino. Consequences of anomalous Ward identities. *Phys. Lett.*, B37:95, 1971.

[59] Edward Witten. Nonabelian bosonization in two dimensions. *Commun. Math. Phys.*, 92:455–472, 1984.

[60] Q.-Han Park and H. J. Shin. Classical matrix sine-gordon theory. *Nuclear Physics B*, 458:327, 1996.

[61] P Bowcock. Boundaries and Defects. *3rd EUCLID School, Trieste, Italy*, 2006.

[62] Ivan Ventura and Gil C. Marques. The Bohr-Sommerfeld Quantization Rule and Charge Quantization in Field Theory. *Phys. Lett.*, B64:43, 1976.

[63] C. Montonen. On Solitons with an Abelian Charge in Scalar Field Theories. 1. Classical Theory and Bohr-Sommerfeld Quantization. *Nucl. Phys.*, B112:349, 1976.

[64] S. Coleman and H. J. Thun. On the Prosaic Origin of the Double Poles in the Sine-Gordon S-Matrix. *Commun. Math. Phys*, 61:31, 1978.

[65] I. V. Cherednik. Factorizing Particles on a Half Line and Root Systems. *Theor. Math. Phys.*, 61:977–983, 1984.

[66] Andreas Fring and Roland Koberle. Factorized scattering in the presence of reflecting boundaries. *Nucl. Phys.*, B421:159–172, 1994, hep-th/9304141.

[67] E. Corrigan, P. E. Dorey, R. H. Rietdijk, and R. Sasaki. Affine Toda field theory on a half line. *Phys. Lett.*, B333:83–91, 1994, hep-th/9404108.

[68] Gustav W. Delius and Georg M. Gandenberger. Particle Reflection Amplitudes in a_n$\hat{(1)}$ Toda Field Theories. *Nuclear Physics B*, 554:325, 1999.

[69] Patrick Dorey, Roberto Tateo, and Gerard Watts. Generalisations of the Coleman-Thun mechanism and boundary reflection factors. *Phys. Lett.*, B448:249–256, 1999, hep-th/9810098.

[70] Peter Mattsson and Patrick Dorey. Boundary spectrum in the sine-Gordon model with Dirichlet boundary conditions. *J. Phys.*, A33:9065–9094, 2000, hep-th/0008071.

[71] Z. Bajnok, L. Palla, G. Takacs, and G. Z. Toth. The spectrum of boundary states in sine-Gordon model with integrable boundary conditions. *Nucl. Phys.*, B622:548–564, 2002, hep-th/0106070.

[72] Z. Bajnok, L. Palla, and G. Takacs. Boundary states and finite size effects in sine-Gordon model with Neumann boundary condition. *Nucl. Phys.*, B614:405–448, 2001, hep-th/0106069.

[73] Z. Bajnok, G. Bohm, and G. Takacs. On perturbative quantum field theory with boundary. *Nucl. Phys.*, B682:585–617, 2004, hep-th/0309119.